Sustained Hydrogel-Based Delivery of RNA Interference Nanocomplexes for Gene Knockdown

Ellen Ngarande

Thesis Presented for the Degree of

DOCTOR OF PHILOSOPHY (Ph.D.)

In the Department of Surgery

Faculty of Health Sciences

UNIVERSITY OF CAPE TOWN

August 2019

Table of Contents

Declaration

I, Ellen Ngarande, hereby declare that the work on which this thesis is based is my original work (except where acknowledgements indicate otherwise) and that neither the whole work nor any part of it has been, is being or is to be submitted for another degree in this or any other university.

I empower the University of Cape Town to reproduce the whole or portion of this thesis for the purpose of research or any manner what so ever.

Signature:… Signed by candidate

Date:2/08/2019……

Acknowledgements

Ass.Prof Neil H. Davies, where to begin. It's been quite a journey, one that seemed like it was never going to end (on my side) but we got there! I am grateful for the patience, guidance, encouragement, a free and safe learning environment and for caring not only about the work but about my wellbeing. It all helped me push through the process. So thank you.

Ass.Prof. Deon Bezuidenhout though we did not interact but your background presence was felt, thank you very much. Anel Oosthuysen thank you for your help with the dendrimers and NMR analysis, I wouldn't have done it without you.

Everyone in the animal unit, most importantly Jabu Magagula and Rodney Lucas, thank you for your help with the mice that made this thesis.

Dr Ousman Tamgue thank you for helping me with the PCR analysis. Hellen Ilsley all that immense histology work thank you for assisting with it.

Emma Doubell and Dr. Kevin Dzobo, thank you for taking the time to assist me with my thesis edits.

My family and friends (basically bonus family), I know you are all as excited as I am to complete this thesis! Collen, Aby, Dyllan, Hilaria, Zimkulu, Selma, Elina, Bootetsi, Bianca, Nancy, Kadi and last but not least Kelvin. For the support, the much needed help at every turn with pretty much everything and listening. I appreciate you all because most of you didn't know exactly what I was doing for 6 years but you were rooting for me every step, every year with no pressure and believed it important that carry on through the difficult times and when I didn't feel my best. So this is for us family.

A very special thank you to my Mother. For your steadfast belief in my abilities and support through my journey, your prayers, patience, love, support, I appreciate you to infinity.

This work would not have been possible without funding from NRF, I am appreciative of the opportunity and the financial assistance.

To the unseen ultimate divine powers, the resolve, revelations, situations and people placed in my path through this journey were not just coincidences. I am grateful.

List of figures

List of appendices

List of Tables

Abbreviations

-ve	Negative
+ve	Positive
≈	Approximately
µg	Microgram
µl	Microlitre
µM	Micromolar
AAV	Adeno-associated virus
AC	Acrylate
ACE	Angiotensin-converting enzyme
ACTN	Actin
ALD	Aldehyde
ApoB	Apolipoprotein B
ASC	Adipose stem cell
AT1R	Angiotensin II (Ang II) type 1 receptor
ATCOL	Atelocollagen
Bp	Base pair
Bcl-2	B-cell lymphoma 2
BHG	Hepes and glucose buffer
BMP	Bone morphogenic protein
Ca2+	Calcium
CD98	Glycoprotein
cRGD	cyclo-Arg-Gly-Asp
CVD	Cardiovascular diseases
CY3	Cyanine dye 3
CY5	Cyanine dye 5
D	G4-PAMAM dendrimer

DAPI	4’,6-diamidino-2-phenylindole
DEPC	Diethyl pyrocarbonate
DMF	N, N-Dimethylformamide
DMF	Dimethylformamide
DMSO	Dimethyl sulfoxide
DNA	Deoxyribonucleic acid
DODAP	1,2-dioleoyl-3-dimethylammonium-propane
DODMA	2-dioleyloxy-N,N-dimethyl-3-aminopropane
DOPC	1,2-dioleoyl-sn-glycero-3-phosphocholine
DOPE	1, 2-dioleoyl-sn-glycero-3-phosphoethanolamine
DOTAP	1,2-dioleoyl-3-trimethylammoniumpropane
Dox	Doxorubicin
Drosha	dsRNA-specific endonuclease
dsRNA	Double stranded ribonucleic acid
DTT	Dithiothreitol
DTX	Docetaxel
ECM	Extracellular matrix
eGFP	enhanced GFP
eNOS	Endothelial nitric oxide synthase
EPR	Enhanced permeability and retention
EthD-1	Ethidium homodimer-1
FACS	Fluorescence activated cell sorting
FBS	Fetal bovine serum
FDA	Food and drug administration
FGF	Fibroblast growth factor
Fig	Figure
FITC	Fluorescein isothiocyanate
FpA	Fibrinopeptide proteins A
FpB	Fibrinopeptide proteins B

FVII	Factor VII
g	Gram
G4	Generation 4
GAPDH	Glyceraldehyde 3-phosphate dehydrogenase
GDF	Growth differentiation factor
GFP	Green fluorescent protein
H&E	Haematoxylin & Eosin
HA	Hyaluronic acid
HBS	Hepes buffered saline
HBV	Hepatitis B virus
HCC	Hepatocellular carcinoma
HCl	Hydrochloric acid
HeLa	Human epithelial cells
HGF	Hepatocyte growth factor
hMSC	Human bone marrow derived mesenchymal stem cells
HPRT	Hypoxanthine phosphoribosyltransferase
hr	Hour
HRP	Horseradish peroxidase
HT1080	Human fibrosarcoma cell line
HT1080-GFP	eGFP stably transfected HT1080 cell line
i.v	Intravenous
IL-6	Interleukin-6
IRF	Interferon regulatory factor
IsoPBS	Iso-osmotic phosphate buffered saline
kDa	Kilo Dalton
LDL	Low density lipoprotein
LDLR	Low density lipoprotein receptor
LV	Lentivirus

MCL1	Myeloid cell leukaemia-1
MCNP	Membrane / core nanoparticles
MD	Modified (G4)-PAMAM dendrimer
Mdr1	Multidrug resistant gene 1
mg	Milligram
MI	Myocardial infarction
Min	Minute
miRNA	Micro ribonucleic acid
ml	Milliliter
mM	Milimolar
mm	Millimeter
MMP	Matrix metalloproteinase
modRNA	Modified mRNA
mol	Mole
mRNA	Messenger ribonucleic acid
Mstn	Myostatin (GDF-8)
mV	millivolts
MW	Molecular weight
Neg	Negative
N/P	Nitrogen / Phosphate ratio
nM	Nano molar
nm	Nanometer
NMR	Nuclear magnetic resonance
ON	Overnight
PAMAM	Poly(amidoamide)
PBS	Phosphate buffered saline
PC	Phosphatidylcholine
PCL	Poly(caprolactone)
PCSK9	Proprotein convertase subtilisin / kexin type 9

pDNA	Plasmid DNA
PE	Phosphatidylethanolamine
PEG	Polyethylene glycol
PEG-AC	PEG-acrylate
PEG-BTC_2	PEG-benzotriazole carbonate
PEG-SG_2	PEG-succinimidyl glutarate
PEG-SMB_2	PEG-succininimidyl methylbutonate
PEG-SMC_2	PEG-Succinimidyl Carboxymethyl Ester
PEG-VS	PEG-vinyl sulphone
PEI	Polyethyleneimine
Penstrep	penicillin and streptomycin antibiotics
PEO	Poly(ethylene oxide)
PG	Phosphatidylglycerol
P-gp	P-glycoprotein
PI	Protease inhibitor
PL	Phospholipid
PLA	Poly (lactic acid)
PLGA	Poly-dl-lactic-co-glycolic acid
PNP	Polymeric nanoparticle
Pos	Positive
PP	Poly(organophosphazene)
PS	Phosphatidylserine
PVA	Poly (vinyl alcohol)
RBCL	Red blood cell lysis
RGD	Arg-Gly-Asp peptide motif
RIPA	Radioimmunoprecipitation
RISC	RNA induced silencing complex
RNA	Ribonucleic acid
RNAi	Ribonucleic acid interference

RT	Room temperature
RT-PCR	Real time polymerase chain reaction
SDS	Sodium dodecyl sulfate
SEM	Scanning electron miscroscope
shRNA	Short hairpin RNA
siFITC	FITC labelled siRNA
siGFP	siRNA against GFP
siMstn	siRNA against Myostatin
siNegative	scramble Negative control siRNA
siRNA	Small interfering ribonucleic acid
SLE	Systematic lupus erythematosus
SNALP	Stable nucleic acid lipid particle
TA	Tibialis anterior
TBE	Tris-Borate-EDTA
TBS	Tris buffered saline
TBST	Tris buffered saline-tween
TAE	Tris base, acetic acid and EDTA
TEA	Triethylamine
TEM	Transmission electron microscope
TGF	Transforming growth factor
TTR	Transthyretin
U	Units
UTR	Untranslated region
UV	Ultra Violet
V	Volts
VEGF	Vascular endothelial growth factor
VS	Vinyl Sulfone
Wwp1	WW domain-containing E3 ubiquitin protein ligase 1

Abstract

Scaffold based delivery of RNA interference (RNAi) molecules such as free small interfering RNA (siRNA) and microRNA has recently begun to be employed towards treatment of diseases such as cancer, bone regeneration, muscular dystrophy and cardiovascular disease. Effective translation from bench side to clinical use of RNAi has been limited in part because upon systemic delivery the RNAi molecules are degraded by RNases and flushed by excretory organs causing an inefficient duration of gene silencing effect at target tissues. These challenges can potentially be minimised by delivering RNAi molecules via non-viral nanoparticle carriers encapsulated in biocompatible, biodegradable and injectable scaffolds such as hydrogels. Various scaffolds have been shown to aid in sustained localised delivery of RNAi molecules and improve gene silencing. This research focused on optimising and establishing such an RNAi hydrogel-siRNA-nanoparticle (hydrogel-nanocomplex) system for targeted and sustained gene knockdown both *in vitro* and *in vivo* using dendrimer and lipid based nanoparticles in combination with synthetic polyethylene glycol (PEG) and natural fibrin hydrogel scaffolds.

Four siRNA nanocarriers were investigated for siRNA delivery, that is, fourth generation dendrimer nanoparticles poly(amidoamine) (D) and its modified version (MD) with PEG and a lipid 1, 2-dioleoyl-sn-glycero-3-phosphoethanolamine (DOPE) molecule, commercial lipid based Lipofectamine® RNAiMax and Invivofectamine® 3.0 nanoparticles. D and MD achieved better RNase protection compared to lipid nanocomplexes though Invivofectamine® 3.0 nanocomplexes protected a small percentage of siRNA over 10 days. The MD nanoparticle displayed improved siRNA release and transfection efficacy compared to D but efficacy of the dendrimers was lower than the lipid particles.

Four hydrogels that have not been investigated for RNAi were assessed for sustainability. Namely, hydrolytically and proteolytically degradable PEG-acrylate (PEG-AC), proteolytically degradable PEG - vinyl sulfone (PEG-VS) hydrogels, unmodified fibrin and PEGylated fibrin hydrogel. The nanocomplex release rate *in vitro* from the various hydrogels showed minimal release from PEGylated hydrogels, burst release from unmodified fibrin and sustained release from PEGylated fibrin. Invivofectamine® 3.0 nanocomplexes retained efficacy optimally after release from PEGylated fibrin hence this hydrogel was utilised for downstream analysis.

For *in vivo* sustained delivery to be effective, determination of hydrogel persistence *in vivo* was required. After injection in the mouse tibialis anterior (TA) muscle PEG-AC and PEGylated fibrin gels degraded within 2 days.

The efficacy of the various nanocomplexes was assayed in a 3D assay that more closely resembled delivery in soft tissue. PEGylated fibrin containing nanocomplexes with cell death siRNA sequences was polymerised around a preformed PEGylated fibrin cell containing droplet. Invivofectamine® 3.0 nanocomplex consistently achieved the highest gene knockdown effect with no evidence of cytotoxicity whilst Lipofectamine® RNAiMax was ineffective. MD showed signs of cytotoxicity when delivered in a sustained fashion. Thus Invivofectamine® 3.0 nanocomplexes in PEGylated fibrin hydrogel were found to be the optimal gel-nanocomplex system to proceed to *in vivo* assessment.

BALB/c GFP transgenic injected in their TA muscle with Invivofectamine® 3.0 nanocomplexes made with siRNA targeting GFP or myostatin (siGFP/siMSTN) in the presence or absence of PEGylated fibrin gel were analysed 7 days post treatment for siRNA retention and GFP and Mstn gene knockdown. Increased retention of siRNA after encapsulation in PEGylated fibrin was observed at 7 days. A non-significant reduction in GFP protein was seen for limbs injected with siGFP- fibrin after 7 days. A substantial and significant reduction in Mstn mRNA levels was elicited by delivery of siMstn–fibrin. Furthermore, only siMstn-fibrin resulted in significant increase in muscle mass.

In this study, dendrimer based nanoparticles were found to effectively protect siRNA against RNases however lipid based nanocomplexes were the most efficacious at gene knockdown. The combination of Invivofectamine® 3.0 and PEGylated fibrin was shown to be the most effective in 3D assays and as an injectable controlled release scaffold into soft tissue suggesting that this approach has therapeutic potential.

1 Introduction

1.1 RNA interference

Ribonucleic acid interference (RNAi) has great potential in providing therapeutic solutions to a wide range of pathologies [4]. RNAi is a conserved post transcriptional gene regulation process carried out by double stranded non-coding small RNA molecules to regulate the expression of proteins [5]. The discovery of RNAi in C. elegans by Andrew Fire and Craig Mello in 1998 [5] allowed for a revolution of research into the elucidation of gene function. Studying gain or loss in function of genes by RNAi has enabled mapping of cellular pathways and deciphering the stages of human development [5-8]. These double stranded small RNA molecules include endogenously expressed micro RNA (miRNA), exogenously applied small interfering (siRNA) and short hairpin RNA (shRNA) [9, 10], which at their mature stage are ≈21-25 nucleotides long with their site of action being in the cytoplasm [7]. siRNA, miRNA mimics and shRNA mirror the endogenous miRNA processing and RNAi pathway in the cytoplasm, that is, they all follow a similar processing and post transcriptional gene silencing path in the cytoplasm but they are differentiated by their origin and number of mRNA targets.

1.1.1 miRNA biogenesis, exogenous RNA processing and RNAi in cells

As illustrated in **Fig.1** miRNA is transcribed from DNA by RNA polymerase II [11] into long transcripts that form pri-miRNA stem loops in the nucleus with matching and mismatching base pairs. siRNA on the other hand is introduced exogenously into the cell cytoplasm as synthetic long complementary double stranded RNA (dsRNA) which is then processed into mature short siRNA in the cytoplasm or introduced as short complementary double stranded siRNA [10]. shRNA sequences are introduced exogenously into cells by plasmid transfection or very commonly via lentiviral vector infection, the latter is particularly used in cells that are not easily transfected [10, 12, 13]. The constructs introduced by lentiviral infection are nuclear imported, with the shRNA sequence stably integrated into the cells' genome. They are transcribed into hairpins known as pre-shRNA that are nuclear exported and later processed into short siRNA or

miRNA depending on the sequence design, resulting in long term gene knockdown. When plasmids are used in cell transfection, they also need to be transported into the nucleus but do not usually integrate into the genome and the resulting gene knockdown effect is transient [10]. Pre-shRNA is transcribed from DNA by RNA polymerase II or III into two complementary sequences of ≈19-22 base pairs (bp) linked by a short loop of ≈4-11 nucleotides, similar to the endogenous pre-miRNA, and join the miRNA biogenesis and processing pathway [9, 10]. Although shRNA are potent gene silencing molecules, they are limited by the need for nuclear transportation and introduction into the host DNA and this process carries a risk of insertional gene mutations. Therefore miRNA mimics and siRNA are commonly used for RNAi [14].

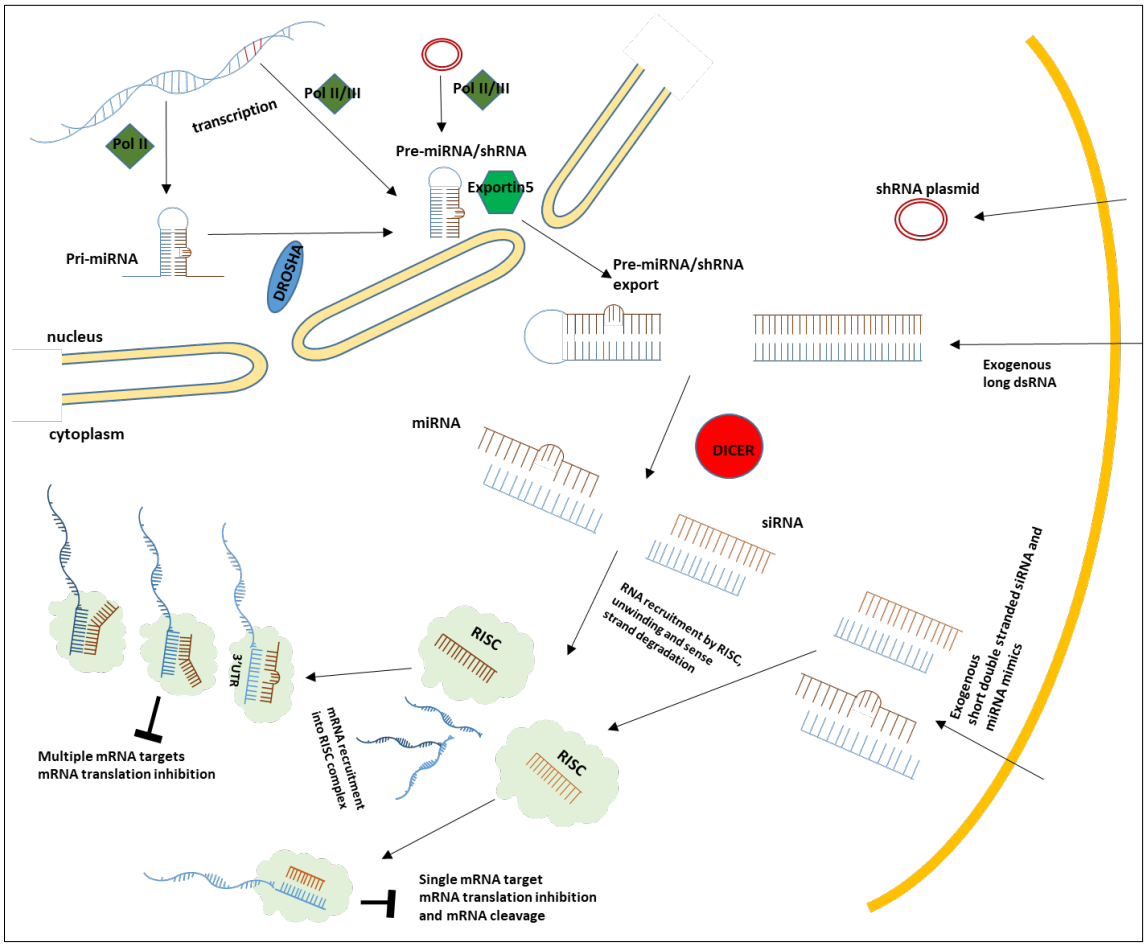

Figure 1: Schematic representation of miRNA biogenesis and exogenous RNA processing in eukaryotic cells RNAi.

In the nucleus, the long pri-miRNA loop transcripts are cleaved by the nuclear enzyme, ribonuclease III Drosha, to shorter 65-75 nucleotide pre-miRNAs. These pre-miRNAs and shRNA are exported to the cytoplasm by nuclear exportin 5 where ribonuclease III

Dicer processes the precursors, pre-miRNA and exogenously introduced long dsRNA into mature miRNA and siRNA duplexes with 2-nucleotide overhangs at the 3' end [10, 15]. The small RNAs (exogenous short siRNA and miRNA mimics, dicer processed mature miRNA and siRNA) are coupled into the RNA-induced silencing complex (RISC) where the duplex is dissociated and the sense strand is cleaved leaving the antisense strand. The RISC complex then binds to complementary mRNA and induces mRNA cleavage in the case of siRNA where the siRNA base pairs perfectly match the target mRNA. For miRNA, the RISC complex inhibits mRNA translation as miRNA has been shown in most eukaryotes to have mismatches with their target mRNA sequences typically at their three prime untranslated regions [16]. The mismatch creates a physical barrier for mRNA transcription and cleavage and allows the molecules to have multiple similar sets of mRNA targets whilst siRNA only has one specific mRNA target [17-20].

1.1.2 RNAi as a therapeutic tool

The aberrant expression and/or mutation of genes is related to the disease state or pathophysiology of many diseases and genetic disorders. These were observations realized partly by the application of the post transcriptional RNAi based tool in *in vitro* and *in vivo* screening studies to characterise gene knockdown phenotypes [21, 22]. The RNAi approach has led to the provision of novel therapeutic targets for many diseases including those previously considered undruggable [21, 23, 24]. Therefore, by knocking down disease causing and promoting genes, RNAi has great potential in bringing a new generation of biodrugs forward to treat diseases such as lung and liver diseases, inflammatory disorders, cancer, viral infections, cardiovascular diseases (CVD), Huntington disease and many other genetic disorders [9, 25-29]. There is however at present, only a relatively small range of RNAi therapeutics that target macular degeneration, cancer, liver, gastrointestinal tract, skin and infectious diseases that are in stage I-III clinical trials [9]. Furthermore, we are aware of just two United States Food and Drug administration (FDA) approved RNAi drugs that are currently on the market that is mipomersen and patisiran [9, 30, 31]. Mipomersen is used for the treatment of inherited familial homozygous hypercholesterolemia disorder [30], and patisiran is being used in the treatment of TTR-mediated amyloid polyneuropathy in adults heart [31]. This relative paucity of RNAi clinical application is in part due to the various systemic barriers encountered by miRNA or siRNA influencing its pharmacokinetics and efficacy *in vivo*.

Since exogenously introduced miRNA mimics and siRNA have similar functions, properties, and encounter similar systemic fates, siRNA is focussed on below.

1.2 Barriers to siRNA transfection and delivery *in vivo*

The progression of RNAi application in the clinic is impeded by systemic and cellular barriers encountered by naked nucleic acids when administered systemically. These barriers include immune response, clearance from the circulatory system by phagocytes and uptake by non-target tissue. They also include a short plasma half-life of less than 10 minutes due to degradation by nucleases, clearance and accumulation in excretory organs such as the kidneys, liver and spleen [32-38]. The cellular challenges faced by exogenous siRNA is a result of their unfavourable physicochemical properties, which inhibit siRNA from passively crossing the cell membrane due to their hydrophilic nature as well as their relatively large molecular weight and size [34, 39]. The phosphate backbone of siRNA results in a highly negatively charged molecule that is naturally repelled by the cellular membrane with a negative surface charge [39]. Furthermore, upon cellular uptake, RNAi molecules need to be able to escape degradation in the endo-lysosomes. These limitations have led to a growing need to find ways to deliver siRNA to the targeted tissue and aid its passage through the cell membrane to their site of action in the cytoplasm. These delivery methods should aid RNAi molecules in stealth systematic movement, transport across the cell membrane and endo-lysosomal escape in order for their implementation as a therapeutic measure in a clinical setting to be more efficacious.

1.3 siRNA delivery methods

There are a variety of emerging measures being explored to increase the efficacy of siRNA that partially evade the above mentioned barriers. Modifying the nucleic acid backbone to improve siRNA stability in systemic circulation and increase cellular transfection is one approach, another is to use nanocarrier transport vehicles such as viruses and non-viral nanoparticles. These nanoparticles, also termed nanomedicines, are defined as nanoscale drugs with various medical purposes including diagnosis, biosensing, imagery and drug delivery [40, 41]. siRNA modifications and the use of nanoparticles afford differing degrees of protection to siRNA during systemic circulation

but have both been shown to improve delivery in various diseases such as neurodegenerative disorders [42] and hepatitis B [43] for example and also target tissues such as the heart [44], tumors [27] and particularly excretory organs [26, 35, 45] where systemically injected biodrugs are highly likely to accumulate . However, each of these delivery methods comes with their limitations which will be discussed separately in the following sections [34, 46].

1.3.1 Modified siRNA

siRNA modifications include changes to the siRNA structure and addition of conjugates to the siRNA. The most commonly used modifications that have been shown to enhance serum stability by elevating RNase resistance, avoiding immune response and increasing circulation time *in vivo* include: cholesterol conjugation, addition of a partial phosphorothioate backbone and 2'- modifications on the sugar ring structures of several bases on the siRNA sense and antisense strands with methyl, methoxyethyl and fluoro groups [38, 45]. For example, cholesterol was conjugated to siRNA targeting apolipoprotein B (ApoB) and delivered intravenously in mice. After intravenous (i.v) injection of the cholesterol-ApoB-siRNA, ApoB mRNA was found to be reduced in the mice liver. ApoB protein levels in the serum as well as total cholesterol were also reduced when compared to cholesterol-siNegative control. In addition, cholesterol-siRNA was found to have improved pharmacokinetics, circulatory retention, accumulation in the liver and jejunum relative to the same negative control [45]. Some of these siRNA modifications are a central aspect to the FDA approved RNAi drug currently on the market, mipomersen [47]. The drug is a modified siRNA (modRNA) sequence that again targets apolipoprotein B-100 (ApoB) mRNA, to reduce ApoB protein production and thus result in low density lipoprotein (LDL) and total cholesterol levels [48]. The antisense oligonucleotide is modified on its 5' and 3' ends with 2' methoxyethyl groups, as well as a modified phosphorothioate backbone to increase nuclease resistance and reduce protein binding and the inflammatory response [30, 48, 49].

Although modifications to the siRNA can be introduced to improve serum stability and allow them to be systemically injected or directly injected at the site of action such as tumors, muscle and myocardial infarction (MI) site, their efficacy is still limited due to off target effects; clearance by the circulatory system; macrophages and excretory organs [34, 39, 50]. In addition, high dosages are needed to reach therapeutic effect, and there

is a reduced gene silencing effect because the RNAi system can only tolerate moderate changes to the RNA structure [51, 52].

1.3.2 Viral nanoparticles

Viral vectors that are being explored in gene therapy as potential therapeutics are recombinant viruses that are devoid of viral integrase and replication proteins. They include retroviruses, lentiviruses (LV), adenoviruses and adeno-associated viruses (AAV) [53-55]. Retroviruses can only infect mitotic cells and they were amongst the first to be developed and used *in vitro* and *in vivo* [56-59], but in recent years research *in vitro* and in clinics has shifted more towards exploring the use of LV and AAV because of their ability to infect both non-dividing and dividing cells hence offering a wider range of target tissues [54, 60, 61]. Viral nanoparticles have the natural ability to infect cells and deliver genetic material with high efficiency and the potential to cause long term gene knockdown effect, a trait desirable in some applications but not others [62, 63]. However they are associated with: immunogenicity, inflammation, pose a risk of insertional gene mutagenicity and the possibility of recombination events during the viral vector manufacturing process that may result in replication-competent viruses [64-69]. There are studies in clinical trials using viral vectors in gene therapy for several genetic disorders and cancer in phases I/II [70]. However regulatory agencies require rigorous testing for replication-competent particles in the viral products before use in trials and patients have longer follow up post treatment to fully establish the safety of the vectors [70]. Despite the advances that have been made in the field to improve viral vector biosafety and application in the clinic, the risk factors mentioned above hinder their clinical translation progress and approval [70]. Therefore non-viral nanoparticles with their more desirable safety profile are considered more immediate candidates for clinical translation [71].

1.3.3 Non-viral nanoparticles

Non-viral nanoparticles come with a range of physicochemical properties which encompass size, charge and material composition and these properties strongly influence a nanoparticles' biocompatibility and clinical application [40, 41]. Particles in the 10-100 nm size range are most widely used and have been shown to have optimal pharmacokinetic properties and improved circulation time *in vivo*. Outside of RNAi, they

have also been shown to have a range of other clinical application such as diagnostics, imaging and drug delivery in many diseases including cancer, CVD and MI [40, 72-74]. All nanoparticles are susceptible to clearance by macrophages as well as biodistribution and clearance by the liver and spleen [75-80], however smaller nanoparticles (<10nm) are especially prone to clearance from the bloodstream by kidneys and larger nanoparticles (>100nm) are more susceptible to opsonisation and phagocytosis [73, 81, 82].

The surface charge of nanoparticles can affect cell membrane interaction differently which results in differing cellular uptake process and toxicity depending on the cell type with which it comes into contact with. Therefore this ultimately affects the nanoparticle's systemic biodistribution, intracellular localisation as well as efficacy [83]. A study of nanoparticles with a range of charges showed that zwitterionic nanoparticles entered human epithelial cells (HeLa) cells by passive membrane fusion whilst anionic and cationic particles crossed their membranes through multiple endocytotic pathways [84]. Charge difference not only affects nanoparticles' intracellular entry pathway and localisation, it also affects their escape ability from the endolysosomal system, thus determining their delivery efficiency [85, 86]. Cationic particles were shown to have a high rate of cellular entry and endosomal escape compared to neutral or anionic particles [86]. Nanoparticles with either a high positive or negative surface charge are more likely to be phagocytosed by endocytotic cells, whilst non-phagocytic cells prefer internalising particles that are positively charged in comparison to highly negative or neutral nanoparticles [87-89]. For example, a study with ovarian cancer cells showed an increase in nanoparticle uptake with a decrease in negative zeta potential ranging from -40mV to -14mV [90]. Inversely another study showed that cationic nanoparticles with an increasing number of amino groups (positive charge) were increasingly taken up by HeLa and human bone marrow derived mesenchymal stem cells (MSC) cells compared to their neutral counterparts [91]. However, although increasing positive charge improves cellular entry, an increase in cytotoxicity of such particles has been reported [92, 93]. Since the cell membrane surface charge is negatively charged, nanoparticles with a high positive charge become more cytotoxic because they can alter the membrane zeta potential and disrupt the plasma membrane [83, 94]. The different uptake preferences of phagocytic and non-phagocytic cells for nanoparticles with varying degrees of charge may influence the selectivity of nanoparticles for drug delivery, their efficacy as well as their fate in distribution. Thus, the effects of these fundamental nanoparticle physiochemical properties of size and charge can serve as a guide towards the design of optimal nanoparticle vectors for drug delivery.

A wide range of materials have been used in the production of nanoparticles as a nanocarrier for RNA molecules for RNAi via complexation, also referred to as nanocomplexes. These materials include organic polymeric, lipid, protein and crystalline based nanoparticles as well as inorganic metallic based nanoparticles [95-98]. Examples of some of the different types of nanoparticles being studied for siRNA delivery *in vivo* are shown in **Table 1** [41, 97-100]. Polymeric and lipid nanoparticles will be discussed further in sections to follow.

Table 1: Selected examples of non-viral nanoparticles used for RNA delivery in vivo.

Material	Nanoparticle (NP)	Condition	Target	Observations	Ref
Organic					
Lipid	Nanoemulsions	Lung cancer	HDM2, c-myc, VEGF	Cell proliferation, angiogenesis and tumor growth suppression in nude mice xenografts.	[101]
Cationic Polymer	Polyethylenimine (PEI)	Parkinson's disease	α-synuden	Reduced α-synuden mRNA and protein expression in mice striatum with no signs of toxicity.	[102]
	Poly(lactic-co-glycolic acid) (PLGA)	Cancer tumors	PLK1	Reduced target mRNA in tumour biopsies and reduced tumor growth of cancer xenografts in the nude mice.	[103]
	Cyclodextrin	Melanoma	RRM2	Accumulation of nanocomplexes, reduced target mRNA and protein in melanoma human patient biopsies and reduced tumor growth.	[104]
	Chitosan	Kidney disease	COX-2	COX-2 immunoreactivity in macrophages reduced in mouse kidneys.	[105]
	Polymeric micelle	Cancer tumors	VEGF, VEGFR2	Inhibited subcutaneous HeLa cell-tumor growth in mice.	[106]
Protein/ peptide	Cell penetrating peptide (CPP)	Pharmaco-kinetics		siRNA-Cy5 improved pharmacokinetic profile, reduced kidney, liver accumulation of siRNA intra-cardially injected in mice.	[107]
	Poly-L-Lysine (PLL)	Cancer tumors	VEGF	Tumor growth inhibition in mice.	[108]
Inorganic & Metallic					
	Gold (AuNP)	Cervical cancer	NF-ĸB p65	Targeted gene knockdown in mice xenografts.	[109]

	Iron oxide (IONP)	Pancreatic ductal adenocarcinoma	Polo-like kinase-1	Superparamagnetic iron oxide (SPIONS) nanocomplexes knocked down Polo-like kinase-1 in tumour bearing mice.	[110]
	Graphene oxide	MI	VEGF-165	Graphene oxide nanocomplexes in hydrogel injected in peri-infarct zone reduced VEGF-165 gene in rat MI.	[111]
	Quantum dots (Q-dots)	Cancer tumors	EGFR	EGFR knockdown and reduced mice tumor xenografts.	[112]
	Nanodiamond	Cancer tumors	survivin	Knockdown of survivin in mice with tumor xenografts and tumor reduction	[113]

Nanocomplex=nucleic acidmolecules complexed to nanoparticle, HDM2= Human doubleminute 2 protein, VEGF=Vascular endothelial growth factor, VEGFR2=VEGF receptor 2, PLK1=Serine/threonine-protein kinase, RRM2=Ribonucleotide reductase family member 2, COX2=Cyclooxygenase-II enzyme, EGFR=estimated glomerular filtration rate, Cy5=Near-infrared.

The reasoning for focusing on lipid and polymeric based nanoparticles is derived from a comprehensive review by Bobo et al. 2016 that found that from 1995-2015, 51 nanomedicines (not restricted to RNAi) have been FDA approved and 77 products with the same definition were in various phases of clinical trials [41]. The list of non-viral nanomaterials being applied in the clinic is dominated by lipid and polymeric nanoparticles, which in combination make up over 60% of approved nanomaterials as well as 40% nanomaterials in various stages of clinical trials, over the protein, metallic, nanocrystals and other materials [41]. The most frequently used non-viral nanomedicines for clinical use are lipid and polymeric based nanoparticles with the main target disease being cancer therapy [72, 98, 100].

Focusing on materials being used for RNAi, the FDA clinical trial database (www.clinicaltrials.gov) was queried using key search terms siRNA and RNAi. The search results yielded an output of 41 RNAi based studies in various stages of clinical trials. Interventions using naked siRNA with or without conjugations or modifications made up 65% of the studies whilst siRNA complexed to or in lipid, polymer, viral and exosome based nanoparticles made up 20%, 10%, 2.5% and 2.5% respectively. Polymeric and lipid based nanoparticles are the most widely used for siRNA delivery because of their relatively simple design and ready interaction with siRNA, feasibility for mass production, ability to interact favourably with cell membranes and high efficiency, therefore these types of nanoparticles will be discussed further [9].

1.3.3.1 *Polymeric nanoparticles*

Polymeric nanoparticles (PNPs) have been made from a number of different synthetic and natural polymers. Some of the synthetic polymeric based PNPs being extensively investigated for the delivery of different therapeutic drugs including plasmid DNA (pDNA) and siRNA are poly (D,L-lactide-co-glycolide) (PLGA) [114] , polylactic acid (PLA) [115], cyclodextrin [116], PEI and dendrimeric polyamidoamine (PAMAM) [95]. Some of the natural polymers being used for siRNA include gelatin [117] and chitosan [95, 118, 119]. PNPs can be further grouped as anionic, neutral or cationic dependent on their net polymeric surface charge [120]. Those used for siRNA delivery, however, are necessarily cationic nanoparticles because they allow for electrostatic interaction with oligonucleotide molecules [121]. Additionally, biodegradable nanoparticles are mostly used because they can be hydrolysed in the body into metabolisable biocompatible nontoxic monomers which can be excreted without affecting normal cellular function [122]. Hence biodegradable cationic polymeric nanoparticles have shown the most success in RNAi therapeutic development and biomaterial application [122-125].

Cationic PNPs are a class of nanoparticles which function by condensing the negatively charged nucleic acids to the positively charged functional groups on the polymers, which are usually primary amines, via non-covalent electrostatic forces [124]. This condensation provides siRNA with protection from RNases, promotes cellular uptake via endocytosis, and improves the delivery of siRNA to the cytoplasm through endosomal and lysosomal escape via the proton sponge effect. This effect is attributed to the polymers strong buffering capacity in the pH range from 5 to 7 due to the presence of the amine groups, which prevents lysosome acidification, promotes H+ proton influx, enhanced chorine ion accumulation followed by osmotic swelling and rupture of the endosome/lysosome releasing the imported siRNA [126-128].

Biodegradable polymers tend to be more soluble and stable in circulation and have reduced immunogenicity, inflammatory and thrombogenic effects [122, 123, 129]. However, when delivered systemically without modifications, these nanoparticles encounter barriers and fate similar to that of naked siRNA. When *in vivo*, nanoparticles may absorb proteins onto their surfaces making them targets for immune response and phagocytosis [130, 131]. Intermolecular interactions between the chemical groups on the surface of PNPs may result in agglomeration with an increase in particle size and surface charge resulting in reduced transfection efficiency and an increased systemic clearance [76, 132, 133]. Large molecules are selected against crossing the endothelium of

capillaries and the extracellular matrix (ECM), a network of fibrous proteins and polysaccharides that presents a physical barrier creating further resistance to the movement of nanoparticles into cells [39, 134]. Further to this, the majority of the nanoparticles or siRNA with weaker buffering capacity that makes it into the cell via endocytosis inadequately escape endosomal entrapment and are either secreted back into the ECM or targeted for lysosomal degradation [135, 136]. These mechanisms, of course, can reduce the efficiency of siRNA.

To avoid these challenges, one approach that is extensively researched is to modify the cationic PNP nanoparticles' surfaces coating through covalently attaching targeting ligands, oligopeptides, lipids and non-ionic surfactant copolymers such as polyethylene glycol (PEG) to the polymeric components of the nanoparticles [95, 137-142]. Modifying PNP surfaces reduces the potential for agglomeration and protein absorption to their surfaces and improves stealth circulation in the system (avoiding eliciting an innate immune response), cell penetration as well as endosomal escape and siRNA release into the cytoplasm [33, 137-139, 143]. Some of the commonly used cationic PNPs being applied *in vivo* for siRNA delivery are shown in **Table 1**. Dendrimer examples are not included in the table as they will be discussed later.

A wide variety of PEI, chitosan, PLGA, cylodextrin and dendrimers PNPs with various formulations, structures, and surface modifications to improve biocompatibility and efficacy in gene silencing have been extensively investigated *in vitro*, but their biocompatibility and efficacy *in vivo* has not been adequately demonstrated [144, 145]. PEI, chitosan and PLGA have proven gene delivery efficiency both *in vitro* and in animal models, however, undesirable cytotoxicity associated with PEI (though it is highly efficacious), low solubility under physiological conditions and poor efficacy associated with chitosan and PLGA nanoparticles remain the most challenging aspects for their use as therapeutics in the clinic [103, 146-148]. According to the clinical trials database, unlike PEI and cyclodextrin, chitosan and PLGA have not been investigated for oligonucleotide delivery in humans though they are FDA approved polymers.

PEI is a commercially available cationic PNP, commonly used as a gold standard polymeric RNAi molecule delivery system and has been used in multiple *in vitro* and *in vivo* studies [126, 149]. PEI is made of repeating units of an amine and two aliphatic carbons and is available in various sizes and charge [150]. Although highly efficacious, high levels of cytotoxicity have been reported limiting its clinical progression as a delivery vehicle. Various efforts have been made to render the nanoparticle less cytotoxic and applicable *in vivo* by adding modifications to the polymer [149, 151]. Two ongoing clinical

trials in phase I and II involving *in vivo*-jetPEI® and pDNA gene therapy of pancreatic cancer have been reported however none have been reported for siRNA delivery [152, 153]. Cyclodextrin, a cyclic (α-1,4)-linked oligosaccharide consisting of a hydrophobic core and a hydrophilic outer surface [121], has been investigated *in vivo* [154-156]. They have also made it to clinical trials for cancer therapy applications but their efficacy is yet to be proven for clinical application [104, 157]. Dendrimers are emerging as PNPs of interest for siRNA delivery. At the right size and charge (to be discussed further below) they are less cytotoxic and can be easily synthesised to exact specifications and geometry making their mass production feasible. The presence of multiple reactive surface groups permits for multiple surface modifications allowing for substantial space for improving efficacy, and because they have been successfully formulated for other FDA approved therapeutic treatments, which will also be addressed further below, they are a good potential candidate for clinical application in RNAi [158].

1.3.3.1.1 Dendrimers

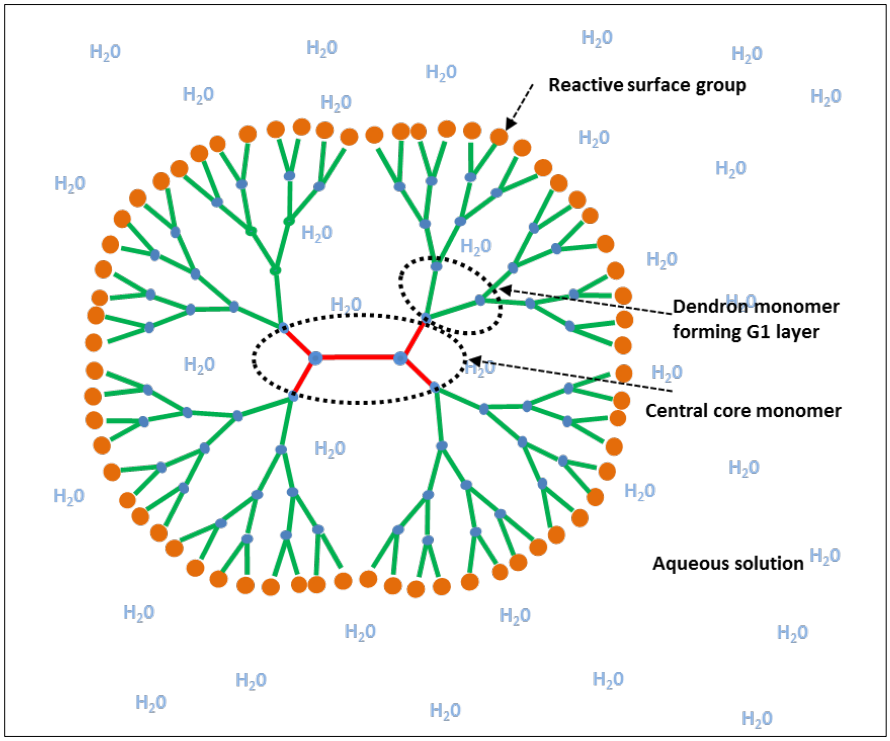

Figure 2: Schematic illustration of generation 4 (G4) dendrimer nanoparticle.

Dendrimers (illustrated in **Fig.2**) are well-defined, multivalent, symmetrically spherical molecules of uniform size with a distinct molecular architecture made up of three layers: (i) a central core monomer, consisting of an atom with at least two identical functional groups (ii) dendrons, which are monomers added to the core molecule forming branched layers (generations, G) and (iii) a charged surface composed of reactive surface groups, usually primary amines. One of the characteristics that make dendrimers a potential candidates for gene therapy application is that it follows a branched dendritic structure, a common architectural structure seen in many biological systems including the naturally occurring nanometric compounds such as glycogen and proteoglycans found in the body [95, 159]. This pattern or architecture offers distinct functional and performance benefits, that is, the hyperbranched nature of the nanoparticle provides flexibility of the particle and creates a high surface area to volume ratio which allows for compact siRNA condensation [144, 159]. There are various types of dendrimers used for siRNA delivery such as poly(prolene imine) [160], triazine [161], carbosilane [162], poly(L-lysine) [163], polyglycerol-based [164] and nanocarbon-containing dendrimers [165], however, emphasis will be placed on PAMAM dendrimers as they are the species of dendrimers most widely studied for RNAi delivery and they are the least complex to manufacture [158].

The biocompatibility, size and charge of dendrimers are determined by their surface groups and generation levels which range from 1-10 [95, 166]. High generation PAMAMs G5-G8 which are large in size and have high cationic charges become more cytotoxic with or without siRNA complexation, therefore lower generations are mostly investigated for siRNA delivery [158, 167, 168]. The known number of multiple reactive groups on the surface of PAMAM dendrimers allows for the precise attachment of various therapeutic compounds, cell targeting ligands and surface modifications such as PEGylation, lipid molecules, amino acids and oligopeptides [169-172]. These modifications can improve dendrimers' biological activities which include efficient siRNA binding and delivery, improved gene silencing effect, reducing cytotoxicity and improving RNase protection [140, 170, 173].

A 4th generation PAMAM dendrimer [G(4)-D, also referred to as D], with an ethylenediamine core was conjugated with PEG_{2K} and lipid molecule 1, 2-dioleoyl-sn-glycero-3-phosphoethanolamine (DOPE), to form a non-cytotoxic lipid triblock amphiphilic copolymer molecule [G(4)-D-PEG_{2k}-DOPE, also referred to as MD] [140]. The PEG molecule was added to D to improve dendrimer flexibility and siRNA condensation [174, 175], whilst the DOPE modification was added to improve transfection [176]. Their *in vitro* experiments showed that both D and MD nanoparticles

were noncytotoxic. MD displayed improved siRNA delivery into cells and green fluorescent protein (GFP) knockdown compared to the unmodified D. In another study various amphiphilic PAMAM dendrons of generation 1, 2 and 3 with a long hydrophobic alkyl chain (varying in length) and generation 3 [G(3)] only dendron without the alkyl chain were formulated [177]. *In vitro* gene knockdown tests with these nanoparticles showed maximal effect was achieved with the alkylated G3 dendron with the longest alkyl chain optimal compared to the other alkylated and unmodified dendrons. They went on to use the effective nanoparticle only in *in vivo* RNAi experiments. Gene silencing experiments were carried out over a week period on nude mice bearing prostate Cancer-3 xenograft tumors. The mice received intratumoral injections twice a week (3mg/kg siRNA) and the alkyl chain modified dendrimer induced ≈50% knockdown of both the oncogene Hsp27 mRNA and protein levels compared to scrambled siRNA nanocomplex control. Additionally, they showed inhibition of tumor proliferation following Hsp27-nanocomplex treatment compared to scrambled siRNA-nanocomplex treatments.

Another interesting *in vivo* study involved modifying a cystamine core G4-PAMAM dendrimer by adding PEG as a crosslinker between the dendrimer and an oligo-arginine cell penetrating peptide. In an MI model, the dendrimer nanoparticle was complexed to siRNA against Angiotensin II type 1 receptor (siAT1R) and showed that both *in vitro* (neonatal cardiomyocytes) and *in vivo* ATR1 mRNA was knocked down. Adult rats had their left descending coronary artery occluded for 30mins and immediately after reperfusion, the peptide modified dendriplex carrying angiotensin II type 1 receptor (AT1R) siRNA was injected in 3 regions of the infarct border zone. 3 days post treatment they observed improved cardiac function, reduced infarct size, and reduced AT1R expression in the rats treated with the dendriplex compared to saline and dendrimer only treated controls [178].

Though few, there are dendrimer based nanomedicines in clinical trials for various non-RNAi based therapies including the clinically approved vaginal microbicide Vivagel® (SPL7013, or astodrimer sodium). It is a lysine-based dendrimer with naphthalene disulfonic acid surface groups in a sodium solution with antiviral and antibacterial properties [72, 97]. This shows that dendrimer PNPs are increasingly gaining momentum as a potential therapeutic nanoparticle. The ability to generate many formulations and modifications to improve their RNAi efficacy further places dendrimers as good candidates for RNAi vehicles.

1.3.3.2 *Lipid based nanoparticles*

The two forms of lipid based nanoparticles with the highest frequency of clinical investigation and FDA approval are micelles and liposomes. Estrasorb™ is an example of a currently clinically approved micelle nanomedicine being applied in hormone replacement therapy [41]. Some of the 10 FDA approved liposomal nanomedicines reported in clinics that have been shown to increase drug delivery to the tumor site with reduced systemic toxicity side effect include Doxil® (liposomal doxorubicin) which is used in therapy of various cancers such as: metastatic breast cancer, multiple myeloma, ovarian cancer and Karposi's sarcoma and the recent Onivyde® (liposomal irinotecan) for pancreatic cancer therapy [41, 179].

Micelles and liposomes come in various forms depending on the phospholipids, helper lipid types, conjugates attached to the lipid molecules as well as the overall surface charge of the nanoparticle when it is completely assembled [180-182]. It is clear from their frequency of use and success rate in the clinic that lipid nanoparticles are effective at drug delivery *in vivo*. They have great potential for use in siRNA delivery due to their high cell transfection efficiency resulting from their direct interaction with the cell membrane which is mainly composed of phospholipid molecules [183].

1.3.3.2.1 Micelles

Micelles are made from long hydrocarbon fatty acid molecules with a polar head that self-assemble to form monolayer spherical structures with a hydrophobic core or hydrophilic core in the case of an inverted micelle (**Fig.3**) [184]. Micelles can be synthetically made to form polymeric micelle structures composed of complex amphiphilic block polymers consisting of a hydrophilic polymeric block and a hydrophobic polymeric block that self-aggregate to form polymeric micelles [106, 140, 182, 184, 185]. Micelle systems made by these complex structures allow for easy incorporation or attachment of oligonucleotides to the molecules. Micelles are mainly used in encapsulation and delivery of hydrophobic and poorly soluble drugs and the block polymers are designed to allow for more efficient anionic nucleic acid interaction and encapsulation [41, 98, 140].

In cancer therapy, micellar drug nanoparticle systems are being explored for simultaneous drug delivery of chemotherapeutic drugs and siRNA to combat drug

resistance in tumors [140, 182, 184, 186-189]. In an elegant study, a polymeric degradable poly(ethylene oxide)-block-poly(caprolactone) (PEO-b-PCL) micellar nanoparticle functionalised on both the PCL and PEO was developed [189]. The PCL block was functionalised to bind to either siRNA against multidrug resistant gene 1 (mdr1-siRNA) which inhibits the expression of drug transporter protein P-glycoprotein (P-gp), or conjugate doxorubicin (Dox). The PEO surface side was also functionalised to bind either cancer targeting ligand RGD4C peptide (ACDCRGDCFCG) or cell penetrating TAT peptide (GRKKRRQRRRPQ). When injected intravenously into murine models with drug resistant MDR-MDA-MD-435 human tumor xenografts that express high levels of P-gp, the multifunctional polymeric micellar system was capable of co-delivering mdr1-siRNA and Dox to target cells. They also showed improved Dox efficacy in animals that received the micelle-mdr1-siRNA system compared to non-micelle, micelle-Dox or micelle-scrambled siRNA controls, indicating inhibition of P-gp-mediated Dox resistance.

In other studies, polymeric micelle nanoparticles have been used for the delivery of various oligonucleotides for cancer therapy [106, 186]. A self-assembling block copolymer containing poly(ethylene glycol)-hydrophilic block-poly(l-lysine) (PEG-b-PLL), with lysine amines modified with 2-iminothiolane that allowed for siRNA binding on the PLL end. The PEG terminus was modified with a cell-surface binding peptide cyclo-Arg-Gly-Asp (cRGD) peptide which specifically binds integrin receptors displayed on the cell surface of tumors as well as endothelial cells associated with growing tumors [106]. When injected intravenously in mice these modified micelles resulted in improved blood circulation time and accumulation in tumors 24hrs compared to naked siRNA or micelles without the targeting cRGD peptide. In the study, siVEGF was in-cooperated into the polymeric micelles and used to knockdown VEGF in mice with subcutaneous HeLa-luc tumors. The modified micelle nanocomplexes showed the highest gene knockdown and tumor size reduction 12 days post treatment compared to micelles complexed with scramble siRNA negative control. Due to the hydrophobic interior of micelles, there is no convenient method for sequestering the hydrophilic oligonucleotides making these nanoparticles less attractive for RNAi and gene delivery than liposomes [184].

1.3.3.2.2 Liposomes

A liposome in its simplest form (**Fig.3**) is composed of amphiphilic phospholipid molecules such as phosphatidylserine (PS), phosphatidylcholine (PC),

phosphatidylethanolamine (PE) and phosphatidylglycerol that self-aggregate to form a lipid bilayer with a hydrophilic core and a surface charge [98]. Lipid nanoparticles have high transfection potential because they fuse easily with the cell membrane, which consists mainly of cholesterol, PC, PS and PE phospholipids; rendering them inherently efficient at cell penetration and escaping endosomes to release their drug payload into the cytoplasm [190, 191]. They are the most easily synthesised nanoparticle that has the ability to incorporate both hydrophilic drugs (in its aqueous core) and hydrophobic drugs (in the lipid bilayer) and hence are increasingly the most commonly investigated in the clinic and were the first nanoparticle approved in FDA clinical trials [41, 98, 192]. The further modification of approved liposome based drugs by changing their chemical groups, stabilising helper lipid molecules and adding surface modifications to enable the delivery of various drugs, improve their therapeutic efficacy in various disease targets, reduce their toxicity and introduce stimuli responsiveness (e.g pH and temperature) [41, 98] is under intensive investigation. In addition to liposomes being the most commonly used nanocarriers in clinics they are the basis of the commercially available transfection reagents such as Lipofectamine® RNAiMAX and Invivofectamine® 3.0, which were developed for the transport of siRNA. A wide range of liposomes can be constructed by using different combinations and proportions of phospholipids, aliphatic chain, conjugates (PEG, cell targeting ligands, antibodies) and helper lipids (such as neutral fusogenic lipids DOPE, DOPC, DSPC , PEG-lipids and cholesterol) in their assembly [47, 98, 180, 193]. Described below are the liposome groups under investigation for siRNA based on charge [2].

1.3.3.2.2.1 Cationic Liposomes

Cationic liposomes are widely used for siRNA delivery and are advantageous over anionic liposomes because they can interact with the negatively charged cell surface allowing for cell penetration and cargo delivery whereas anionic liposomes are repelled by the membrane [180, 193]. Cationic liposomes are made from cationic lipids such as 1,2-dioleoyl-3-trimethylammoniumpropane (DOTAP) and 2-dioleyloxy-N,N-dimethyl-3-aminopropane (DODMA) in combination with neutral helper lipids [2]. The right balance in ratio of these different types of lipids that make up the liposome however needs to be achieved in order to produce nanocomplexes with the right charge tolerable to cells in order to prevent eliciting an immune response and cytotoxic effects linked to production

of reactive oxygen species and induction of high calcium levels in cells, a common feature associated with liposomes with a high cationic charge [194-196].

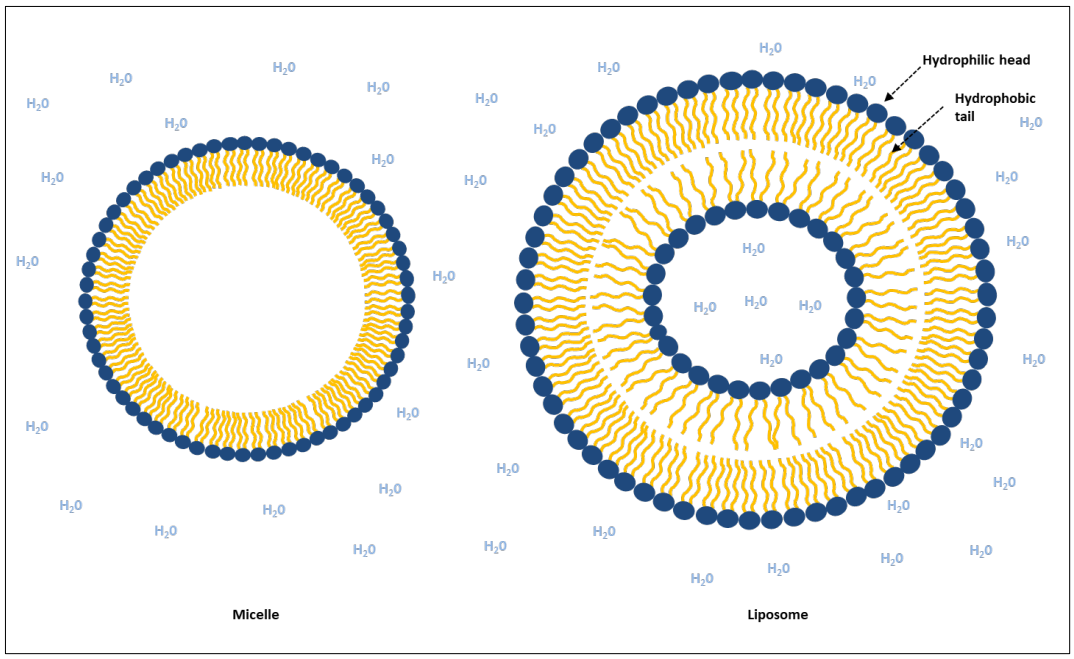

Figure 3: Schematic illustrations of micelle and liposome nanoparticles.

For example, a study with four liposomal formulations, composed of DOTAP and Cholesterol (Chol)-derivative cationic lipids in combination with different ratios of the neutral DOPE and cholesterol helper lipids, were made to produce cationic liposomes that had similar +ve surface charges (≈ 50mV) [197]. When the nanoparticles were complexed to siRNA at nanoparticle nitrogen (N) to siRNA phosphate (P) molar ratios (N/P) ratio of 2.5, 5 and 10, all nanoparticles had similar rates of transfection and gene knockdown effect, but the groups of nanoparticles with less helper lipid (DOPE and cholesterol) ratios were more cytotoxic compared to the DOTAP/Chol/DOPE liposome with the highest helper lipid ratio. Cell cytotoxicity was also shown to be influenced by siRNA concentration (40nM and 100nM) and the N/P ratio of (2.5, 5 and 10). All four cationic liposome formulations at any N/P ratio were cytotoxic when 100nM siRNA was complexed to the nanoparticle, whilst at lower 40nM siRNA concentration, only the nanocomplexes at higher N/P of 10 and consequently a high cationic charge were more cytotoxic compared to lower N/P ratios 2.5 and 10 with lower cationic charge [197].

This *in vitro* study demonstrated the effects of cationic liposomes' physicochemical properties, lipid composition, cationic liposome and siRNA concentration on cell

cytotoxicity. In this case, a lower concentration of siRNA and liposome had to be used in order to achieve non-cytotoxic gene knockdown effect. Cationic liposomes incorporate negatively charged siRNA via electrostatic interactions easily and they demonstrate great potential candidate nanoparticles for *in vivo* gene knockdown. However because of the potential immune trigger and cytotoxic effect they are likely to induce, special consideration of the nanocomplexes overall charge and siRNA concentrations to be used is required to ensure optimal efficacy.

The cationic lipids in liposomes effectively condense nucleic acid with the negatively charged siRNA molecules via electrostatic interaction to form multiple structural conformational possibilities (**Fig.4**) such as lipoplexes, lipopolyplexes, membrane/core nanoparticles (MCNP) and stable nucleic acid lipid particles (SNLPs) [2]. Lipoplexes are formed when the lipids form multiple bilayers and the siRNA is embedded within the adjacent lipid bilayers [2]. Lipopolyplexes are single bilayer liposomes containing polyplexes (a cationic-polymer / siRNA complexation) [2]. MCNP are made of a single bilayer as a shell encasing an inorganic core loaded with siRNA molecules [198].

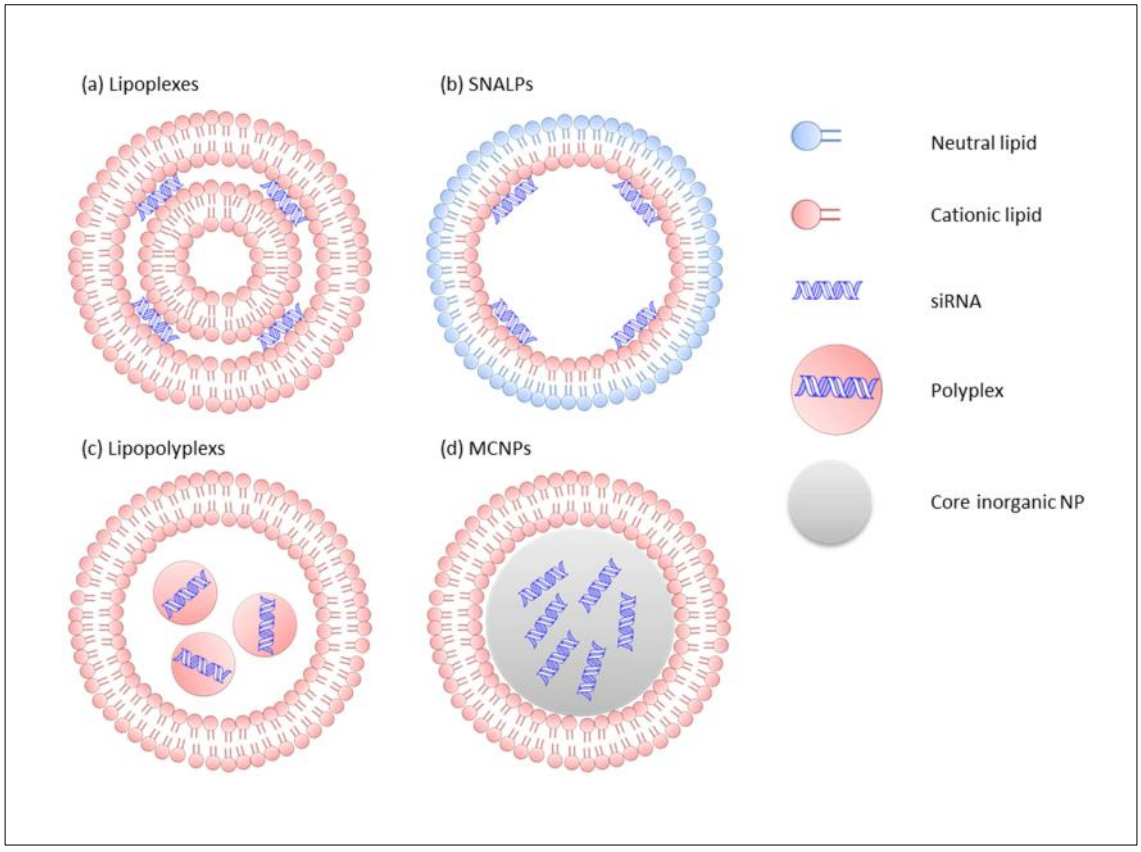

Figure 4: Possible structural conformations made from complexing siRNA to cationic liposomes. *Figure reprinted from Xia et al. 2013 [2], with permission from Elsevier.*

SNALPs are also single bilayered membranes with a neutral surface charge and their siRNA is encapsulated in the interior of the liposome interacting with the inner wall of the bilayer which is positively charged. This is made possible because the liposomes are composed of titrable pH-sensitive lipids, that is, cationic at pH=4 and neutral at pH 7.4 [2, 199]. SNALPs include PEGylated lipids in their composition for enhanced nanocomplex stability and evading mononuclear phagocyte system [43, 200]. There are a number of examples of efficient siRNA delivery *in vivo* by SNALPs that have been reported [43, 201-203]. The initial SNALP formulation for RNAi in hepatitis B virus (HBV) therapy was developed by Morrissey et al 2005 [204]. In a mouse HBV model, the SNALP achieved siRNA delivery which resulted in persistent HBV inhibition, in a dose dependent manner [43]. Since then SNALPs have emerged as one of the leading liposome formulations under clinical development and are in different stages of clinical trials for diseases such as hypercholesterolemia, hereditary transthyretin (TTR)-mediated amyloidosis and various cancers [200]. Patisiran is an example of SNALP liposome produced by Alnylam® Pharmaceuticals that was recently approved by the FDA. Patisiran (ALN-TTR02) is an RNAi SNALP, the first and only approved RNAi nanoparticle being applied in the clinic for the treatment TTR-mediated amyloid polyneuropathy in adults. TTR-mediated amyloidosis is a slowly progressive disease caused by TTR gene mutations and the deposition of hepatocyte-derived TTR amyloids in the peripheral nerves and heart [31, 205]. The cationic liposomal SNALP complexes are introduced intravenously into patients and contain siRNA molecules against TTR mRNA. This RNAi drug reduces hepatic synthesis of TTR protein in patients and therefore improves multiple polyneuropathy and cardiomyopathy clinical manifestations of TTR amyloidosis [31, 206].

In another study, a group again in association with Alnylam® developed a SNALP-ApoB siRNA formulation that was used to reduce LDL cholesterol levels for hypercholesterolemia therapy in non-human primate animal models [203]. The SNALP was composed of the lipids [methoxypoly (ethylene glycol)$_{2000}$)carbamoyl]-1,2-dimyristyloxy-propylamine (PEG-C-DMA), cationic lipid 1,2-dilinoleyloxy-N,N-dimethyl-3-aminopropane (DLinDMA), and helper lipids 1,2-distearoyl-sn-glycero-3-phosphocholine and cholesterol, in a 2:40:10:48 molar ratio. A single systemic injection of the SNALP-siApoB formulation resulted in ApoB gene silencing (in a dose dependent manner) in the liver of cynomolgus monkeys, 48hrs after administration, with maximal silencing of over 90%.

In later studies they developed more lipid nanoparticles termed lipidoids, similar to their initial SNALP described above but with one less helper lipid [207, 208]. A lipidoid library

of 1200 structurally diverse lipidoids was synthesised and used to formulate lipidoid particles that could be either complexed with siRNA or miRNA. Using a luciferase screening assay in HeLa cells, they selected lipidoids that resulted in high levels of gene silencing *in vitro* after cells were treated with firefly luciferase targeting siRNA-lipidoid complexes [207]. Seventeen lipidoid formulations composed of various types of amine-alkyl-acrylate/acrylamide lipidoid conjugates, cholesterol and $mPEG_{2000}$-DMG (Alnylam® product) in a 42:10:48 molar ratio, was selected from *in vitro* assays for further *in vivo* screening. The lipidoid formulations were complexed to serum Factor VII siRNA (siFVII) and systemically introduced into mice to target serum FVII protein. Seven lipidoids were identified to achieve significant reduction of FVII with the largest reduction being caused by the $98N_{12}$-5 (5-tailed) lipidoid. The $98N_{12}$-5 lipidoid was complexed with various siRNAs and miRNAs to test for efficacy in various animal and disease models when locally or systemically delivered. For example, siFVII and siApoB were intravenously injected into rats and resulted in significant gene knockdown of the respective gene targets in the liver compared to lipidoids formulated with siControl. The lipidoid was also complexed to anti-miR122 (which targets miR122 and results in target gene upregulation) and was systemically delivered which resulted in repressed miR122 (compared to mismatched anti-miR122 control) in the liver. In non-human primates cynomolgus monkeys were given i.v injection of lipidoid-siApoB formulation and monitored up to 30 days post treatment. Serum ApoB reduction was observed (compared to animals treated with lipidoid-siControl) in a dose dependent manner with the lowest levels achieved rapidly by day 3, >50% silencing still maintained at 2 weeks and full recovery of expression achieved 1 month later. Silencing duration extended their previous reports for systemic RNAi in nonhuman primates where the study terminated at 11 days [203]. In a separate study, they used the same $98N_{12}$-5 lipidoid particle to complex siRNA against proprotein convertase subtilisin/kexin type 9 (PCSK9) for hypercholesterolemia using rat and mice models [208]. PCSK9 protein regulates LDL receptor (LDLR) protein levels. Reduction of PCSK9 causes increased LDLR levels in the liver and reduction of plasma LDL cholesterol. Lipidoid-siPCSK9 reduced PCSK9 mRNA levels in the liver by 50–70% which was associated with up to a 60% reduction in plasma cholesterol levels compared to lipidoid-siControl. This liposome has entered and completed phase I clinical trial as ALN-PCS02 with a positive outlook where the drug reduced LDL cholesterol in healthy participants with raised cholesterol concentrations [209]. Further progress on this is yet to be reported and it may have been hindered by the competing FDA approved modRNA drug, mipomersen (discussed in prior section 1.3.1), used in the clinic for therapy in patients with homozygous and severe heterozygous familial hypercholesterolemia. These studies demonstrate the positive

outlook on efficacy of cationic liposomes, SNALP in particular, *in vivo* for various targets when systemically injected.

Other cationic lipid particles that are not SNALPs, have been able to illustrate their use in various therapeutic miRNA and siRNA delivery *in vivo.* A liposome nanoparticle composing DODMA/egg-PC/Cholesterol/PEG-cholesterol at molar ratios of 45:15:35:5, with a slight +ve charge (≈ 4mV) at pH 7.4 and a slight –ve charge (≈ 4mV) when complexed to siRNA was developed for gene knockdown in murine tumor xenografts model. The nanoparticles were again complexed with miR-122, a liver-specific tumor suppressor miRNA sequence commonly downregulated in hepatocellular carcinoma (HCC), and injected intratumorally twice a week over 26 days in nude mice xenografts. The experimental groups yielded efficient miR-122 knockdown of its target genes by >95% in the liver and tumor xenografts, as well as reduced angiogenesis and tumor growth reduction by 50% compared to a control siRNA group without causing systemic cytotoxicity. This liposome nanoparticle demonstrated therapeutic potential, in particular for HCC therapy, and it demonstrated efficient miRNA mimics delivery and gene knockdown *in vivo* [210]. The use of cationic lipid nanoparticles in various *in vivo* studies and the approval of patisiran application in the clinic shows the advancement of cationic liposome nanoparticles as RNAi delivery vehicles.

Lipofectamine® RNAiMAX and Invivofectamine® 3.0 are examples of very widely used commercial cationic lipid transfection reagents developed to optimise siRNA/gene delivery and efficacy *in vitro* and *in vivo*. The structures and formulations of these liposomes are proprietary but direct communication with the manufacturer indicated that post siRNA complexation, Lipofectamine® RNAiMAX remains cationic whilst Invivofectamine® 3.0 has a neutral charge. Lipofectamine® RNAiMAX has mainly been used in multiple *in vitro* studies but has also been utilised in a few *in vivo* studies [211-213]. It was used in a study that demonstrated intracardiac injection of pro-regenerative miRNA mimics for cardiac repair [213]. In this study, Lipofectamine® RNAiMAX was used as delivery vehicles of miRNA mimics (has-miR-199a-3p, has-miR-1590a-3p) in a mouse MI model. These miRNAs were previously shown when expressed in the heart using viral vectors to stimulate cardiomyocyte proliferation and thus induce cardiac regeneration post MI [214]. One dose of 1.4ug miRNA complexed to Lipofectamine® RNAiMax nanoparticles were directly injected to the infarct border zone of the mice. Results showed improved cardiac function and repair compared to control untreated mice, reduced infarct size 8 weeks post MI and increased the number of cardiomyocytes in a proliferative state. This is an important study were liposome nanocomplexes were directly injected at the site of action in soft tissue.

Invivofectamine® 3.0 is a newer and more costly transfection reagent that has been shown in a number of studies to be an effective transfection reagent for RNA delivery in various tissues *in vivo* when injected systemically [38, 215-219] but studies that show direct injection of this liposome in solid tissue at the site of action is limited [213, 220]. A recent study that investigated vascular lung-targeted delivery of miRNA (with no mammalian homologue) complexed to PEI and Invivofectamine® 3.0 showed that, systemic i.v injection via the jugular vein of rats with both miRNA nanocomplexes resulted in a lack of pulmonary selectivity and led to broad elevated miRNA levels in the lungs, heart and excretory organs (spleen, liver and kidneys), 2 and 24hrs post injection [216]. Preferential transfer of miRNA was observed in the spleen and liver, and less in the kidneys for both PEI and Invivofectamine® 3.0 nanocomplexes. The study shows the potential ability to deliver miRNA in various tissue when delivered intravenously however it also emphasised that off target gene knockdown may occur in various tissues where the nanocomplexes accumulate, which may not necessarily be the intended target. Another study utilised Invivofectamine® 3.0 in the delivery of miR-302d nanocomplexes into peritoneal cells of adult mice with induced lupus-like phenotype, a model of systematic lupus erythematosus (SLE) [219]. miR-302d was established as a therapeutic target in this study where it was shown that miR-302d levels negatively correlated with disease severity in SLE patients and that miR-302d down regulated interferon regulatory factor (IRF)-9 thus decreasing expression of interferon stimulated genes. Lupus induced mice were given an intraperitoneal injection of miR-302d mimics and control miRNA complexed with Invivofectamine. Seven days post injection, results showed significant downregulation of IRF-9 and interferon-stimulated genes expression in the extracted peritoneal cells, kidneys, lungs and blood of the miR-302d treatment group with a concomitant reduction in inflammation in comparison to the control miRNA group. In this study, it was shown that inhibition of the type I interferon pathway through miR-302d delivery via Invivofectamine has potential benefits for SLE patients.

It is important to note that multiple studies illustrate the use of cationic liposomes and show great prospective as nanoparticles to use for RNAi *in vivo* when introduced systemically. Other than the discussed cancerous tissue and a few intramyocardial injection studies, there is limited evidence of these nanoparticles being applied in solid tissue. Hence the use of liposomes to demonstrate targeted gene knockdown at the site of injection in other various soft tissue requires further investigation.

1.3.3.2.2.2 Neutral Liposomes

Neutral liposomes are made from lipids with a neutral charge such as zwitterionic 1,2-dioleoyl-sn-glycero-3-phosphocholine (DOPC) and 1,2-dioleoyl-3-dimethylammonium-propane (DODAP) to improve blood circulation and reduce the potential toxicity and immunogenicity arising from the charged cationic liposomes [2, 193, 221]. Neutral liposomes function by entrapping siRNA in their hydrophilic core [222]. However, the lack of interaction between the oligonucleotides and the neutral lipids at physiological pH results in low siRNA entrapment efficiency by passive loading resulting in complex siRNA incorporation processes [223]. Among other methods, the use of ionisable pH-sensitive lipids such as DODAP with a pK_a of 6.6 and ethanol dialysis, to allow siRNA interaction in the lipid's cationic state has been shown to improve siRNA entrapment [223]. In addition, the cellular uptake of neutral liposomes is less efficient in comparison to that of cationic liposomes [224].

Despite this, a variety of neutral liposomes have been investigated for RNAi and shown efficacy *in vivo*. Examples of such a study include the use of DOPC neutral liposomes in cancer therapy. The liposome was used in the delivery of siRNA in orthotopic xenograft mice models for ovarian cancer targeting EPH Receptor A2 [225] and breast cancer targeting B-cell lymphoma 2 (Bcl-2) [221]. Systemic injection of the DOPC liposomal nanocomplexes with their respective siRNA in these studies showed localisation of siRNA in target tumors and consequentially resulted in tumor growth suppression [221, 225]. Another example of a neutral liposome used *in vivo* is a PEGylated DOPE derived neutral liposome composed of (DOPE, N-(carbon-methoxypolyethylene-glycol-2000)-1,2-distearoyl-sn-glycero-3-phosphoethanolamine and cholesterol lipids) which was formulated and complexed to siRNA against Myeloid cell leukaemia-1 (MCL1) with high encapsulation efficiency [226]. MCL1 is an anti-apoptotic protein in macrophages responsible for disease progression in rheumatoid arthritis. The *in vitro* gene knockdown experiments showed MCL1 mRNA (60%) and protein (90%) knockdown and resulted in an increase in the number of dead cells compared to liposome controls with negative siRNA.

1.4 Barriers of nanoparticle efficacy

Though nanoparticle based approaches have shown good transfection efficiency and RNAi efficacy *in vitro*, the majority of them are in their formative stages and there are relatively few that have reached the pre-clinical stage and very few are being investigated clinically [41, 97, 98]. Their clinical translation and FDA approval success rate is still limited owing to a variety of systemic barriers which include: eliciting an immune response, lack of targeted and localised tissue delivery of the RNAi nanoparticles resulting in off target effects, accumulation in clearance organs (liver, kidneys and spleen) which potentially results in cargo dependent toxicity in those tissues and concomitant failure at the intended peripheral target tissues [38, 227-231].

One approach to overcome the above issues is the development of a RNA delivery vehicle/system to localise and sustain release of siRNA in the targeted tissue. This siRNA delivery system should holistically address the barriers encountered by siRNA or nanocomplexes namely: RNAse attack and consequential short plasma life span, off target delivery, immunogenicity, cytotoxic effects as well as satisfactory efficacy [232]. Increasing siRNA availability at the required site and preventing off target effects should reduce the dosage and frequency of delivery required to achieve gene knockdown effect before RNase attack and systemic clearance by both phagocytic cells and secretory organs. A promising approach that has begun recently to receive significant attention is the delivery of RNAi nanoparticles in combination with scaffolds [232, 233].

1.5 Scaffolds and nanocomplex delivery

Scaffolds can be defined as biologically compatible biomaterials and are currently used in tissue engineering for a wide range of purposes which include structural support, adhesion, and as sealant and surface coatings [234]. Most importantly scaffolds are increasingly being investigated as an efficient way of providing localised and sustained therapeutic effect of drugs, cells, growth factors and nucleic acids *in vivo* [234, 235]. The combination of RNAi and scaffolds is a relatively new but growing offshoot of this research. As for other drugs and biomolecules, sustained and localised release of RNAi molecules encapsulated in a scaffold is expected to improve efficacy, specifically by achieving a more prolonged gene silencing effect than the transient effect of 2-4 days achieved by that of a single dose [168, 236]. Through creating a local reservoir of siRNA

or siRNA nanocomplexes in target tissue as opposed to systemic delivery, scaffolds may limit exposure to RNases, circumvent global immune response and prevent off target effect and systemic clearance by excretory organs [233, 235].

Factors that need to be considered in scaffold design for RNAi purposes not only include tissue biocompatibility and biodegradability into non-toxic by-products but also include injectability, biomaterial type (synthetic or natural), scaffold structure (pore size and connectivity), degradation time and electrostatic/reactive inertness [235, 237]. The latter might reduce nanocomplex interaction and/or cause aggregation which may result in nanocomplex inactivity.

Some of the scaffolds being used for RNAi and previously reviewed include macroporous scaffolds [238, 239], microparticles [240, 241], electrospun nanofibres [242-245] and hydrogels [246]. Pre-crosslinked scaffolds such as microparticles, electrospun fibers and surface coating scaffolds for medical devices and implants have a pre-conceived shape and size and will require surgical implantation [233, 234, 246, 247]. As they are more invasive, they are less ideal for siRNA delivery *in vivo*. Injectable and *in situ* forming scaffolds such as hydrogels on the other hand carry the advantage of having the ability to mould to the required shape, access unreachable areas and importantly they have the potential to be delivered in a minimally invasive fashion, therefore, allowing for possible shorter recovery time for patients [234]. Nonetheless, mild gelation conditions and gelation rates during the crosslinking process of these *in situ* forming hydrogels are essential to prevent overheating and tissue damage, to allow injecting and retention of the gel precursors and therapeutics at the site of action before diffusion occurs [235]. Another unique feature of hydrogels that makes them advantageous and highly favoured in research for clinical application as a biomaterial compared to other scaffold types mentioned above is that they characteristically retain a high volume of water content identical to human tissue and provide cells or tissue with structural support emulating that of the ECM [248, 249]. Therefore hydrogels and their use in the controlled delivery of RNAi molecules will be the focus of further discussion.

1.5.1 Hydrogels

Hydrogels are water swollen 3D networks of porous and hydrophilic polymers that are made of either synthetic or natural material [247, 249, 250]. They have been

demonstrated to permit cellular invasion and provide cues for surrounding tissue to regenerate [250-253]. They have also been shown to allow for entrapment of biomolecules and cells as well as offer controlled release of the encapsulated cargo without destroying tissue structure or function [235, 251-253]. Hydrogels can be engineered in ways that promote degradation/porosity and drug release. This improvement in adjustable biodegradability and porosity of the scaffold would theoretically equate to improved localised release of nanocomplexes over the required time at the injected site, therefore providing sustained release of RNAi molecules at the target site. Wang and Burdick 2017 [235] extensively reviewed the various types of modifications that can be applied to the hydrogels' design to enhance their degradability in response to surrounding stimuli *in vivo* such as pH, temperature, hydrolysis, and enzymatic degradation and hence improve cargo delivery [235].

Hydrogels used in sustained release of RNA molecules can be made by synthetic polymers, naturally derived polymers or combinations thereof [237, 254]. Most synthetic biomaterials, without any modifications, lack the inherent ability to provide cues for cellular interaction and tissue regeneration, but they do allow for greater tunability of properties compared to natural polymer hydrogels [237]. RNAi molecules require optimal integration into scaffolds without significantly reducing their gene silencing effect. A summary of the various hydrogels that have been used in preclinical RNAi studies is given in **Table 2**. As reflected in the table PEG based hydrogel scaffolds are one of the most commonly used scaffolds for *in vivo* siRNA delivery. PEG hydrogels are favourable because they are electrostatically inert and they can easily incorporate nanocomplexes during their formation and gelation process and will not directly interact with charged nucleic acids or nanocomplexes. In addition, PEG hydrogels are injectable, have the ability to crosslink *in situ* and they can be designed to have various engineerable physical, mechanical and chemical properties. Therefore they will be deliberated upon further in sections to follow.

Table 2: Summary of in vivo scaffold mediated RNAi in therapeutics.

Condition	Hydrogel	Nanoparticle	Target	Observations	Ref
Cancer					
	Chitosan	Naked siRNA	TG2	Inhibition of tumor growth in melanoma and breast cancer tumor mice models.	[255]
	CLA-coupled poloxamer	PEI/pDNA$_{shRNA}$	Akt1	Reduced Akt1 expression, enhanced cell apoptosis and	[256]

				inhibited tumor growth in breast cancer mice model.	
	PLGA-PEG-PLGA	PEI/$pDNA_{shRNA}$	PLK1	PLK1 expression inhibition, enhanced cell cycle regulation, apoptosis and tumor growth in osteosarcoma mice model.	[257]
	PAMAM-Dextran	PEI/siRNA	Luciferase	Improved transfection efficiency and luciferase silencing in mice with tumors expressing luciferase.	[258]
	PAMAM-Dextran	PAMAM/RNA-triple-helix	miR-205/221 targets	Tumor size reduction in breast cancer mice model.	[259]
	Collagen-PEG	Naked siRNA & $pDNA_{eNOS}$	Interleukin-6	Reduced inflammatory cells, increased blood vessel density, growth factor binding,	[260]
	Collagen	PEI/siRNA	Id1	Improved siRNA delivery, prolonged Id1 expression suppression, inhibition and reduced tumor growth in gastric cancer xenograft mice model.	[261]
	PEI-PEG-PP	Naked siRNA	cyclin B1	Reduced cyclin B1 expression (30 days) and decreased tumor volume in prostate cancer mice model.	[262]
	PEI-PEG-fPP	Naked siRNA	VEGF	Extended VEGF gene silencing (21 days) and reduced tumor sizes in breast cancer mice model.	[263]
	PEI-PEG-PP	Naked siRNA	Bcl-2	Reduced Bcl-2 expression (30days) and tumor volumes in mice cancer xenografts.	[264]
Inflammation					
	Alginate/chitosan biomaterial	PEI/siRNA	CD98	CD98 expression and colitis reduction in mouse colic tissue.	[265]
	Chitosan	Naked siRNA	VEGF	Hydrogel extended siRNA retention, reduced VEGF expression, decreased mucosa thickness in rats.	[266]
	Sericin silk protein	Naked siRNA	RelA	Reduced ear thickness and clinical skin severity in AD-induced ear skin of mice.	[267]
	Collagen-PEG	Naked siRNA & $pDNA_{eNOS}$	Interleukin-6	Reduced inflammatory cells, increased blood vessel density, growth factor binding,	[260]
Bone regeneration					
	PLA-DX-PEG	Naked siRNA	BMP-2	BMP-2 induced Noggin gene expression suppression and improved bone formation in mice	[268]

	HP-HA-PEG (Glycosil™)	Naked miRNA	miR-26a targets	System led to increased vascularization and complete bone repair in rats with calvarial bone defect	[269]
	PEG-b-PLA-b-DM	Diblock cationic polymer/siRNA	Wwp1	Wwp1 silencing at fracture, accelerated bone formation and increased biomechanical strength in mice	[270]
	8-arm-PEG	PEI/siRNA & miRNA	Noggin & miRNA-20a targets	Noggin and miR-26a targets reduction, accelerated bone formation in rats with calvarial bone defect.	[271]
CVD					
	Cationised pullulan	Naked siRNA	MMP2	siRNA uptake, and reduced MMP2 activity in arterial walls of rabbits.	[272]
	Dex-PCL-HEMA/PNIPAAm	$pDNA_{shRNA}$	ACE	Reduced ACE expression, inhibited cell apoptosis, reduced infarct size, and improved cardiac function in rat MI model.	[273]
	PEI-PEG hydrogel	Naked siRNA-Cy5.5	GFP	Improved siRNA uptake and reduced GFP fluorescence in GFP-expressing rat hearts.	[274]
	HA-PEG hydrogel	Naked miRNA	miR-29B targets	Decreased elastin, less collagen deposition, increased vascularisation and improved myocardial function in mice.	[275]
	HA	Naked miRNA	miR-302	Sustained local cardiomyocyte proliferation and improved myocardial function in mouse MI model.	[276]
	HA	Naked siRNA	MMP2	Improving myocardial thickness and myocardial function in a rat MI model.	[1]

TG2=transglutaminase, Akt1=serine/threonine-protein kinase, CLA=Conjugated linoleic acid, PLK1=Polo-like kinase 1, PLGA=poly(d,l-lactide-co-glycolide), pBAE=oligopeptide-terminated poly(β-aminoester), Id1=Inhibitor Of DNA Binding 1,PEI-PP=Polyethyleneimine-poly(organophosphazene), fPP=folate PP,PLA-DX-PEG=poly-D,L-lactic acid-dioxanone-poly(ethylene glycol), BMP=Bone morphogenetic proteins, HP-HA-PEG=heparin-thiol- hyaluronic acid-poly(ethylene glycol), PEG-b-PLA-b-DM = EG-b-poly(lactide)-b-dimethacrylate, Wwp1=WW domain-containing E3 ubiquitin protein ligase 1, PEG-PLA-DM=poly(ethylene glycol)-poly(lactic acid)-dimethacrylate, PEI=polyethylenimine, ACE=angiotensin-converting enzyme, Dex-PCL-HEMA/PNIPAAm=dextran-poly(e-caprolactone)-2-hydroxylethylmethacrylate-poly(N-isopropylacrylamide),RelA= NF-κB subdomain, MMP=matrix metalloproteases, VEGF=Vascular endothelial growth factor, ACE=Angiotensin-converting enzyme, GFP=green fluorescent protein, CD98=glycoprotein.

Compared to synthetic polymers, fewer natural polymer derived hydrogels have been investigated for siRNA delivery both *in vitro* and *in vivo* and these include carbohydrate based (chitosan, hyaluronic acid (HA), alginate) and protein based (gelatin, collagen, fibrin) hydrogels [249, 254, 277]. Of the mentioned natural polymers, fibrin based hydrogels have not been adequately evaluated *in vitro* and they have not been demonstrated *in vivo* therefore further investigation of this scaffold material is desirable as it offers advantages that will be discussed and explored further. Hydrogels made of naturally derived polymers have an added advantage over synthetic based scaffolds because they play a role in cell interaction, signaling and adhesion. However, without modifications, they tend to lack adequate mechanical properties and engineerability that is afforded by synthetic hydrogel polymers, thereby compromising their application *in vivo* [234, 278]. The combination of synthetic and natural polymers to develop hybrid hydrogel scaffolds with improved combined properties for sustained delivery is now being widely investigated. Hence synthetic PEG hydrogels, naturally derived fibrin hydrogels and their modifications with potential for RNAi molecules delivery will be discussed.

1.5.1.1 *PEG hydrogels*

PEG hydrogel scaffolds are inert, biocompatible, water swollen synthetic polymer networks. They are made of reactive PEG polymer molecules with reactive linear or branched structures (referred to as arms) and reactive crosslinker segments [234, 277]. PEG polymers are one of the most advantageous synthetic biomaterials to use for hydrogel formation in tissue regeneration because, in addition to what was discussed above (section **1.5**), PEG is an FDA approved conjugate molecule with various biomedical applications in the clinic which include many FDA approved protein-PEG conjugates for treatment of diseases such as cancer and hepatitis [279, 280]. PEG hydrogels can be engineered to be degradable or non-degradable by adding crosslinker segments with various characteristics during polymerisation [277] and the hydrogel crosslinking process is easily achieved in response to conditions such as heat, pH, radiation and photopolymerisation [254, 277, 281-283]. In addition to degradability other characteristics such as pore structure and hydrogel function can be achieved by altering (i) PEG polymer type (ii) crosslinker type (iii) the ratio of these reaction components (that is PEG polymer, crosslinker) used during the hydrogel polymerisation and (iv) conjugating various bioactive molecules onto the polymer depending on application

requirements [234, 277, 284-286]. These functional bioactive groups that can be added include heparin, RGD peptide motif and growth factors, they can also be used to engineer the hydrogels for specification of function [277, 284, 287, 288].

There are various types of PEG polymers that are determined by the kind of functional group they consist of on their reactive arms, for instance: amine, thiol, carboxyl, acrylate (AC) and vinyl sulfone (VS) functional groups [277]. Some of the crosslinker types include hydrolytically degradable poly (lactic acid) (PLA), polyglycolic acid molecules, and reactive enzyme sensitive peptide sequences such as matrix metalloprotease (MMP) [277, 284, 286].

An example of a particularly useful and widely explored form of PEG hydrogel system that is a powerful synthetic ECM mimic is an enzymatically degradable PEG hydrogel initially developed by the Hubbell group [289]. A representation of such an enzymatically degradable PEG hydrogel formation is shown in **Fig.5**. Where a multi arm (typically 4 or 8-arm) PEG with acrylate (AC) or sulfhydryl (VS) reactive end groups is crosslinked with a reactive bis-cysteine protease sensitive peptide. This protease sensitive sequence can be tailored to be MMP sensitive and there has been a wide range of applications and studies using the MMP sequence GCRE**GPQGIWGQ**ERCG developed by the Hubbell group containing the MMP1 enzyme cleavage motif GPQG↓IWGQ (arrow indicates cutting site for the MMP1 enzyme) [285, 290].

The advantage of enzymatically degradable hydrogels over hydrolytically degradable ones is that non-enzymatic hydrolysis is uncommon *in vivo*. Naturally, the ECM is degraded by migrating cells that secrete proteases such as, serine proteases, collagenase, plasmin, MMPs, and ECM proteolysis is essential for cell migration and invasion [289, 291]. The peptide sequence incorporated within the hydrogel is sensitive to degradation by the corresponding protease, therefore the degradation rate of the hydrogel (as well as the release of encapsulated drugs) adjusts to the rate of cell infiltration as well as the specific enzymes secreted by those migrating cells [291]. Enzyme sensitive PEG hydrogels have not been used for RNAi but have been used for plasmid delivery *in vitro* [292]. In this study, they explored the use of a 4-arm PEG-VS hydrogels in the delivery of PEI complexing a pDNA (carrying various reporter transgenes) to clusters of MSCs cells also encapsulated within the hydrogel prior to crosslinking. Cells were either suspended as a cluster within a fibrin clot or as a homogenous mix of single cells throughout the gel. The PEG-VS was functionalised for cell adhesion with RGD and the gel crosslinking was facilitated by the bis-cysteine MMP1 peptide. Gene transfer to the migrating infiltrating cells was measured by quantifying the

fluorescence of the reporter gene microscopically. Results showed cell clusters produces cumulative increasing gene expression over 21 days whereas homogenous cells produced a plateauing cumulative gene expression by day 7. The study showed that the gel was capable of maintaining viable transfecting polyplexes over time and cells could migrate through the gel and take up the polyplexes.

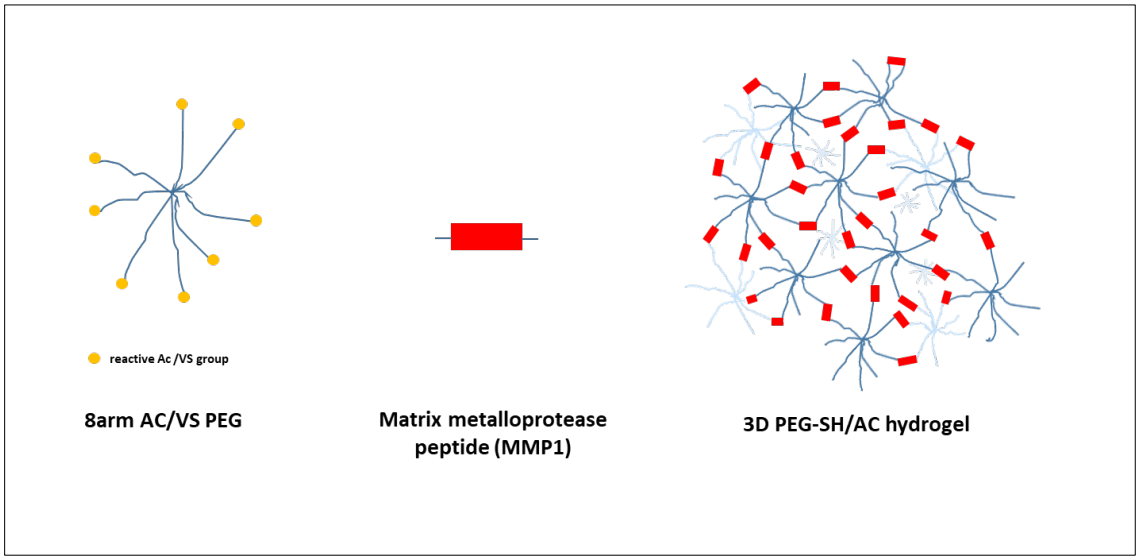

Figure 5: A schematic representation of an 8-arm PEG- VS/AC hydrogel formation crosslinked with MMP peptide crosslinker containing the MMP enzyme recognition and cleavage motif.

As discussed hydrogels have the ability to control the delivery and release of growth factors [252, 253], siRNA [293], cells [294], and other biodrugs [233, 251]. In addition, the design principles of hydrogels have been influenced by their ability to mimic the ECM. Since the ECM has been demonstrated to play a vital role in cell interaction, signal transduction and providing mechanical support to tissue [295, 296], developing scaffolds that provide similar functions has become an emerging research area. The use of an injectable engineered hydrogel without therapeutic biomolecules or cells in MI therapy is one classic example where hydrogels are being applied for their discussed injectability, tunable degradability, engineerability and ECM mimic characteristic features to provide cardioprotective function [247, 297].

1.5.1.2 *Scaffold mediated RNAi in therapeutics.*

Currently, there are no injectable scaffold based RNAi for targeted delivery strategies being used in clinics or in clinical trials as determined by using the key search words siRNA and RNAi in the Clinical Trials database [179]. There is however one study in phase I/II trials, where a surgically implanted miniature biodegradable polymer Local Drug EluteR containing siRNA against an oncogene K-RasG12D (siG12D), is being tested as a treatment for pancreatic cancer therapy [298-300]. As outlined in **Table 2**, there is a relatively low number of early stage preclinical applications of engineered hydrogels for local and sustained delivery of RNAi [235]. RNAi through controlled release from hydrogel scaffolds has primarily been applied in cancer therapy studies [255-259, 261-264], but also in inflammation [260, 265-267], bone regeneration [268-271], muscular dystrophy [301, 302] and CVD therapy studies [1, 111, 272-276].

1.5.1.2.1 Cancer

The majority of the studies on sustained localised delivery of siRNA or nanocomplexes has been towards targeting cancer cells. This is because in part most of the subcutaneous xenograft tumour models used in the studies can be directly and simply intratumorally injected. In addition, the enhanced permeability and retention effect associated with cancerous tissue allows for ready uptake of siRNA or nanocomplexes and therefore facilitating targeted delivery and accumulation of therapeutics in this tissue [134, 303].

One of the earliest proof-of-concept studies to investigate the delivery of localized RNAi molecules for cancer therapy was by Han et al. [255]. The delivery of siRNA against the oncogene transglutaminase (TG2), which is highly expressed in multiple cancers, was done with a temperature sensitive chitosan hydrogel. Initially to show localisation of siRNA they intratumorally injected mice once with the *in situ* gelling chitosan hydrogel containing Alexa 555-fluorescently labelled siRNA. Tumor explants 24 and 48hrs post injection showed that the gel was capable of releasing siRNA to surrounding tumor cells as well as being invaded by tumor cells. It was noted that the gel they used degraded within 3-4 days, hence to show efficacy, melanoma and breast cancer murine tumor models received a single intratumoral injection per week of hydrogel containing siTG2 and Docetaxel (DTX) drug over a 30 day period. Their results indicated that one month post treatment this combinatorial treatment had a significant reduction in tumor growth and an increase in apoptotic cells versus the gel-siTG2 alone and gel-DTX alone

treatment controls. This study showed localisation of siRNA and improved efficacy when siRNA and drug are delivered using the chitosan hydrogel.

A collagen hydrogel was used for localised and sustained delivery of siRNA against oncogene Id1 responsible for cell proliferation and migration in gastric cancer [261]. The siRNA was mixed in the collagen gel either alone or complexed to PEI nanoparticles and its release profile and bioactivity was determined in vitro. It was shown that PEI-siRNA nanocomplexes were released more slowly (50%) than siRNA alone (100%) over 10 days, and that proliferation of cells within hydrogels containing PEI-siRNA or naked siRNA was significantly lower than gel only controls with a more substantial gene knockdown effect seen in the PEI-siRNA group. In a gastric cancer xenograft tumour animal model, gastric cancer cells were mixed with either media only or siRNA only controls, siRNA-gel or PEI-siRNA-gel and injected into nude mice. They found reduced tumor weight, size and cell proliferation in siRNA-gel or PEI-siRNA-gel treated groups and an enhanced effect in PEI-siRNA-gel. The study showed the feasibility of using collagen hydrogel for localised and sustained delivery of siRNA in cells incorporated within the gel. Though a proof of concept, it should be noted that pre-mixing of siRNA with cancer cells prior to injection might create an artificially favourable environment for siRNA uptake.

A sophisticated approach has been extensively investigated by the Song group since 2012 [262]. They developed a linear PEI - conjugated poly(organophosphazene) (PP) hydrogel that was modified with hydrophobic isoleucine ethylester and a hydrophilic thermosensitive amino PEG such that the polymer would electrostatically interact with siRNA (via PEI interaction) and also transition to a hydrogel upon exposure to $37^{O}C$. The hydrogel can through both dissolution and degradation release siRNA polyplexes for efficient uptake. This sustained delivery thermosensitive gelling approach has great potential for minimally invasive delivery and their findings suggested that the PP hydrogel delivery. With this PP hydrogel system they encapsulated various RNAi molecules such as PEI-siCyclin B1 [262] and PEI-siVEGF [263] for cancer therapy. In another study, they encapsulated protamine (a potent transfection reagent) complexed with siVEGF within the thermosensitive PP hydrogel system without PEI conjugation (**Fig.6**) [3]. When the hydrogel was administered intratumorally or subcutaneously in murine models, it demonstrated anticancer effect caused by RNAi and gene knockdown of the oncogenes in question at the tumor sites. In a more recent study [264] they co-delivered siBcl-2 and Docetaxel (DTX) drug via the PEI and hydrophobic isoleucine ethylester interaction within the PP hydrogel. When injected intratumorally in mice the PP complex system

showed successful delivery of drug and siRNA as well as efficacious Bcl-2 gene knockdown. They showed enhanced tumor size and weight reduction in the PP-DTX-siBcl-2 treated groups (in a dose dependent manner) when compared to DTX and PP-siGFP negative controls over 30 days. Here, they demonstrated the potential use of the gel in cancers that require combinatorial therapy.

In addition to the discussed, there are several other hydrogel based approaches that have utilised a mouse subcutaneous xenograft model and intratumoral injection of RNAi molecules [256-258, 261]. Given that this is the most investigated disease for RNAi application and although promising results have been observed, there has not been translated to the clinic as of yet. This may reflect the novelty of this approach but also that the animal model may not be ideal [304]. Therefore finding other ways to model the disease as well as broadening the spectrum of disease focus for RNAi therapeutic application is essential for progression in this field.

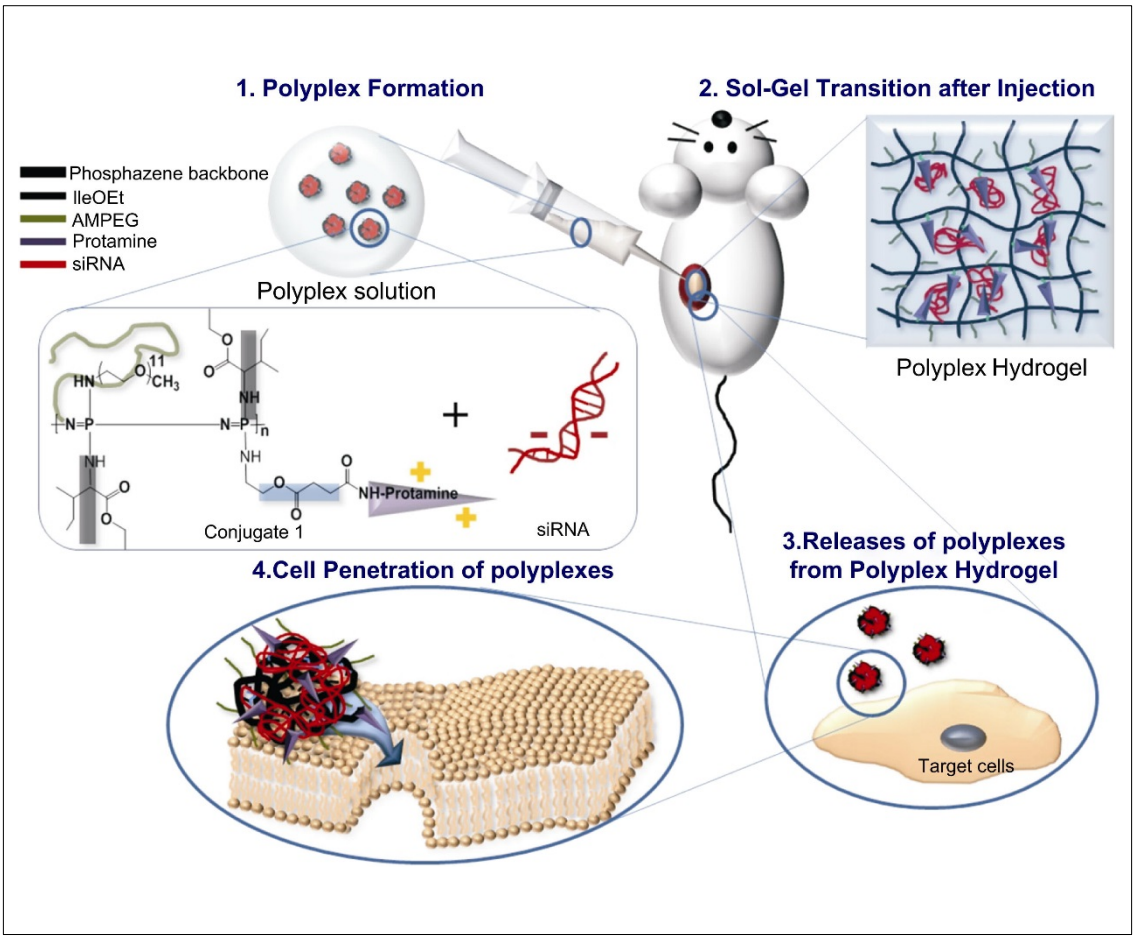

Figure 6: Schematic diagram of a thermosensitive poly(organophosphazene) nano-polyplex assembled hydrogel system. *Figure reprinted from Kim et al. 2013 [3], with permission from Elsevier.*

1.5.1.2.2 Inflammation

Hydrogels are also being investigated as delivery vehicles for RNAi molecules in chronic inflammatory diseases such as rhinosinusitis [266], atopic dermatitis where the treatment is topically applied on the skin [267], and inflammatory bowel disease. In a combinatorial approach, controlled release from a hydrogel was used to target inflammation in the colon of an induced colitis mouse model [265]. PEI-siRNA nanocomplexes against a pro-inflammatory glycoprotein (CD98) gene were encapsulated in an alginate chitosan hydrogel that would release the nanocomplexes at pH 5-6 thus avoiding the stomach and small intestines (with pH lower than 4 and higher than 6 respectively) and targeting the colon. Colitis mice received daily gavages of the nanocomplex-hydrogel over 8 days, and then their colons were excised and analysed for pro-inflammatory cytokines. Efficient uptake of nanocomplexes by macrophages and epithelial cells in the colon, reduction of CD98 expression, inflammatory cytokines and weight loss was observed relative to scrambled siRNA negative control. Results from this study demonstrated the ability of the nano-hydrogel system to locally release nanocomplexes in the colon and decrease colitis in a pH depended manner. Though not an injectable hydrogel depot approach, this study demonstrated a novel manner in which hydrogels can target a specific organ.

An injectable collagen sphere-in-hydrogel system was designed to target transplant rejection problems that result from the foreign body response against tissue engineered organs and implants during organ replacement [260]. Endothelial nitric oxide synthase (eNOS) pDNA, encoding for a pro-angiogenic enzyme eNOS, was complexed to partially degraded PAMAM dendrimer to form polyplexes. The polyplexes were loaded into hollow 1μm collagen microspheres by agitating the mixture of negatively charged collagen microspheres and positively charged polyplexes. The polyplex loaded microspheres were then resuspended in a collagen/pentaerythritol poly(-ethylene glycol) ether tetrasuccinimidyl glutarate solution containing free Interleukin-6 (IL-6) siRNA. The collagen sphere-in-hydrogel system with eNOS-pDNA and IL-6 siRNA (a pro-inflammatory cytokine involved in inflammatory cascade and increase in inflammatory cells) was subcutaneously injected into the rat dorsum and at 7 and 14 days post treatment the animals were sacrificed and implants excised and analysed. Results from the explants confirmed a reduction in inflammatory cells and an increase in the length and density of blood vessels at both time points in the groups treated with scaffold

+eNOS pDNA+IL-6 siRNA compared to scaffold+IL-6 siRNA. They also showed that this therapeutic eNOS-pDNA delivery system caused temporary changes in the ECM composition as seen by the increase in the binding capacity of the sulfated glycosaminoglycan to growth factors $VEGF_{165}$ and fibroblast growth factor (bFGF) at day 7 which returned to baseline by day 14. The increase in binding capabilities of growth factors may cause the increase in angiogenic inducing capabilities of the ECM in the treated area. This study showed that the developed injectable collagen sphere-in-hydrogel system could deliver nucleic acids over a period of 2 weeks, modulate inflammation and increase angiogenesis *in vivo*.

1.5.1.2.3 Bone regeneration

There are presently few reports on scaffold mediated RNAi in bone regeneration. In one study, siRNA against WW domain-containing E3 ubiquitin protein ligase 1 (Wwp1), was complexed via electrostatic interaction with polymer diblock nanoparticles (NP) composed of dimethylaminoethyl methacrylate [270]. The NP-siWwp1 nanocomplexes were encapsulated within a hydrolytically degradable hydrogel formed from ultraviolet (UV)-photopolymerization of photo-initiator, lithium arylphosphanate, with poly(ethylene glycol)-b-poly(lactide)-b-dimethacrylate (PEGa-b-PLA-b-DM). The hydrogels were precast with NP-siWwp1 prior to assessment. *In vitro* assays showed that the hydrogels released 75% of NP-siRNA over 30 days compared to 100% release of non-complexed siRNA in 1 day. When cells were seeded in wells with NP-siWwp1 hydrogels placed above in transwell inserts, knockdown of Wwp1 was found to be maintained for at least 12 days relative to the 3 days achieved by siRNA/NP alone. The localization and release of NP-siRNA hydrogels, using near-infrared (Cy5) labelled siRNA and their gene silencing efficiency (using siWwp1), was investigated *in vivo* in a murine mid-diaphyseal femur fracture model. Hydrogels encapsulating NP- siRNA Cy5 labelled were implanted at the fracture site and localised NP-siRNA was observed at the fracture site over 28 days compared to free siRNA which was only present for 3 days. 2 and 3 weeks post NP-siWwp1 hydrogel treatment, mice were sacrificed and real time polymerase chain reaction (RT-PCR) showed a significant 77% reduction of Wwp1 mRNA expression at the fracture callus and accelerated bone formation and improved biomechanical strength of the harvested femur specimens in the treatment group relative to NP-siWwp1 only injections and untreated fractures which had no significant effect. This study indicates that the NP-siRNA hydrogel system has significant therapeutic promise to augment

fracture healing, but because their hydrogel is prepared and set outside the body and requires surgical implantation, this approach may be limited in applicability for other pathologies such as CVD as the involved organs may be less amenable to the implantation of precast hydrogels.

In situ forming hydrogels offer substantial advantages as they can be less invasively delivered and can take the form of complex 3D shapes and have been investigated for the controlled delivery of RNAi nanoparticles in bone regeneration [271]. In an initial *in vitro* study, sustained delivery of PEI-siNoggin and PEI-miRNA-20a nanocomplexes to human derived MSCs (hMSCs) that were encapsulated within an 8-arm-PEG-acrylate (8-arm-PEG-AC) hydrogels was observed. The 8-arm-PEG-AC was crosslinked with 8-arm-PEG-SH. Results indicated increased osteogenic differentiation of the hMSCs over a 28 day period compared to PEI-control siRNA [305]. It should be noted that the siRNA nanocomplexes and cells were premixed during hydrogel formation which does allow for direct interaction of the cells with siRNA whilst the hydrogel is still liquid thus it is not entirely clear that this setup reflects a sustained delivery of siRNA to the cells.

More recently the same 8-arm-PEG-AC hydrogel system was modified by covalently attaching a GRGDSPC cell adhesion peptide through their cysteine thiol prior to crosslinking. They encapsulated hMSCs + siNoggin and/or miRNA-20a to assess their ability to accelerate bone formation in a rat model with calvarial bone defect [271]. The thiolated cell adhesion peptide sequence containing RGD was used to enable the encapsulated hMSCs' attachment and survival in the hydrogel microenvironment. 5mm bilateral circular defects were drilled on both sides of the sagittal suture on the rats' cranium and the hydrogels encapsulating human bone marrow derived MSC cells and PEI-RNA complexes were implanted in the defects. Rats were sacrificed 2 and 12 weeks post-surgery and the implants were excised and analysed for cell differentiation, RNA analysis (at 2 weeks) and bone formation at 12 weeks. Their results showed sustained significant knockdown of Noggin and miRNA-20a target in hMSCs encapsulated in the hydrogel 2 weeks post-surgery as well as an increase in osteogenic markers in those samples compared to siRNA negative controls. At 12 weeks histology showed that explants treated with hydrogels containing hMSCs and miRNA-20a-nanocomplexes resulted in more bone formation than the hydrogels containing hMSCs without siRNA or with negative control siRNA. It was concluded that the hydrogel system developed in this study may provide a platform for filling and healing bone defects, additionally, it is a promising system for localised and sustained gene delivery in a variety of tissue applications. Though the hydrogel system developed has *in situ* forming capabilities, the animal model and defect studied by the group required surgical implantation of pre-made

gel discs, as well as mixing the cells being targeted for transfection with the nanocomplexes occurred within the hydrogel prior to polymerisation. It would be of interest to investigate its systemic capability when injection of a hydrogel and release of nanocomplexes to knockdown genes in surrounding tissue is required.

1.5.1.2.4 Muscular dystrophy

RNAi is being applied to enhance and accelerate skeletal muscle regeneration as a therapeutic measure for skeletal muscle injuries and muscular dystrophy therapy targeting proteins such as myostatin [306-308]. Myostatin is an important key regulatory protein in muscle regeneration as it acts as a negative regulator of skeletal muscle growth. In brief, myostatin is a protein that belongs to the transforming growth factor – Beta family and it is also referred to as growth differentiation factor (GDF-8) [309]. It is a secreted protein whose precursor form goes through two proteolytic processes in the cell to produce a biologically active 12-14 kDa active C terminal fragment [310, 311]. Myostatin gene sequence is conserved across various species such as fish, cattle, mice and humans. In adult tissue, it is almost exclusively expressed in skeletal muscles and adipose tissues, though the expression levels vary in each muscle [309]. The function of myostatin was first elucidated in mice and cattle with mutated myostatin, where it was observed that the absence of functional myostatin results in increased muscle fibre mass through hyperplasia and hypertrophy [310, 311]. The mice and cattle with mutant myostatin presented with a double muscle phenotype compared to wild-type animals [309-312]. Understanding the mechanism by which myostatin regulates muscle growth has become important in developing new strategies for human therapeutics in treating muscular atrophy diseases and as well as agricultural function in livestock production [301, 309, 311]. One of the therapeutic measures being explored as therapy for diseases such as muscular dystrophy is the inhibition of myostatin to increase muscle mass.

Atelocollagen (ATCOL) is a cationic naturally derived polymer that has been used for local myostatin siRNA (siMstn) delivery in skeletal muscle for muscle mass increase and muscle function recovery [301, 302]. It is a collagen derivative produced by pepsin-treatment of collagen type I to remove telopeptides on the C and N terminals of the collagen molecule [313]. ATCOL was developed and optimised for siRNA delivery *in vivo* and is commercially available in two forms depending on the desired method of administration and target tissue. That is, it can be used to deliver nanocomplexes or

siRNA in the form of a hydrogel with gelation capabilities for local injection or it can be used as a solution for systemic administration that does not gel [302].

The effect of ATLCOL-siMstn complexes in three murine models using ATLCOL-scrambled siRNA as control was investigated. In their first investigation, ATLCOL-siRNA was injected into the masseter and bicep femoris of normal mice. These nanocomplexes were also injected into the masseter and tibial muscles of dystrophin deficient mice, a muscular dystrophy animal model. In both these animal models, muscle morphology was examined 2 weeks post treatment. Their third animal model involved systemic injection 4 times over 3 weeks of the ATLCOL-siMstn complex into normal mice to show global silencing effect of myostatin. In this animal study, muscle morphology was examined on lower limbs and masseter muscles 3 weeks post treatment. In all their animal models they observed similar results which included significant increase in muscle mass and muscle fibre (larger myofibrils) as well as a decrease in myostatin protein in the ATLCOL-siMstn compared to the scrambled siRNA control group. In a follow up study, ATLCOL-siMstn and similar control nanocomplexes were injected in masseter muscles of transgenic mice expressing mutant caveolin-3, an animal model for muscular dystrophy showing severe myopathy [301]. In addition to determining muscle mass and fibre size; the Mstn protein, myogenic transcription factors (MyoD and Myogenin) and adipogenic transcription factors (CCAAT/enhancer-binding protein, glitazone receptor) RNA levels were quantified. Both adipogenic transcription factors and Mstn RNA levels were found to be downregulated whilst the myogenic transcription factors were upregulated, this would result in the replacement of adipose cells with skeletal muscle growth. Supporting this conclusion was the observation that Mstn treated tissue was found to be lean and had reduced connective tissue compared to the ATLCOL-scrambled siRNA control. In addition, they showed that muscle activity in the treatment group was increased compared to the negative control. The results from both their studies indicated that local and systematic application of ATLCOL-siMstn stimulated muscle growth and could potentially be used to treat muscle atrophic disorders.

1.5.1.2.5 CVD

There has been a recent increase in research into the application of scaffolds for RNA delivery in MI therapy. RNAi has shown promising outcomes with improvements in a wide range of MI therapeutic targets such as fibrosis, infarct size, apoptosis, hypertrophy, angiogenesis, inflammation and cardiac regeneration by reprogramming surviving

cardiomyocytes [214, 314, 315]. There is now interest in using various injectable scaffolds to deliver many of these RNA interfering molecules for MI therapies.

One of the earliest studies to demonstrate the use of a scaffold in sustained efficacious gene knockdown *in vivo* with siRNA targeted neointimal hyperplasia or restenosis of coronary stents [272]. Reduction of MMP2 was the goal as the expression of this protease by vascular cells is upregulated during restenosis of the stented vessel. A rabbit model which was subjected to balloon carotid artery injury had metal stents coated with unmodified pullulan and dextran polysaccharides crosslinked with sodium-trimetaphosphate to form a hydrogel and then impregnated with cationised-pullulan-siRNA nanoparticles implanted 15 days post injury. This study used surface coated stents into which nanocomplexes were swollen and they illustrated localised delivery and uptake of Tamra-tagged siRNA in the carotid artery 24hrs post implantation and a notable 30% decrease in pro-MMP2 activity [272]. In this very preliminary study, no assessments were carried out at more relevant later time points and can be viewed as a proof of concept. In a later study, a modified thermosensitive biodegradable dextran hydrogel encapsulating shRNA plasmids complexed to Lipofectamine 2000 was used to inhibit angiotensin converting enzyme (ACE) in a rat MI model [273]. Post MI, angiotensin-converting enzyme (ACE) has been shown to enhance myocardial cell death and increase infarct size [316, 317]. When the shRNA-hydrogel was injected directly into the infarct zone, an improved cardiac function at 30 days was observed with a concomitant decrease in ACE mRNA, apoptosis and the infarct size compared to the negative control shRNA-hydrogel group [273].

The use of a scaffold based delivery system for RNAi molecules as a therapy for MI has been most intensively investigated by the Burdick group. The overall approach incorporates degradable guest host hydrogels with shear-thinning properties that rapidly self-heal for controlled delivery of miRNA mimics and siRNA. In one of their initial studies, GFP silencing siRNA was locally delivered by a self-eroding hydrogel into rat myocardium [274]. Here, PEI was modified with guest molecule β-cyclodextrin (CD) and PEG with host molecule adamantine (Ad). siRNA was complexed to the CD-PEI to form polyplexes, and these polyplexes were combined with Ad-PEG to form an injectable, shear thinning, guest-host PEI-PEG hydrogel encapsulating siRNA that self-erodes into smaller spherical PEI-PEG polyplexes in a size range of 20-300nm (**Fig.7**). The polyplexes were capable of transfecting HT1080 and GFP expressing C166 endothelial cells *in vitro* as assessed with Cy3-labelled siRNA and siGFP siRNA respectively. They encapsulated GFP-Cy5.5 labelled siRNA into the self-eroding-hydrogel system and injected it to the left ventricle of GFP transgenic adult rats. Quantification of GFP and

Cy5.5 signal by thresholding confocal micrographs of frozen sections suggested 40% GFP knockdown in proximity to Cy5.5 labelled siGFP siRNA and not the control siRNA containing gel at 24hrs. Knockdown was also suggested at 7 days from qualitative observation (no quantification). When delivered in a hydrogel there was significantly more Cy5.5 label retained at 2 and 7 days though the label had substantially dispersed by day 7. This study indicated the potential of this type of siRNA delivery system for cardiac pathology therapy.

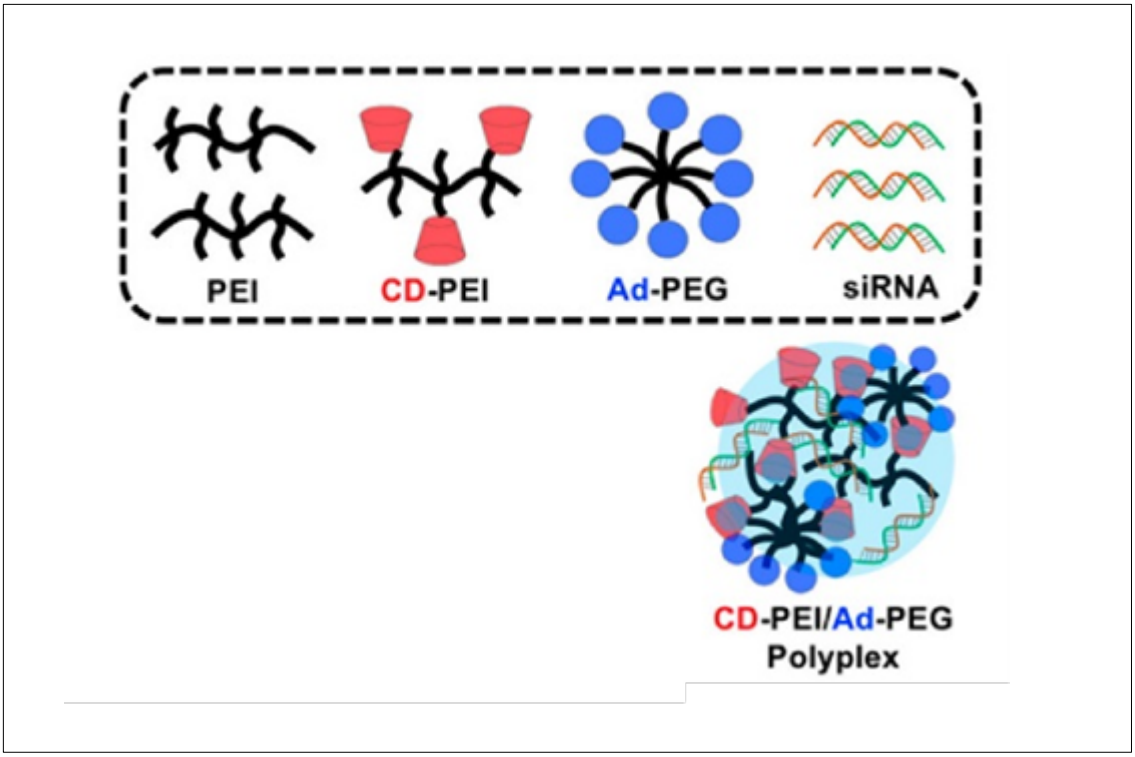

Figure 7: Schematic representation of CD-PEI/Ad-PEG polyplex. *Figure reprinted and adapted with permission from Wang et al. 2017 [1].*

In a later study, a guest host injectable HA hydrogel was used to deliver a cholesterol modified miR-302, a cardiomyocyte proliferation regulator [276]. HA was modified with CD and Ad molecules to again interact and form a shear thinning and self-healing hydrogel that entrapped siRNA due to its cholesterol modifications affinity to CD. A single injection of this hydrogel system was delivered to the infarct in a mouse MI model and optical imaging of explanted hearts showed that 90-95% of siRNA was lost by 7 days with the remainder dissipating over the next 3 weeks. Improved cardiac function was observed and an increase in cardiomyocytes in the infarct border zone 28 days post treatment relative to PBS and gel-siRNA negative control miRNA [276]. In their most

recent study, cholesterol modified siMMP2 was investigated as MMP2 is implicated in deleterious heart remodeling post MI [1]. Here the siMMP2 was delivered into infarct cardiac tissue of a rat using a guest-host HA hydrogel that had been further modified to be protease sensitive. The HA was modified with guest molecule CD to react with the cholesterol modified siRNA, additionally guest molecule aldehyde (ALD) and heterobifunctional MMP-cleavable peptide with host molecule hydrazide (which reacts with ALD via an hydrazone bond to form the protease responsive aspect of the shear-thinning, self-healing hydrogel) were added to the HA polymer [1] . Controlled release of siRNA was observed over 15 days and 4 weeks post injection in the infarcted area, reduced wall thinning and improved cardiac function was seen in comparison to PBS and gel/negative siRNA controls. This powerful and modifiable system has great potential to be delivered via catheter based approaches. It would be of interest to determine whether the short term loss of siRNA could be alleviated through greater protection against RNase activity and tighter entrapment.

In another recent study, a miRNA mimic to miR-29B was delivered to an infarct in a controlled release fashion [275]. A thiolated hyaluronic acid polymer (Glycosan HyStem®) was crosslinked with thiol-reactive PEG diacrylate to form a hydrogel that encapsulated miRNA-29B (miR-29B), a miR-29 mimic. The miR-29 family is known to target inhibition of multiple ECM genes which include fibrillins, elastin, collagens type I and III [318]. Adult mice were subjected to ischemia/reperfusion and immediately received 5 X 10µl injections of gel mixture on the border zone of the infarcted myocardium. At 2 and 5 weeks following MI myocardial function was maintained and, increased vasculature and decreased elastin protein expression and collagen fibre deposition at the border zone of the infarct were observed [275]. Furthermore, using Raman microscopy they managed to show location specific alteration of ECM organisation and maturity in areas were the miRNA-hydrogel was loaded. Hence, in this case, improved functional recovery of the myocardium through modification of ECM was achieved through sustained delivery of siRNA.

1.5.1.3 *Fibrin hydrogels*

Fibrin is an FDA approved naturally derived scaffold which is desirable in regenerative medicine due to its elasticity, minimal immunogenicity, permeability and biocompatible degradation products [235, 319]. Fibrin hydrogels are formed from the major components of the coagulation cascade, fibrinogen and thrombin [320]. Fibrinogen plays an important

role in several pathologies and its biological functions are homeostasis and wound healing [321]. Considering the advantages of fibrin as a biomaterial, it has not been sufficiently explored as a potential scaffold candidate for localised and sustained delivery of siRNA.

1.5.1.3.1 Fibrinogen structure and fibrin clot formation *in vivo*.

Fibrinogen is a soluble fibrous 340 kDa glycoprotein made primarily in the liver. It is present in human blood at 1.5 - 4mg/ml concentration. This concentration increases dramatically when an injury occurs in the body [321]. Human fibrinogen is made up of 3 pairs of polypeptide chains $(A\alpha B\beta\gamma)_2$, that is, α,β and γ chain pairs with small fibrinopeptide proteins A and B (FpA, FpB). The fibrinopeptides attach the 2 α chains to the (middle) E region [322-325]. The 2 sets of βγ chains are linked to form two dimers (D regions), that sit on either side of the middle E region. The two D regions (made of βγ chains) are then linked to the middle E region by an α-helical coiled segment. All 6 chains of the fibrinogen are linked together by 29 disulphide bonds [326]. In fibrin synthesis post vascular injury, thrombin, a protease enzyme in the plasma is activated to cleave off FpA and FpB in a pH and Ca^{2+}-dependent manner via a complex enzymatic activation cascade [327, 328]. Thrombin first cleaves FpA off the fibrinogen monomers causing conformational changes in the monomer structure allowing them to spontaneously join and lengthen to form double stranded protofibrils. Thrombin subsequently cleaves off FpB from the protofibrils releasing α chains allowing the protofibrils to aggregate laterally and longitudinally forming insoluble fibrin fibres and a 3D fibrin network clot or gel. The gelation or formation of the fibrin clot occurs when 15-20% of the fibrinogen has been converted to fibrin, new branch points and fibres continue to form within the clot network [321, 329]. The clearing of fibrin clots *in vivo* after completing their haemostatic function follows a controlled proteolytic degradation process termed fibrinolysis by the plasmin protease [330, 331].

1.5.1.3.2 Fibrin clot (hydrogel) formation *in vitro*

Formation of fibrin gels *in vitro* mimics the *in vivo* fibrinogen cleavage process which leads to fibrin hydrogel formation [234]. When formed, fibrin hydrogels also follow the natural *in vivo* fibrinolytic systemic degradation process, which makes them highly favoured for clinical application [320, 332, 333]. In tissue engineering and regeneration

as a whole, fibrin hydrogels have demonstrated their potential in skin, cartilage, neural and cardiac tissue repair [319, 320, 334-340]. In addition fibrin hydrogels are widely used in surgery as a bioadhesive and sealant in wound closure [320, 341-343].

There is extensive investigation into the use of fibrin hydrogels for the delivery of growth factors such as transforming growth factor (TGF), bFGF, and VEGF [234, 332, 337, 344-347], and fibrin hydrogels have also been utilised for cell delivery both *in vitro* and *in vivo* [320, 332, 348-353]. However, there are a limited number of studies investigating the delivery of nucleic acids with the majority assessing gene (pDNA) delivery [348, 354, 355] and only one to our knowledge that examined siRNA delivery [356]. Uptake and expression of lipoplexes of plasmids carrying GFP (Lipofectamine 2000 [348]) or luciferase (Transfast™ [354]) were found to be highly efficient when cells and DNA-lipolexes were mixed during polymerisation and less so when cells were seeded upon DNA containing fibrin hydrogels. It was noted that the highly efficient transfection observed upon mixing was most likely due to the proximity of lipoplexes and cells when incubated together during polymerisation [348]. Knockdown of noggin expression was observed when lipofectamine 2000 complexes with noggin siRNA were layered onto preformed fibrin hydrogels [356]. In a form of reverse transfection, cells were seeded onto the hydrogel surface which was decorated with lipoplexes thus ensuring direct contact. Therefore, though this study was an initial proof that fibrin could allow for RNAi agent delivery, it was not designed to examine controlled release. The above studies demonstrate the potential of fibrin as a nucleic acid delivery vehicle but have only assessed its suitability *in vitro*. A concern with the use of fibrin *in vivo* is its limited duration after implantation due to proteolytic degradation [357]. One relatively gentle modification that has been shown to limit proteolytic degradation *in vitro* is the crosslinking of fibrin with bivalent PEG molecules [337]. This approach has also shown utility *in vivo* [358, 359].

1.5.1.3.3 PEGylated fibrin hydrogel

The PEGylation of fibrin by bivalent PEG crosslinkers has been most extensively developed by the Suggs group [337, 351, 358-362]. In their early studies, they showed that reaction of fibrinogen with benzotriazole carbonate derivative of PEG (PEG-BTC_2) to form a PEGylated fibrin patch consisting of pig bone marrow MSCs *in vitro* improved cell migration, cell viability and facilitated MSC differentiation into endothelial cell

phenotypes [351]. They then in another study injected this PEG-BTC_2 PEGylated fibrin gel type in a mouse MI model with or without hepatocyte growth factor (HGF), cells or both. It was shown that 2 to 4 weeks post treatment, animals that received gel-HGF-cells had high cell retention, low cell apoptosis and improved cardiac function compared to all other groups.

In a later study they showed that reaction of fibrinogen with bivalent succininimidyl methylbutonate PEG (PEG-SMB_2) significantly delayed degradation by plasmin relative to the unmodified fibrin [337]. The *in vitro* release study kinetics showed that release of TGF-β1 from the fibrin gels was dependent on the degree of PEGylation and that the release rate of growth factors correlated with gel degradation rate (which is controlled by PEGylation degree). Bioactivity of the released growth factor up to 8 days was maintained as they observed a reduction in cell proliferation rate versus untreated cells.

In earlier *in vivo* studies, they PEGylated fibrin with another different bivalent PEG derivative, succinimidyl glutarate (PEG-SG_2) [360]. It was found that when combined with insulin-like growth factor-I (IGF-I), it improved skeletal muscle function and structure in the rat hind limb ischemic reperfusion injury model relative to PEGylated fibrin or IGF alone. The behavioural effects of the PEG-SG_2 PEGylated fibrin gel versus unmodified fibrin or collagen gels on encapsulated adipose derived stem cells (ASCs) was determined *in vitro* [358]. They demonstrated that the PEGylated fibrin gel enabled cells to have an elongated interconnected morphology compared to other gels. The gel also caused increased expression of a haemostasis glycoprotein (von Willebrand factor) and secretion of angiogenic factors from the ASC cells compared to the other gel types. Their results suggested the PEGylated fibrin matrix provided better mechanical and biochemical support to cells, therefore, offering a better therapeutic angiogenic advantage. More recently in 2016, two studies utilised the same PEG-SG_2 PEGylated fibrin in delivering stem cells *in vivo* [359, 362]. In both instances the PEGylated-fibrin groups resulted in significantly increased vascularisation when (i) ASCs were delivered in a rat burn injury model [362] and (ii) when bone marrow MSC were delivered in rat hind limb ischemic model [359] relative to the no treatment, PEGylated fibrin gel only and MSCs only controls.

Thus PEGylation of fibrin in this manner reduces protease degradation and appears to increase its functionality *in vivo* although a direct comparison to unmodified fibrin *in vivo* has to our knowledge not been reported.

2 Research aim

The overall aim of this study was to develop a novel RNAi delivery system with utility for delivery to soft tissue based on hydrogel entrapment of siRNA-nanocomplexes.

Two commercial cationic lipid nanoparticles Lipofectamine® RNAiMAX and Invivofectamine® 3.0, a commercial cationic polymeric nanoparticle G(4)-PAMAM dendrimer nanoparticle and it's modified triblock G(4)-D-PEG_{2k}-DOPE version previously developed by Biswas et al. [140] were assessed for their sustainability for scaffold based delivery with particular emphasis on their ability to protect their siRNA cargo from serum RNase cleavage, as it is considered a critical aspect for prolonged delivery *in vivo*.

Two variants of a synthetic based PEG hydrogel and natural fibrin and a PEGylated fibrin hydrogel were assayed *in vitro* with respect to controlling release of the mentioned siRNA-nanocomplexes, and supporting transfection of cells in a 3D model assay developed to more closely resemble *in vivo* delivery to soft tissue.

Finally, the delivery of siRNA against GFP and myostatin into the TA of mice was used to assess the efficacy of the hydrogel-nanocomplex system *in vivo*.

3 Results and discussion

3.1 Characterisation of nanoparticles for scaffold based delivery

3.1.1 Dendrimer nanoparticles *In vitro* characterization

The initial nanoparticle vector assessed as a vehicle for siRNA delivery from a hydrogel scaffold was a PAMAM dendrimer-based nanoparticle, due to its good biocompatibility and potential for protection from RNases [140]. RNA protection from degradation by ribonucleases is an important factor *in vivo* for prolonged RNAi efficacy to be achieved. Cationic particles have the ability to condense and protect siRNA from serum RNases and therefore this warrants further exploration. Modifying nanoparticle surfaces with molecules such as PEG and lipid molecules improves biocompatibility by reducing chances of nanoparticle agglomeration, protein absorption to their surfaces that makes them targets for opsonisation, improve stealth circulation in the system (avoiding eliciting innate immune response), improve RNA complexing and protection, cell penetration, endosomal escape and siRNA release into the cytoplasm [33, 137-139, 143]. Hence the PAMAM dendrimer nanoparticle was modified with a nitrophenyl carbonate derivative of PEG (PEG_{2K}-NPC_2) and DOPE molecules to form a triblock PAMAM dendrimer-based copolymer previously developed by Biswas et al. [140]. The initial focus was towards replicating the findings of Biswas et al. and the examination of the potential of their modified dendrimer to protect siRNA from serum RNases in greater depth.

3.1.1.1 *MD synthesis*

The 4th generation PAMAM dendrimer G(4)-D (referred to further as D), with 64 free reactive primary amines was modified as described in 5.1 by coupling of PEG_{2K}-NPC_2 and DOPE molecules to form a triblock G(4)-D-PEG_{2k}-DOPE modified dendrimer (MD) nanoparticle at a stoichiometry that would reduce primary amines in D to 63. D and the schematic synthesis reaction of MD is shown in **Fig.8A**. To confirm the successful modification of the dendrimer, starting materials D, modifying tail group PEG-DOPE and the final product MD were analysed by ^{1}H nuclear Magnetic Resonance (NMR) (**Fig.9**). Characteristic peaks of PEG-DOPE were assigned and indicated. The two terminal

methyl (-CH3) groups give rise to the peaks at δ 0.91 ppm (j). Peaks at 1.33-1.35 ppm (i), 1.62ppm (h), 2.05 ppm (g), 3.32 ppm (f) and 3.48 ppm (e) are from methylene (-CH2-) protons in the lipid chains. CH2 peaks from the PEG are indicated at 4.55-4.57 ppm (m), 3.82-3.84 ppm (n) and 3.54-3.80 ppm (p). The peak at 5.38 ppm (a) represents the vinylic protons (-CH=CH-). Doublets at 8.34-8.36ppm and 7.51-7.53 ppm (k and l) are indicative of protons in the nitrophenyl group. Successful coupling of PEG-DOPE to D to form MD are confirmed by a) the disappearance of CH-proton signals (present in nitrophenyl groups of PEG-DOPE) from the MD spectrum, and b) presence of characteristic CH2-proton signals from both PEG and D, as well as CH2- and CH3-proton signals from DOPE in the spectrum of MD.

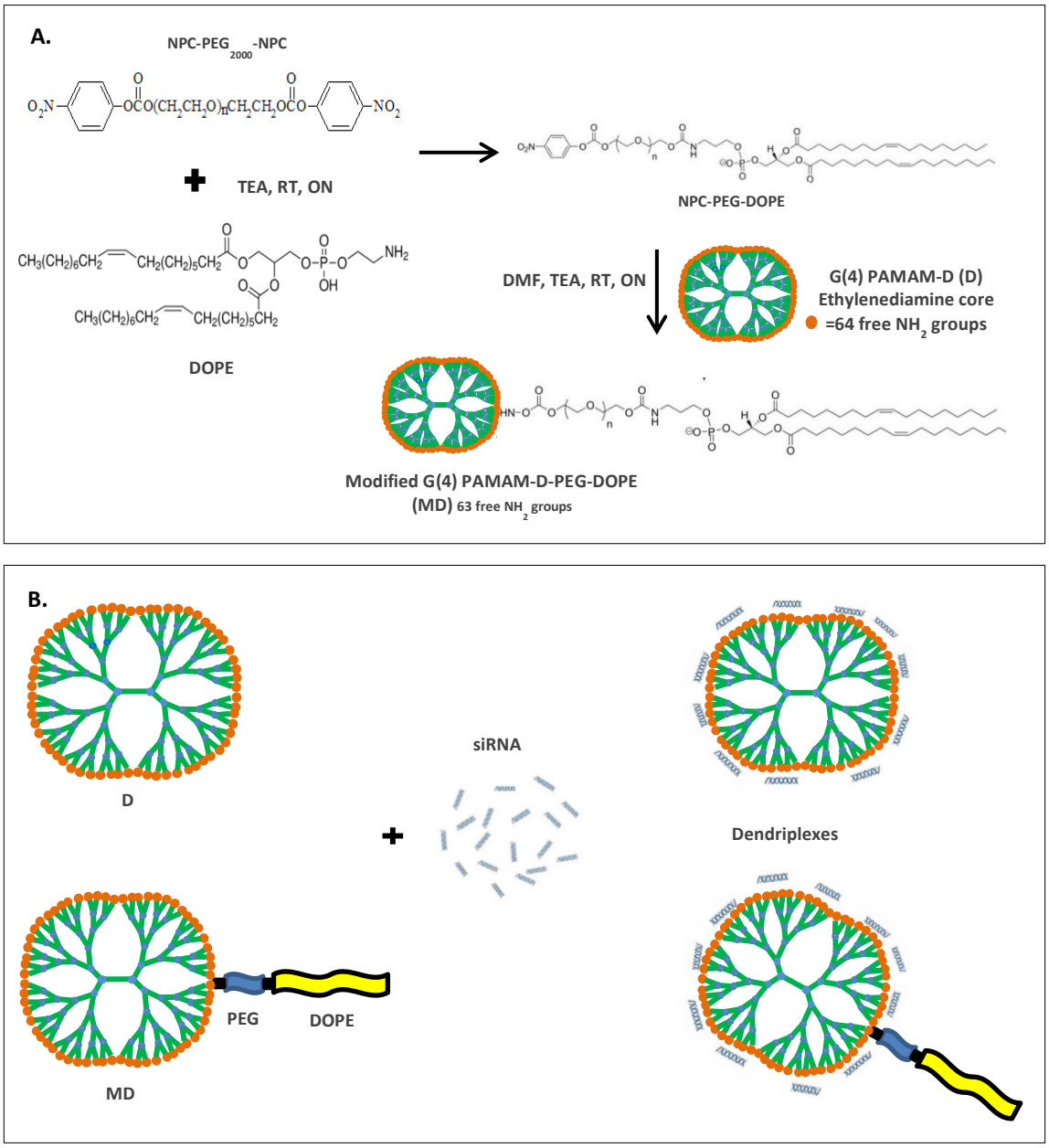

Figure 8: Schematic representation of (A) MD synthesis and (B) Dendriplex formation by complexing siRNA to D and MD nanoparticles*. DMF (N, N-Dimethylformamide),TEA (Triethylamine), RT (room temperature), ON (overnight)*

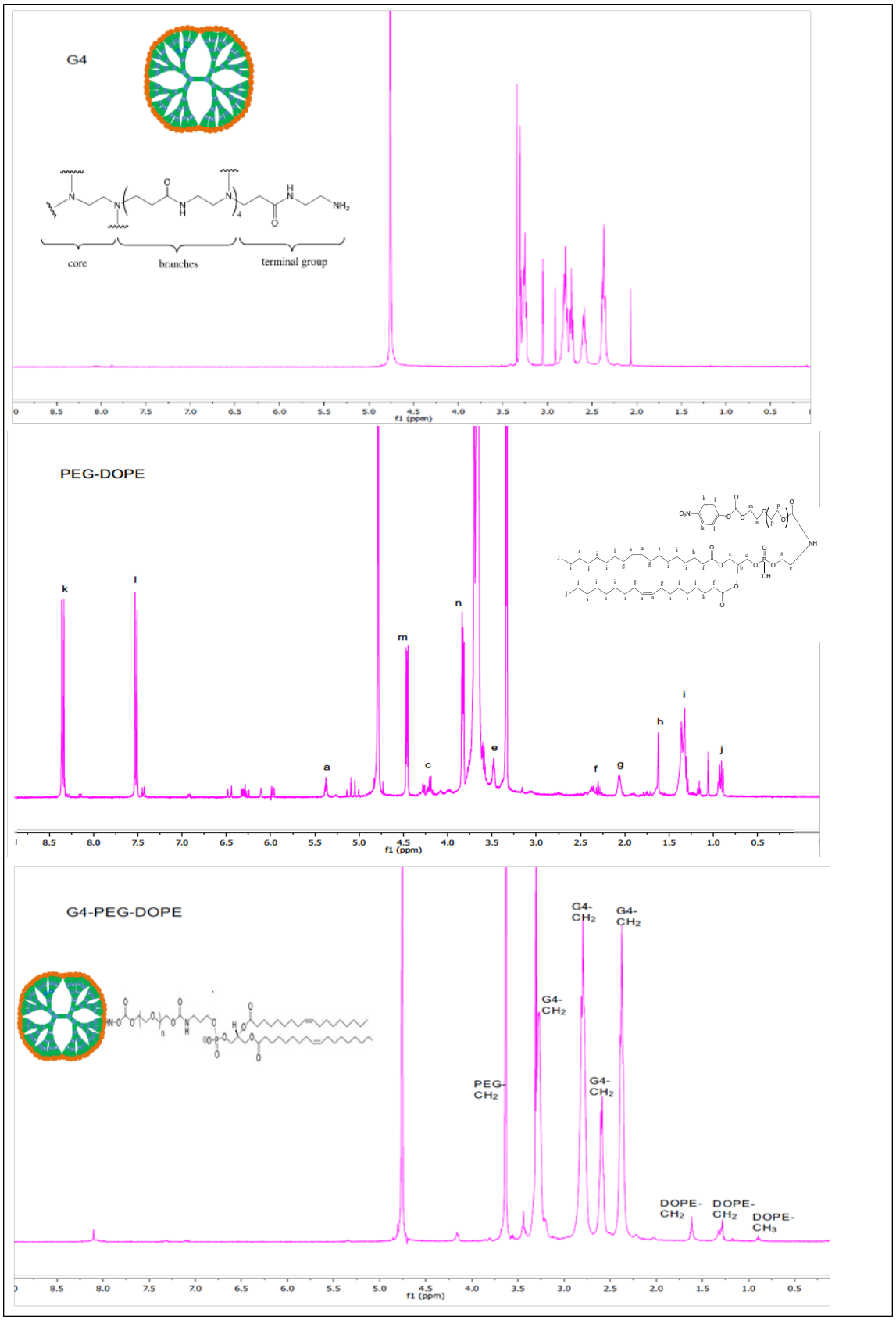

Figure 9: ^{1}H NMR spectra of the starting materials G(4) PAMAM-Dendrimer (D) and NPC-PEG$_{2K}$-DOPE and the modified G(4) PAMAM-Dendrimer-PEG-DOPE (MD).

3.1.1.2 *siRNA binding and dissociation capacities of D and MD nanoparticles.*

The abilities of D and MD nanoparticles to bind siRNA were assayed by agarose gel shift. The D and MD dendriplexes were formed by complexation with a negative control sequence siRNA (siNegative) at different nanoparticle to siRNA ratios (N/P ratios) as described in section 5.2. When positively charged nanoparticles bind to negatively charged siRNA, they prevent the siRNA migrating in the electric field. Hence the siRNA complexing abilities were analysed by gel shift assay a method commonly used to assess siRNA binding affinity to [363]. MD was capable of fully complexing siRNA at an N/P ratio as low as 0.5 whilst D formed complexes from N/P of 1 (**Fig.10**). Thus both nanoparticles condensed siRNA effectively at low N/P ratios. These results confirm the findings of Biswas et al. [140].

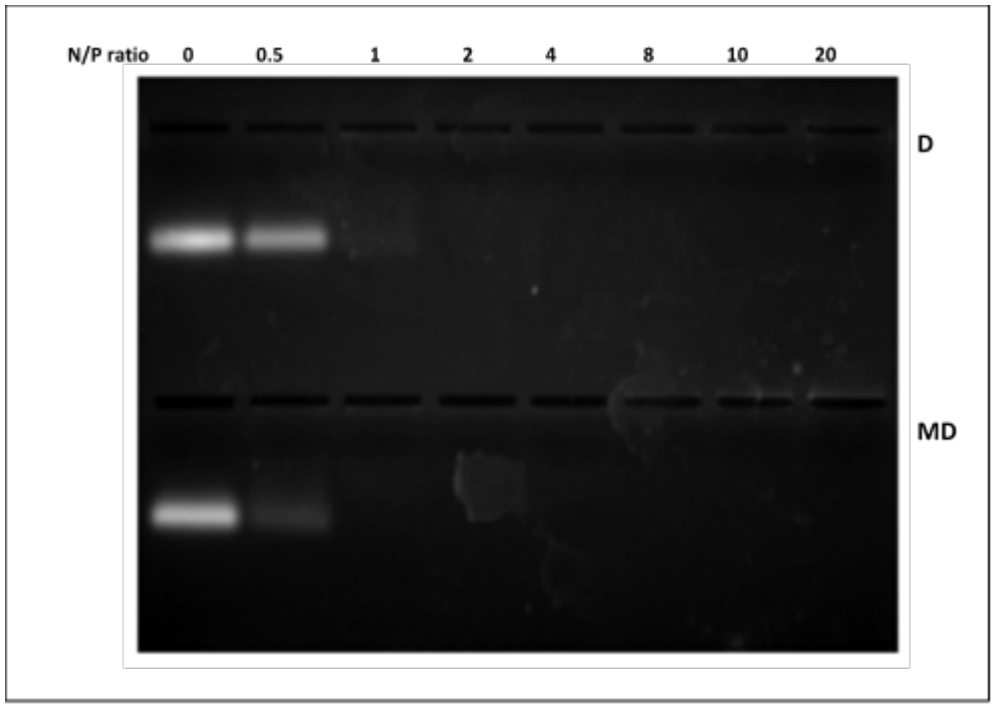

Figure 10: The siRNA binding abilities of nanoparticles (D and MD)*. This was assessed by agarose gel shift. Dendriplexes were formed at different N/P ratios of 0 to 20. siRNA concentration was kept constant at 200ng. The image of unbound siRNA recovered after dendriplex formation and electrophoresis on 2% agarose gel to show siRNA complexation was taken. This image is a representation of three experiments.*

Subsequent to establishing the binding capacity of the various N/P ratios, the nature of the siRNA binding to the dendrimers was further characterised using a RiboGreen™ RNA fluorescent label exclusion quenching assay followed by a heparin sulphate dissociation assay (**Fig.11**).

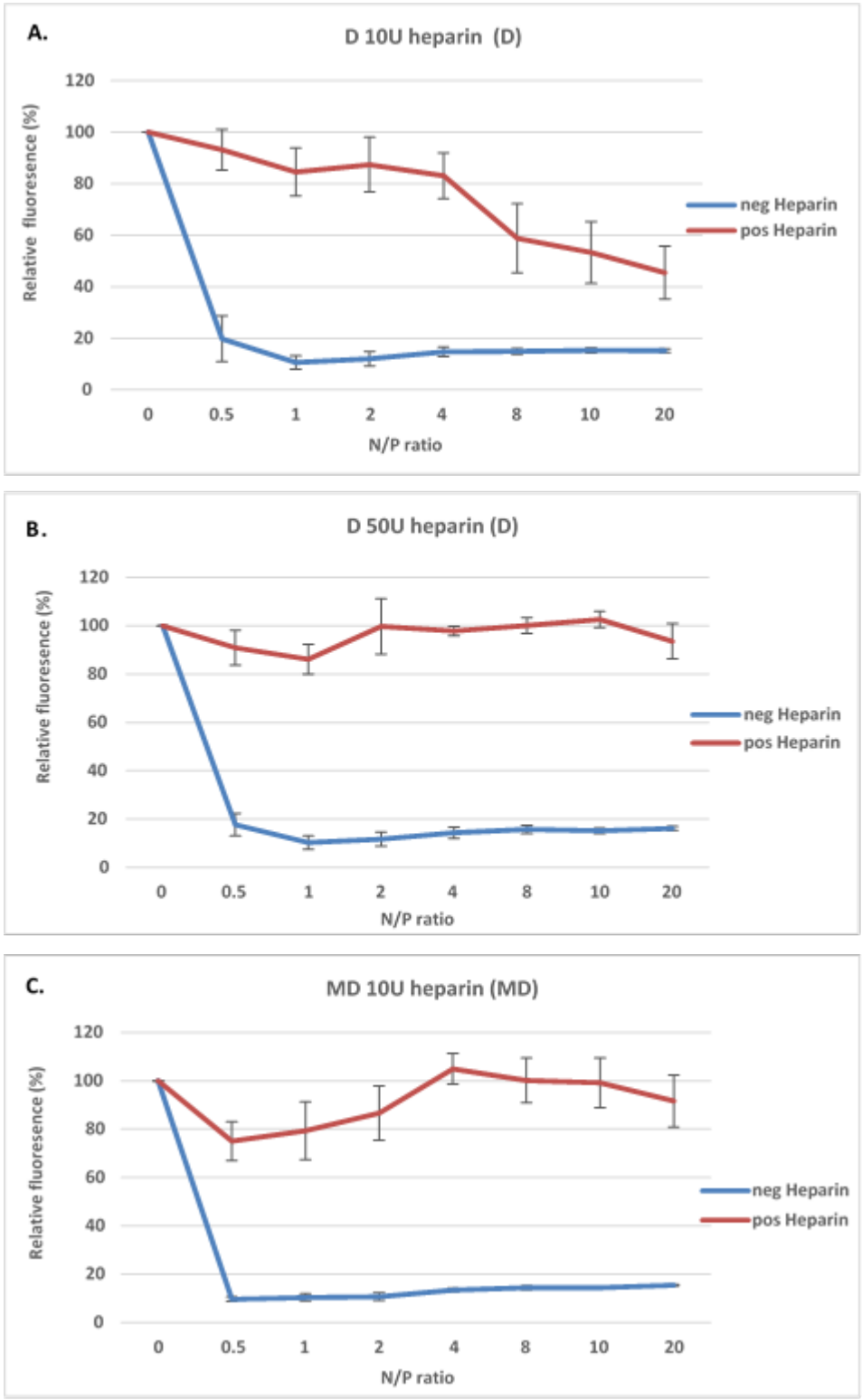

Figure 11: The siRNA binding abilities of D and MD assessed by quenching assay. *D and MD at N/P ratio of 0-20 were formed using 200ng siFITC scramble siRNA. The quenching of fluorescence from siRNA bound RiboGreen™ RNA label was determined. Subsequently reversal of quenching after addition of heparin sulphate was quantified. (A) and (B) siRNA fluorescence quenching for D and fluorescence recovery after addition of 10 and 50U/µg siRNA of heparin sulphate respectively. (C) siRNA fluorescence quenching and recovery for MD in the presence of 10U/µg siRNA of heparin sulphate. Graphs represent three experiments done with 3 technical repeats per experiment.*

A maximum quenching of siRNA fluorescence from N/P ratios of 1 and 0.5 for D and MD nanoparticles respectively was observed, corresponding to the gel shift assay findings above. When 10U/μg siRNA of heparin sulphate was added to disrupt the ionic bonds between the negatively charged siRNA phosphate backbone and the positively charged surface of the nanoparticles, fluorescence quenching of MD was reversed. At the same concentration of heparin, siRNA dissociation from D appeared incomplete at higher N/P ratios from 8 upwards and it required addition of 50U heparin per μg siRNA to reverse quenching at all ratios. This finding suggests that though siRNA is complexed at similar ratios for D and MD, D complexation is tighter.

The siRNA complexing abilities of D were comparable with what has been previously observed [140] however, in this study MD was found to be slightly more effective at binding siRNA (from N/P 0.5) compared to binding only being observed at N/P 2 in the original report. Another discrepancy was observed with heparin sulphate induced dissociation of the dendriplexes. Dissociation of D in this study required 5 times higher concentration of heparin sulphate to achieve complete siRNA recovery than that previously reported for D. Particularly this inconsistency observed for heparin sulfate dissociation might reflect the necessary use of different batches of reagents though this does not entirely explain the same concentration achieving dissociation of MD in both studies.

3.1.1.3 *siRNA protection ability of dendriplexes from degradation in serum*

In the original study, complete protection over 24hrs from serum RNases was observed for both particles at an N/P 10 ratio [140]. Protection of siRNA from RNases is a critical area for any vehicle that will carry siRNA within an implanted scaffold for extended periods and therefore was explored with a serum protection assay over a longer period. D and MD-siNegative dendriplexes were incubated in 50% FBS over a period of 10 days. The ability of the dendriplexes to protect siRNA from RNases at different N/P ratios in serum was determined by agarose gel after 0.5% sodium dodecyl sulfate (SDS) decomplexation (**Fig.12**). Naked siRNA (N/P ratio 0) was completely degraded in less than 24hrs. This is expected and has been reported in many other studies [43, 140, 204, 364, 365]. There was limited protection observed for both D and MD at N/P ratios 0.5 and 1 whilst substantial siRNA presence was detected up to 10 days in both D and MD samples for higher ratios (N/P 2-20). The results suggest that the higher N/P ratios efficiently condense and protect siRNA from degradation. Previous RNA degradation

studies have generally considered serum protection/stability of siRNA over a short time period (24hrs) [140, 204, 364, 365]. siRNA appeared to be protected slightly more effectively in the D samples which correlates with the stronger interaction with siRNA that was observed in the heparin stability assay (**Fig.11**). As the higher N/P ratios (2-20) for both D and MD provided siRNA protection for longer compared to the lower N/P ratios (0.5-1), these ratios were included in follow up experiments. These findings suggest that dendrimer based protection of siRNA is suitable for controlled release studies *in vivo*.

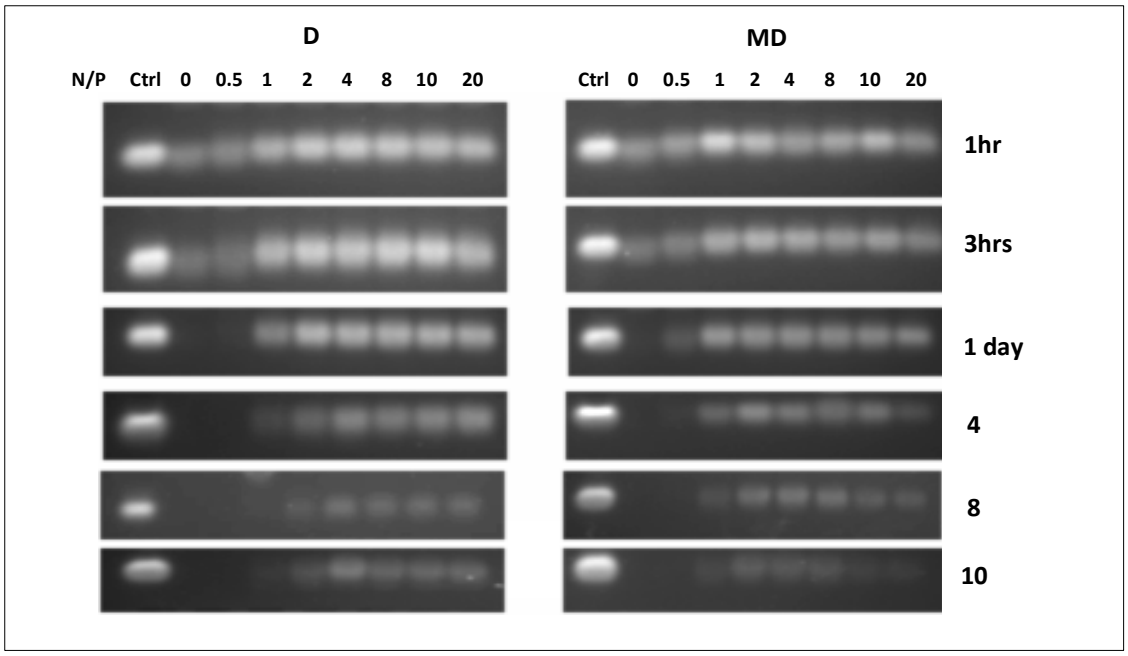

Figure 12: siRNA protection from degradation by D and MD nanoparticles*. Dendriplexes formed with 200ng siNegative, at N/P ratio of 0-20. D and MD dendriplexes were incubated with 50% FBS over 10 days. After denaturation in 0.5% SDS, 100ng equivalent siRNA was resolved on 2% agarose gel. Fresh siRNA (100ng) was loaded as a control (Ctrl) at each time point. Image is a representation of three experiments.*

3.1.1.4 *Cytotoxicity analysis of D and MD dendriplex*

The potential cytotoxicity of D and MD dendriplexes was assayed with HT1080 cells (**Fig.13**). Both D and MD dendriplexes at N/P ratio of 2-8 showed no cytotoxic effect relative to siRNA alone. MD at N/P ratio of 10 and 20 showed a non-significant reduction in viable cells by 5% and 19% respectively. The inherent cytotoxicity effect of the dendriplexes alone, with no siRNA complexation, on C166-GFP and A549 cells, was previously shown to be non-cytotoxic [140]. In this study dendrimers complexed to siRNA were shown to have a similar effect.

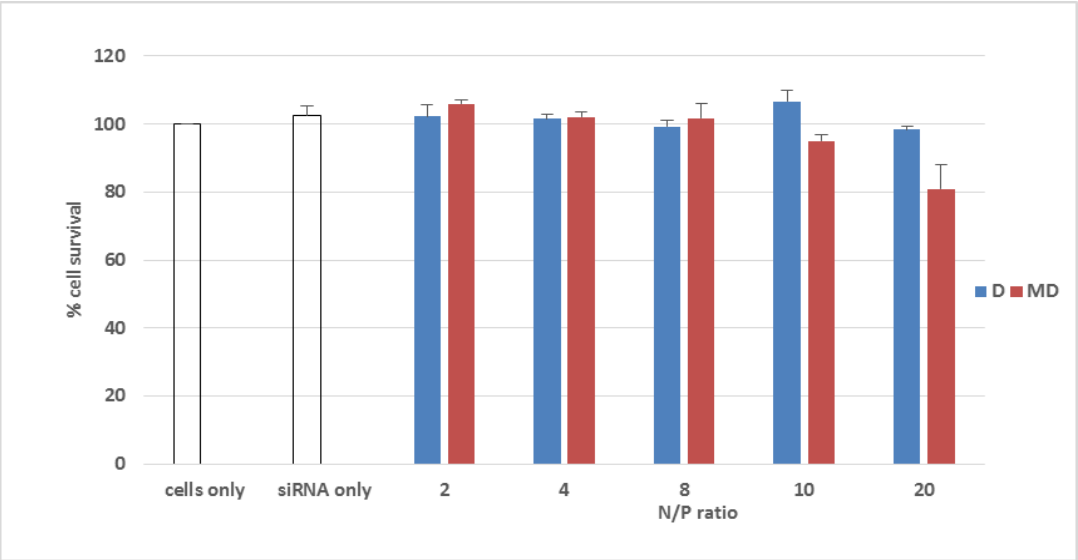

Figure 13: The cytotoxic effect of dendriplexes D and MD on HT1080 cells. *D and MD were complexed with scrambled siNegative at N/P ratios of 2-20. After 4hr transfection and 48hr incubation cells were assayed for cell survival using the Cell Titre Glo® assay. Untreated cells (cells only) and free siNegative (siRNA only) treated cells were included as controls. Percentage cell survival is represented as standard error mean of three biological repeats with 3 technical repeats per experiment.*

3.1.1.5 *Cellular uptake and transfection efficacy of dendriplexes*

Initially, the ability of dendriplexes at different N/P ratios to deliver siRNA into cells was determined with a fluorescently labelled scrambled siRNA sequence with fluorescein isothiocyanate (siFITC), procedure described in section 5.7. Fluorescent micrographs (**Fig.14**) showed that there was no discernible uptake of naked siFITC but that D and MD-siFITC dendriplexes were equally capable of efficiently delivering siRNA into cells for all N/P ratios as evidenced by the bright fluorescence of all cells which was more pronounced in N/P 8. In comparison to the previous report where only N/P=10 dendriplexes made with siRNA-Cy5 were considered for transfection efficiency, and it was observed then that D showed less internalization of D dendriplexes compared to MD [140]. The reason for the apparent reduction in uptake at N/P 20 is not clear but possibly reflects a tighter interaction of the siRNA with the dendrimer such that dissociation in the cytoplasm is inhibited.

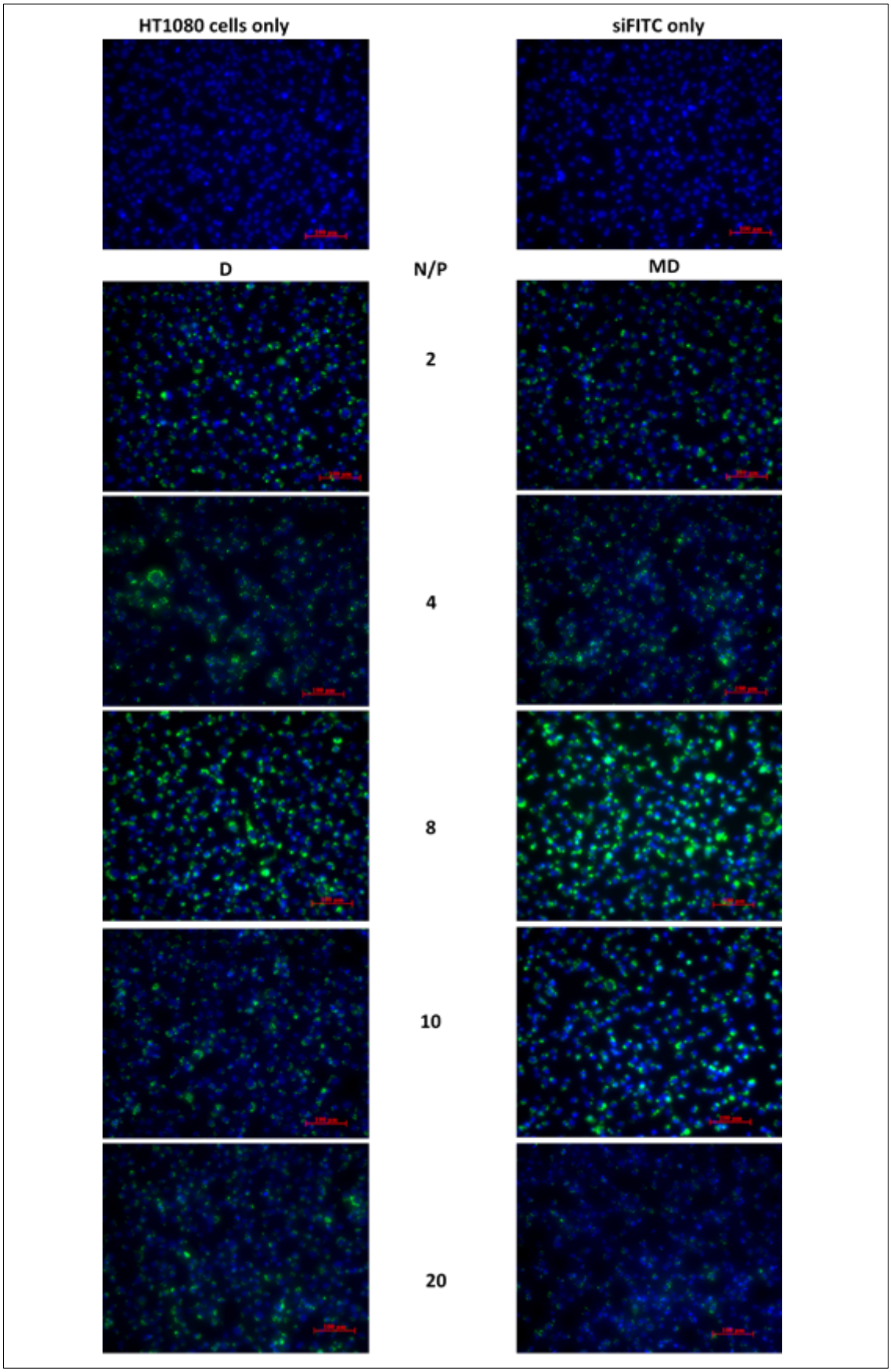

Figure 14: Uptake of siFITC D and MD dendriplexes at N/P of 2-20*. Dendriplexes were made with 200ng siFITC scramble siRNA. Hoechst stained nucleus (blue) and siFITC (green). Untreated cells served as negative control. Scale bar = 100µm.*

Though uptake is of course necessary for delivery, the siRNA delivered into the cell must be efficiently released to interact with its target mRNA sequences in the cytoplasm. The efficacy of delivery was assayed using a mixture of commercial siRNA sequences (siDeath) that have been shown to elicit cell death after their cellular delivery allowing for efficacy to be determined by measuring cell viability after transfection. When naked siRNA or D dendriplexes at any N/P ratio were delivered as described in section 5.8.1, cell viability relative to untreated cells or those receiving the scrambled siNegative sequence did not decrease (**Fig.15A**). MD dendriplexes elicited significant decreases in cell viability at N/P ratios of 4 and 8 relative to their equivalent siNegative complexes reaching a maximum at 8 with a 36 ± 2% reduction in viable cell number ($p<0.05$ vs siNegative) (**Fig.15B**). At the higher N/P ratios of 10 and 20, similar levels of cell death to N/P ratio of 8 were observed but significance against their siNegative controls were lost. This presumably reflects the cytotoxicity observed above (**Fig.13**) with reductions in viability for the MD dendriplexes with siNegative at N/P ratios 10 and 20 of 12 ± 7% and 24 ± 13% respectively. Because N/P of 8 showed the most efficient siRNA delivery, no cytotoxic effect and most efficacious delivery of the siDeath, it was the chosen ratio to use throughout the following experiments that further characterized the dendrimers.

3.1.1.6 *TEM analysis of D, MD and dendriplexes*

Structural analysis of the D and MD nanoparticles at N/P ratio of 8 by transmission electron microscope (TEM) was carried out (**Fig.16A**). MD nanoparticles were larger than D with diameters of 33 ± 2nm and 18 ± 1nm respectively (**Fig.16B**). When complexed to siRNA the size of D increased significantly to 24 ± 1nm, and that of MD increased to 44 ± 4nm ($p<0.01$ vs uncomplexed dendrimers). The sizes of D and MD nanoparticles without siRNA complexation are similar to what was previously seen in the original study [140]. Additionally, it was observed in this present study that when complexed to siRNA the dendriplexes nearly double in size.

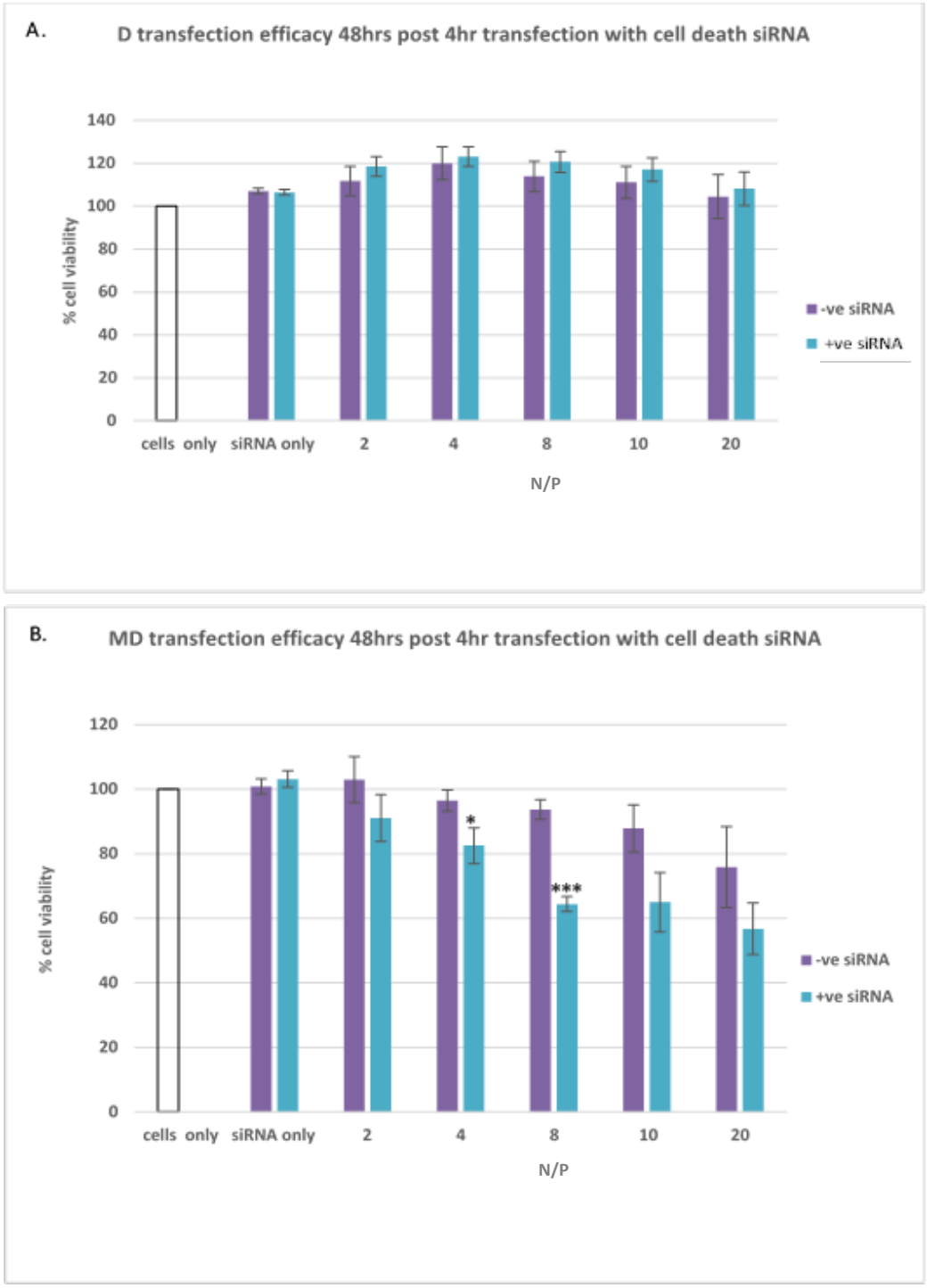

Figure 15: Transfection efficacy of D and MD dendriplexes determined by cell death assay*. D (A) and MD (B) nanocomplexes at N/P ration of 2-20 were formed with either 200ng siDeath (+ve siRNA) or siDeath-Negative control (-ve siRNA). Cells only and siRNA only cells treated with free +ve siRNA or -ve siRNA served as negative controls. After transfection, cell viability was determined with the Cell Titre Glo® assay. Percentage cell survival is represented as standard error mean of three biological repeats with 3 technical repeats per experiment. * p<0.05 and *** p<0.005 vs cells treated with free +ve siRNA only.*

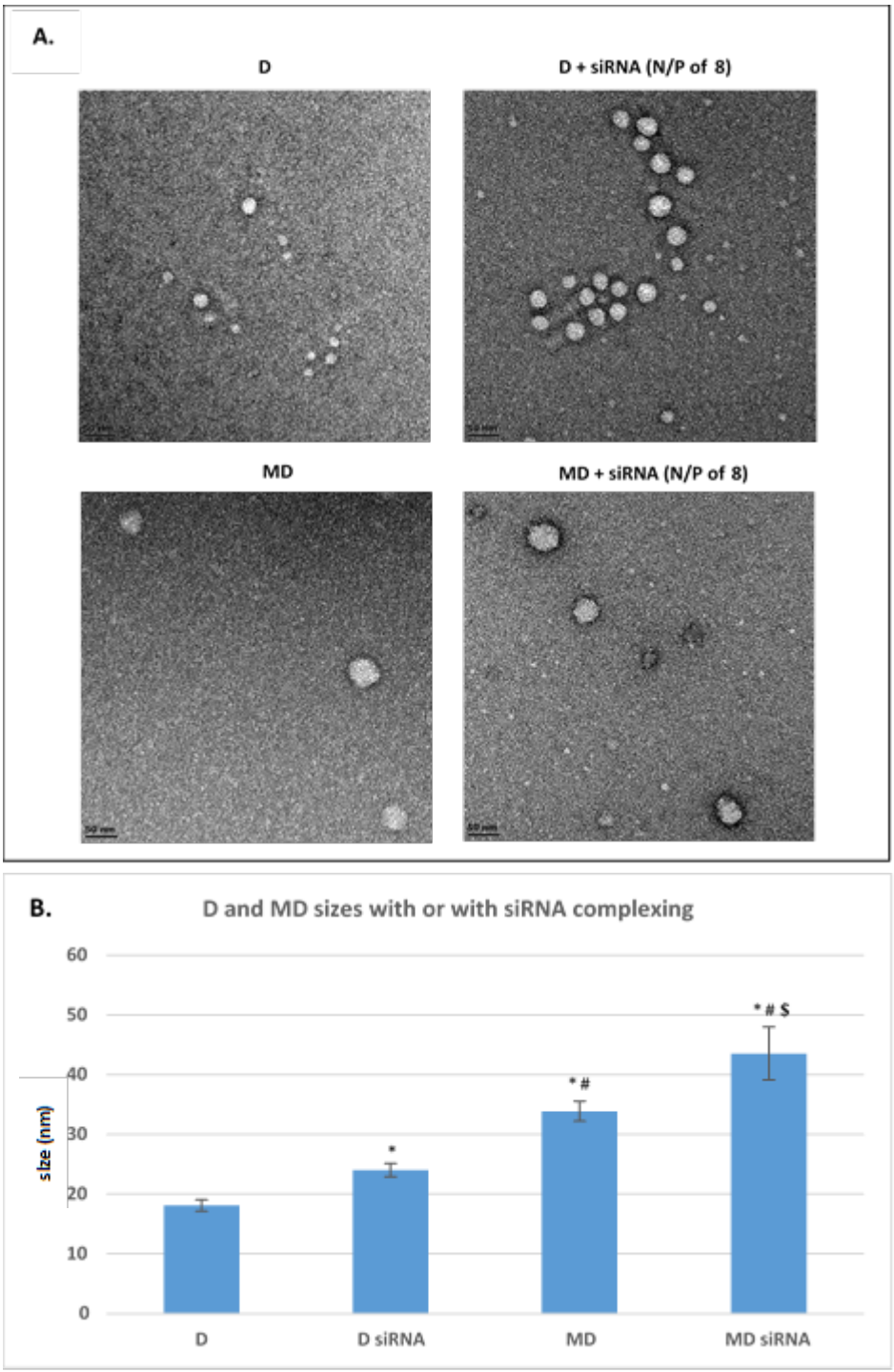

Figure 16: Transmission electron microscopy of dendrimer nanoparticles. *TEM micrographs (A) of D, MD and their respective siNegative dendriplexes formed at (N/P ratio of 8) using 200ng siRNA. (B) The nanoparticles average diameter in nm. 20 nanoparticles were analysed per group. *p<0.0005 vs D, #p<0.0005 vs D siRNA. $p<0.05 vs MD. Scale bar =50nm.*

3.1.1.7 *Complementary assays of D and MD dendriplex uptake and efficacy*

D and MD dendriplexes at N/P ratio of 8 were further investigated for siRNA delivery efficiency by flow cytometry to assay uptake of siFITC by HT1080 cells. It can be clearly seen (**Fig.17A**) that naked siRNA is not taken up at a detectable level but is when complexed to both D and MD, 24hrs after transfection. There was no significant difference noted in the uptake amount between D and MD. When A549 cells were transfected with siFITC-dendriplexes and analysed 1hr and 4hrs post transfection by Biswas et al [140] a higher siRNA up take with MD than D was reported which was not observed in this study.

An alternative reporter assay was established to confirm the above findings of the cell death assay. A stably transfected cell line of HT1080 cells expressing green fluorescent protein (HT1080-GFP cells) under the control of the CMV promoter (**Appendix 1**) was generated following the procedure described in 5.5.1. The HT1080-GFP clones with varying levels of GFP expression were made (**Appendix 2A**). Clone 9 with the highest GFP expression was chosen for use in *in vitro* GFP expression experimental analysis throughout this study.

The established HT1080-GFP cells were used to analyse the knockdown of the GFP gene by dendriplexes made with siGFP at N/P of 8. Both flow cytometry and immunoblots were employed to quantify the knockdown. The geometrical mean analysis determined by flow cytometry (section 5.8.2.1) showed a reduction of GFP based fluorescence by both D and MD dendriplexes in the HT1080-GFP cells by 25% and 37% 48hrs post transfection as seen in **Fig.17B** ($p<0.05$ and $p<0.01$ vs their respective D and MD-siNegative dendriplexes). 72hr knockdown effect was included to determine any further decrease in GFP KD effects that may occur over time. The transfection efficacy had started to reduce slightly by 72hrs after transfection with 24.5% and 32% for D and MD (**Appendix 3**) however the GFP knockdown remained significant ($p<0.01$). As the D particle showed no efficacy of gene knockdown when assessed with the cell death assay (**Fig.15**) and a weaker effect when assayed for GFP inhibition (**Fig.17**), it was decided to continue only with the MD particle in downstream experiments.

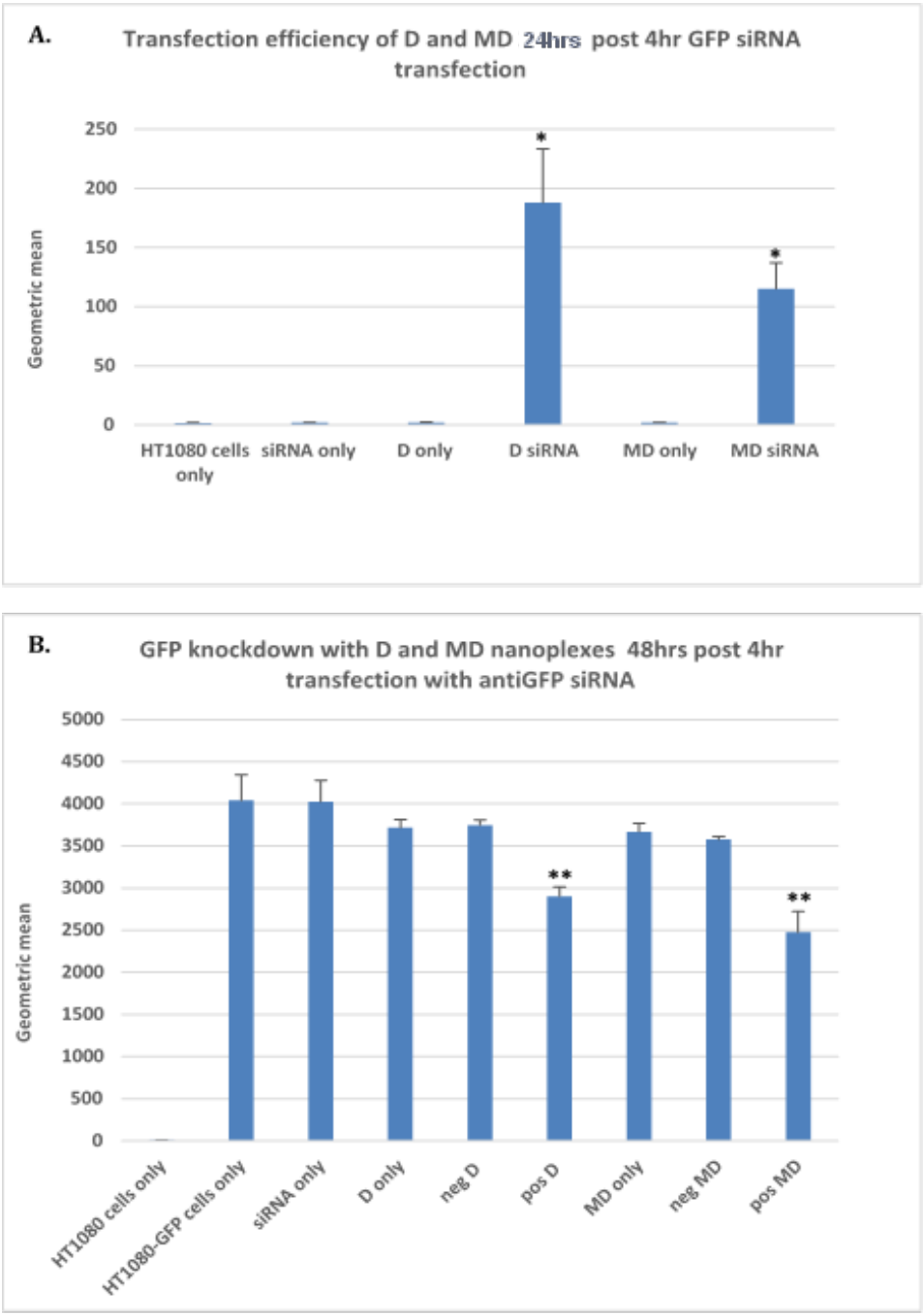

Figure 17: The transfection efficiency and efficacy of D and MD nanocomplexes (N/P of 8). *(A) The ability of D and MD to efficiently deliver siFITC into HT1080 cells. Dendriplexes were made with 200ng siFITC. (B) The efficacy of the delivered siGFP with D and MD on HT1080-GFP cells. Here dendriplexes were made with 500ng siGFP (pos D/MD groups) or siNegative (neg D/MD groups). Results were analysed by flow cytometry three biological repeats with 3 technical repeats per experiment. * p<0.05 vs siRNA only control group and ** p<0.005 vs respective D/MD-siNegative dendriplexes control.*

The GFP knockdown by MD was further confirmed by immunoblot in **Fig.18**. Initially before western blot analysis of GFP expression could occur the co-probing of GFP and loading control β-Tubulin, as well as the amount of protein to load for detection, was optimised (see section 5.10 and **Appendix 2B**). Once the western blot was optimised,

HT1080-GFP cells were transfected with siGFP- dendiplexes and 48hrs post transfection whole cell lysate was probed with an anti-GFP monoclonal antibody (following procedure in section 5.8.2.2). Two bands were observed at 27 and 30 kDa which accords with the molecular weights reported for GFP according to the manufacturer's product description [366, 367]. Both bands were quantified by densitometry and showed a significant 32% knockdown of GFP protein by MD ($p<0.05$ vs naked siRNA) and a 69% knockdown with Lipofectamine® RNAiMAX ($p<0.01$ vs naked siRNA). Thus, the knockdown efficacy of MD was shown to be reproducible with the two different assays (cell death assay and GFP knockdown) but also that the commercial liposomal carrier used as a positive knockdown control in this experiment was more efficacious than MD ($p<0.05$).

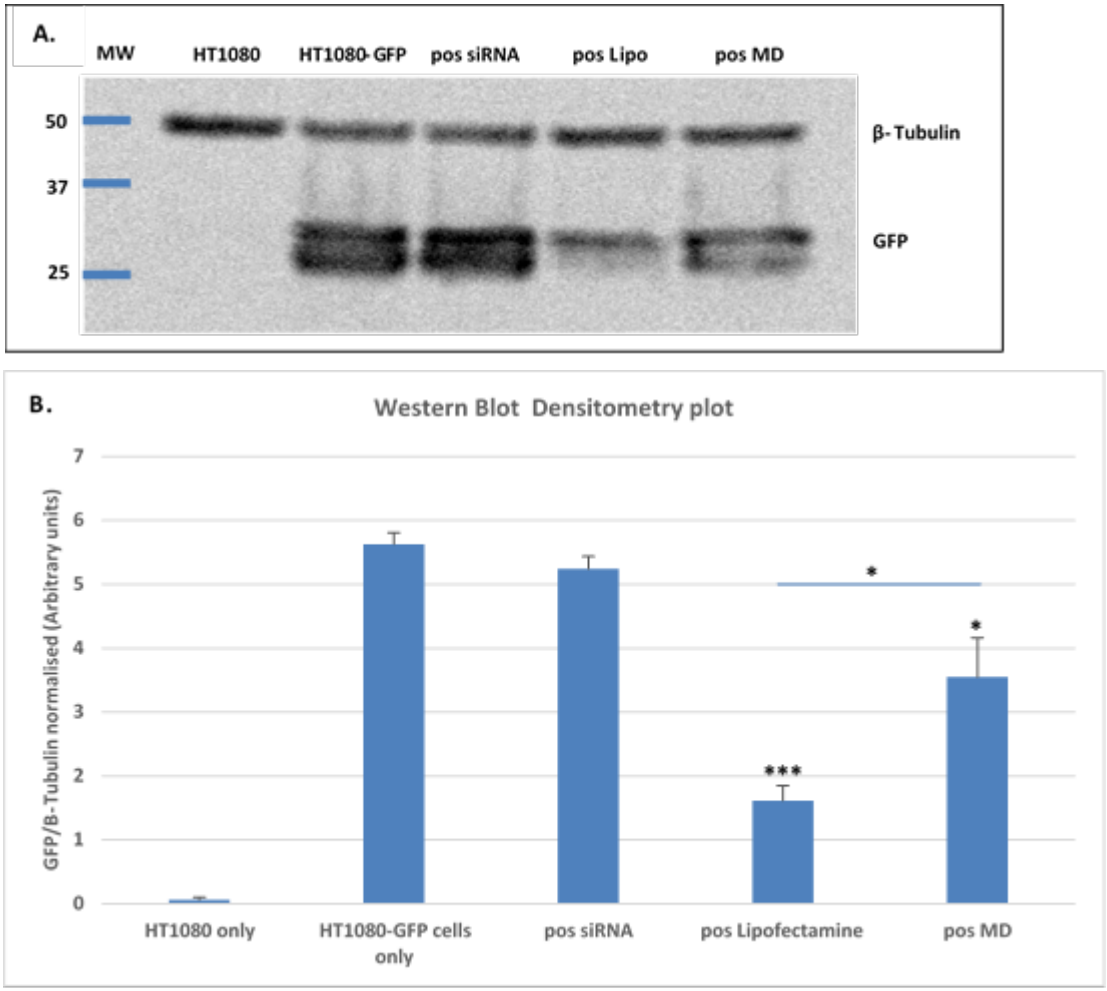

Figure 18: GFP knockdown in GFP-HT1080 cells with MD (N/P of 8) dendriplexes 48hrs post transfection with siGFP*. (A) Immunoblot of GFP with β-tubulin as a loading control. (B) Densitometric analysis of GFP levels normalised to β-tubulin levels. HT1080-GFP cells were either untreated or treated with naked siGFP Lipofectamine® RNAiMAX as a positive control or MD dendriplexes made with 200ng siRNA. Image and graph represents three biological repeats with 3 technical repeats per experiment. * $p<0.05$ (pos siRNA<MD<Lipofectamine) and *** $p<0.0005$ vs Lipofectamine. MW= molecular weight marker in kDa.*

Both D and MD dendrimers have the ability to efficiently deliver siRNA in HT1080 cells with minimum cytotoxicity, however this high siRNA delivery efficiency does not translate to efficacious gene knockdown with the D dendrimer, as shown by the nanoparticle's inability to cause cell death with siDeath and achieve a lower GFP knockdown compared to that of MD. When D and MD siGFP dendriplexes were used on a stably expressing GFP C166 cell line in the original study, a 10 and 22% GFP knockdown respectively was observed [140]. A similar but more pronounced knockdown with MD of around 35% ± 3% was observed across all assays in this study. This may reflect the use of HT1080 cells. As noted above, the low efficacy of D can possibly be attributed to the stronger interaction of siRNA with D as indicated by the requirement of high levels of heparin sulphate to achieve dissociation. This may have resulted in the failure of D dendriplexes to effectively disassociate and release siRNA into the cytoplasm to for efficacious knockdown in contrast to its counterpart MD.

Adding the PEG and lipid DOPE modification to the dendrimer achieved adequate siRNA condensation/binding, non-cytotoxicity, improved siRNA delivery and siRNA dissociation capabilities as well as gene knockdown effect compared to D. In addition, it is possible that this modification improved the endosomal escape ability of MD dendriplexes and therefore played a role in the improved gene knockdown efficacy compared to D. Even though MD achieved higher efficacy, it is important to note that the GFP knockdown effect was of lower magnitude when compared to Lipofectamine® RNAiMax. Thus though it was considered viable to proceed with MD due to its good biocompatibility and pronounced protection against RNase degradation as a potential vehicle for sustained delivery from a hydrogel, it was considered prudent to also assess commercial liposomal vehicles due to their high efficiency. Therefore Lipofectamine® RNAiMAX and another related liposome based carrier (Invivofectamine® 3.0.) were also assessed in downstream experiments.

MD was theoretically modified with PEG-DOPE in a 1 to 1 molar ratio, because of the multivalent nature of PAMAM (64 free reactive amines) other molar ratios, different conjugates as well as different lipid molecule lengths, can be explored to possibly optimise the efficacy of this G(4)-PAMAM-D. The effects of varying lengths of hydrophobic alkyl lengths on G(3) dendrimer's efficacy was tested *in vitro* by one group [177]. Another looked at the toxicity effects of a variety of PAMAM to lipid ratios as well as PAMAM to PEG molecules was tested by another group however no biological effects of these modifications on the nanoparticle was verified *in vitro* [169], suggesting that many multiple modifications can still be done to further interrogate the efficacy of this

dendrimer. It should also be noted at this stage the work reported by Biswas et al. [140] was confirmed by the findings described above with only minor differences.

3.1.2 Lipid nanoparticles *In vitro* characterization

The two lipid based vehicles Lipofectamine® RNAiMax and Invivofectamine® 3.0 had recently been shown to have substantial efficacy after direct delivery to the mouse heart *in vivo* by Giacca et al. 2016 [213]. Although Lipofectamine and Invivofectamine® 3.0 are established transfection reagents commonly used in research as positive controls in *in vitro* transfection assays, characterizing their siRNA binding, RNase protection, toxicity and confirming their efficacy *in vitro* in our hands was essential prior to exploring their utility for encapsulation in and release from hydrogels.

3.1.2.1 *siRNA binding capacities of Lipofectamine® RNAiMAX and Invivofectamine® 3.0 nanoparticles*

Lipofectamine® RNAiMAX and Invivofectamine® 3.0 nanoparticles' siRNA binding abilities were assayed by gel shift assay as was done for the dendrimers and as described in 5.3.1. The amount of Lipofectamine® RNAiMAX used in transfections in this study (0.6µl Lipofectamine® RNAiMAX / 200ng siRNA communicated with Giacca laboratory for the ratios used in their *in vivo* study [213]) and the commercially recommended undiluted concentration of Invivofectamine® 3.0 (0.36µl Invivofectamine® 3.0 / 200ng siRNA) were tested. The agarose gel shift **Fig.19A** and quantified in **Fig.19B** shows that Lipofectamine® RNAiMAX does not stably condense siRNA whilst Invivofectamine® 3.0 complexed 70% of the loaded siRNA. However, when increasing amounts of Lipofectamine® RNAiMAX (in the range of 0.6-5µl / 200ng siRNA) were used to complex the siRNA, stable siRNA condensation begins to occur from 3µl / 200ng siRNA with full complexation at 5µl/200ng siRNA (**Appendix 4**). Unfortunately, in this study, these high concentrations of Lipofectamine were found to be cytotoxic to the HT1080 cell line substantial cytotoxicity of cells was observed and therefore the 0.6µl / 200ng dosage was used throughout the study.

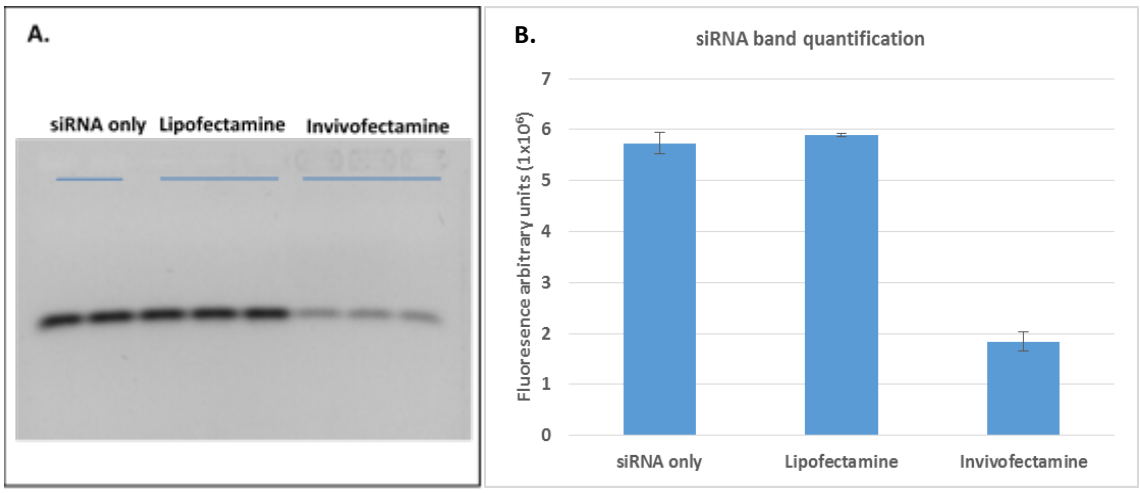

Figure 19: The siRNA binding abilities of Lipofectamine® RNAiMAX and Invivofectamine® 3.0: *This was assessed by agarose gel shift. To show siRNA complexation image of unbound siRNA recovered after electrophoresis of Lipofectamine® RNAiMAX and Invivofectamine® 3.0 nanocomplexes made with 200ng siNegative on 2% agarose gel was taken (A). (B) shows quantification of the siRNA bands. Image and graph represent an experiment done with 3 technical repeats of nanocomplexes.*

3.1.2.2 *siRNA protection ability of nanocomplexes from degradation in serum*

The ability of the lipid nanocomplexes to protect siRNA from serum RNases was again assayed by incubation of complexes in 50% FBS over 10 days following the protocol in section 5.4. Lipid nanocomplexes were formed by complexing 200ng siNegative with 0.6µl siRNA for Lipofectamine® RNAiMAX and with the recommended 0.1mg/ml Invivofectamine® 3.0. Lipofectamine® RNAiMAX at the concentration used did not provide siRNA protection in serum as siRNA was completely degraded in 24hrs, thus at least the same rate as naked siRNA indicating no meaningful protection (**Fig.20**). The Lipofectamine® RNAiMAX serum protection of siRNA seen here supports the siRNA complexing data (**Fig.19**) confirming that because of the weak siRNA condensation ability it is unlikely to effectively protect siRNA from degradation. Invivofectamine® 3.0 had a curious pattern of protection. A substantial proportion of the siRNA was degraded by 24hrs but ≈10% of siRNA remaining at that time point persisted over the entire period assayed. The RNA binding assessment by gel shift and their protection against RNase for Lipofectamine® RNAiMAX and Invivofectamine® 3.0 particles has not to our knowledge been reported before. Others have shown the complexing ability [368] of different types of lipid nanocomplexes as well as their ability to protect siRNA in serum for periods up to 24hrs [369, 370] and 48hrs [371] whereas here extended 10 day period was considered. This study's findings show that the binding and the protection against RNase of the lipid based particles is much more reduced relative to the MD. However, it

was not clear what level of knockdown from the RNase resistant siRNA from Invivofectamine® 3.0 preparations might be achieved.

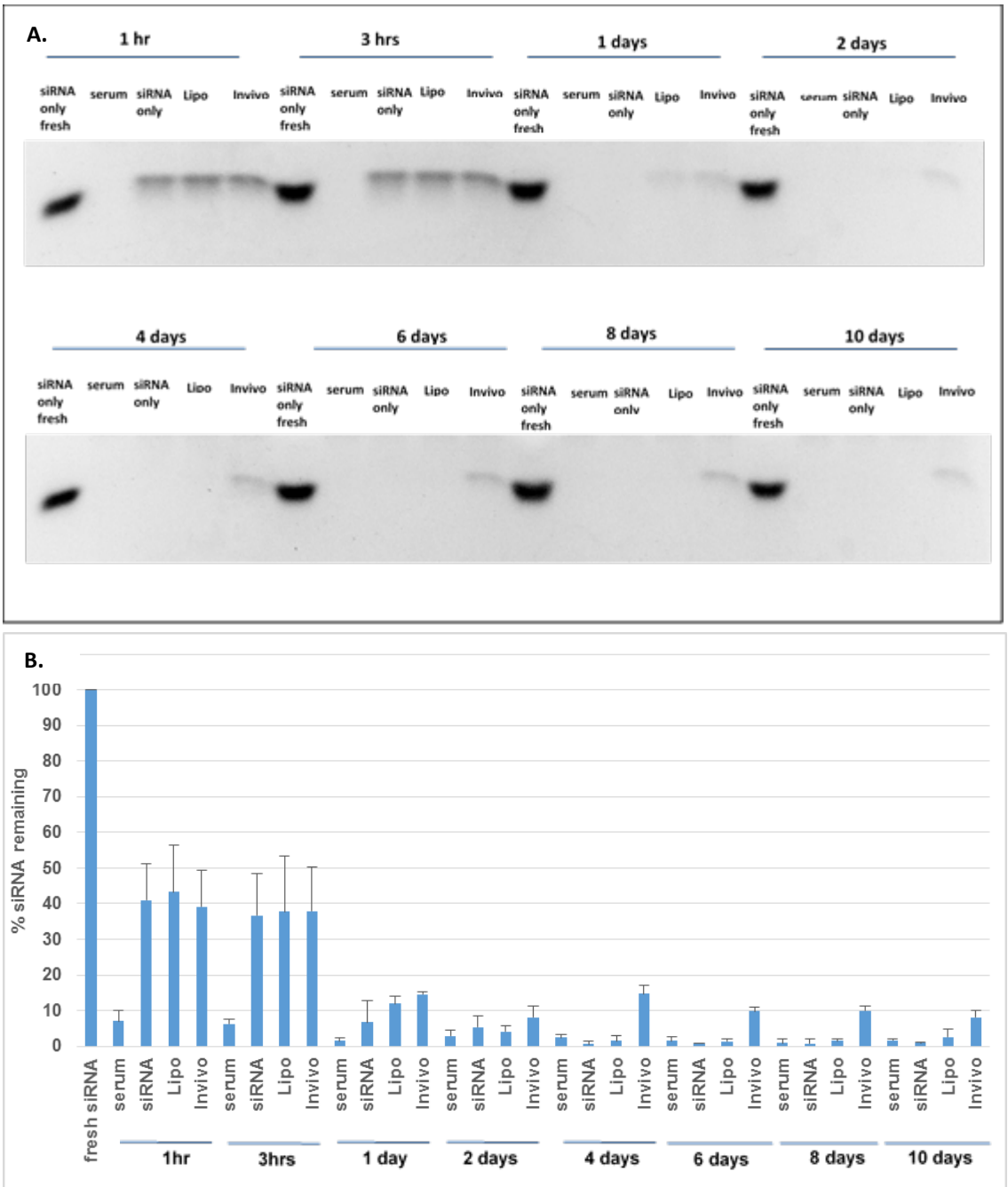

Figure 20: siRNA protection from degradation by Lipofectamine® RNAiMAX and Invivofectamine® 3.0 nanoparticles. *Nanocomplexes were made with 200ng siNegative, and incubated with 50% FBS over 10 days. After denaturation in 0.5% SDS, 100ng equivalent siRNA was resolved on agarose gel and imaged (A). Fresh siRNA (100ng) was loaded as a control at each time point. (B) Shows quantification of the remaining siRNA. Image and graph represent 2 experimental repeats. Lipo and Invivo = Lipofectamine® RNAiMAX and Invivofectamine® 3.0*

3.1.2.3 *Cytotoxicity analysis of Lipofectamine® RNAiMAX and Invivofectamine® 3.0 nanocomplexes*

Nanocomplexes made with siNegative were tested for cytotoxicity on HT1080 cells **Fig.21**. Invivofectamine® 3.0 showed no signs of cytotoxicity whilst Lipofectamine® RNAiMAX showed a very minimal (6.5 ± 1%) but significant reduction in cell viability ($p<0.001$ vs untreated cells). Cationic transfection reagents such as Lipofectamine with a high transfection efficiency have been associated with high cell cytotoxicity [372, 373]. Lipofectamine® RNAiMAX has been shown in one particular study to have cell type dependent cytotoxicity [374]. When Lipofectamine® RNAiMAX nanocomplexes made according to manufacturer specifications complexing single-stranded oligonucleotide were used to transfect various cells it displayed a relative high transfection efficiency as well as cytotoxicity of 20% [374]. An interesting observation in this study is that of the 10 cell lines were considered in the study, 7 of the cell lines where Lipofectamine® RNAiMAX exposure resulted in various levels of cytotoxicity were cancer cells. It is also important to note that single stranded nucleotides were used in this screening study. Given that the cells used in this study are also cancer cells and a low of toxicity was observed, it may suggest though Lipofectamine® RNAiMAX is efficacious it may have toxic effects in cancer cells.

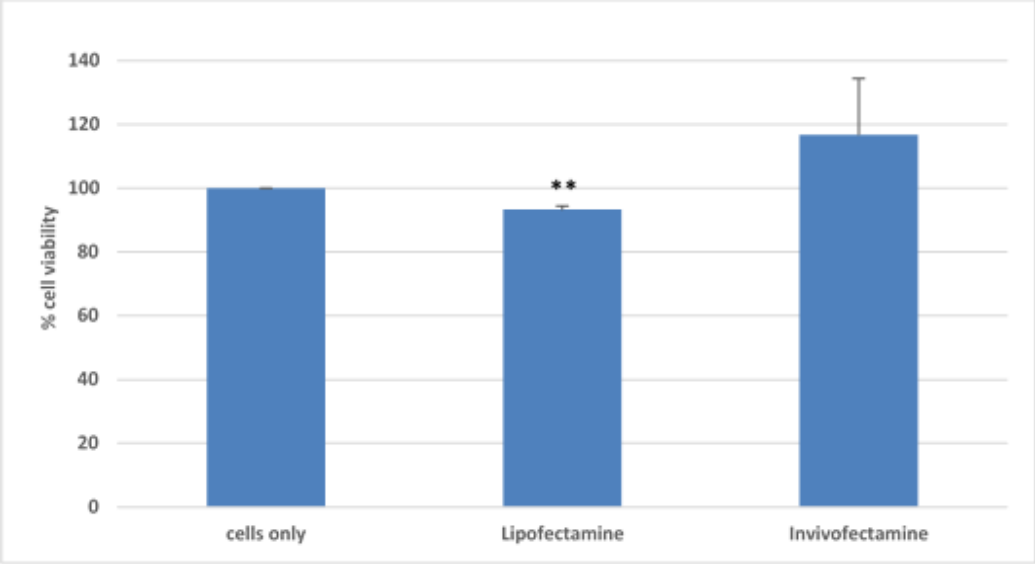

Figure 21: The cytotoxic effect of Lipofectamine® RNAiMAX and Invivofectamine® 3.0 nanocomplexes on HT1080 cells. *Cells were treated with nanocomplexes made with 200ng siNegative. After 4hr transfection and 48hr incubation cells were assayed for cell survival using the Cell Titre Glo® assay. Untreated cells (cells only) were included as control. Percentage cell survival is from three biological repeats with 3 technical repeats per experiment. * p<0.005 vs cells only.*

3.1.2.4 *Gene knockdown effects, Lipofectamine® RNAiMAX and Invivofectamine® 3.0 nanocomplexes*

The efficacy of Invivofectamine® 3.0 and Lipofectamine® RNAiMAX nanocomplexes made with siGFP-Cy3 (1000ng) was determined by GFP knockdown in HT1080-GFP cells. MD knockdown was repeated in this experiment for direct comparison with the lipid nanoparticles. The GFP levels measured by flow cytometry (**Fig.22**) shows that MD, Lipofectamine® RNAiMAX and Invivofectamine® 3.0 resulted in 25%, 70% and 43% GFP knockdown ($p<0.01$) when compared to their respective nanocomplex negative controls. Though Lipofectamine® RNAiMAX has the lowest level of siRNA binding and serum protection capacity (**Figs.19 to 21**), it was the most efficacious at gene knockdown in these 2D *in vitro* assays. MD has better siRNA condensation and serum protection however compared to lipid nanocomplexes it is less effective at gene knockdown but more effective than D. Invivofectamine® 3.0 showed some degree of binding and protection and an intermediate level of gene knockdown. As all three nanocomplexes displayed efficacy with minimal cytotoxicity as well as varying degree levels of serum protection, they were all investigated in scaffold release experiments.

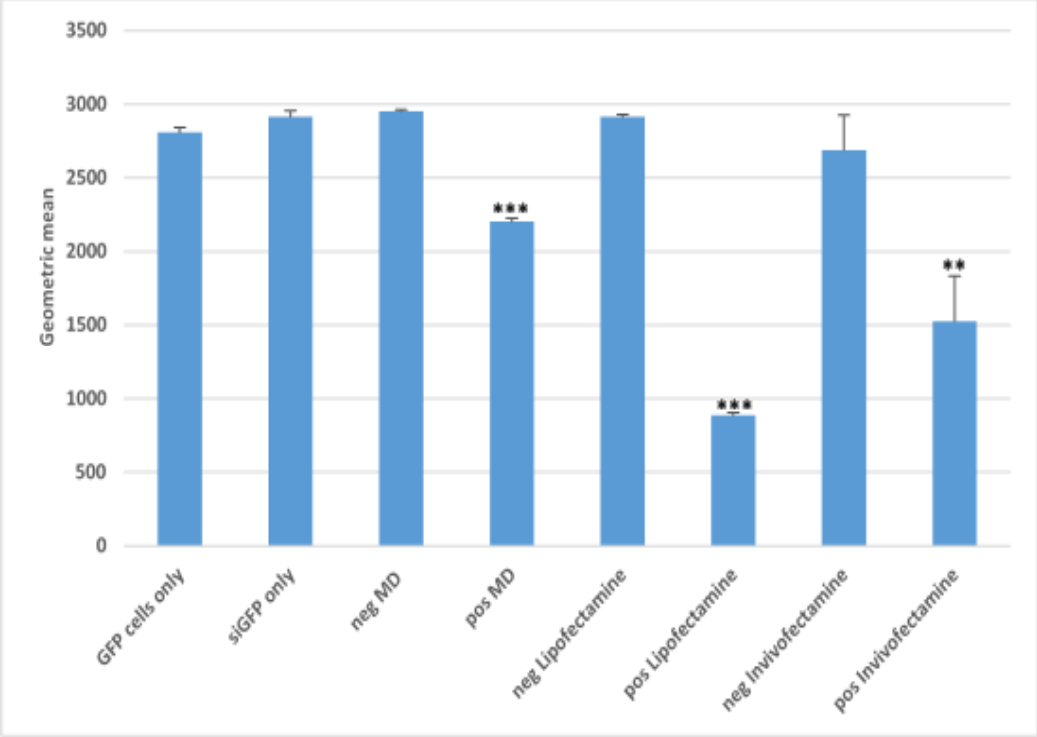

Figure 22: GFP knockdown in HT1080-GFP cells with the MD, Lipofectamine® RNAiMAX and Invivofecatamine nanoparticles*. HT1080-GFP cells were transfected by nanocomplexes made with 500ng siGFP-Cy3 or siNegative for 4hrs with and incubated for 48hrs post transfection. Flow cytometry was used to measure the GFP geometric mean. siNegative control was included. Data represents of an experiment done with 3 technical repeats per experiment. ** p<0.005 vs neg Invivofectamine and *** p<0.0005 vs respective neg MD/Lipofectamine.*

3.2 Hydrogel optimisation

3.2.1 Fibrin and PEG hydrogel characterisation

Due to their potential for controlled and localised delivery of RNAi agents, hydrogels have begun, as detailed in chapter 1.5, to be increasingly investigated. Synthetic PEG based hydrogels have been assessed by a number of investigators in pre-clinical small animal studies with a particular emphasis on targeting cancer, bone regeneration, inflammation and MI [257, 260, 262-264, 268-271, 274, 275]. One form of PEG hydrogel has been developed to function as an ECM mimic containing cell adhesion peptides and enzymatically degradable crosslinkers [285, 290, 375]. Our laboratory has refined these hydrogels to control their interactions with cells and tissue [284, 290, 375] and utilised them to mechanically reinforce the infarcted heart [376, 377] and deliver growth factors and mesenchymal stem cells to the heart [287, 378]. Thus it was thought relevant to explore this type of hydrogel that is centered on the PEG-VS 8-arm 20 kDa molecule that allows for stable crosslinks to thiol containing compounds. Further to this, the utility of a PEG-Ac variant [379] that allows for the formation of hydrolytically degradable crosslinks with thiols was investigated.

In addition, it was deemed useful to consider the natural FDA approved fibrin hydrogel. Fibrin has been widely used to deliver proteins such as growth factors and to a lesser extent DNA [337, 348, 354, 355] and only one in vitro study to our knowledge examining RNAi [356]. It was considered likely that chemical modification of fibrin, such as PEGylation as pioneered by the Suggs group [337, 351, 359, 380] to increase it's *in vivo* stability might be required. Thus initially, PEGylation of fibrin hydrogels needed to be established in our hands.

3.2.1.1 *Fibrinogen PEGylation*

Fibrinogen was PEGylated (described in section 5.12) by reaction with the succinimidyl carboxymethyl ester derivative of PEG (PEG-SMC_2) at PEG to fibrinogen molar ratios of 5:1 (lane 2) and 10:1 (lane 3). The use of this homo-bifunctional PEG allows for crosslinks to be forms with positive amine groups in the protein. It can be clearly seen that the three fibrinogen chains seen around 46, 52 and 66 kDa shift up towards higher

molecular weights (**Fig.23**). The shift is more pronounced for the 10:1 ratio. The presence of bands at molecular weights higher than 250 kDa are suggestive that there is a portion of the fibrinogen molecules that have intermolecular crosslinks. These findings are similar to those reported by others [351, 380].

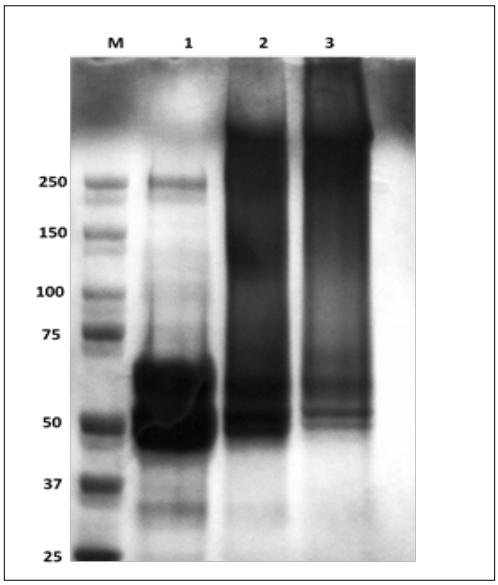

Figure 23: PEGylation of fibrinogen at 5:1 and 10:1, PEG to fibrinogen molar ratio*. Image of SDS-PAGE gel stained for protein with Coomassie Brilliant Blue R-250. M lane=molecular weight marker in kDa. Lane 1 is unmodified fibrinogen. Its PEGylation with PEG-SMC_2 was at ratios 5:1 (lane 2) and 10:1 (lane 3). Image is a representation of two experiments.*

3.2.1.2 *Fibrin and PEGylated fibrin hydrogel structure*

It has been observed by the Suggs group [381] that PEGylation of fibrinogen at ratios similar to those reported here resulted in changes in structure from the entangled fibrillar nature of unmodified fibrin to an amorphous sheet-like structure as visualised by scanning electron microscope (SEM). The fibrin hydrogels in this study were polymerised within highly porous polyurethane foams (150-180 μm diameter pores with 80-90 μm diameter interconnections [382] that allowed for support of the hydrogels during SEM processing (section 5.2.1.4). A SEM micrograph of an empty foam is given in **Fig.24A**. It can be seen that similarly to what was observed by the Suggs group, upon PEGylation, even at the lower level of 5:1 PEGylation (**Fig.24C**), a fibrillar structure of unmodified fibrin **Fig.24B** was replaced by a flat sheet-like morphology. It is possible that this structural change is in part desirable for a hydrogel to be utilised for controlled release as this change was correlated with slower diffusion through the PEGylated fibrin by a 10

kDa dextran and thus might allow for a more prolonged release of siRNA-nanoparticles [381]. PEGylation also increased the gelling time after activation with thrombin from 3minutes for unmodified fibrin to ≈20minutes (mins) for the 10:1 ratio and the 5:1 intermediate in time. This again is not necessarily a disadvantage for an injectable hydrogel as it allows for more time to set up an experiment. Furthermore, PEG hydrogels injected into rat hearts showed that a formulation that took 20mins to polymerise was retained as effectively as one that took 2-3mins [376, 377].

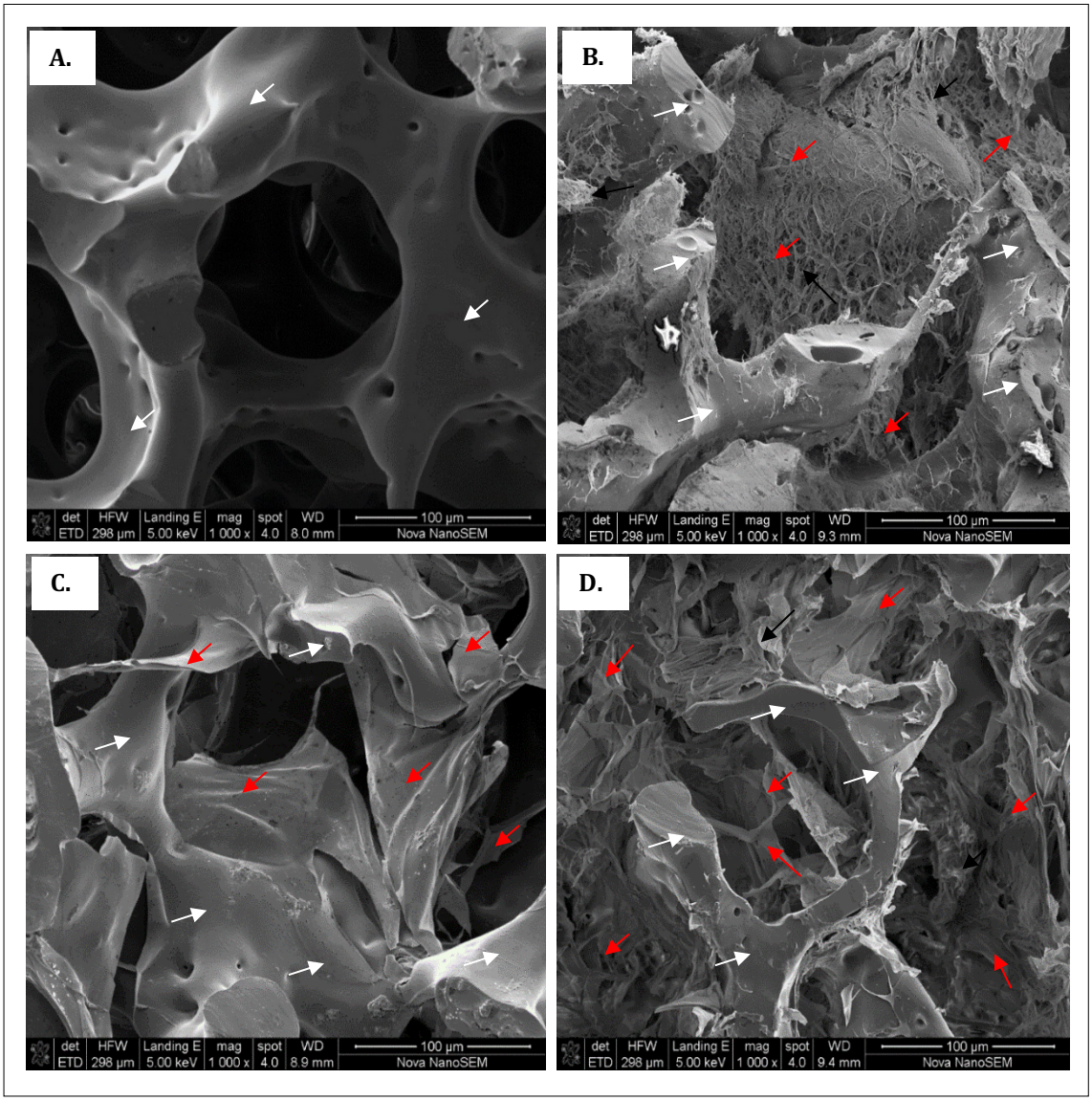

Figure 24: Fibrin gel characterisation by scanning electron microscope*. SEM micrograph images of unmodified fibrin (B), 5:1 PEGylated fibrin (C) and 10:1 PEGylated fibrin gels (D) that were polymerised in a porous polyurethane (PU) foam (A). The white and red arrows indicate the PU and fibrin gel respectively.*

3.2.1.3 *Stability of fibrin hydrogels in aqueous buffers.*

Fibrin hydrogels spontaneously degrade in aqueous buffers as previously observed by the Suggs group [337]. This could be due to the presence of proteases and in communication with the Suggs laboratory, they indicated that aprotinin stabilizes fibrin under these conditions. This shows that the protection against degradation that the group observed after PEGylation was due to protection against proteases and might translate to greater longevity *in vivo*. It is intended that PEGylation of fibrinogen increases the hydrogel duration *in vivo*, therefore, a simple assay to determine the rate of the fibrin hydrogels degradation over time was employed. Following the procedure in section 5.12.1.5, 50µl (10mg/ml) fibrin hydrogels were formed and incubated in Hepes buffered saline (HBS) pH 7.4 buffer at 37^{o} under sterile conditions. The eluents of the fibrin hydrogel were collected at various time points over 18 days until the gels completely degraded, and the breakdown products were quantified by Bradford's assay. Unmodified fibrin hydrogel degraded faster showing complete degradation by day 3 (**Fig.25**) an observation similar to Suggs' group that showed complete degradation by day 4 [337]. 5:1 PEGylated fibrin hydrogel degraded by day 10, however, macrosegments of the fibrin were possibly lost during sample collection therefore 100% protein was not recovered as assayed by Bradford's protein quantification. 10:1 PEGylated fibrin hydrogel took the longest to degrade as it was still present by day 18. These results are comparable to previous observations [337]. It was shown here that there is an inverse relationship between the degree of fibrin PEGylation and rate of degradation. The Drinanan et al. study [337] showed that mono-functionalised PEG-(succinimidyl α-methylbutanoate) (PEG-SMB) had generated similar protection to PEG-SMB, suggesting steric hindrance of proteases by the PEGs.

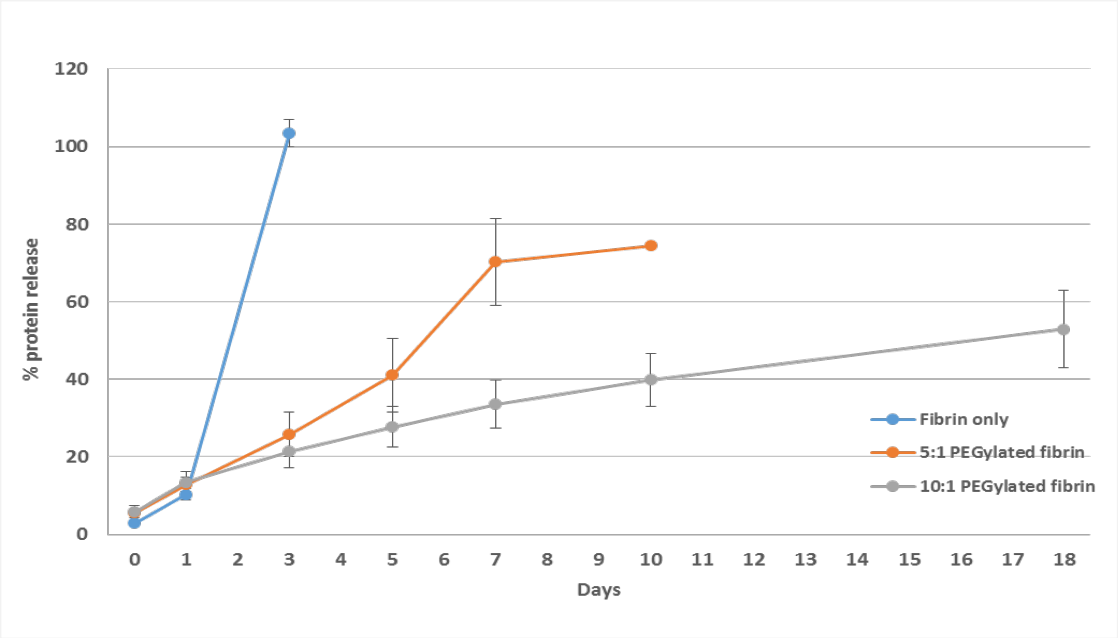

Figure 25: non-PEGylated, 5:1 and 10:1 PEGylated fibrin gel degradation rate measured by fibrin release from the hydrogel. *50µl (10mg/ml) fibrin hydrogels were formed and incubated at 37^{O}C over 18 days. The release of the hydrogel/protein breakdown in HBS pH 7.4 over 18 days was measured and quantified by Bradford's assay. Data represents % protein release for three experiments with 3 technical repeats.*

3.2.2 Controlled and sustained release of nanocomplexes from PEG and Fibrin hydrogels.

3.2.2.1 *siRNA and nanocomplex release from PEG-AC and PEG-VS hydrogels*

Successful scaffold based controlled and sustained delivery of RNAi molecules requires a reasonable release profile of molecules as well as maintenance of active RNAi molecules over time. Hydrogels encapsulating free siNegative or nanocomplexes were eluted in HBS and eluents were collected and quantified following the procedure in section 5.13. In aqueous buffers, PEG-AC hydrogels begin to visibly break up after 7 days [288], whilst the PEG-VS hydrogels are hydrolytically stable [376]. Both free siRNA and Lipofectamine® RNAiMAX nanocomplexes show up to 30% release in the initial 30min wash, almost complete elution by day 1 and elution appears complete by day 3 from PEG-AC hydrogel (**Fig.26**). Though there may be a stable proportion of Lipofectamine® RNAiMAX nanocomplexes entrapped that were released whilst the PEG-AC degraded from day 7 to day 10. MD and Invivofectamine® 3.0 nanocomplexes show slow release over the first 7 days then approximate full release by day 10 which again coincides with hydrogel degradation. Very similar release behavior was observed

from stable PEG-VS hydrogel. Free siRNA and Lipofectamine® RNAiMAX nanocomplexes essentially show fast release by day 1 with a small proportion on MD released upon the enzymatic degradation of the peptide crosslinked PEG-VS hydrogel with Proteinase K on day 10. Again there was limited release of ≈20% of MD and Invivofectamine® 3.0 nanocomplexes until degradation of the PEG-VS. Thus it appears that naked siRNA and Lipofectamine® RNAiMAX nanocomplexes are not sterically hindered from rapidly diffusing out of the PEG hydrogels. For Lipofectamine® RNAiMAX this may reflect weak binding of siRNA as indicated by the gel shift assay (**Fig.19**). It appeared that ≈70-80% of MD and Invivofectamine® 3.0 nanocomplexes were entrapped until hydrogel degradation. Certainly for MD the particle would be sterically entrapped as 4% 8-arm hydrogel is expected to have a mesh size of less than 25nm [290], which is smaller than the size of MD-siRNA nanocomplexes (**Fig.16**).

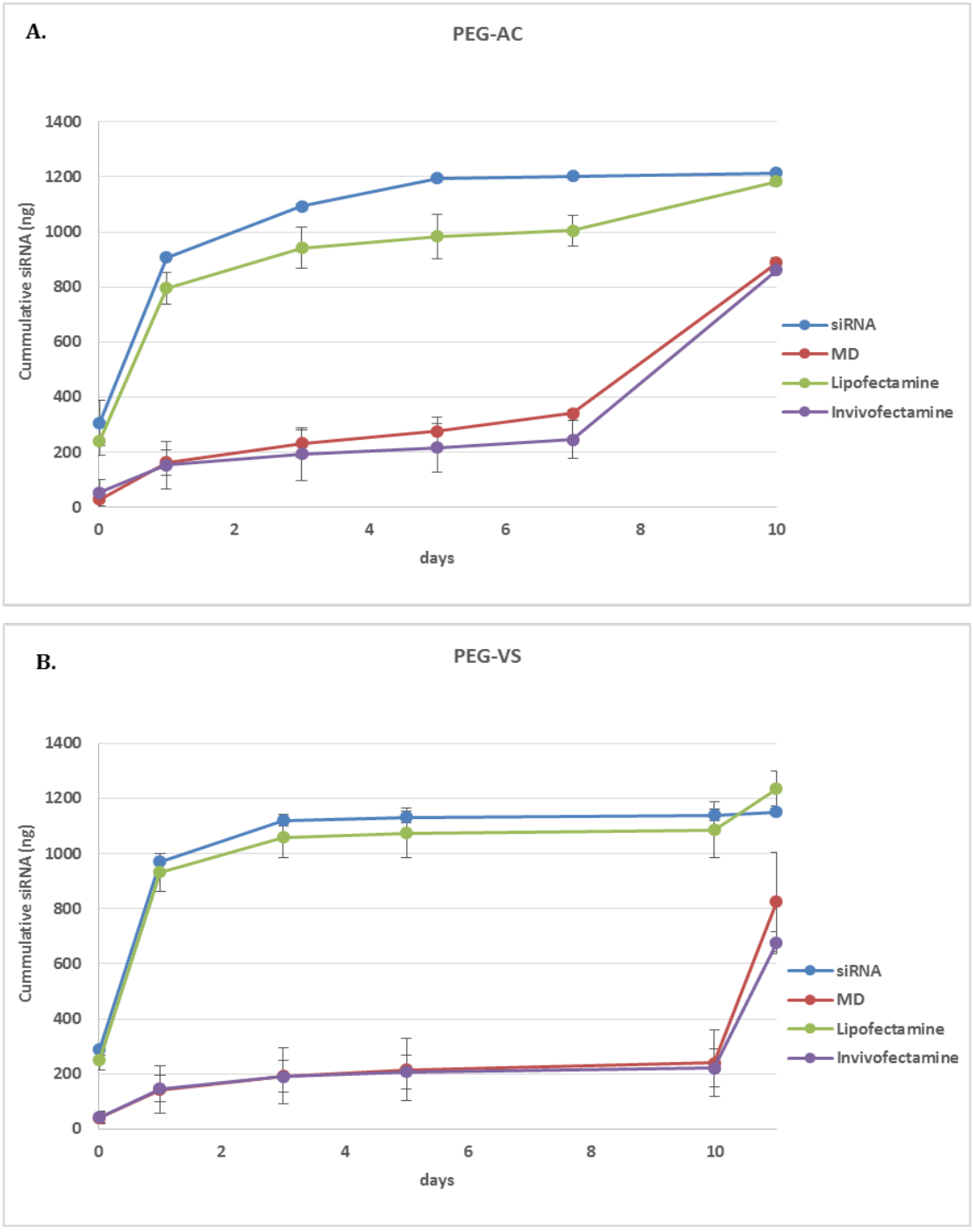

Figure 26: siRNA and nanocomplex release from PEG-AC and PEG-VS hydrogels over 10 days. *1000ng siNegative nanocomplexes encapsulated in PEG-AC (A) or PEG-VS (B) were incubated in HBS and collected over 10 day period. Collected nanocomplexes were denatured (0.5% SDS), resolved on a 2% agarose gel and the siRNA bands were quantified. PEG-VS gels were digested over night from day 10 to 11 by Proteinase K (1mg/ml). Results represents three experiments with 3 technical repeats per experiment.*

3.2.2.2 *Effects of animal derived fibrin hydrogel components on siRNA degradation*

The fibrin hydrogel components used in this study (fibrinogen and thrombin) are animal derived and therefore could potentially contain RNases. Before conducting siRNA encapsulation experiments with this hydrogel type, naked siRNA was incubated under sterile conditions with human serum derived fibrinogen and bovine plasma derived thrombin in HBS at 37°C (as prescribed in section 5.14). The samples were collected over 5 days for siRNA detection. In **Fig.27** the gel components showed no degradation effect on the free siRNA which is normally observed within 24hrs in the presence of serum as seen in this study (**Figs.12 & 13**). In fact, siRNA was persistently present over the tested 5 day period, through signs of degradation were apparent at day 5. The result here suggested that the fibrin gel components were essentially RNase free and could be used in siRNA release assays.

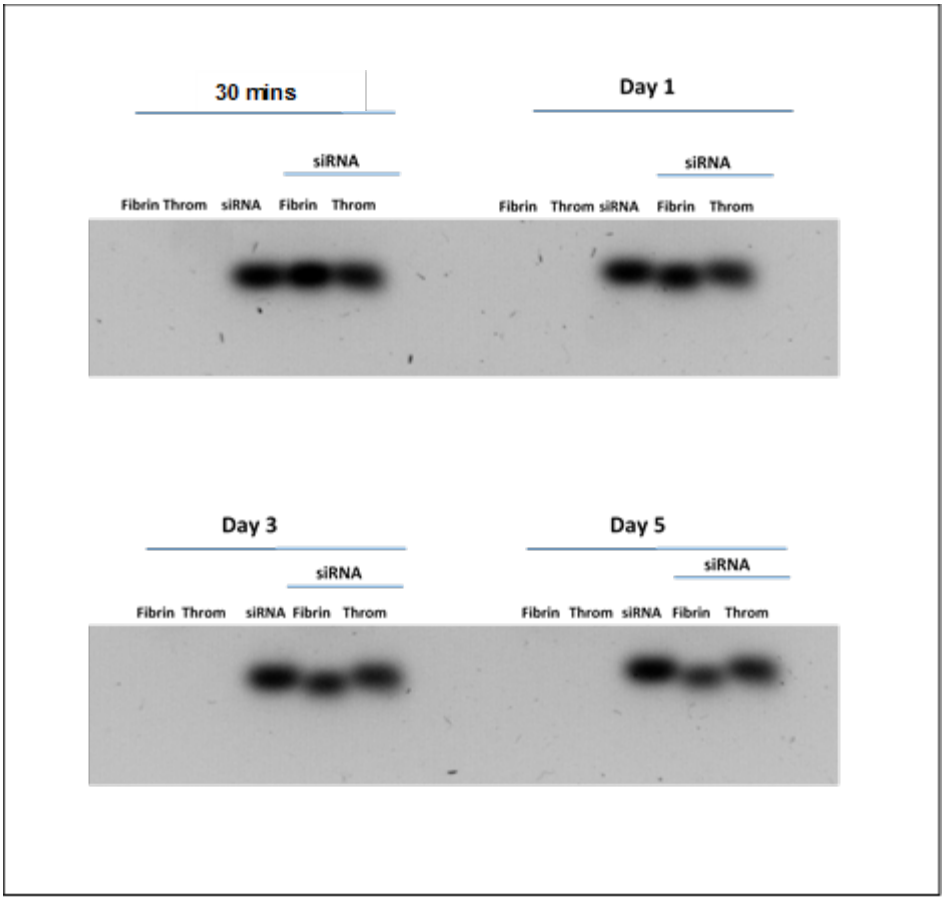

Figure 27: Effects of fibrin gel components (fibrin and thrombin) on siRNA degradation over time. *200ng of siNegative was incubated over 5 day period with fibrinogen (10mg/ml final concentration) in HBS buffer and 0.624U/ml thrombin in 40mM $CaCl_2$ HBS buffer. Fibrinogen, thrombin and fresh 200ng siRNA were included in the 2% agarose gel electrophoresis as controls. Throm: thrombin. Image is a representation of an experiment with three technical repeats.*

3.2.2.3 *siRNA and nanocomplex release from fibrin hydrogels*

Unmodified fibrin hydrogels also showed a more rapid release of naked and Lipofectamine® RNAiMAX nanocomplexes than MD and Invivofectamine® 3.0 nanocomplexes. However, unmodified fibrin hydrogel released most of the siRNA formulations by day 3 when there was breakup of the hydrogel. Because this hydrogel degraded rapidly controlled siRNA release over a lengthier time period was not feasible.

The PEGylated fibrin gels however degraded slowly over time, as shown in **Fig.28**. Consequently they slowly released MD and Invivofectamine® 3.0 nanocomplexes over time and therefore showed improved siRNA release over 10 days compared to the PEG-AC and PEG-VS hydrogels. Again naked siRNA and Lipofectamine® RNAiMAX were essentially completely released by day 3. The PEGylated fibrin hydrogels showed sustained release of MD and Invivofectamine® 3.0 nanocomplexes over 10 days. From day 1-10, 5:1 PEGylated fibrin released Invivofectamine® 3.0 nanocomplexes at ≈48ng/day and MD nanocomplexes at ≈56ng/day. 10:1 PEGylated fibrin released Invivofectamine® 3.0 nanocomplexes at ≈42ng/day and MD nanocomplexes a ≈40ng/day. The release of both nanocomplexes was more linear in nature for the 5:1 than observed in 10:1.

What was apparent in all the release studies is that naked siRNA had a similar fast release profile as Lipofectamine® RNAiMAX. As speculated above, Lipofectamine® RNAiMAX at the nanoparticle/siRNA ratio used in this study, did show weak siRNA condensation abilities in prior siRNA binding assays (**Fig.19**), it is possible that the Lipofectamine® RNAiMAX nanocomplexes fell apart in the HBS within a day and hence produced a release pattern similar to that of naked siRNA. PEG-AC, -VS and non-PEGylated fibrin hydrogels had less optimal release profile relative to PEGylated hydrogels which showed gradual siRNA release in an aqueous environment over at least 10 days.

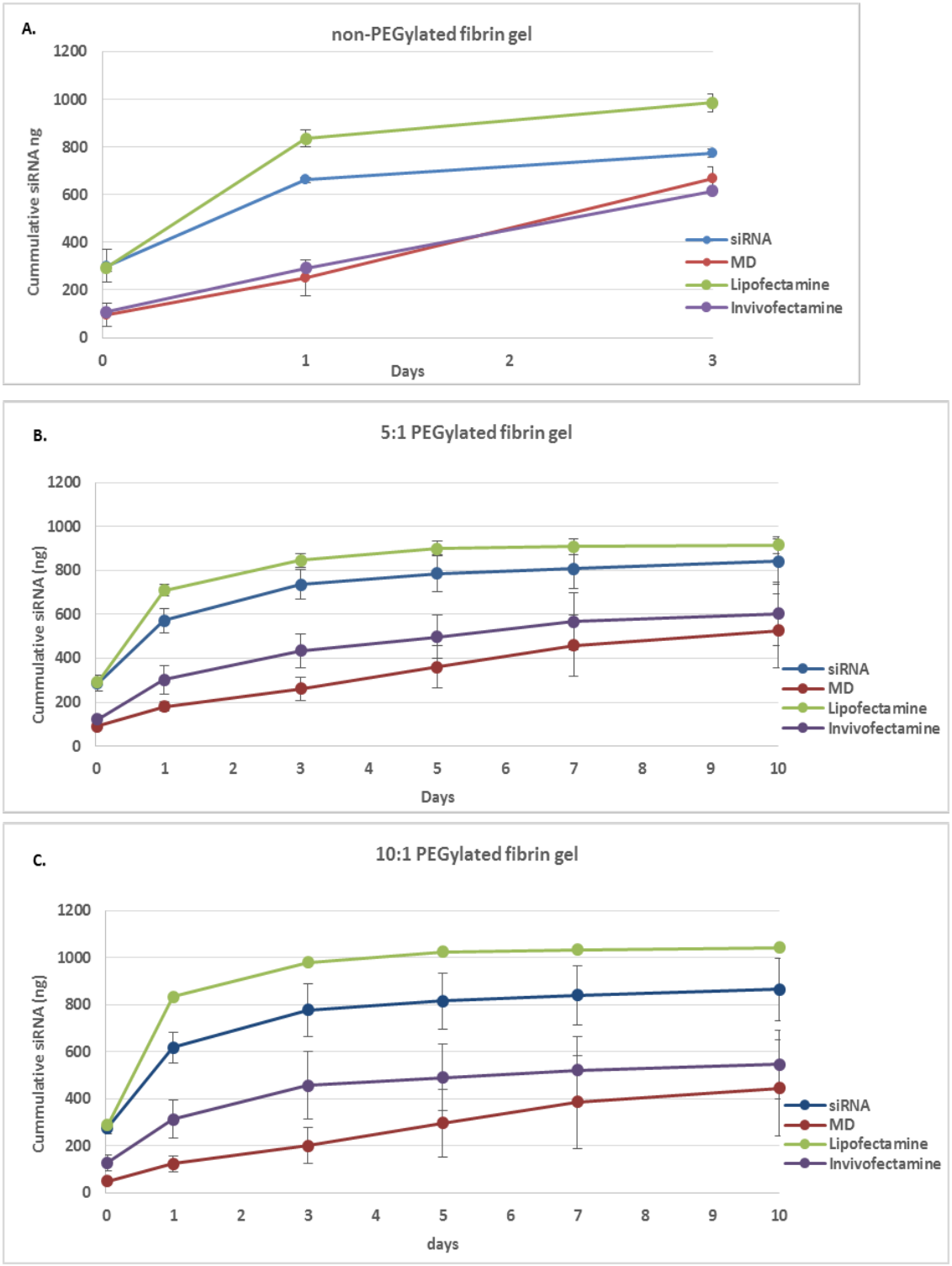

Figure 28: siRNA and nanocomplexes release from non-PEGylated and PEGylated fibrin hydrogels over a period of 10 days. *1000ng siNegative nanocomplexes encapsulated in unmodified (A), 5:1 (B) and 10:1 (C) PEGylated fibrin were incubated in HBS and eluents collected over a 10 day period. Collected nanocomplexes were denatured (0.5% SDS), resolved on a 2% agarose gel and the siRNA bands were quantified. Results represents three experiments with 3 technical repeats per experiment.*

Unmodified fibrin hydrogels have a known fibrous structure [356, 383] and since it is recognized that adding modifications to fibrin polymer changes their structure,

viscoelasticity, gelation time and degradation rate of the resulting hydrogel [320, 321, 331], it was shown here that the addition of PEG in fibrin hydrogels affects the fibrous structure of fibrin into a flat sheet-like structure altered its gelation, degradation time and may have variably influenced their nanocomplex release rates. Findings in this study indicate that naturally derived fibrin polymers without modifications lack the adequate stability and tunable properties that are required for sustained release, but introducing modifications and forming hybrid gels by adding a synthetic polymers such as PEGylation improves the hydrogels characteristics, function and stability particularly and improve controlled release of their cargo [337, 351, 359, 361, 384-387]. Certainly, it was clear from these release studies that the PEGylated fibrin hydrogel had the most promising controlled release of MD and Invivofectamine® 3.0 nanocomplexes *in vitro*. Subsequently, the bioactivity of the releasates from these hydrogels was analysed.

3.2.2.4 *Bioactivity of eluted nanocomplexes from PEGylated fibrin hydrogels in vitro*

The free siRNA nanocomplex release experiment was repeated using 1000ng siGFP and 5:1 or 10:1 PEGylated fibrin hydrogels (section 5.15.1 no serum). The initial 30min wash eluent was discarded and the rest collected after 0-5 day and 5-10 day incubation periods.100ng siGFP equivalent nanocomplexes released from each 0-5 day and 5-10 day pool was used to transfect HT1080-GFP cells. It can be seen from **Fig.29** that only Invivofectamine® 3.0 nanocomplexes from both PEGylated fibrin hydrogels showed efficacy at both time points. siRNA, MD and Lipofectamine® RNAiMAX evidenced no efficacy. Eluents from 5:1 PEGylated fibrin (**Fig.29A**) consistently knocked down GFP expression by around 45% ± 10% (0-5 days) and 42 ± 13% (5-10 days), $p<0.05$ against cells only control. 10:1 PEGylated fibrin (**Fig.29B**) knocked down GFP expression by 56 ± 34% from 0-5 days and the knockdown was reduced to 36 ± 1% from 5-10 days, suggesting a possible decline in efficacy over time. It is clear that Invivofectamine® 3.0 appears to maintain stability and efficacy. This may result from the nanoparticles' development for *in vivo* delivery. It is curious that the other nanocomplexes showed no efficacy at either time points. For Lipofectamine® RNAiMAX it does again suggest that the nanocomplexes were unstable. It is not clear why MD nanocomplexes have lost all efficacy as these nanocomplexes were shown to be relatively stable up to 10 days (RNase protection **Fig.12**).

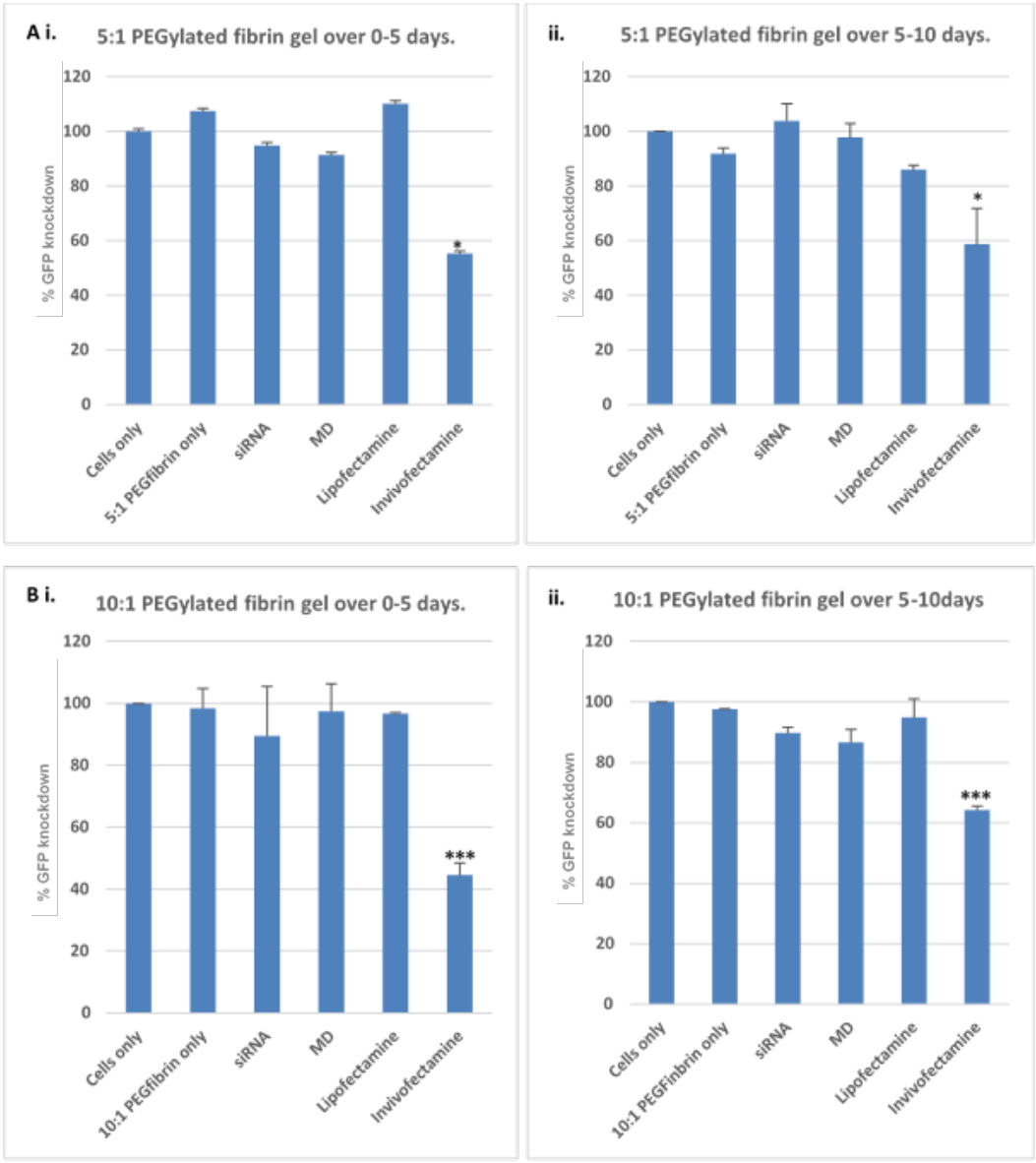

Figure 29: Bioactivity of eluted siRNA and siRNA-nanoparticles over 0-5 and 5-10 days from PEGylated fibrin gels in HBS. *The pooled eluted and quantified nanocomplexes (100ng siGFP equivalent) from 5:1 (A i-ii) and 10:1 PEGylated fibrin gel (Bi-ii) over 0-5 and 5-10 days was used to transfect HT1080-GFP cells for 4hrs. 48hrs post transfection flow cytometry was used to measure the GFP geometric mean shift. Untreated cells only and PEGylated fibrin only eluents (PEG fibrin) were included as negative controls. The % GFP knockdown represents three biological repeats with 3 technical repeats per experiment. * and *** p<0.05 vs PEGfibrin only.*

3.2.3 *In vivo* degradation of 4% 8-arm PEG-VS, PEG-AC, fibrin and PEGylated fibrin hydrogels

In order to assist in choosing the most promising hydrogel candidate, the *in vivo* rate of degradation of all the hydrogels was qualitatively assayed. The tibialis anterior (TA) muscle of mice was chosen as the target soft tissue due to its small size (to facilitate

downstream analysis) and ease of access for injection. It was established by assessing the spread of Coomassie Brilliant Blue R-250 stained PBS in the injected tissue, that to achieve optimal TA muscle coverage with one injection of the hydrogel, 30µl volumes of the gels were to be injected parallel to the long axis of the TA muscle. The procedure is fully described in section 5.17.2.

All gels were conjugated with a Cy5 fluorescent tag, PEG gels were labelled via Fluor® 660 C2-maleimide as described before [376] and in section 5.12.3. This procedure had been shown effective for verifying PEG hydrogels in rat hearts for up to 3 months with non-degradable 8-arm-PEG-VS gel [376]. Purchased fibrinogen with Alexa Fluor™ 647 conjugate was used in combination with the natural human fibrinogen (with no Alexa label) as described in section 5.12.1.1&2. This resulted in highly fluorescent fibrin gels that polymerised at equivalent rates. Pilot injections in the TA muscle of BALB/c mice with the optimised injections of the Cy5 labelled PEG and fibrin hydrogels was shown to result in effective fluorescence in the tissue (**Appendix 5**).

To determine the distribution and degradation rate of the PEG and fibrin hydrogels *in vivo* over 7 days, the mice were injected in their TA with the hydrogels (2 legs per gel) in a randomised manner. The animals were euthanised at 30mins, 2, 4 and 7 day time points post injection. At 30mins all hydrogels are clearly visible throughout the muscle tissue. It is possible that fibrin is more effectively retained as evidenced by the high fluorescence intensity and greater coverage (**Fig.30**). However, this may also reflect different staining efficiencies. By day 2 PEG-AC (**Fig.30B**) hydrogel was no longer visible [288] and unmodified fibrin gel (**Fig.30C**) at this time showed only minor traces of the gel present. H&E stain (data not shown) found no evidence of PEG-AC presence suggesting that the absence of fluorescence is not simply indicative of loss of fluorescent label. Such a loss is possible as the label will also detach from the PEG-AC due to hydrolysis, but here it seemed that the loss of hydrogel was complete. This suggests that hydrolysis coupled with enzymatic degradation of peptide crosslinker caused a much more rapid degradation *in vivo* compared with what was seen *in vitro* where only hydrolytic degradation takes place. Rapid unmodified fibrin degradation was not unexpected as its stability was found to be limited *in vitro* (**Fig.25**).

PEG-VS (**Fig.30A**) showed a gradual degradation over the 7 day period with still significant PEG gel left at day 7. This accords previous experience in the laboratory with injection into rat hearts [377]. 5:1 (**Fig.30D**) and 10:1 (**Fig.30E**) PEGylated fibrin also showed evidence of degradation over the 7 day period with a more pronounced

degradation for the 5:1 PEGylated gel. This might be expected as degradation *in vitro* was more rapid for this hydrogel.

Thus this first *in vivo* study allowed for the clear exclusion of PEG-AC and unmodified fibrin gels as potential delivery vehicles due to rapid degradation. Of the remaining 3 gels it was decided that the 5:1 PEGylated fibrin gel was the optimal candidate to proceed with. PEG-VS allowed minimal nanocomplex release *in vitro* though it had a promising degradation rate *in vivo*. This hydrogel can be investigated in the future to study the delivery of siRNA or nanocomplexes in invasive cells. It was considered that the trial period for determining the scaffold mediated siRNA-nanoparticles delivery in the selected TA muscle was to be 7 days in these initial proof of concept studies. The 5:1 PEGylated fibrin gel showed perhaps a more controlled release over a 10 day period (**Fig.28**), faster degradation rate *in vitro* and possibly *in vivo*, and represented less modification of natural fibrinogen and therefore was chosen over the 10:1 PEGylated fibrin to assess delivery of nanocomplexes in 3D assays.

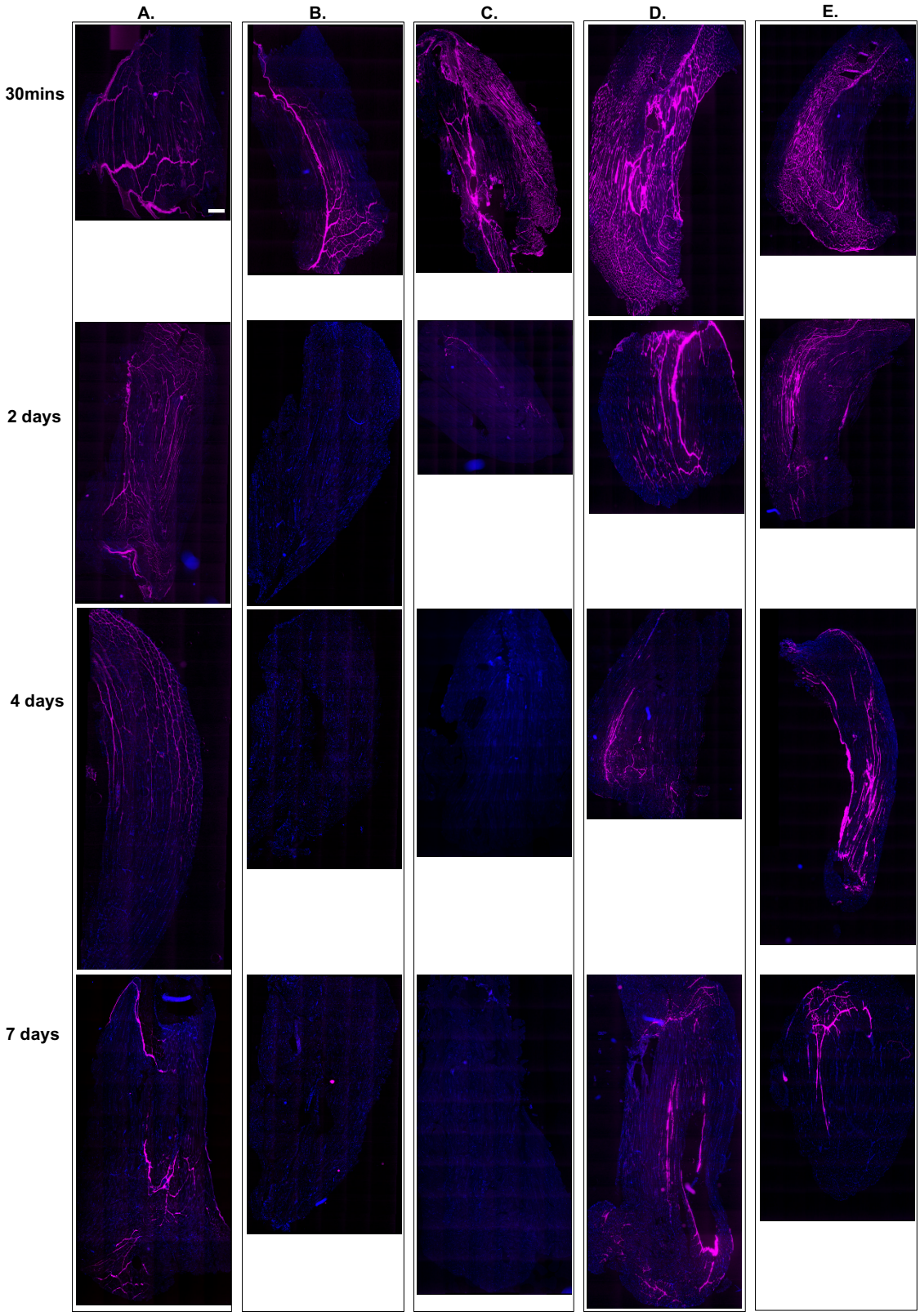

Figure 30: PEG and fibrin hydrogel degradation time in the TA muscle of BALB/c mice over 7 days. *30µl hydrogels of 4% 8-arm PEG VS (PEG-VS) (A), 4% 8-arm PEG-AC (PEG-AC)(B), unmodified fibrin gel (C), 5:1 (D) and 10:1(E) PEGylated fibrin gel was imaged 30mins to 7 days post injection. All hydrogles were Cy5 labelled (pink) and whole TA muscle tissue nuclei is 4',6-diamidino-2-phenylindole (DAPI) stained (blue). The images of the whole TA muscle tissue are a representation of n=2 legs per group. Scale bar =500µm.*

3.2.3.1 *Bioactivity of eluted Invivofectamine® 3.0 nanocomplexes in serum*

Prior to establishing a 3D assay for investigating efficacy of nanocomplexes delivered by 5:1 PEGylated hydrogel and subsequent *in vivo* analysis, the bioactivity of the eluted Invivofectamine® 3.0 nanocomplexes was assayed in the presence of serum. This was considered necessary as the nanocomplexes will be exposed *in vivo* to serum components. The release of nanocomplexes, was repeated in the presence of 10% FBS in media rather than HBS (section 5.15). Invivofectamine® 3.0 nanocomplexes were eluted in 10% serum containing media and collected at day 2, 4 and 7 time points. Transfections with the collected releasates were carried out in serum rich media (10% FBS) for 24hrs (2 day releasates) or 72hrs (4 and 7 day releasates).

It can be seen that there was a highly effective knockdown as determined by flow cytometry (**Fig.31**). The nanocomplexes collected at day 2, 4 and 7 resulted in 76.4%, 86.5% and 82.4% GFP knockdown effect. This result not only confirms the sustained bioactivity of Invivofectamine® 3.0 in previous observations (**Fig.29**) but also show a substantially more effective knockdown efficacy compared to the knockdown effects observed in the previous 4hr transfection experiments carried out in the absence of serum. This again may reflect the design of the Invivofectamine® 3.0 for systemic *in vivo* use. In addition, there was no significant knockdown difference between 48hr and 72hr transfections as established prior by dendriplexes (comparing **Fig.17 and Appendix 3**). The result here does indicate probable protection against RNase degradation. There was a prolonged protection of a limited quantity of siRNA when the nanocomplexes were incubated in 50% FBS (**Fig.20**) and it may be that this protection effect is more pronounced in less serum/FBS concentration.

Even though the nanocomplex release and bioactivity data thus far shows that Invivofectamine® 3.0 nanocomplexes are efficacious in 2D assays all three nanocomplexes, however, were investigated for bioactivity upon release from the PEGylated fibrin hydrogels in further 3D assays because each nanoparticle displayed its own advantages prior. MD dendriplexes are the most effective at siRNA complexing and serum protection compared to lipid based nanoparticles but the least efficacious. At the concentrations used in this study Lipofectamine® RNAiMAX is the least effective at forming stable nanocomplexes and serum protection, however the most efficacious in 2D *in vitro* assays (4hr transfections in the absence of serum), compared to Invivofectamine® 3.0. Therefore it was also considered worthwhile to investigate all 3

nanocomplexes in the 3D assays to compare how the three would compare in an environment that best mimics the tissue microenvironment.

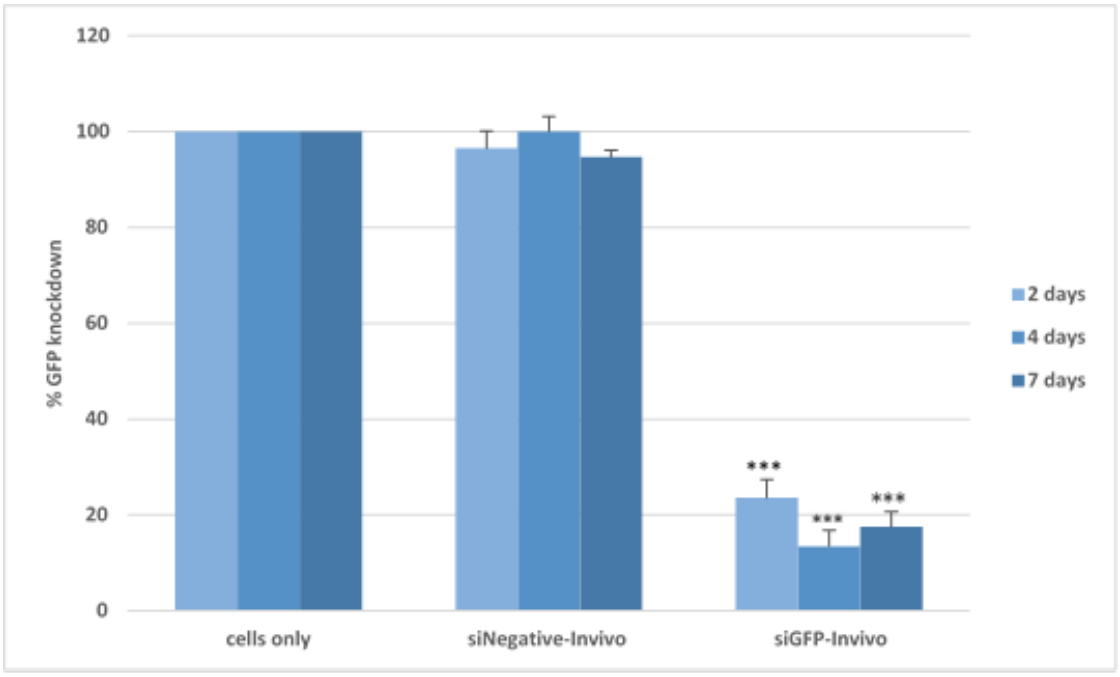

Figure 31: Bioactivity of Invivofectamine® 3.0 nanocomplexes eluted from 5:1 PEGylated fibrin hydrogel gel in the presence of serum. *Invivofectamine® 3.0 nanocomplexes (1000ng siGFP-Cy3) in PEGylated fibrin were incubated in media (10% serum) and eluted over 7 days. The eluted nanocomplexes were used to transfect HT1080-GFP cells in the presence of 10% serum for 48-72hrs. Post transfection flow cytometry was used to measure the GFP geometric mean. Untreated cells and siNegative Invivofectamine® 3.0 nanocomplexes (siNegative-In vivo) were included as negative controls. Data represents 3 technical repeats per experiment. *** p<0.0005 vs siNegative-Invivo.*

3.3 Controlled and sustained release of nanocomplexes in Fibrin hydrogels

3.3.1 3D RNAi *in vitro* assays

In order to advance to *in vivo* assays of scaffold base RNAi, it was necessary to develop a 3D model that mimicked the *in vivo* scenario. It was considered important that the cells and RNAi agents were not exposed to each other whilst the hydrogel scaffold polymerised and was in liquid form. Hence in this study, two 3D *in vitro* assays were developed to investigate controlled sustained release of nanocomplexes from 5:1 PEGylated fibrin hydrogels.

3.3.1.1 *3D chemotaxis Transwell assay*

The initial approach investigated was a variation of a standard transwell chemotaxis assay. Here a layer of fibrin hydrogel containing MD, Lipofectamine® RNAiMAX and Invivofectamine® nanocomplexes made with siGFP-Cy3 was polymerized in fibrin hydrogels, onto the membrane of transwell with 8 micron pore size as illustrated in **Fig.32** (procedure described in section 5.16.1). Onto this was layered another fibrin hydrogel containing HT1080-GFP cells. The transwell was placed into media in the lower chamber containing 10% FBS as a chemoattractant. Unfortunately, it was found that both the PEGylated fibrin hydrogels limited the cell invasion to an extent that very minimal cells were seen to navigate through the transwell membrane or on the surface of the lower chamber. This observation did not change significantly over 10 days and therefore there were insufficient cells to allow for analysis. The fast degrading non-PEGylated fibrin gel however allowed faster cell migration through the transwell membrane to the surface of the lower chamber that allowed sufficient cells to be analysed. Though this was not the hydrogel formulation that was targeted, the ability of this type of assay to determine 3D RNAi was assessed. The efficacy of the nanocomplexes was determined 48hrs post cell seeding, a day earlier than the hydrogel has been shown to completely degrade *in vitro* (**Fig.25 and 29**) This was so it could be ensured that the nanocomplexes being assessed for efficacy were from hydrogel release.

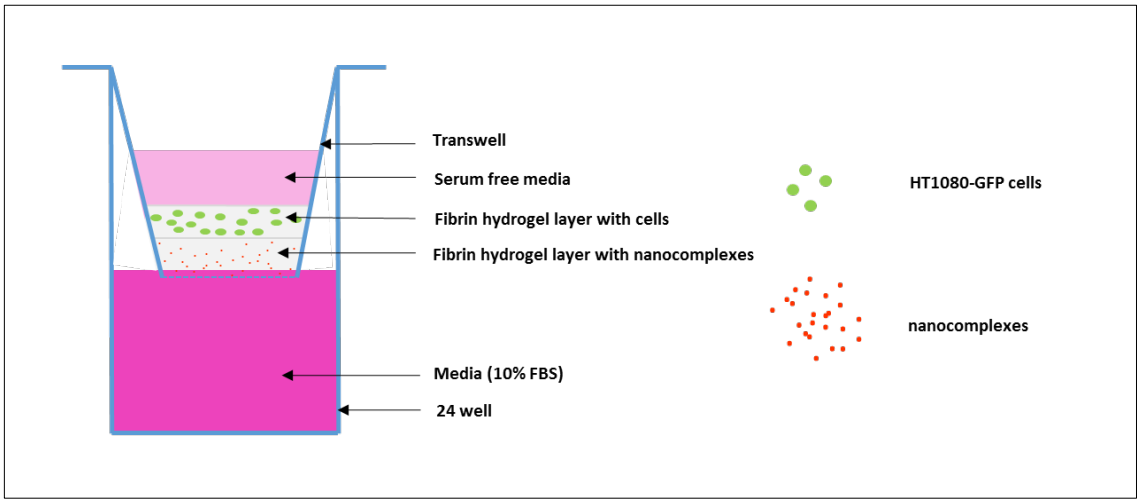

Figure 32: Schematic representation of the 3D chemotaxis Transwell assay*. A layer of 50µl fibrin hydrogel encapsulating HT1080-GFP cells was seeded on top of a layer of 50µl fibrin hydrogel encapsulating nanocomplexes in a transwell.*

It can be seen from the micrograph of the underneath of the transwell membrane (**Fig.33A**) that uptake of siGFP-Cy3 could be seen for all complexes but not the free siGFP-Cy3. However, a clear drop in GFP cells could be seen for Lipofectamine® RNAiMAX and Invivofectamine® 3.0 treated cells. It was also apparent that fewer cells as determined by DAPI stain can be seen on Lipofectamine® RNAiMAX nanocomplexes suggesting a level of toxicity by the nanocomplex. As Lipofectamine was found to be minimally cytotoxic in the previous 2D assay (**Fig.21**), this might reflect a more prolonged exposure of cells to the nanocomplex therefore may result in more cell loss. These micrograph images confirm previous results that although MD is efficient at cell transfection (indicated by more cells with siGFP-Cy3 compared siGFP-Cy3 only group) it has the least gene knockdown effect indicated by the presence of more green cells compared to Lipofectamine® RNAiMAX or Invivofectamine treated cells. Lipofectamine® RNAiMAX though highly efficacious (less green cells present) is more toxic, indicated by less live DAPI stained cells compared to the other nanoparticles. This result demonstrated that Invivofectamine® 3.0 is the optimal nanoparticle as it is efficient at transfecting cells and causing significant gene knockdown without being toxic. The qualitative GFP gene knockdown shown by the images was confirmed by GFP expression analysis of cells from the bottom well by flow cytometry in **Fig.33B**. MD, Lipofectamine® RNAiMAX and Invivofectamine® 3.0 nanocomplexes caused 42 ± 8%, 69 ± 5% and 72 ± 6% GFP knockdown ($p<0.01$ against positive siGFP-Cy3 only control group).

Although somewhat limited in applications to hydrogels that the cells can invade through in a reasonable number, this assay may be of use due to quantitative nature.

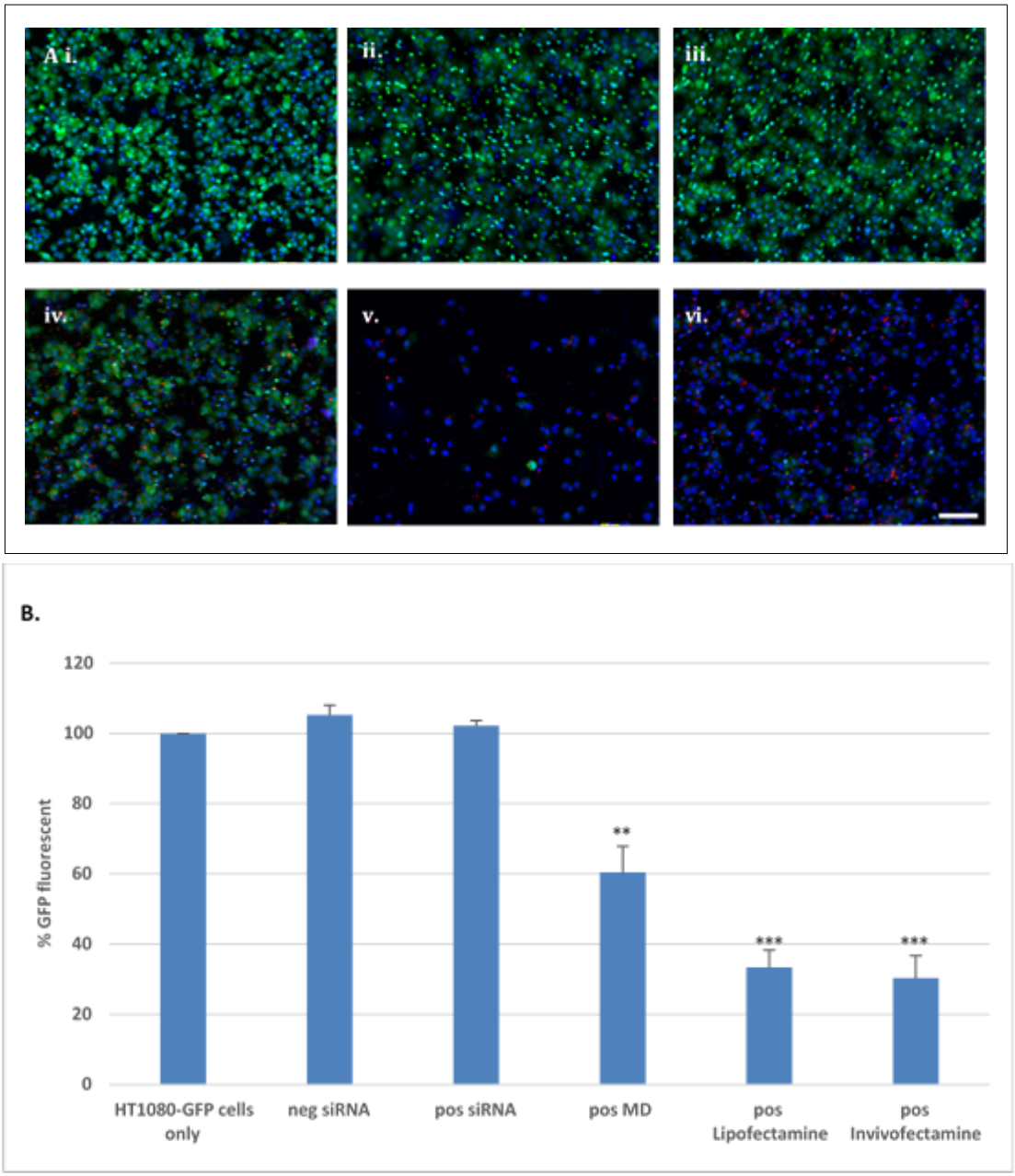

Figure 33: GFP knockdown in a 3D chemotaxis Transwell assay*. A non-PEGylated fibrin gel containing 500ng free siNegative-Cy3 (neg siRNA) or free siGFP-Cy3 (pos siRNA) or MD/Lipofectamine® RNAiMAX/ Invivofectamine® 3.0-siGFP nanocomplexes was polymerised onto the Transwell membrane. It was overlaid by another non-PEGylated fibrin gel encapsulating HT1080-GFP cells. 72hrs post incubation, (A) cells that migrated to the bottom of the transwell membrane were DAPI stained and imaged by fluorescent microscopy (i-vi) representing untreated cells, siNegative-Cy3, siGFP-Cy3, MD, Lipofectamine® RNAiMAX and Invivofectamine® 3.0 treatments respectively. (B) Cells that migrated to the bottom of the well were tripsonized and quantified for GFP knockdown by flow cytometry. Untreated cells were included as controls. Data represents three biological repeats with 2 technical repeats per experiment. ** p<0.005 and *** p<0.0005 vs positive siRNA group. Scale bar = 100 µm.*

3.3.1.2 *3D embedded cell cluster assay*

Thus an additional 3D assay was developed. Here a droplet of 5:1 PEGylated encapsulating HT1080-GFP cells was overlaid with 5:1 PEGylated fibrin containing nanocomplexes made with 500ng siRNA as illustrated in **Fig.34** (and described in 5.16.2). GFP expression was considered as evidence of cell viability (green cells) and dead cells were stained red with ethidium homodimer-1 (EthD-1). Limited cells were seen to migrate out of the PEGylated fibrin into the surrounding 5:1 PEGylated fibrin similar to their behavior in the Transwell assay (data not shown). However, it was surmised that release of siGFP into the cell droplet could be assessed.

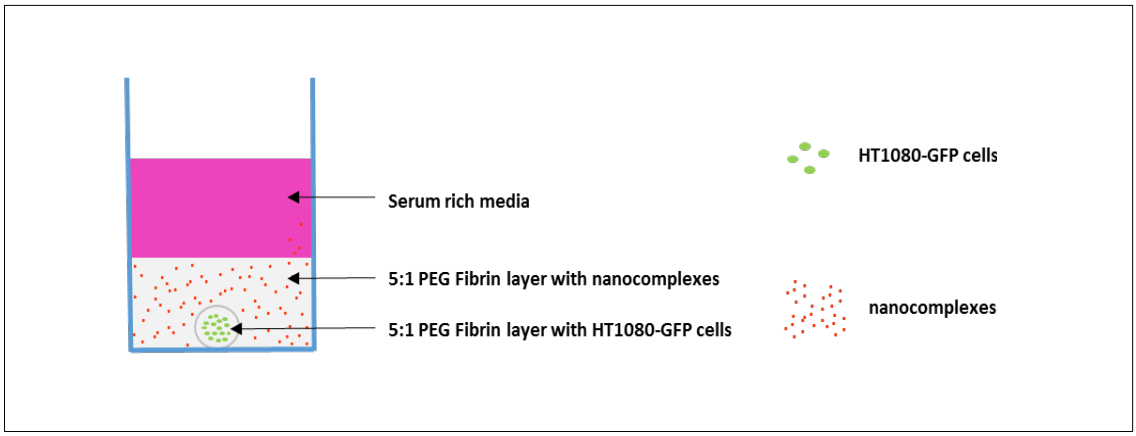

Figure 34: Schematic representation of 3D embedded cell cluster assay. *HT1080-GFP cells were encapsulated in 5µl 5:1 PEGylated fibrin hydrogel and a layer of 50µl 5:1 PEGylated fibrin hydrogel containing nanocomplexes was set on top of the cells.*

Uniform distribution of GFP expressing cells could be seen at day 0 for all groups, (**Appendix 6**). Cells in the central droplet were visualised by fluorescent microscopy **Fig.35**. and the imaged live (green) or dead (red) cells were quantified by image analysis **Fig.36.** At day 3 there was no significant change in the number of GFP expressing cells in all groups. However, an increase in dead cells was observed for cells surrounded by PEGylated fibrin containing MD-siDeath and Invivofectamine® 3.0-siDeath with 8 and 6 fold increase relative to MD-siDeath-Negative or Invivofectamine® 3.0-siDeath-Negative respectively ($p<0.01$).

At 7 days there was a 69% reduction in GFP expressing cells in the central droplet surrounded by Invivofectamine® 3.0-siDeath relative to Invivofectamine® 3.0-siDeath-negative ($p<0.01$). There was also a significant reduction in GFP expressing cells in the

Invivofectamine® 3.0-siDeath group compared to all other groups ($p<0.01$). When assessing the number of dead cells, Invivofectamine® 3.0-siDeath was again significantly increased by 7 fold relative its negative control group, Invivofectamine® 3.0-siDeath-Negative, and also against both Lipofectamine® RNAiMAX groups and cells only ($p<0.01$) but not relative to MD-siDeath group (p=not significant). Both MD-siDeath and siDeath-Negative treated groups for live cells showed significant reduction relative to cells only group ($p<0.01$). Dead cells were significantly increased for both MD groups relative to cells only ($p<0.01$) and MD-siDeath showed a significant 2 fold increase relative to MD-siDeath-Negative ($p<0.01$).

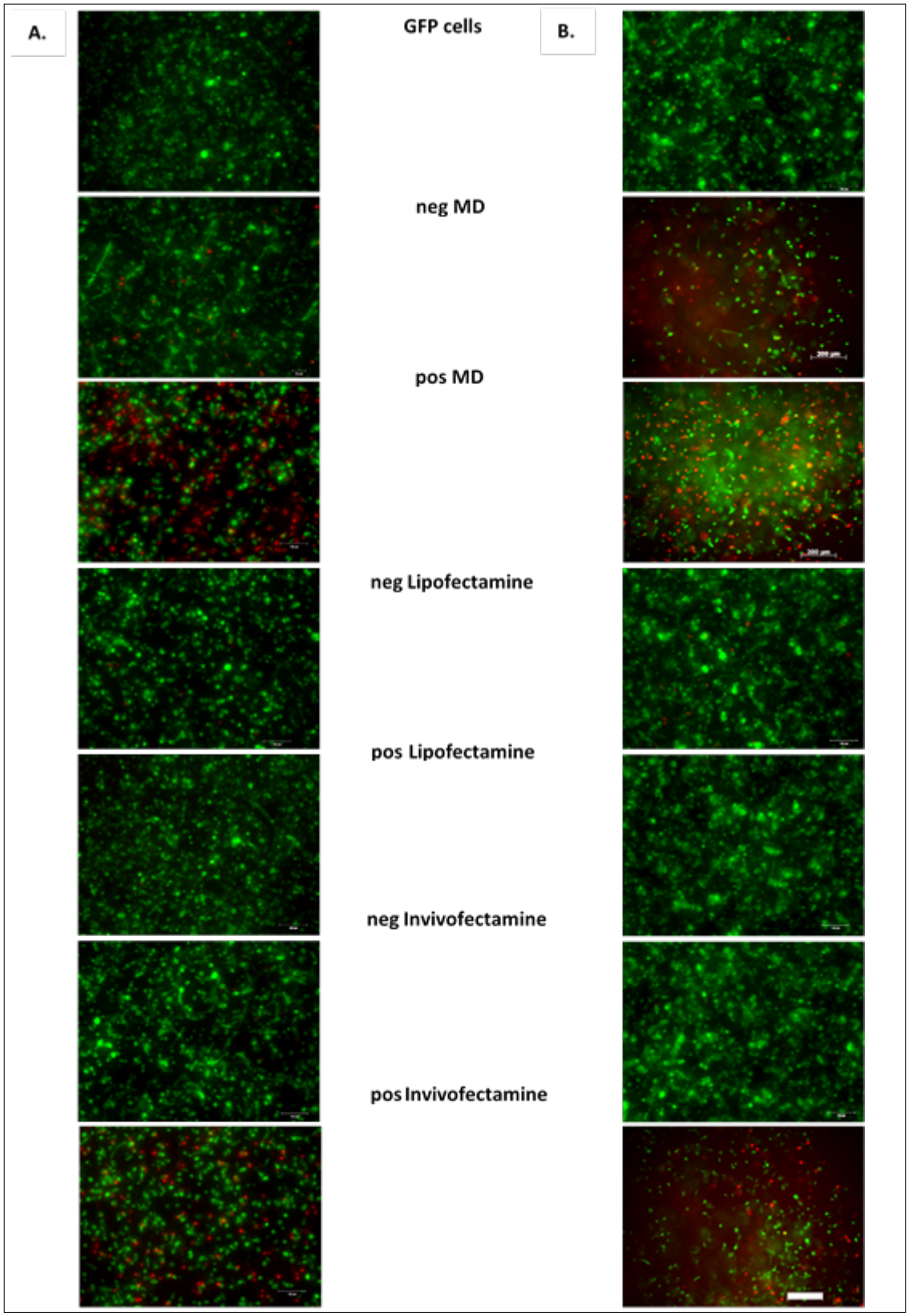

Figure 35: Transfection efficacy of HT1080-GFP cells in 3D embedded cell cluster assay. *Maximum projection Z-stack images of cells encapsulated in 5ul 5:1 PEGylated fibrin droplet covered with a layer of 50µl 5:1 PEGylated fibrin gel containing: MD/Lipofectamine® RNAiMAX/ Invivofectamine® 3.0 nanocomplexes made with 500ng siDeath (pos siRNA groups) or siDeath-Negative control (neg siRNA groups). 3 days (A) and 7 days (B) post incubation EthD-1 (2mM) from the Live/Dead™ cell viability assay was used to stain dead cells red and imaged by confocal microscopy. Green indicates viable/live HT1080-GFP cells. Cells only were included as negative controls. Micrograph images are representation of three biological repeats with 4 technical repeats per experiment. Scale bar = 200µm.*

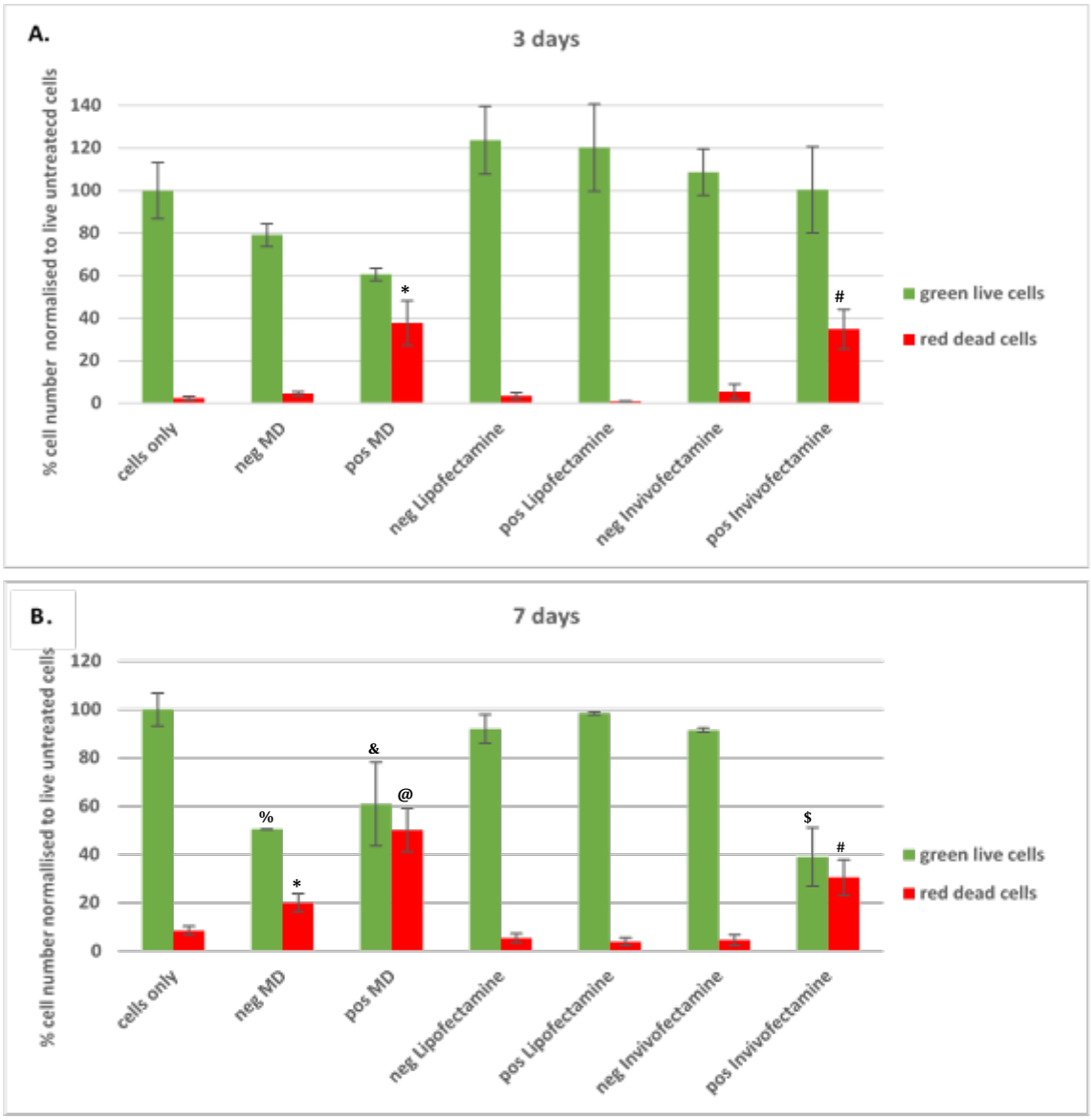

Figure 36: Efficacy quantification of the 3D embedded cell cluster assay z-stack images. *3 days (A) and 7 days (B) post incubation EthD-1 (2mM) staining and confocal microscopy imaging (**Fig.32**), the average number of living (green) and dead (red)HT1080-GFP cells were counted by Image J cell counter (4 fields/well). Data represents three biological repeats with 4 technical repeats per experiment. In (A) *p<0.05 for dead cells: pos MD vs neg MD and all groups except pos Invivofectamine. #p<0.05 for dead cells: pos Invivofectamine vs neg Invivofectamine and all groups except pos MD. In (B) #p<0.05 for dead cells: pos Invivofectamine vs neg Invivofectamine and all groups except the MD groups. $p<0.05 for live cells: pos Invivofectamine vs all groups. &p<0.05 for live cells, pos MD vs cells only, %p<0.05 for live cells, neg MD vs cells only. *p<0.05 for dead celsl: neg MD vs posMD and cells only. @p<0.05 for dead cells: pos MD vs neg MD and cells only.*

This assay allows for the relatively simple quantification of the efficacy of the release of siRNA into cells in 3D. It was clear that Lipofectamine® RNAiMAX nanocomplexes again had no efficacy when released from PEGylated fibrin hydrogel. This is in contrast to the positive effect observed when assayed in the previous Transwell assay (**Fig.33**). A major difference between these two assays is the presence of serum in the 3D cluster assay. Manufacturers recommendations are to transfect in serum free media and this may have

impacted Lipofectamine® RNAiMAX efficacy. However, Lipofectamine® RNAiMAX nanocomplexes released from fibrin hydrogels were assayed for efficacy (**Fig.29**) in 2D transfections under serum free conditions. The lack of efficacy in that study suggests that Lipofectamine® RNAiMAX nanocomplexes at the concentration used in the study are relatively unstable. In a previous study, Lipofectamine® RNAiMAX nanocomplexes absorbed on the surface of unmodified fibrin hydrogel were shown effective at noggin gene knockdown in a 3D *in vitro* assay when MC3T3-E1 pre-osteoblasts cells were directly seeded on top of the hydrogel [356]. In another study, these nanocomplexes were injected into the myocardial tissue and showed effective RNAi [213]. However, in this study, the release assay and the 3D assays showed that Lipofectamine® RNAiMAX nanocomplex eluents either failed to demonstrate efficacy or showed signs of toxicity. In the studies mentioned, cytotoxicity of the nanocomplexes *in vitro* was not assessed as they were in this present study.

The lipid nanoparticles used here vary in overall charge post siRNA complexation according to their manufacturer. Lipofectamine® RNAiMax has an overall positive charge whilst Invivofectamine® 3.0 has an overall neutral charge when complexed to siRNA. It has been reported that nanoparticles with an overall neutral charge are optimal carrier nanoparticles compared to cationic particles when in the presence of serum as cationic nanoparticles are prone to aggregation [388-390].

The apparent efficacy of MD-siDeath at 3 days was surprising as MD had not shown efficacy in the release studies. However, the conditions of the experimental set up were different which could possibly impact efficacy. Nanocomplexes were incubated 5 days in the release assay prior to use, whereas in the 3D assays nanocomplexes could start transfecting as soon as the experiment was set up. The reduction in GFP expressing cells and increases in dead cells over 7 days observed for both the MD-siDeath and MD-siDeath-Negative (negative control), suggests cytotoxicity of MD nanocomplexes when exposed to cells for longer periods of time. In the previous 2D cytotoxicity assay (**Fig.13**) experiment the cells were only exposed to nanocomplexes for 4hrs whereas in the 3D cell cluster assay cells were incubated with the nanocomplexes up to 7 days.

The 3D cell cluster assay showed Invivofectamine® 3.0 was the most consistent with cell death occurring at both 3 and 7 days and no sign of toxicity in the Invivofectamine® 3.0-siDeath-Negative group. This finding confirmed it is the optimal candidate for assessment of scaffold based delivery of RNAi in the in vivo.

This is the first study to attempt dendrimer, Lipofectamine® RNAiMax and Invivofectamine® 3.0 encapsulation in a PEGylated fibrin hydrogel for gene knockdown *in vitro*. The scaffold studies in literature, fibrin hydrogel included, show controlled siRNA release and prolonged gene silencing mostly in *in vitro* studies using 3D assays that have *in vivo* mimicking limitations [239, 293, 305, 391-395]. For instance, a commonly used 3D approach to demonstrating gene knockdown efficacy of RNAi scaffolds involves mixing single cells and nanocomplexes in the gel components prior to polymerisation [293, 305, 391] or 2D assays were cells are seeded directly on top of a layer of nanocomplexes on the scaffold [395]. In both these methods, cells are immediately in contact with the nanocomplexes which is not always the case when hydrogel-nanocomplexes are injected in solid tissue. Other studies use transwell experiments were gels with nanocomplexes are set in the well and single cells seeded in 2D on the top side of a transwell [393] or vice versa [270]. This approach effectively assays release but does not incorporate a 3D aspect for the cells. The 3D assays developed in this study were designed to limit the immediate contact of cells with the nanocomplexes and allow cell transfection to occur via the release and diffusion of nanocomplexes through the separate hydrogel layers or by means of cell migration through the hydrogel layers past the nanocomplexes towards the serum rich media.

Collectively the 2D and 3D nanocomplex release and gene knockdown assay results with the tested three nanocomplexes have shown that Invivofectamine® 3.0 is the optimal nanoparticle which consistently showed minimal toxicity, high transfection efficacy, and when encapsulated in 5:1 PEGylated fibrin hydrogel over 7/10 days, maintained bioactivity compared to MD and Lipofectamine® RNAiMAX. Therefore Invivofectamine® 3.0 nanocomplexes encapsulated in 5:1 PEGylated fibrin hydrogel were used in *in vivo* model to knockdown GFP protein and myostatin mRNA in TA muscle.

3.3.2 In vivo RNAi assays

The mouse hind limb is technically attractive as it allows for easy minimally invasive access with low potential of harm to the animal. However skeletal muscle has generally been reported to be challenging tissue to gene transfect with non-viral nanocomplexes [396-398]. To assist in transfection a number of studies suggest the use of electroporation and hydrodynamic injection. Electroporation is the application of an

electrical pulse to the muscle tissue to make the cells more permeable and susceptible to transfection [398-405]. Earlier studies showed that the use of electroporation to transfect interleukin-5 pDNA into TA mice skeletal muscle [400] and pDNA expressing β-galactosidase in soleus or extensor digitorum longus muscles of adult rats [402] was more efficient than simple intramuscular DNA injection. Later studies showed electroporation effectively transfect TA muscle with shRNA against inositol 1, 4, 5-triphosphate receptor [405], 5′-Nucleotidase (NT5C1A) [403]and myostatin [404]. This, therefore, suggested that evidence of knockdown using PEGylated fibrin-nanocomplex system would be a strong indication of its ability.

As the mice used in this study expressed enhanced GFP (eGFP) ubiquitously, siGFP used in the above experiments was employed. GFP is a common gene knockdown reporter in 2D *in vitro* experiments and it was used in this study for the same purpose, to investigate downstream effects of gene knockdown at a protein level both *in vitro* and now *in vivo* using BALB/c GFP transgenic mice. However, GFP would not result in a measurable functional effect *in vivo* hence myostatin was additionally investigated to show gene knockdown effect as well as providing the possibility of measuring physical changes in the mouse muscle after gene knockdown. As previously discussed (section 1.5.1.2.4), myostatin is an important key regulatory protein in muscle regeneration and has been investigated in developing new strategies for human therapeutics in treating muscular atrophic diseases [301, 309] including the use of hydrogel based Mstn RNAi to knockdown its expression *in vivo* [301, 302]. Hence in this study, it was considered advantageous to employ the siRNA sequence that had been shown previously by Magee et al. [312], Noji group [301, 302, 406] and Mosler et al. [308] to knockdown myostatin in the masseter, gastrocnemius and quadriceps femoris muscles.

3.3.2.1 *Establishment of in vivo model*

Prior to commencing the *in vivo* study, there were a number of aspects of the RNAi and downstream analysis that required characterisation. As it was clear from the literature that skeletal muscle gene knockdown was demanding it was deemed that a maximal amount of siRNA that could be feasibly loaded in the 30µl injection volume of the TA muscle should be used. Direct communication with the manufacturer indicated that dialysis of the nanocomplexes prior to animal delivery due to lack of dilution was desirable. This was tested for its influence on cytotoxicity and efficacy as described in section 5.18 (**Appendix 7**). No significant difference in the parameters was observed

after dialysis but as these experiments were to be carried out *in vivo* and no negative influence of dialysis was observed, this dialysis modification was retained.

3.3.2.1 *Detection of GFP and Mstn gene knockdown*

In an initial study with total RNA extracted from TA of a BALB/c GFP transgenic mice, it was used to identify the optimal housekeeping gene primer to use in conjunction for RT-PCR analysis (procedure described in section 5.18.3). It was decided that GAPDH primers gave the least variation in cycle threshold (Ct) values and were therefore used in data analysis (**Appendix 8**). Mstn primers generated an acceptable Ct value at 32 cycles and the amplification efficiencies of the primers was accounted for through the analysis of RT-PCR data with the LinRegPCR software program [407]. Immunoblotting of Mstn with the purchased anti-myostatin primary antibody [404] was unsuccessful in our hands. The purchased myostatin antibody was optimised by dot blotting and western blotting to reduce background and unspecific binding (**Appendix 9**), however, analysis of myostatin from muscle tissue sample produced multiple unspecific bands rendering it impossible to discern the right size bands for myostatin. Therefore it was decided to rely on RT-PCR data of mRNA levels to determine myostatin gene knockdown. Gene knockdown of GFP by siGFP for potential protein knockdown was carried out by western blotting. GFP could be effectively extracted from TA muscle tissue and showed a higher level of expression relative to β-Tubulin as compared to HT1080-GFP (clone 9) levels (**Appendix 10**). The expression pattern also appeared different as the GFP from the BALB/c transgenic mice extract was predominantly 27 kDa whereas the HT1080-GFP extract mainly contained the 30 kDa band.

Once knockdown analysis assays were in place, an *in vivo* study looking at PEGylated fibrin hydrogel based RNAi was carried out. siMstn-Cy3 and siGFP-Cy3 complexed to Invivofectamine® 3.0 was injected alone or with 5:1 PEGylated fibrin hydrogel into the TA of BALB/c GFP transgenic mice as described in 5.18.

3.3.2.2 *Nanocomplex retention in TA over 7 days*

GFP transgenic BALB/c mice were treated with Cy3 labelled siRNA Invivofectamine® 3.0 nanocomplexes in the presence or absence of 5:1 PEGylated fibrin hydrogel

following the procedure fully described in 5.18. In short 16 mice were randomly injected in both their TA hind limbs with four groups of treatments of PEGylated fibrin hydrogel encapsulated or free siMstn-Cy3 Invivofectamine® 3.0 and siGFP-Cy3 Invivofectamine® 3.0 nanocomplexes. 7 days post treatment, TA muscles were dissected and a central ≈1mm cross section was assessed for siRNA content and the rest was used for protein and mRNA analysis. As the 1mm cross-sectional tissue samples were small (to allow maximal tissue to be made available for RNA and protein extraction in further experiments) some difficulty was experienced with processing for histology and 3 tissue samples were lost from the PEGylated fibrin-nanocomplexes (Invivofectamine® 3.0-siGFP-Cy3 and siMstn-Cy3) group and 3 samples from free nanocomplexes (Invivofectamine® 3.0-siGFP-Cy3 and siMstn-Cy3) group were lost. Cy3 labelled siRNA could be detected in the stitched micrographs in **Fig.37.** siRNA was only detected in 5 out of 14 explants for free nanocomplex group represented in **Fig.37A** and 11 out of 13 for PEGylated fibrin-nanocomplexes group represented in **Fig.37B**. Blinded image analysis showed that significantly more siRNA was present in the TA muscle tissue per total area of muscle tissue in the PEGylated fibrin nanocomplexes group by 87% versus the free nanocomplexes group (**Fig.37C**) ($p<0.05$). The results not only indicating that muscles injected with encapsulated nanocomplex localised and retained more nanoparticles in the muscle by day 7, but also that a portion of the siRNA was kept protected from RNase cleavage. This finding is in line with others who have shown that siRNA retention at the site of delivery improved in tumors, sinus mucosal lining and bone fracture targets sites when a scaffold is used in the siRNA/nanocomplex delivery [255, 262, 263, 266, 270]. Scaffold mediated nucleic acid retention in cardiac muscle tissue has also been seen in two studies where rat MI models were intramyocardially injected with either gel-siRNA-Cy5.5 or gel-pDNA [273, 274]. siRNA was detected to be more in the gel-siRNA group compared to siRNA alone 24hrs post injection. In this present study siRNA retention of nanocomplexes was seen to be increased in mouse skeletal muscle after 7 days when injected with PEGylated fibrin.

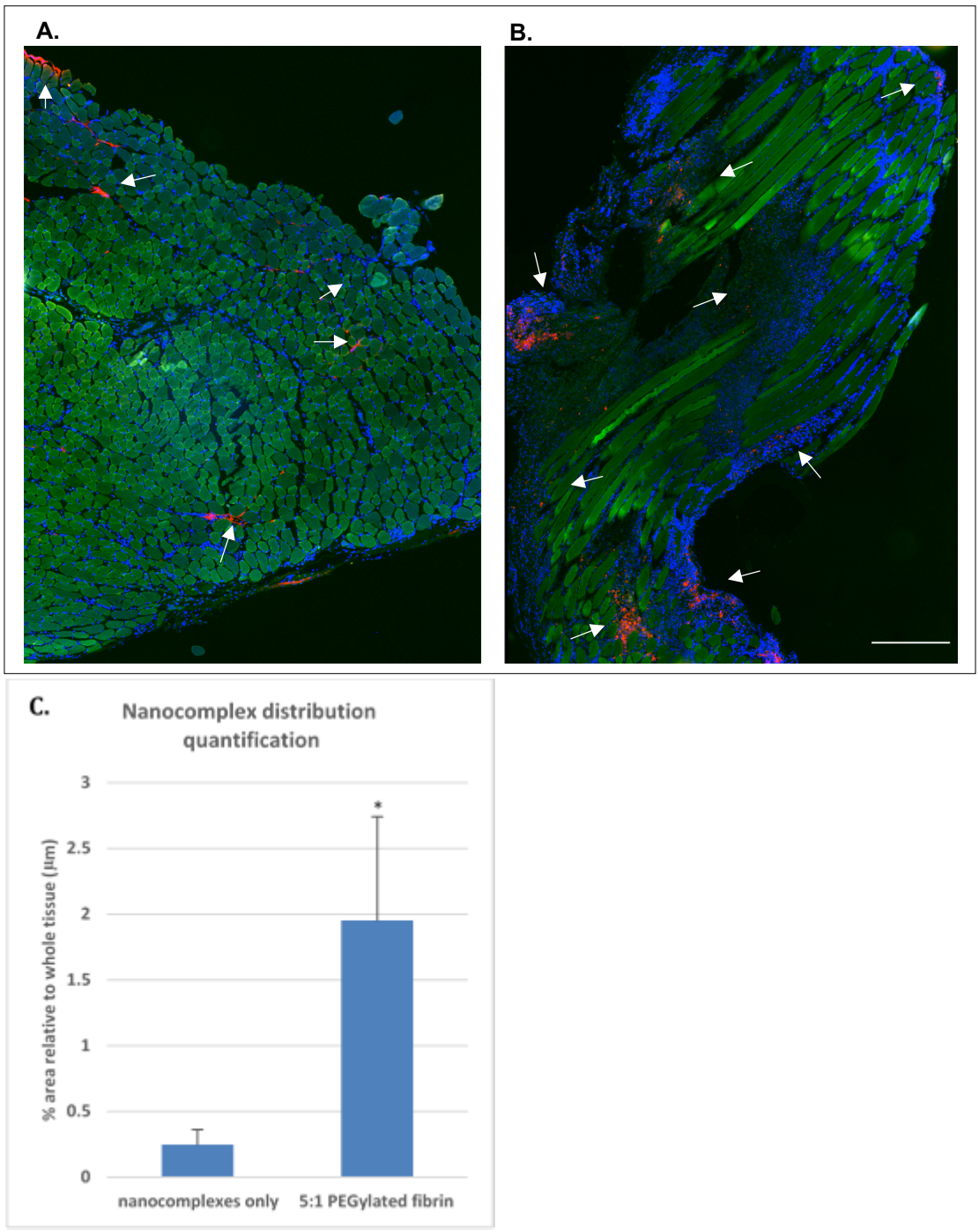

Figure 37: Tibialis Anterior muscle tissue retention of free Invivofectamine® 3.0 nanocomplexes or encapsulated in 5:1 PEGylated fibrin gel. *16 mice (32 legs) were randomly injected in their left and right TA muscle with Invivofectamine ® 3.0 nanocomplexes made with 5µg siMstn-Cy3 or siGFP-Cy3 with or without 5:1 PEGylated fibrin hydrogel encapsulation. For nanocomplex retention analysis, 7 days post treatment mice were then grouped into free nanocomplexes group and nanocomplexes in 5:1 PEGylated fibrin group (16 legs per group). 1mm crossections extracted from each TA muscle was used for fluorescent imaging of the retained siRNA in the tissue without (A) or with (B) 5:1 PEGylated fibrin hydrogel. Blue is DAPI stain, green is GFP and red is the Cy3 labelled siRNA. Arrows indicate some of the areas with nanocomplexes. (C) Quantification of the % area covered by Cy3 labelled nanocomplexes relative to total tissue by Visiopham image analysis software. Data is representation of 14 tissues samples without fibrin gel and 13 samples with fibrin gel. * p<0.05 vs nanocomplexes only group. Scale bar = 500µm.*

3.3.2.3 *GFP knockdown in vivo over 7 days*

It was considered reasonable to use siMstn treated tissue as control for their siGFP treated counterparts and siGFP nanocomplex alone treated tissue as control for the influence of fibrin as Mstn knockdown would not be expected to influence GFP expression. The converse was used for analysis of Mstn expression. The siGFP/Mstn-nanocomplex treated tissue samples were analysed for GFP knockdown by western blot analysis in **Fig.38**. No significant protein reduction was observed in the siGFP experimental groups against their siMstn treated negative control groups or for siGFP in PEGylated fibrin against siGFP nanocomplex alone. However, there was a decrease in GFP expression of 24% for Invivofectamine® 3.0-siGFP versus Invivofectamine® 3.0-siMstn (p=0.91) and 13% versus Invivofectamine® 3.0-siMstn nanocomplexes in PEGylated fibrin (p=0.98). Furthermore, Invivofectamine® 3.0-siGFP nanocomplexes in PEGylated fibrin had a reduction in GFP expression relative to all other groups: 52% vs. free Invivofectamine® 3.0-siMstn (p=0.46), 37% vs free Invivofectamine® 3.0-siGFP (p=0.85) and 46% vs Invivofectamine® 3.0-siMstn in PEGylated fibrin (p=0.67).

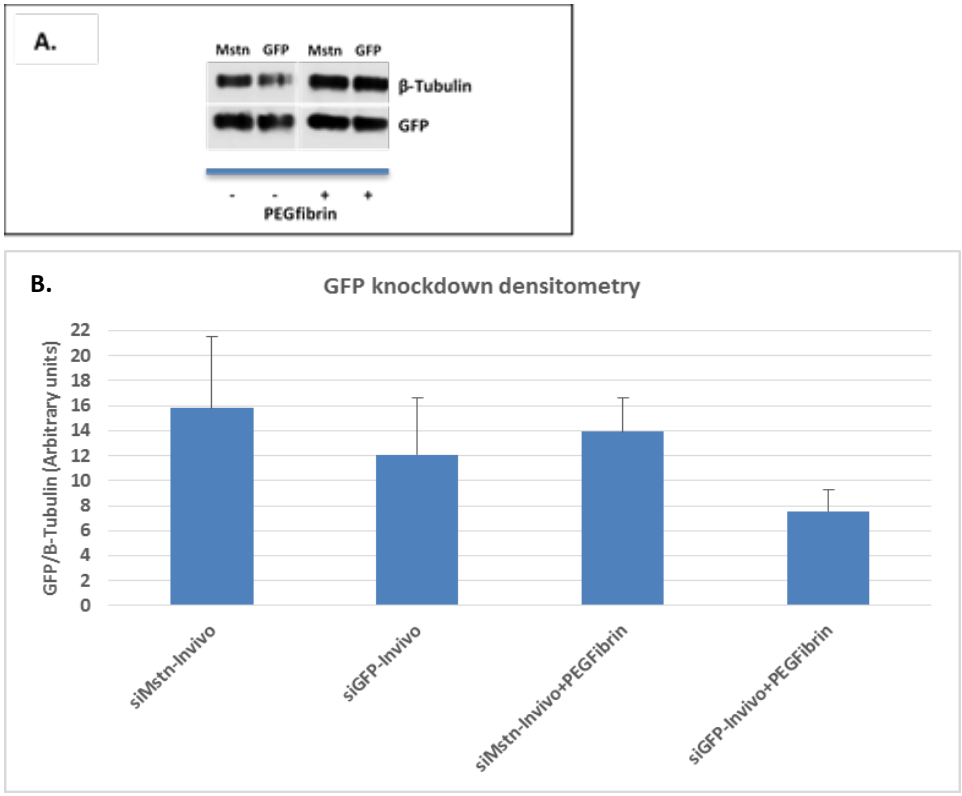

Figure 38: In vivo GFP knockdown with or without PEGylated fibrin over time. *Mice were injected in their TA muscle with Invivofectamine ® 3.0 nanocomplexes of siMstn-Cy3 or siGFP-Cy3 with or without PEGylated fibrin hydrogel encapsulation. 7 days post treatment GFP expression was determined by western blot analysis. A. GFP levels at day 7 (B) Quantification of GFP normalised to β-Tubulin, n=8. Statistical significance p=non significant.*

GFP is a protein that is commonly used as a visual and quantitative reporter for monitoring gene expression in biological assays [408, 409]. It is clear from literature that quantification of GFP knockdown is easily achieved on single cells by flow cytometry and by western blots in *in vitro* assays. eGFP protein is a stable variant of GFP that has a longer half-life which presents a challenge in studies where quantifying protein levels after transient GFP knockdown studies over a limited time period is required [409-411]. Indeed many studies investigating siRNA knockdown *in vitro* use a destabilized form of the GFP that possibly renders knockdown more detectable [52, 293, 408, 412-416]. There is a relative scarcity of *in vivo* RNAi knockdown of GFP expression studies reported in literature [274, 293, 417-422] and all were conducted using eGFP.

In an early study, 14 days after implantation of GFP expressing glioblastoma cells in the flanks of mice, siGFP attached to magnetic nanoparticle carrying a membrane translocation peptide was delivered systemically [422]. Tumor accumulation of siRNA was observed 48hrs after delivery and a significant drop in GFP fluorescence (% decrease not given) was observed with optical imaging. In a more recent but similar study, GFP expressing T-lymphoma cell tumors in mice were targeted with siGFP complexed to acid-degradable ketalized PEI were delivered systemically 10 days after cell implantation. 3 days post treatment, flow cytometry indicated a 30% reduction in GFP expressing cells from the tumors but a GFP ELISA indicated a non-significant drop in GFP expression and RT-PCR was not conclusive with respect to mRNA knockdown [419]. As noted above, tumors with their leaky vasculature may be more susceptible to RNAi reagents than soft tissue.

In skeletal muscle studies, GFP expression was achieved through plasmid transfection where GFP plasmid was delivered in conjunction with naked siGFP to TA of mice followed by electroporation [421]. An 80% knockdown in GFP expression, as determined by whole body imaging, was observed over 23 days when the plasmid was delivered in conjunction with the siRNA. Interestingly if siRNA was delivered 2 days after plasmid delivery only ≈40% knockdown was observed and this was only significant transiently at day 5, suggesting that established GFP expression and translation may make knockdown more challenging. In another skeletal muscle based study, GFP expression was achieved in mice limb through transfection with a recombinant adenovirus that expresses GFP [417]. Delivery of siGFP in a cationic nanogel achieved a 58% knockdown as determined by fluorescence of the limb. However, it should be noted that the fluorescence capture methodology and time of analysis were not supplied.

In a study that used transgenic mice expressing GFP under control of the β-actin promoter (heterozygotes as compared to homozygotes used in this present study), delivery to mouse bronchial epithelial cells was undertaken through nasal spray of siGFP/chitosan nanoparticles daily for 5 days [420]. These particles were observed to knockdown GFP expression *in vitro* by 80% whilst bronchial epithelial cell knockdown in mice was observed by fluorescent microscopy to achieve ≈40% knockdown. A limited number of replicates (2-3) were used in this study. Transgenic rats expressing GFP from the CAG promoter in their cardiac tissue (see section 1.5.1.2.5) had guest host assembled PEI hydrogel carrying siGFP-Cy5.5 injected into heart tissue [417]. Here cardiac GFP expression was assayed with confocal microscopy whereby GFP fluorescence intensity that co-localised with siGFP-Cy5.5 signal was determined. At 24hrs a 40% reduction in GFP fluorescence was observed when siGFP-Cy5.5 signal was present.

RNAi knockdown of GFP expression *in vivo* appears to be in the majority assayed by fluorescence based methodologies which are more quantitatively challenging than methods such as western blot and Elisa. In one study described above, significance observed with flow cytometry was lost when analysed with ELISA suggesting that this latter type of analysis should be employed more frequently.

The mice used in this study were eGFP expressing mice with expression driven by a ubiquitin C promoter and the mice were homozygotes. Therefore, there were potentially high levels of expression of the more stable variant and consequently, it is possible that the turnover of the protein may not have been rapid enough to reliably detect protein reduction.

The observation above that knockdown was more effective when carried out in parallel with the initiation of GFP expression in skeletal muscle than when knockdown was delayed by only 2 days further suggests that the stability of the eGFP variant may render GFP knockdown detection challenging [421]. Though not significant, a reduction in GFP protein levels was observed with the most pronounced reduction in the hydrogel group.

3.3.2.4 *Myostatin knockdown in vivo over 7 days*

The knockdown of Mstn in TA tissue samples treated with the free or PEGylated fibrin encapsulated siMstn-Cy3 or GFP-Cy3 Invivofectamine® 3.0 nanocomplexes was determined by RT-PCR (section 5.18.3). Mstn expression was normalised against

GAPDH taking into account the individual primer efficiencies acquired from LinRegPCR program output (determined from averaging primer efficiencies for each sample run) [407].

RT-PCR analysis (**Fig.39** amplification curves in **Appendix 11**) showed that only delivery of siMstn-Cy3 complexed on the 5:1 PEGylated fibrin hydrogel resulted in a significant knockdown against all groups that is, 91 ± 17% versus free Invivofectamine® 3.0-siGFP-Cy3, 93 ± 22% versus free Invivofectamine® 3.0-siMstn-Cy3 and 86 ± 62% versus 5:1 PEGylated fibrin hydrogel encapsulating Invivofectamine® 3.0-siGFP-Cy3 groups ($p<0.01$). All other changes were not significant. This result indicates that the entrapment and release of Invivofectamine® 3.0-siMstn-Cy3 nanocomplexes in PEGylated fibrin hydrogel over the 7 days was effective.

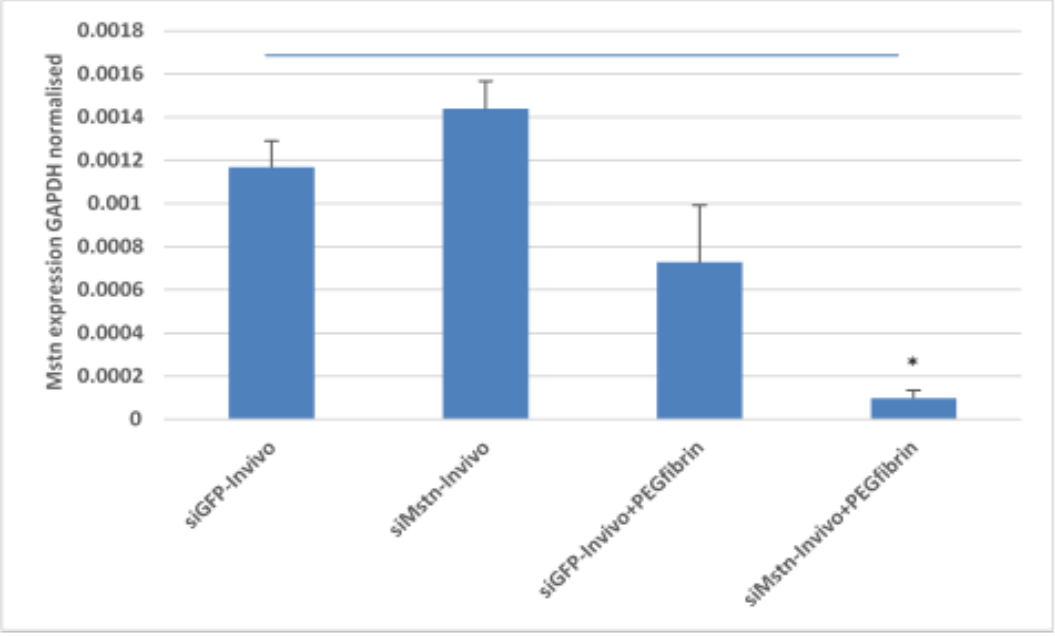

Figure 39: Myostatin knockdown with Invivofectamine® 3.0 nanocomplexes in the presence or absence of 5:1 PEGylated fibrin over 7 days. *Mice were injected in their TA muscle with Invivofectamine ® 3.0 nanocomplexes of siMstn-Cy3 or siGFP-Cy3 with or without PEGylated fibrin hydrogel encapsulation. 7 days post treatment, Mstn expression was quantified by RT-PCR normalised to GAPDH. n=8. * p<0.05 vs all groups.*

Since Mstn is known to promote muscle growth through muscle cell hypertrophy and hyperplasia [423], the mass of the excised TA was quantified (**Fig.40**). Only the fibrin hydrogel encapsulating Invivofectamine® 3.0-siMstn-Cy3 group showed a significant increase in mass of 26% and 25% against the free Invivofectamine® 3.0-siGFP-Cy3 and Invivofectamine® 3.0-siGFP-Cy3 nanocomplexes groups respectively. There was only a non-significant 9% increase against the fibrin hydrogel encapsulating Invivofectamine®

3.0-siGFP-Cy3 group. This suggests that retention of fibrin and associated fluid might contribute to the observed mass gain.

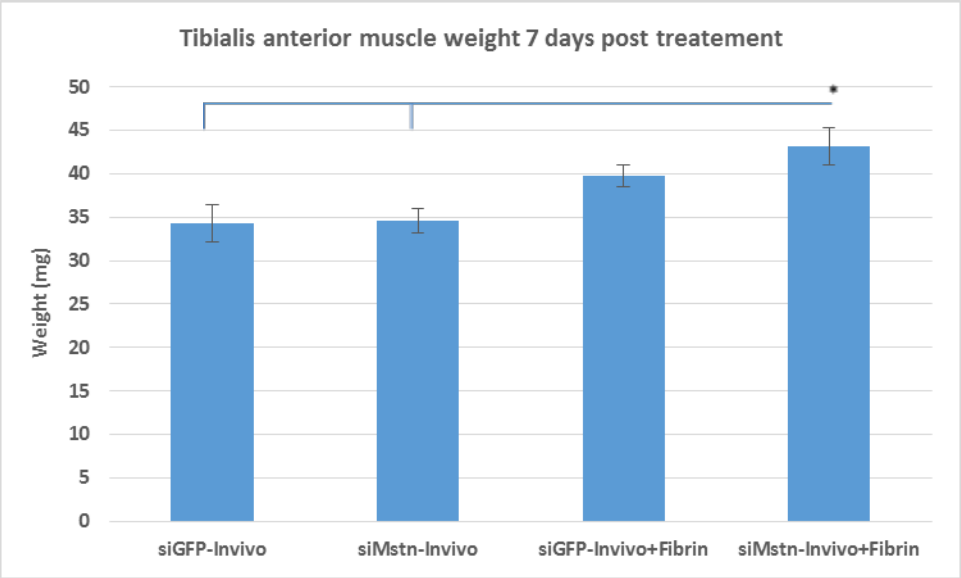

Figure 40: Effects of Mstn knockdown over 7days on TA muscle tissue weight. *Mice were injected in their TA muscle with Invivofectamine ® 3.0 nanocomplexes of siMstn-Cy3 or siGFP-Cy3 with or without PEGylated fibrin hydrogel encapsulation were analysed for muscle weight gain 7 days post treatment. The excised TA tissue was weighed. n = 8. *p<0.05 vs siGFP-Invivofectamine and siMSTN-Invivofectamine.*

There have been several studies investigating the influence of siMstn sequence used in this present study on skeletal muscle mass. They all examine mass gain after 2-4 weeks. In the original study that identified the sequence as being an effective Mstn mRNA inhibitor, the sequences incorporated in a shRNA plasmid was electroporated in the TA of rats and the muscle excised after 2 weeks [312]. Only a 25% mRNA knockdown was achieved but this resulted in a 10% increase in muscle mass. In two related studies where the sequence was delivered with atelocollagen into masseter muscles [301] and biceps femoris [302] of mice, a 20-60% increase in muscle size was observed in the earlier study in the biceps femoris and around 35% increase in masseter mass with a 75% knockdown of mRNA at 2 weeks. In a study that examined the effect of combining mice exercise with RNAi, the siRNA sequence was delivered systemically using a mini-osmotic pump [308]. After 28 days, only the combination of siRNA and exercise resulted in an increase of the mice's gastrocnemius muscle mass of 8%. This was associated with a knockdown of Mstn mRNA of approximately 30-40%. Interestingly for both this and the first Mstn RNAi study above, in a comprehensive Cre recombinase study in mice with floxed Mstn genes, it was found that a 60% knockdown of Mstn mRNA was required

to achieve an increase in muscle mass [424]. In a recent study using an alternative sequence conjugated to a highly chemically modified cholesterol, systemic administration in mice achieved 85-95% knockdown of Mstn mRNA [425]. Here an ≈8% increase in mice gastrocnemius muscle size (as determined by microcomputed tomography) was observed after 7 days. The apparent increase in mass of the TA in this present study coupled with a 90% mRNA knockdown is comparable to the findings discussed above, suggesting that delivery from PEGylated fibrin hydrogel is advantageous. It should be noted that the level of knockdown observed in vivo was similar to that achieved in the experiments above where cells were transfected with siRNA complexed with Invivofectamine® 3.0 in the presence of serum.

In total, the results reported above for delivery of siRNA into the challenging environment of the skeletal muscle is efficacious when encapsulated within PEGylated fibrin. This improved efficacy most likely resulted from the improved retention and controlled release of the lipid nanocomplexes.

Future work to further investigate this system should consider longer implant periods whereby a potentially more pronounced increase in muscle mass might be achieved. Additionally, the impact of delivery into a muscle damage model where the impact on muscle function could be assessed would be informative.

4 Conclusions

The present study confirmed the observations shown in literature that the PAMAM dendrimer effectively condenses siRNA, and efficiently delivers siRNA in *in vitro* 2D cell culture with minimal cytotoxicity. Efficacy of the dendrimers in this study was demonstrated in two ways, by GFP knockdown and using a cocktail of siRNA sequence that result in cell death. It was confirmed that the unmodified version of the nanoparticle was not as effective in GFP knockdown in HT1080 cell line compared to the modified version, additionally, it was observed to have no effect at all when cell death was assessed. This highlights the importance of using various assays to show efficacy of nanoparticles. These siRNA interactions and gene knockdown were improved when the nanoparticle was modified with PEG polymer and DOPE lipid molecule, again confirming the work from the original study. In an extension to previous work, both dendrimers were shown to effectively protect against RNase attack for at least 10 days. Even though the dendrimer nanoparticles could effectively knockdown genes, when compared to the commercial lipid nanoparticles their efficacy paled in comparison. As these lipid based nanoparticles were intended for sustained delivery *in vivo* from scaffolds, which has never been reported in literature, their siRNA binding capacity and RNase protection capacity was also examined. Invivofectamine® 3.0 was verified to be non-cytotoxic and to effectively bind around 70% of its siRNA. Although the majority of complexed siRNA was degraded within 24hrs, the nanoparticle persistently protected 10% of its siRNA over 10 days.

Enzymatically degradable PEG and fibrin hydrogels have not been comprehensively investigated for controlled siRNA delivery thus they were assessed here. The modification of fibrin by adding PEG molecules to stabilise degradation of fibrin *in vitro* and allow sustained release of cargo has been shown by the Suggs group. They also showed a structural change of the fibrin from a network of fibrillary structure to sheet-like morphology. This study confirmed these well-defined effects of fibrin PEGylation *in vitro* and went further to show for the first time the comparisons of non-PEGylated and PEGylated fibrin degradation rate *in vivo*. Unmodified fibrin degraded *in vivo* by day 2 whilst the PEGylated fibrin gradually degraded and was still present in tissue after 7 days. The hydrolytically and enzymatically degradable PEG-AC hydrogel had a much faster degradation rate *in vivo* compared to that *in vitro*, and this was presumably due to the exposure of the enzymatically degradable crosslinker by the hydrolytic degradation.

PEG-AC, like unmodified fibrin, was completely degraded by day 2 and therefore would not be useful for *in vivo* sustained release, however, PEG-VS showed similar degradation rate to the PEGylated fibrin gels. Because PEG-VS did not degrade *in vitro* and release siRNA or nanocomplexes, the efficacy of those releasates could not be verified *in vitro*. This type of gel may be an interesting candidate for nanocomplex delivery to invasive cells in the future. This present study proceeded with the PEGylated fibrin hydrogel which did release siRNA nanoparticles in a sustained manner *in vitro* and whose efficacy could be verified. It was determined that of the nanoparticles used in the study, Invivofectamine® 3.0 nanocomplex releasates remained effective over 10 days of release.

A 3D assay was designed to more closely mimic *in vivo* delivery to soft tissue, whereby PEGylated fibrin hydrogels containing cells or nanocomplexes were polymerised separately were employed. Though other variations of these assays have been used, it is the first time they were used for a RNAi assay. The 3D assays showed that Invivofectamine® 3.0 nanocomplexes were consistently efficacious with no evidence of cytotoxicity. It was also found in these assays that though the modified dendrimer nanocomplexes were effective at gene knockdown at early time points, with longer exposure to cells there were evident signs of toxicity. Based on these results, it was determined that Invivofectamine® 3.0 and PEGylated fibrin hydrogels were the optimal siRNA delivery combination and were investigated *in vivo*.

To our knowledge, PEGylated fibrin hydrogel has not been used for sustained *in vitro* or *in vivo* RNAi. Furthermore to this, RNA interfering lipid nanocomplexes specifically have not been shown to be delivered in a sustained manner by any scaffold. This study is the first to show *in vivo* RNAi in mouse skeletal muscle, which is considered a challenging tissue to transfect, via localised and sustained delivery of lipid based nanocomplexes encapsulated in PEGylated fibrin hydrogel. The direct injection of this novel hydrogel-lipid nanocomplex (PEGylated fibrin hydrogel- Invivofectamine® 3.0 nanocomplex) RNAi system into the TA muscle resulted in (1) improved siRNA or nanocomplex retention at the target site compared to free nanocomplexes (2) the knockdown of target Mstn mRNA, and a significant muscle weight increase as well as an observed reduction in GFP level (through this reduction was not significant) compared to free lipid nanocomplexes or the hydrogel-lipid nanocomplex control groups within the 7 day period. Future work will investigate the effect of Mstn knockdown over a longer period on muscle growth.

In this present thesis, Invivofectamine® 3.0 nanocomplexes were shown to be the optimal nanoparticle for sustained siRNA delivery from the nanoparticles assessed.

Encapsulating the lipid nanocomplexes in PEGylated fibrin hydrogel improved the efficacy of free lipid nanocomplexes in skeletal muscle gene knockdown. A novel PEGylated fibrin hydrogel- Invivofectamine® 3.0 nanocomplex RNAi system established in this preliminary proof of concept study, is potentially a delivery system for RNAi molecules for various human diseases and presents further opportunity for possible improvement and clinical development.

5 Methods

5.1 Modified dendrimer nanoparticle formation

5.1.1 G(4)-D-PEG$_{2K}$-DOPE Polymer synthesis

Synthesis of G(4)-D-PEG$_{2K}$-DOPE was prepared following the procedure previously detailed by Torchilin et al. and Biswas et al. with minor modifications described below [140, 426].

5.1.1.1 *Synthesis of NPC-PEG$_{2K}$-DOPE (starting polymer)*

PEG$_{2K}$-NPC$_2$ (1g, 0.5mmol) was dissolved in 5ml chloroform (≈10 fold molar excess to DOPE). 20µl tris base, acetic acid and EDTA (TAE) buffer solution was added to 50mg/ml solution of DOPE (37.2mg, 0.05mmol) in chloroform [37.2mg DOPE +744µl chloroform + 20µl TAE]. The DOPE-TAE mixture was added dropwise to the PEG$_{2K}$-NPC$_2$ solution. The reaction mixture was incubated at room temperature (RT) overnight with stirring. Chloroform was removed with a rotary evaporator and freeze dried. The crude reaction mixture was dissolved in 1 ml 0.01 M hydrochloric acid (HCl) solution with water bath sonication to form NPC-PEG$_{2K}$-DOPE micelles. The micelles were purified from the unbound PEG$_{2K}$-NPC$_2$ and released -NPC by dialysis of the mixture against 0.01 M HCL using cellulose ester dialysis membrane with 12-14000 kDa molecular weight (MW) cut off. Dialysis was carried out with changes of HCl three times at 2X1.5hrs and overnight. The purity of NPC-PEG$_{2K}$-DOPE product was determined by thin layer chromatography (TLC). The initial pure fractions of NPC-PEG$_{2K}$-DOPE were freeze dried.

5.1.1.2 *Synthesis of G(4)-D-PEG$_{2K}$-DOPE (Modified Dendrimer, MD)*

In a pre-weighed 50ml flask methanol was evaporated from 0.62ml of G(4)-D solution on a rotary evaporator for 20mins to get 69mg of G(4)-D. 10µl of TEA was added to 69mg G(4)-D re-suspended in 25ml DMF, and NPC-PEG$_{2K}$-DOPE solution in DMF (12.6mg in 2.5ml DMF] was added in a 1:1 molar ratio. The MW of NPC-PEG$_{2K}$-DOPE 2663.51g/mol and that of G(4)-D is 14214.17 /mol. The reaction mixture was stirred overnight at RT to create a modified dendrimer nanoparticle theoretically with 63 free primary amines. DMF

was removed by rotary evaporator. The crude mixture was dissolved in 1ml water and dialyzed against water as described above. The collected G(4)-D-PEG_{2K}-DOPE (modified dendrimer, MD) product was freeze dried in pre-weighed vials using Virtis-Freeze Dryer for 24hrs and characterized by nuclear magnetic resonance (NMR) spectroscopy using Varian 400 MHz spectroscope. In preparation for NMR analysis, product MD, starting materials G(4)-D (which is referred to as D) and NPC-PEG_{2K}-DOPE were dissolved in d-methanol (10mg/ml).

5.2 Nanocomplex formation

5.2.1 D-siRNA dendriplex formation and Nitrogen:Phosphate (N/P) ratio determination

Following nanocomplexing protocol by Biswas et al. [140], 200ng siRNA in a 10µl volume of Hepes and glucose buffer (BHG) buffer pH 7.4 (**Appendix 14**) was added to appropriate dendrimer concentration determined by the N/P ratio (0 – 20 range), also in a 10µl volume of BHG buffer. N refers to the number of moles of nitrogen (N) on the dendrimer, while P refers to the number of moles of phosphates (P) on the backbone of siRNA. N/P ratios of 0:1, 0.5:1, 1:1, 2:1, 4:1, 8:1,10:1 and 20:1; were considered in this study. The amount of N (dendrimer) required, as P (siRNA) remained constant at 200ng, was determined by the formula in **Equation 1**. The mixture was incubated for 20mins at RT to allow dendriplexes/nanocomplexes to form. **Fig.8** shows the schematic representation of how MD was synthesised and how dendriplexes possibly occur.

Equation 1: N/P ratio calculation formula

$$\mathrm{N/P} = \frac{number\ of\ moles\ of\ G{-}(4){-}Dendrimer \times 64\ (free\ amines)}{number\ of\ moles\ of\ siRNA \times 42\ (Phosphate\ groups\ in\ backbone)}$$

5.2.2 Lipofectamine® RNAiMAX nanocomplex formation and optimisation for transfection

Lipofectamine® RNAiMAX was used as a positive control for GFP knockdown *in vitro* as well as one of the lipid based nanoparticle in addition to the dendrimer. Nanocomplexes

with Lipofectamine® RNAiMAX were made following Lipofectamine® RNAiMAX manufacturers guide specifications with a few modifications as follows. 5000 cells were seeded per well in a 96 well plate a day prior to transfection. A range of 0.6µl - 5ul Lipofectamine was used to complex 200ng siNegative in serum free MCDB media pH 7.4 instead of recommended Opti-MEM® Medium. Cells were transfected with the nanocomplexes and monitored over 72hrs microscopically. 0.6µl Lipofectamine® RNAiMAX had the least cytotoxic effect on the HT1080 cells and was considered optimal volume to use in all the *in vitro* transfection experiments instead of the recommended 0.3µl per ≈13.3ng siRNA (4.5µl per 200ng). 0.6µl Lipofectamine® RNAiMAX was used to complex 200ng or 500ng siRNA depending on experimental needs.

5.2.3 Invivofectamine® 3.0 nanocomplex formation

Invivofectamine® 3.0 was used as the second lipid based nanoparticle of interest in our study. The Invivofectamine® 3.0 nanocomplexes were made following Invivofectamine® 3.0 manufacturers guide specifications with the following modifications: 10µl of Invivofectamine was added to an equal volume of siRNA and complex solution to give a final concentration of 0.6mg/ml siRNA in 20µl. The 20µl mixture was incubated for 30mins at 50^{o}C and no further dilution (6X dilution) of the nanocomplexes as recommended by the manufacturer was implemented to keep the concentration of nanocomplexes as high as possible for later scaffold delivery studies. The change in protocol of using nondiluted nanocomplexes was tested *in vitro* in GFP knockdown experiments (section 5.8.2). 6X, 3X, 2X and 0X dilution of nanocomplexes all containing (1000ng siGFP/Mstn-Cy3) were used in the transfection of HT1080-GFP cells to ensure efficacy of the nanocomplexes was maintained when used in their concentrated form (**Appendix 12**). This would allow smaller volumes with more siRNA-nanocomplexes to be loaded in the 30µl volume hydrogels without compromising nanocomplex efficacy. Once nanocomplexes were made they were immediately used in knockdown transfection experiments or stored at 4^{o}C up to 1 week until use as recommended by the manufacturer. It was established that using diluted or non-diluted stock nanocomplexes had no effect on transfection, all experiments involving Invivofectamine® 3.0 nanocomplexes *in vitro* were made following manufacturers guide without the final 6X dilution.

5.3 Nanocomplex formation and dissociation ability tests by:

5.3.1 Gel shift assay

D and MD Dendriplexes N/P ratios of 0 – 20 as well as Lipofectamine® RNAiMAX and Invivofectamine® 3.0 nanocomplexes were prepared in as described in section 5.2 using siNegative. After incubation of the nanocomplex mixtures for the recommended times, nanocomplex formation was tested by gel shift assay. After nanocomplex incubation, for dendriplexes, 20µl aliquots for each ratio were mixed with GelRed™ nucleic acid dye (final concentration 1X) to label siRNA and loaded into wells of a 2% (w/v) agarose gel for electrophoresis using a Biorad nucleic acid electrophoresis system (55V for 30mins). When nanoparticles condense the siRNA it renders it unable to migrate through the agarose gel pores, only free unbound siRNA migrates towards the anode. The siRNA bands were visualized under UV light using Syngene InGenius^3 Gel Documentation system and micrograph images were taken by the system's GeneSys image capture. Quantification of the siRNA bands was done by Syngene GeneTools image analysis software.

5.3.2 Fluorescent siRNA quenching and dissociation assay

Dendriplex formation and dissociation ability was tested by RiboGreen™ RNA label exclusion quenching assay and heparin sulphate RNA dissociation method following Biswas et al. [140] with modifications as follows: Dendriplexes N/P ratios of 0 – 20:1 were prepared using siFITC**.** RiboGreen™ (with an excitation/emission wavelength of 500 / 525nm) was included in the dendriplex mixture to label and amplify the fluorescent signal of free siRNA. FITC has an excitation/emission wavelength of 485/520 nm similar to RiboGreen™. Firstly the 200ng siFITC in 9µl BHG buffer was incubated with 1µl RiboGreen™ stock solution for 10mins at RT to label siRNA before nanocomplexes are made. The labelled siRNA was incubated with 10µl D/MD for 20mins at RT to form dendriplexes in BHG buffer. The 20µl dendriplex solution with label was added to 40µl Tris-EDTA pH 8 (TE, **Appendix 14**) buffer to make a 60µl volume that would cover the well of a 96 well white opaque pate. BHG and TE buffer only with RiboGreen™ was included as background control. The fluorescence intensity of any free siRNA was detected and measured by a 96 well plate reader fluorescence spectrophotometer (Cary

Eclipse), at 500/525 excitation and emission wavelengths. 10 and 50U of heparin sulphate per 1µg siRNA was added to the dendriplex mixture with mild shaking to dissociate siRNA from the dendrimers and fluorescence was measured again.

5.4 D, MD, Lipofectamine® RNAiMAX and Invivofectamine® 3.0 nanocomplexes siRNA serum protection ability.

1000ng scramble siNegative was complexed to D and MD at an N/P ratio of 0-20:1 (as above in section 5.2.1) in BHG buffer pH 7.4, a total volume of 100µl master mix for each N/P ratio 0-20. 100µl FBS was added to each reaction tube (50% final serum concentration). Lipofectamine® RNAiMAX (0.6µl) and Invivofectamine® 3.0 master mix was also made following manufacturers guide and the protocol above in sections 5.2.2 and 5.2.3; nanocomplexes with 1000ng siRNA were made and diluted to a total volume of 100µl with Iso-osmotic PBS (IsoPBS) pH 7.4. 100µl fetal bovine serum (FBS) was added to the reaction tubes containing the 100µl nanocomplex solutions (50% final serum concentration). Each reaction tube contained 200µl solution of nanocomplex and serum. Over a period of 10 days, 10µl aliquots of serum + nanocomplex sample (100ng siRNA) from each nanocomplex (D, MD, Lipofectamine® RNAiMAX and Invivofectamine® 3.0) were collected and snap frozen in liquid nitrogen and stored at -20^{0}C. Samples were vortexed before each collection. After 10 days, SDS was added to each collected 10µl (100ng siRNA) sample to dissociate the siRNA from the nanoparticles (0.5% final SDS concentration). 1X Loading dye with nucleotide labelling dye GelRed™ was added to the samples. Fresh 100ng siRNA was included as positive control. Samples with SDS were incubated for 5mins after which samples were subjected to electrophoresis according to protocol in section 5.3.1.

5.5 Cell culture

Table 3: Cell plating protocol for tissue culture

Cell Type	Plate size	Cell number plated	Volume of media
HT1080 (GFP or non-GFP)	96 well	5000	100µl
	24 well	30000	500µl
	Transwell	15000	200µl top well 500µl bottom well

HT1080 and HT1080-GFP cells were cultured in MCBD media in an incubator at 37^0C with 5% carbon dioxide. The number of cells used in the experiments and the volumes of media in which they were maintained is indicated in **Table 3**. The media contained 10% FBS, 1% penstrep antibiotics (100U penicillin and 100ug streptomycin). HT1080-GFP cells were maintained in full growth media with 200ng/ml G418 (Geneticin antibiotic), during the growth phase only, to keep positively selecting for GFP expressing cells.

5.5.1 Making a stable HT1080 cell line expressing GFP (HT1080-GFP)

800000 cells were seeded in two 60mm cell culture plates. The following day cells in one plate were transfected with PolyFect transfection reagent according to supplier's guide complexing 2.5ng pEGFP-C1 plasmids with a neomycin resistant gene for selection (**Appendix 1**). No DNA was added in the control plate. 24hrs post transfection media was removed and cells were maintained in full growth media with 600µg/ml G418. G418 selects against non-transfected over time, and maintains selection for cells that stably incorporated the eGFP plasmid in their genomic DNA. After 3 weeks, 3 stable clones (9, 10 and 16) were selected by limiting dilution following Life Technologies protocol. Cells seeded for experiments were maintained in normal MCDB growth media without G418. Flow cytometry described in section 5.6 below was carried out on the 3 clones to show positive GFP expression in the 3 clones, non GFP expressing cells HT1080 cells were included as a negative control (**Appendix 2A**). Clone 9 which showed the highest GFP expression indicated by higher geometric shift was chosen for all *in vitro* experiments.

5.5.2 Cytotoxicity analysis for D, MD and Invivofectamine® 3.0 nanocomplexes

200ng siNegative complexed to Lipofectamine® RNAiMAX, Invivofectamine® 3.0, D and MD (N/P ratios of 0-20:1) were added to 5000 cells in a 96 well white opaque plate that were seeded in triplicate 24hrs prior (150nM final siRNA concentration). Untreated cells or siRNA only treated cells were included as controls. The transfection was allowed to occur over 4hrs without serum, and cells were incubated at 37^oC for 48hrs in 100µl volume of growth media. Cell death was detected 48hrs post transfection using the CellTiter-Glo® luminescent Cell Viability Assay as per the manufacturer's guide protocol. 100µl of CellTiter-Glo® Reagent was added to the transfected cells and incubated for 10mins. CellTiter-Glo was also added to 2500, 5000, 10000 and 15000 cells seeded in triplicates on the day of detection to generate a standard curve. The reagent lyses the

cells and enables the detection of ATP present in viable live cells which is proportional to the number of cells present ATP dependent luminescence was quantified on a Promega GloMax 96 microplate luminometer. The number of viable cells was determined from the standard curve and expressed as percentage cell survival normalised to untreated control cells. The same was done for cells treated with Invivofectamine® 3.0 nanocomplexes. Cells were treated with nanocomplex solution containing 200ng siRNA (0.36µl Invivofectamine® 3.0-siRNA) for 4hrs in the absence of serum and further incubation and ATP detection was done as indicated above.

5.6 Flow cytometry

Treated and untreated HT1080 or HT1080-GFP cells with siGFP or fluorescently labelled siRNA (siFITC) were washed with warm PBS (pH 7.4) to remove media, trypsinised from the base of the plate and centrifuged at 1500rpm. The cell pellet was suspended in 500µl of FACS buffer and the GFP fluorescence intensity was measured and represented as geometric shift from the mean as measured on a Beckon Dickson FACSCalibur flow cytometer. 10000 cells were counted for analysis and gated using forward-scatter versus side-scatter to exclude debris and dead cells.

5.7 D and MD dendriplex transfection efficiency in HT1080 cells.

The FITC labelled siRNA dendriplexes were prepared as described in 5.2.1 for N/P ratios of 2 – 20:1. 20µl of complexes were added to 5000 HT1080 cells seeded in triplicates the day before in 96 well plates containing 180µl volume of serum free fresh growth media. Cells only and siRNA only negative controls were included in the experiment. After 4hrs of incubation at 37^{o}C, cells were carefully washed 1X with PBS pH 7.4. Full growth media was added and cells were incubated for 24hrs. Cells were then washed with PBS pH 7.4 and nuclei stained with Hoechst stain at a final concentration of 2µg/ml in media for 10mins. Post staining cells were washed with PBS pH 7.4 to remove excess staining solution. 200µl growth media was added and cells were imaged by inverted fluorescent microscope (Zeiss Axiovert 200M Inverted Fluorescent Microscope).

5.8 Nanocomplexes transfection efficacy

5.8.1 Cell death assay

D and MD dendriplexes were formed with 200ng siDeath/siDeath-Negative at ratios 0-20:1. 5000 HT1080 cells seeded in triplicates a day prior in 96 well plates were transfected for 4hrs without serum with the dendriplexes. Untreated cells and free siDeath/siDeath-Negative were included as negative controls. After 4hrs full growth serum was added to the cells and 48hrs post transfection CellTiter-Glo® Luminescent cell viability assay was performed as described in section 5.5.2.

5.8.2 Complimentary D and MD dendriplex uptake and efficacy.

5.8.2.1 *siFTC uptake by D and MD dendriplexes (N/P 8)*

To determine transfection efficacy with siFITC, in 24 well plates, after determining the best transfection ratio (N/P 8) which would be applied throughout the study, 30000 HT1080-GFP cells were seeded in triplicate. The following day the cells were transfected with D and MD dendriplexes containing 1000ng siFITC at (N/P of 8). Dendrimers only or free siFITC where included as controls. 24hrs post transfection, efficacy of the dendriplexes was determined by flow cytometry, which measured and quantified the geometric shift from control untreated cells. Flow cytometry procedure fully described in 5.6.

5.8.2.2 *GFP knockdown with D and MD dendriplexes (N/P 8)*

Transfection efficacy of D and MD dendriplexes was measured by flow cytometry and western blotting. 30000 HT1080 cells or HT1080-GFP cells were seeded in a 24 well plate in triplicate, the following day cells were transfected for 4hrs in serum free media with D and MD (N/P 8) made with 1000ng siGFP or scramble siNegative siRNAs. 48 or 72hrs post 4hr transfection, GFP knockdown in cells was determined and analysed by either flow cytometry (section 5.6) or western blot analysis (section 5.10) depending on experimental needs. GFP knockdown analysis by flow cytometry was made 48hrs and 72hrs post transfection. Untreated HT1080 cells, untreated HT1080-GFP cells, free siGFP only treated cells and D/MD nanoparticles only treated cells were included as negative GFP knockdown controls. Untreated HT1080 cells were used as an indication

of GFP knockdown. GFP knockdown analysis by western blot was made 48hrs post transfection. Here, Lipofectamine® RNAiMAX (0.6µl/1000ng) and untreated HT1080 cells were used as positive controls for GFP knockdown whilst untreated HT1080-GFP cells and free siGFP only treated cells were included as negative GFP knockdown controls. 48hrs post transfection whole cell lysate protein was extracted from cells (section 5.9) in preparation for western blot analysis.

5.8.3 GFP knockdown with MD, Lipofectamine® RNAiMAX and Invivofectamine® 3.0 nanocomplexes.

Transfection efficacy of all nanocomplexes was measured by flow cytometry. 30000 HT1080 cells or HT1080-GFP cells were seeded in a 24 well plate in triplicate, the following day cells were transfected for 4hrs in serum free media with MD (N/P 8), Invivofectamine® 3.0 and Lipofectamine® RNAiMAX (0.6µl/1000ng) nanocomplexes were made with 1000ng siGFP or siNegative control siRNAs. Untreated HT1080-GFP only cells, free siGFP, and all three nanoparticles complexed with siNegative siRNA were included as negative knockdown controls. 48hrs post transfection GFP knockdown was and analysed in cells by flow cytometry (section 5.6).

5.9 Protein extraction from HT1080-GFP cells *in vitro* for western blot analysis

After cells were treated with MD nanocomplexes in the GFP knockdown experiment (section 5.8.2.2), cells were washed 3X with warm PBS pH 7.4, trypsinized and centrifuged at 1500 rpm. 50µl Ice cold radioimmunoprecipitation assay (RIPA) buffer with protease inhibitor (PI) cocktail (1µl /100µl RIPA) was added to the cells on ice were subjected to one short burst of sonication with a microprobe and incubated for 10mins on ice to allow complete cell disruption. After incubation, the samples were centrifuged at 14000rpm (4^0C for 5minutes) to remove debris and DNA. The supernatant was transferred to a fresh Eppendorf and the extracted protein quantified by Bradford's assay according to Pierce™ Detergent Compatible Bradford Assay Kit manufacturer's guidelines. Samples were stored at -80^0C prior to analysis for GFP expression (western blot section 5.10).

5.10 Western blot analysis

The protein concentration to use in western blot analysis experiments for GFP expression and detection with the listed antibodies (**Table 2**) was optimised to reduce background. 30µg protein samples was optimal for analysis (**Appendix 2B**). 30µg of protein from either HT1080 cells or mouse tissue was electrophoresed under reducing conditions using 5% β-Mercapthoethanol. The sample was boiled for 10mins in the reducing loading dye. The proteins were then separated on a 12% SDS-page BioRad TGX™ FastCast™ Acrylamide gel at constant 200 volts (V) for 40mins. A Precision Plus Protein™ dual colour molecular weight marker was included in the protein separation to estimate the protein sizes. Protein transfer onto nitrocellulose membrane was done using semidry transblot system for 15mins at constant 10 V. To prevent nonspecific antibody binding the membrane was blocked for 1hr at RT with 5% non-fat milk in Tris buffered saline tween (TBST). GFP (≈27 kDa), myostatin (≈50 kDa) and the loading control β-Tubulin (≈50 kDa) protein were probed for rabbit anti-GFP, rabbit anti-myostatin and rabbit anti-β-Tubulin primary antibodies in 5% non-fat milk in TBST overnight at 4^0C. Membranes were washed 3 times for 10minutes with TBST. Anti-rabbit HRP tagged secondary antibody in 5% non-fat milk and TBST was added to the blot and incubated at RT for 1hr. Membranes were washed 3X 10mins with TBST and protein band detection and imaging was carried out using WesternBright™ECL western blotting detection kit and the Syngene GeneGnome gel doc system. Since both GFP and β-Tubulin primary antibodies were raised in rabbit and had different sizes they were where co-detected on the same immunoblot. For Myostatin and β-Tubulin which are the same size (≈50 kDa) myostatin was probed for first and the membrane was stripped for β-Tubulin detection. The list of antibodies and concentrations used are listed in **Table 4**.

5.10.1 Nitrocellulose membrane stripping

After probing for myostatin protein, the membrane was incubated for 2hrs with shaking at RT in stripping buffer (**Appendix 14**). The membrane was washed 3X 10mins with TBST buffer before blocking with 5% milk powder in TBST for 1hr. β-Tubulin primary antibodies in 5% non-fat milk and TBST was added and incubated overnight at 4^0C antibody. Membranes were washed 3 times for 10minutes with TBST and Anti-rabbit HRP tagged secondary antibody was added the protein band detection procedure repeated as mentioned above (5.10).

Table 4: Antibody concentrations used for western blotting

Primary Antibody	Primary antibody conditions (2.5% non-fat milk powder in TBST)	HRP Secondary Antibody	Secondary Antibody conditions (2.5% non-fat milk powder in TBST)
Rabbit anti-GFP	1:10000	Goat anti-Rabbit	1:20000
Rabbit anti-Myostatin	1:5000	Goat anti-Rabbit	1:20000
Rabbit anti-β-Tubulin	1:2500	Goat anti-Rabbit	1:20000
Rabbit anti-GAPDH	1:5000	Goat anti-Rabbit	120000

5.11 Transmission electron microscopy (TEM) analysis of D,MD and dendriplexes

D and MD nanoparticles (5mg/ml in nanopure water) without siRNA and with scramble siNegative at N/P of 8 were prepared as above in section 5.2.1. Samples were primed for TEM and imaging by taking 3µl of each sample and loading it onto a copper grid plate, left for 30 seconds and excess liquid was dabbed off. Samples were left to dry for 10mins at RT nanoparticle and nanocomplex images were taken by FEI Tecnai G2 TEM. The diameter of 20 nanoparticles per group were measured.

5.12 Scaffold formulation

5.12.1 Fibrin hydrogel formulation, PEGylation and characterisation

5.12.1.1 *Fibrin gel formulation with or without Cy5 fluorescent label*

A 35µl 10mg/ml Fibrin gel was prepared by mixing 8.75µl 40mg/ml stock Fibrinogen (in HBS pH 7.8), 4µl of 0.624 U/ml of thrombin in 40mM Ca^{2+} and the volume made up to 35µl by adding HBS pH 7.4. To label fibrin gels with a Cy5 label, 2µl of 3mg/ml fibrinogen with Alexa Fluor™ 647 conjugate was added to the solution before thrombin and the final volume of HBS pH 7.4 added adjusted to make the final gel volume 35µl. For 50µl gels used in siRNA elution profiles, the volumes of the gel components were adjusted accordingly. When free siRNA, MD, Lipofectamine® RNAiMAX and Invivofectamine® 3.0 nanocomplexes were required, they were added to the pre-gel mixture adjusting the volume of HBS pH 7.4.

5.12.1.2 *5:1 or 10:1 PEGylated Fibrin gel formulation with or without Cy5 fluorescent label*

A 35µl 10mg/ml Fibrin gel was prepared by first conjugating PEG-SMC_2 to fibrinogen for 1hr at 37^0C. 1.75µl of 10 mg/ml PEG-SMC_2 or 3.5µl of 10mg/ml PEG-SMC_2 was added to 8.75µl 40mg/ml stock Fibrinogen in HBS pH 7.8 (for a 5:1 or 10:1 PEG to fibrinogen ratio respectively). The volume was made up to 20µl by HBS pH 7.8. After incubation 4µl of 0.624U/ml of thrombin in 40mM Ca^{2+} was added and the volume made up to 35µl by with HBS pH 7.4.

5.12.1.3 *Fibrinogen electrophoresis to show PEGylation*

Following protocols by Zhang et al. [351] with some modifications. 0, 5:1 and 10:1 PEGylated fibrinogen was prepared as described above (5.12.1.1 & 2) in 20µl HBS pH 7.8. After PEGylating, 5µl (125ng of fibrinogen protein) of the fibrinogen was added to 8.3µl 3X loading dye with 15% β-mercapthoethanol and volume made up to 25µl with distilled water. Samples were boiled for 10mins, loaded onto a 7.5% SDS PAGE BioRad TGX™ FastCast™ Acrylamide gel and electrophoresed at 200 V for 45mins. After electrophoresis fibrinogen protein on the gel was stained by coomassie stain for 30mins and distained for 2hrs with mild shaking at RT. The images of the gel stains were taken by the gel doc system using white light.

5.12.1.4 *Scanning electron microscopy (SEM) imaging of fibrin hydrogels*

50µl 10mg/ml of 0, 5:1 and 10:1 PEGylated fibrin were made as above in 5.12.1.1 & 2. Immediately after adding thrombin, the gels were absorbed into interconnecting microporous polyurethane foam discs (84% porosity, with pore sizes 125 - 180µm in diameter). The fibrin gels were polymerised within the foam to support the hydrogels during sample preparation for SEM. The polyurethane foams containing fibrin gels were fixed with 2.5% glutaraldehyde for 30mins. Foams were rinsed 3X with distilled water and freeze dried overnight. They were then gold sputter coated with Palaron range SC 7640 sputter coater for SEM imaging. SEM images of the fibrin gel structure were then acquired on a FEI Nova Nano SEM 230 operating at an acceleration voltage of 5 kV.

5.12.1.5 *Stability of fibrin hydrogels in aqueous buffer*

50µl 10mg/ml (total 504ng of protein) 0, 5:1 and 10:1 PEGylated fibrin gels were prepared in triplicates as above 5.12.1.1 & 2 in 2ml eppendorfs. 150µl HBS pH 7.4 was incubated for 30mins, 1, 3, 5, 7, 10, 18 and 26 days with 150µl HBS pH 7.4 buffer replacement in between each time interval collection until the gels completely degraded. The collected released fibrin protein samples were snap frozen and quantified after the gels had degraded. Knowing the quantity of the starting material, the protein released was measured by Bradford's assay following manufacturer's guidelines. Serially diluted (504 – 0ng) fibrinogen was used to create a standard curve which allowed for quantification of the released fibrin over time.

5.12.2 4% 8-arm PEG-VS gel and PEG-AC gel formulation

PEG hydrogels were formed by crosslinking either 8-arm 20 KDa PEG-VS or PEG-AC with MMP1 recognition peptide (GCREGPQGIWGQERCG 1733Da MW). PEG-VS hydrogels were only enzymatically degradable whilst PEG-AC hydrogels were both enzymatic and hydrolytically degradable. For a 50µl final volume, 10µl 20% m/v PEG VS or AC in IsoPBS pH 7.4 was mixed with 0.88mg MMP1 recognition peptide in 20µ IsoPBS pH 7.4 (4 peptide : 1 PEG) and IsoPBS pH 7.4 added to 50µl. The hydrogels polymerised spontaneously over 20mins at 37^0C or in situ after injection in the tibialis anterior muscle of mice. When free siRNA, MD, Lipofectamine® RNAiMAX and Invivofectamine® 3.0 nanocomplexes (1000ng siRNA) were needed, they were added to the pre-gel mixture adjusting the volume of additional isoPBS pH 7.4.

5.12.3 4% 8-arm PEG-VS and PEG-AC gel Cy5 labelling and formulation

A far red label was introduced into the PEG hydrogels through the addition of a thiol to a far-red labelled maleimide. Alexa Fluor® 660 C2-maleimide (Alexa) was reacted with DTT as follows: 1ul Alexa (10mg/ml) dimethyl sulfoxide was reacted with 9ul DTT (1.1mM in IsoPBS pH 7.4 at a 1 Alexa per DTT molecule) for 30mins and 37^0C. The Alexa-DTT was then added to PEG monomer at 1 Alexa-DTT molecule per 100 PEG molecules and reacted at 37^0C before adding all other gel components as described above (5.12.2).

5.13 siRNA release from PEG- AC and PEG-VS hydrogels

1000ng siNegative alone or MD (N/P 8), Lipofectamine® RNAiMAX and Invivofectamine® 3.0 nanocomplexes were made and encapsulated in PEG hydrogels. 50µl 4% 8-arm PEG-VS or 4% 8-arm PEG-AC were prepared as described in 5.12.2. after polymerisation incubated in 150µl HBS pH 7.4 over 30mins, 1, 3, 5, 7 and 10 days with 100µl HBS pH 7.4 buffer replacements. At each collection time point 150µl HBS pH 7.4 buffer with eluents was collected and snap frozen for siRNA quantification. On day 10, undegraded PEG hydrogels was digested Proteinase K in 150µl HBS pH 7.41 at a final 1mg/ml final concentration. The digest was collected and the siRNA or nanoparticles released were quantified by running samples on a 2% agarose gel (section 5.3.1). Fresh 100, 50, 25, 12.5, 6.25 and 0ng siRNA was included per gel run and used as a standard curve to determine the amount of eluted siRNA at each time point. 4µl 5X loading dye, SDS (0.05% final concentration) was added to 10µl of the released samples, to dissociate the nanoparticles and volume made up to 20µl with DEPC treated water. Samples were loaded onto the agarose gel and run for 30mins at 55V. siRNA bands were visualised, imaged and quantified by Syngene GeneTools software.

5.14 Effects of fibrin hydrogel components on siRNA degradation

Fibrin hydrogel components fibrinogen and thrombin were incubated with siRNA over a period of 5 days to assay potential degradation of siRNA as they are animal derived products that could possibly contain RNases. 200ng siNegative was incubated at 37^0C 10mg/ml fibrinogen or 0.624U/ml thrombin in 20µl HBS pH 7.4. Samples were taken master mix at 30mins, 1, 3 and 5 days. Samples were incubated under sterile conditions at 37^0C. At each time point 20µl samples were removed, snap frozen in liquid nitrogen and kept at -20^0C until further analysis after experiment completion. siRNA, fibrinogen and thrombin only were included as controls. After 5 days all samples including fresh siRNA were subjected to gel electrophoresis on 2% agarose gel (section 5.3.1).

5.15 siRNA release from PEGylated and non-PEGylated fibrin gels

50µl (10mg/ml) of 0, 5:1 and 10:1 PEGylated fibrin gels encapsulating siRNA and nanocomplexes were prepared following procedure described in 5.12.1.1&2: 12.6µl 40mg/ml stock Fibrinogen, 13.6µl HBS pH 7.8 and 2.5µl or 5µl PEG-SMC_2 10mg/ml (for 5:1 an 10:1 PEG-fibrin respectively) were combined, vortexed and incubated for 1hr at

37^0C. After incubation, 5.7µl of 0.624U/ml thrombin in 40mM Ca^{2+} (in HBS pH 7.4) was added and volume made up to 50µl with HBS pH 7.4 with or without 1000ng siNegative alone, MD, Lipofectamine® RNAiMAX and Invivofectamine® 3.0 nanocomplexes. 3 gels per group were polymerised in and incubated in 150µl HBS pH 7.4 over 30mins, 1, 3, 5, 7 and 10 days with 100µl HBS pH 7.4 buffer replacements. At each collection time point 150µl HBS pH 7.4 buffer with eluents was collected and snap frozen for siRNA quantification. By day 3 and day 10, unmodified fibrin and 5:1 PEGylated fibrin had completely degraded respectively, hence sample collection stopped at those time points. The collection point for 10:1 PEGylated fibrin gel stopped at Day 10 though it had not completed degradation. The siRNA or nanoparticles released were quantified by running samples on a 2% agarose gel and quantified as described above (5.13).

5.15.1 Bioactivity testing of the siRNA or nanocomplexes released from PEGylated fibrin gels in the presence or absence of serum.

50µl (10mg/ml) 5:1 and 10:1 PEGylated fibrin gels encapsulating 1000ng siGFP-Cy3 or MD / Lipofectamine® RNAiMAX /Invivofectamine® 3.0 nanocomplexes were prepared as above in 5.15. 3 gels per group were polymerised and washed in HBS pH 7.4 for 30mins, with the initial wash excluded from the transfection experiment. Then samples incubated 150µl HBS pH 7.4 0-5 days and for 6-10 days with 150µl HBS pH 7.4 buffer replacements. At 5 and 10 days the eluent was immediately quantified and used in transfection experiments to test bioactivity of the released nanoparticles. For siRNA/nanocomplex release in the absence of serum: Gels without siRNA or nanocomplexes were included in the release profile and used as negative controls. After siRNA quantification (described in section 5.14), 100ng of the eluents in HBS pH 7.4 per treatment group (if sufficient siRNA was present) added to 30000 HT1080-GFP cells seeded in 24 well plates a day prior. 4hrs post transfection media was changed and 48hrs later cells were analysed for GFP knockdown by flow cytometry (section 5.6). HT1080-GFP cells only, 5:1 and 10:1 PEGylated fibrin only eluents with no siRNA were used as negative controls. For siRNA release in the presence of serum, 50µl 5:1 PEGylated fibrin gels were prepared in triplicate with siGFP or siNegative. The hydrogels were incubated at 37°C under sterile conditions in 200µl eluent (10% FBS in MCDB media) over a period of 7 days. Eluents were collected at day 4 and 7. The extracted eluent was immediately used to transfect cells seeded a day prior in a 24 well plate (in the presence of fresh full growth media) for 48hrs. Cells only were included as negative

controls. 48hrs after each transfection cells were analysed for GFP knockdown with flow cytometry as described in 5.6.

5.16 3D cell culture assays pre *in vivo* experiments

5.16.1 3D Transwell chemotaxis assay

MD, Lipofectamine® RNAiMAX and Invivofectamine® 3.0 nanocomplexes were made with siGFP-Cy3 as described in section 3.1. Lipofectamine® RNAiMAX, MD and Invivofectamine® 3.0 was complexed to 500ng siGFP-Cy3. siGFP only, Cy3 labelled scramble siRNA (siNegative-Cy3) and HT1080 cells only were used as negative controls. 50µl (10mg/ml) non-PEGylated fibrin gels with 500ng siGFP-Cy3 and nanocomplexes were polymerised onto the transwell membrane (bottom gel layer, see **Fig.32**). 50µl (10mg/ml) non-PEGylated fibrin gels with 15000 HT1080-GFP cells suspended in serum free MCDB media was polymerised on top of the gel-siGFP-Cy3 (top gel layer). The Transwell set up was then incubated for 24hrs the lower chamber containing MCDB media with 10% FBS (as chemoattractant), and the insert of the Transwell was filled with serum free MCDB media. 24hrs post seeding media was changed to remove excess released nanocomplexes. HT1080-GFP cells only (no siRNA or nanocomplexes), fibrin hydrogels with HT1080-GFP cells and free siNegative-Cy3 or siGFP-Cy3 (no nanocomplexes) were used as negative controls. The same experimental set up was used to assay invasion through 5:1 and 10:1 PEGylated fibrin hydrogel. Cells were monitored from 24hrs to 10 days (with media change every 48hrs.

48hrs post treatment, cells that migrated to the surface of the Transwell membrane and bottom chamber were quantified by fluorescent microscopy and flow cytometry (section 5.6) respectively. For fluorescent microscopy, cells and excess fibrin gel on the top side of the transwell membrane were scraped off and the cells at the bottom of the membrane were washed 2X with isoPBS pH 7.4 and fixed with 10% formalin. Post fixing and washing 3X with isoPBS pH 7.4 the membrane was cut off the well, placed on a glass slide and stained with Fluoroshield™ with DAPI. A coverslip was placed on top of the membrane and cells were imaged by Nikon Eclipse 90i fluorescent microscope at 20x magnification, with the same exposure settings.

3D embedded cell cluster assay

96 well plates were siliconized with Sigmacote® prior to cell seeding. HT1080-GF cells were mixed with 5µl 5:1 PEGylated fibrin gel at 1000 cells/µl prior to polymerisation. A 5µl droplet was pipetted in the center of each transwell for 15mins at 37^0C. Then a 50µl 5:1 PEGylated fibrin gel encapsulating MD / Lipofectamine® RNAiMAX / Invivofectamine® 3.0 nanocomplexes made with 500ng siDeath was polymerised onto the 5ul droplet. siDeath-Negative control siRNA was included as control. After the top gel-layer polymerised full growth media was added to the well (see **Fig.34**). Cell droplets were, immediately imaged by Zeiss Axiovert fluorescent microscope at 10X magnification. The experimental set up was then incubated for 3 and 7 days with media change every 48hrs. At day 3 or 7 cell death was assayed by addition of EthD-1 from the Live/Dead™ cell viability assay. Green HT1080-GFP cells were used as indicator of live cells in this experiment. At day 3 and 7 wells with cells were washed 3X with isoPBS pH 7.4, 2mM EthD-1 was added to the cells and incubated for 20minutes to stain dead cells red. Maximum intensity projection images of the cell droplets was then imaged by Zeiss LSM510 confocal microscope at 10X magnification. 4 fields of view across the cell droplet were taken per well and quantified by Image J cell counter.

5.17 *In vivo* studies gel degradation and gene knockdown analysis

5.17.1 Animals

Animals were bred and housed at the Animal Unit, Faculty of Health Sciences, University of Cape Town (UCT), under standard research facility conditions. The handling of all mice and experiments complied with the Principles of Laboratory Animal Sciences as well as the UFAW Handbook on the care and management of laboratory Animals and followed the protocol for this study approved by UCT Faculty of Health Sciences, Animal Ethics Committee protocol number 014/022.

6-8 week old, GFP transgenic or non-GFP mice (male and female) were used. The non-GFP (UCT4) – BALB/c wildtype mice were obtained from the UCT Animal Unit and BALB/c GFP transgenic mice heterozygote (Cby.B6-Tg (UBC-GFP) 30Scha/J from Jackson laboratory) were provided by Frank Brombacher's laboratory at UCT. The GFP transgenic mice express eGFP under the transcriptional control of a

human ubiqutin C promoter. Homozygote eGFP expressing transgenic parental mice were bred to provide the mice used in the study. Homozygote eGFP expressing mice were reported to be normal by Jackson laboratory and this was considered more convenient. Confirmation of the GFP mouse genotype during the breeding process was done by flow cytometry on cells isolated from the mice blood. 2ml of red blood cell lysis (RBCL) buffer (**Appendix 14**) was added to 100µl of mouse blood and incubated for 2mins at 37^{o}C. After incubation cells were centrifuged at 1500rpm for 3mins, and supernatant discarded. If the red blood cell lysis was not complete an additional cell lysis step was added until a clear pellet of white blood cells was visible. The cell pellet was resuspended in FACS buffer and GFP levels within the cells determined by flow cytometry (section 5.6). As seen in (**Appendix 13**) homozygotes GFP mice had approximately double the GFP fluorescence of heterozygote mice. Once parental homozygote GFP mice for breeding were established, their offspring were used in the *in vivo* studies.

All injections on live mice with nanocomplexes and hydrogels with or without nanocomplexes were done using a 0.3mm 30G needle following the approved animal ethics protocol as follows. Animals were first anaesthetised by placing them one at a time in a box containing an atmosphere of 5% isoflurane in 100% oxygen for 2mins. Animals were placed on a nose cone with 1.5% isoflurane in 100% oxygen at 0.3l/minute. The injection site was swabbed with ethanol swabs and 30µl of samples (nanocomplexes, hydrogels or both) was injected into the tibialis anterior (TA) muscle of the mouse's lower hind limb 2-5mins post mixing the gel components. Both limbs of each mouse were utilised to reduce the number of mice used. At appropriate time points (30min, 2, 4 and 7 days) mice were euthanized with 5% isoflurane for 5mins and cervical dislocation to confirm death. Their TA muscle were excised and analysed by histology, western bot and RT-PCR.

5.17.2 Hydrogel injection and distribution optimisation *in vivo*

For hydrogel injection optimisation to get optimal tissue coverage with the hydrogel, Injections were done on dead BALB/c mice donated by the Animal Unit that had been euthanised for animal breeding maintenance. Coomassie Brilliant Blue R-250 stained PBS pH 7.4 was used as a dye for this exercise. Various injection volumes, needle injection depth and angle, as well as number of injections and injection site, were tried to get optimal spread in the TA muscle without injection leakage.

5.17.3 Hydrogel degradation *in vivo*

For this experiment, 35µl PEG-VS/AC gels, non-PEGylated and PEGylated fibrin gels with Alexa Fluor® 660 C2-maleimide and Alexa Fluor™ 647 were prepared as prescribed in section 5.12 without siRNA or nanocomplexes. 30µl of the gel components were injected into BALB/c mice TA muscle 5-10mins post mixing, 2 legs per group of hydrogel. The mice were sacrificed 30mins post injection or at day 2, 4 and 7. Histology and image analysis for hydrogel degradation rate *in vivo* over 7 days was performed on whole TA tissue samples. Whole TA muscle samples were immediately fixed in 10% formalin for at least 24hrs. Post formalin fixing tissue samples were wax embedded, sectioned into 2 micron slices, mounted and DAPI stained by fluoroshield DAPI stain. Stitched fluorescent images of the whole muscle sections were taken by Nikon Eclipse 90i fluorescent microscope at 10x magnification, with the same exposure settings, to image the distribution of nanocomplexes.

5.18 *In vivo* analysis of RNAi

Invivofectamine® 3.0 nanocomplexes were made with 5µg of siGFP-Cy3 or siMstn-Cy3 following protocol 5.2.3. Before the Invivofectamine® 3.0 nanocomplexes were used in experiments, they were first dialysed under sterile conditions in isoPBS pH 7.4 for 2hrs using Slide – A - Lyzer® Mini dialysis device kit. This was done (as per recommendation in communication with the manufacturer) to remove any uncomplexed nanoparticle reagents that may cause cytotoxicity as high concentrations of the nanocomplexes were going to be used *in vivo*. After dialysis, the toxicity and transfection efficiency of the nanocomplexes was tested using cell viability Cell Titre Glow assay and GFP geometric shift by flow cytometry (**Appendix 7**). 16 mice were injected in both their TA muscles with the dialysed nanocomplexes encapsulated in 30µl 5:1 PEGylated fibrin. The various groups were randomly distributed (n=8). Post injection, mice were monitored and sacrificed 7 days post treatment. Their TA muscle tissue was extracted, weighed and the samples were immediately immersed in RNAlater® solution to protect all RNA from RNases. Tissue samples were later processed for histology, RNA and protein analysis.

5.18.1 Nanocomplex retention

For nanocomplex distribution analysis in the muscle tissue, a small piece ≈1mm thick was cut from the middle cross section of the extracted TA muscle tissue (illustrated in **Fig.41** below) and fixed in 10% formalin in preparation for histology as described in 5.17.3. The remaining larger pieces were placed back in RNA later in preparation for protein and total RNA extraction at a later stage. The distribution of nanocomplexes in the presence or absence of PEGylated fibrin hydrogel relative to tissue size was further quantified by Visiopharm image analysis software.

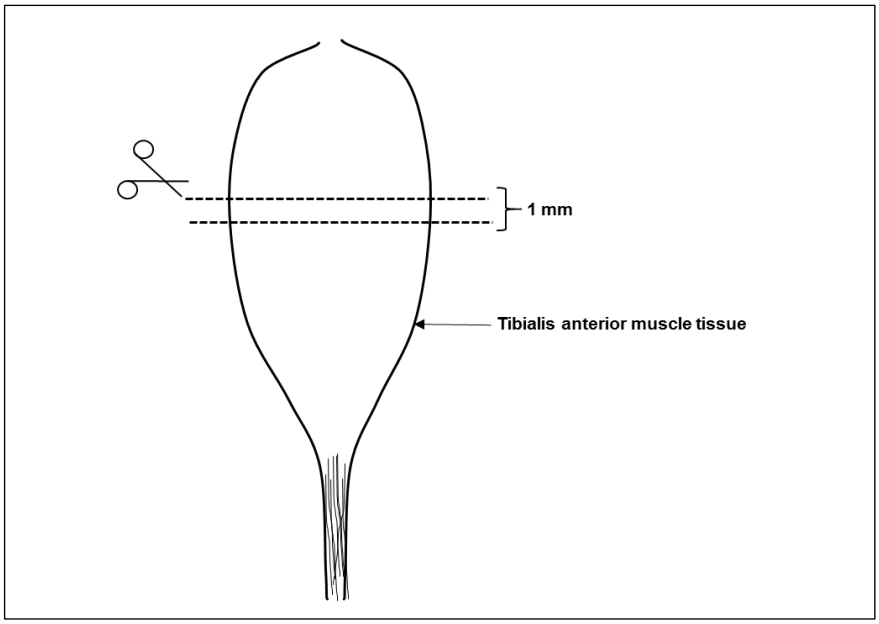

Figure 41: Illustration of how the tibialis anterior muscle cross sectioned for nanocomplex distribution analysis.

5.18.2 Protein and siRNA extraction from mouse AT muscle.

Prior to analysis of tissue samples from the *in vivo* experiment GFP expression in TA of the GFP transgenic mice needed to be analysed. TA muscle samples of GFP expressing mice were excised from the mice and preserved in the RNAlater® in preparation for protein. Protein was extracted using mirVana™ miRNA Isolation Kit as per manufacturer's instructions. The tissue samples were minced with a scalpel blade into the smallest possible pieces. Samples were kept on ice and subjected to two short bursts of sonication by Virsonic Sonicator. Protease inhibitor (PI) cocktail (1µl/100µl) was added

to the isolated protein to prevent protein degradation. Protein concentration was quantified using Bradford's assay. GFP protein in the tissue samples was analysed by western blot as described in 5.10. Non-GFP expressing TA tissue samples and HT1080-GFP cell lysate were included as negative and positive controls. The expression of eGFP protein in the transgenic mice was confirmed in **Appendix 11.B**&**C**

For the *in vivo* study described in in 5.18, after excision and RNAlater®, preservation of the tissue samples to be used in siRNA and protein analysis, the siRNA and protein in the samples was extracted using mirVana™ miRNA Isolation Kit as per manufacturer's instructions and again as described above with additions as follows: The tissue samples were weighed and minced with a scalpel blade into smallest possible pieces. Samples were kept on ice and subjected to two short bursts of sonication by Virtis Virsonic Sonicator at speed level 2. Samples were split in half for separate protein and siRNA isolation following extraction kit protocol. Protease inhibitor (PI) cocktail (1µl/100µl) was added to the isolated protein to prevent protein degradation. Protein and siRNA were quantified using Bradford's assay and Nanodrop respectively. Samples were stored at -80^{0}C until analysis for Mstn mRNA (by RT-PCR, section 5.18.3) and GFP expression by western blot as described (in section 5.10)**.**

5.18.3 Quantitative RT-PCR analysis

After extraction and quantification of total RNA from tissue samples in all groups, Mstn mRNA levels was quantified using the Roche RT-PCR system. The primer concentrations to use in the study for RT-PCR was initially optimised, these primer sequences and concentrations are listed in **Table 5**. The housekeeping gene to be used in the experiments was optimised before sample analysis as well (amplification and melting curves in **Appendix 8A**.). Mstn primers were obtained from literature [301, 302, 308, 312] and purchased from Qiagen. The ACTN, HPRT and GAPDH primers were self-designed using NCBI gene sequence database and primer sequence blast and purchased from Qiagen. Firstly cDNA synthesis was made from the extracted total RNA using Roche Transcriptor first strand cDNA synthesis kit following manufacturers guide. mRNA levels were detected using LightCycler® 480 SYBR Green I master mix again following manufacturers guide. 20µl PCR reaction tubes were subjected to the following PCR cycle conditions were as follows: Hold at 95^{o}C for 5mins; 45 cycles of denaturing at 95^{o}C for 10secs, annealing at 60^{o}C for 15 secs, elongation at 72^{o}C for 15secs, detecting at 78^{o}C; and a final melting step ramping from 60^{o}C to 95^{o}C. Water controls were always included in the RT-PCR runs to monitor for or primer dimer formation.

GAPDH was chosen as the optimal housekeeping gene to use in sample analysis. GAPDH (237bp) and Mstn (167bp) primer/RT-PCR products were confirmed by electrophoresing 5µl of the 20µl products from the reaction tube on a 2% agarose gel with GelRed™ loading dye (final concentration 1X) (**Appendix 8B**). For sample analysis of Mstn gene expression, the PCR efficiency values for each primer set (that is Mstn and GAPDH) was determined per sample run in each PCR repeat using the LinRegPCR software program [407]. Per every sample run the PCR efficiency is obtained by fitting a line of regression to a subset of data points (Ct values) in the log-linear phase using linear regression. The mean PCR efficiency for each primer is then calculated for the PCR reaction. The Mstn expression was calculated from the Roche CT value output taking into account the mean PCR efficiency for each primer obtained from the LinRegPCR program and presented normalised to the housekeeping gene GAPDH.

Table 5: Primer sequences used in RT-PCR analysis

Primer gene target name	Forward Primer	Reverse primer	Concentration (nM)
Myostatin	5'-CAGCCTGAATCCAACTTAGG-3'	5'-TCGCAGTCAAGCCCAAAGTC-3'	250
β Actin	5'-TGGAATCCTGCATCCAGAAAC-3'	5'-TAAAACGCAGCTCACTAACAGTCC-3'	500
HPRT	5'-GTTGGATATGCCCTTGAC-3'	5'-AGGACTAGAACACCTGCT-3'	500
GAPDH	5' -TTCACCACCATGGAGAAGGC-3'	5' -GGCATGGACTGTGGTCATGA-3'	500

5.19 Statistical analysis

Data was tested for normality. One-way ANOVA with post-hoc Tukey testing for significance was performed on normally distributed data. For non-parametric data Kruskal Wallis followed by Steel-Dwass post hoc testing significance was performed. P values less than 0.05 were considered statistically significant. Statistical analysis was performed using JMP statistical analysis, a SAS software (Cary, North Carolina, USA). Data are presented as the mean ± standard error mean.

6 Appendices

Appendix 1

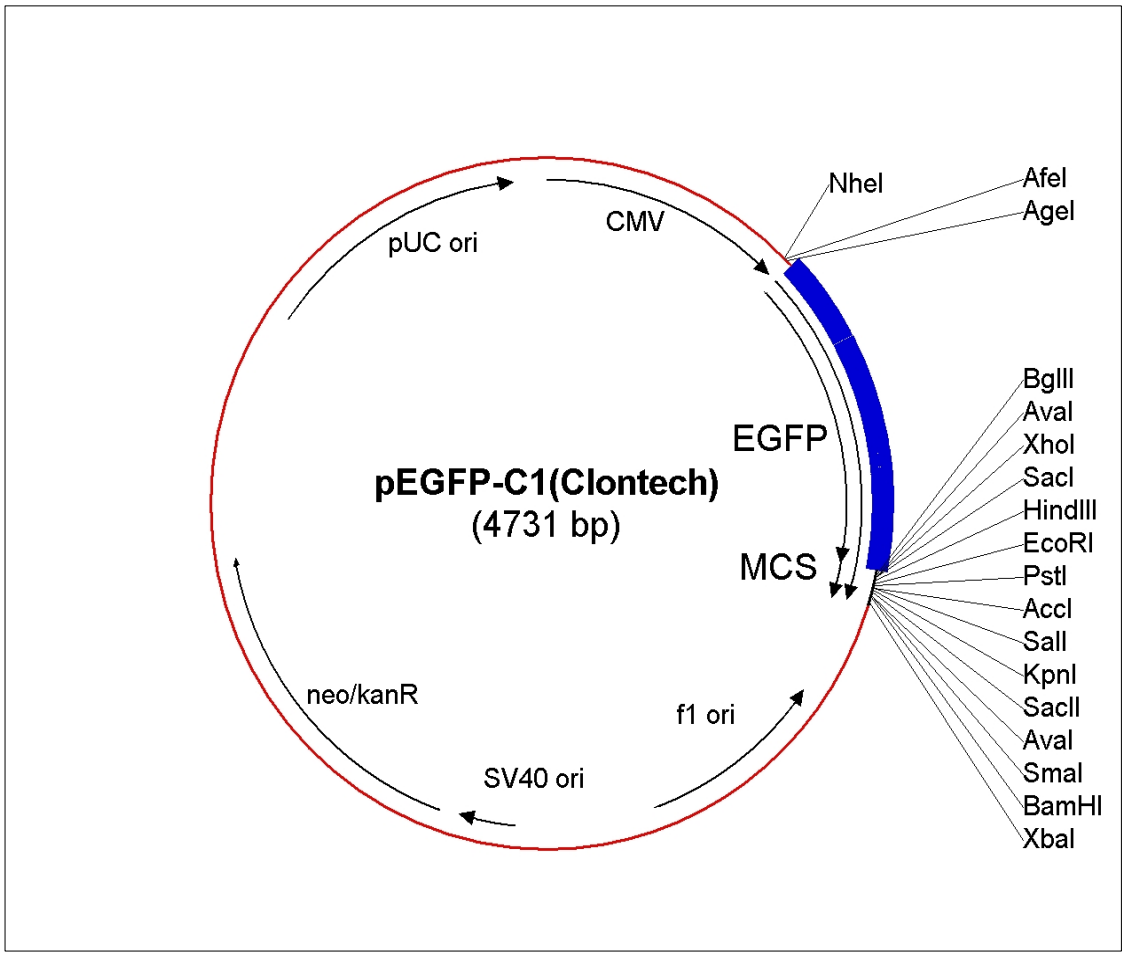

Appendix 1: pEGFP-C1 plasmid used in the production of an HT1080 cell line stably expressing GFP (HT1080-GFP). *The Image was obtained from: http://www.bioss.uni-freiburg.de/toolbox/products.php?PL-558 and the plasmid was purchesed from Clontech.*

Appendix 2

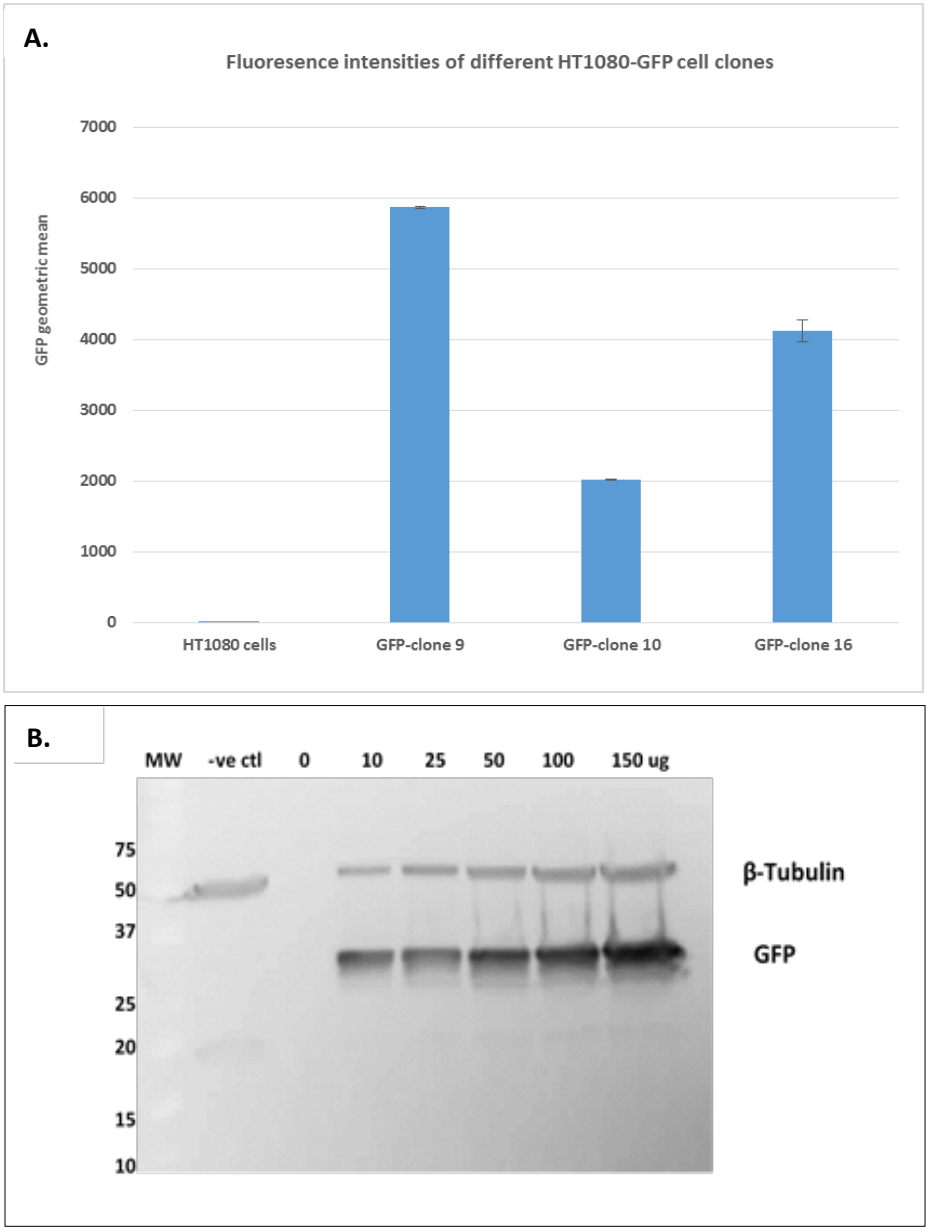

Appendix 2: GFP expression levels in 3 established HT1080-GFP clones and western blot optimisation. *(A) HT1080-GFP Clone 9 with the most intensity was used through throughout the study. Data is a representation of an experiment done with 3 technical repeats. HT108 cells were included as negative control. (B) Shows protein loading optimisation using HT1080-GFP clone-9 cell lysate. 0-150ng protein was loaded on the 12% SDS page gel. HT1080 cell lysate was used as negative control and β-Tubulin was used as loading control in all GFP expression or knockdown experiments. 40ug was used in all follow up experiments. HT1080 cell lysate was included as negative control. MW= molecular weight marker in kDa.*

Appendix 3

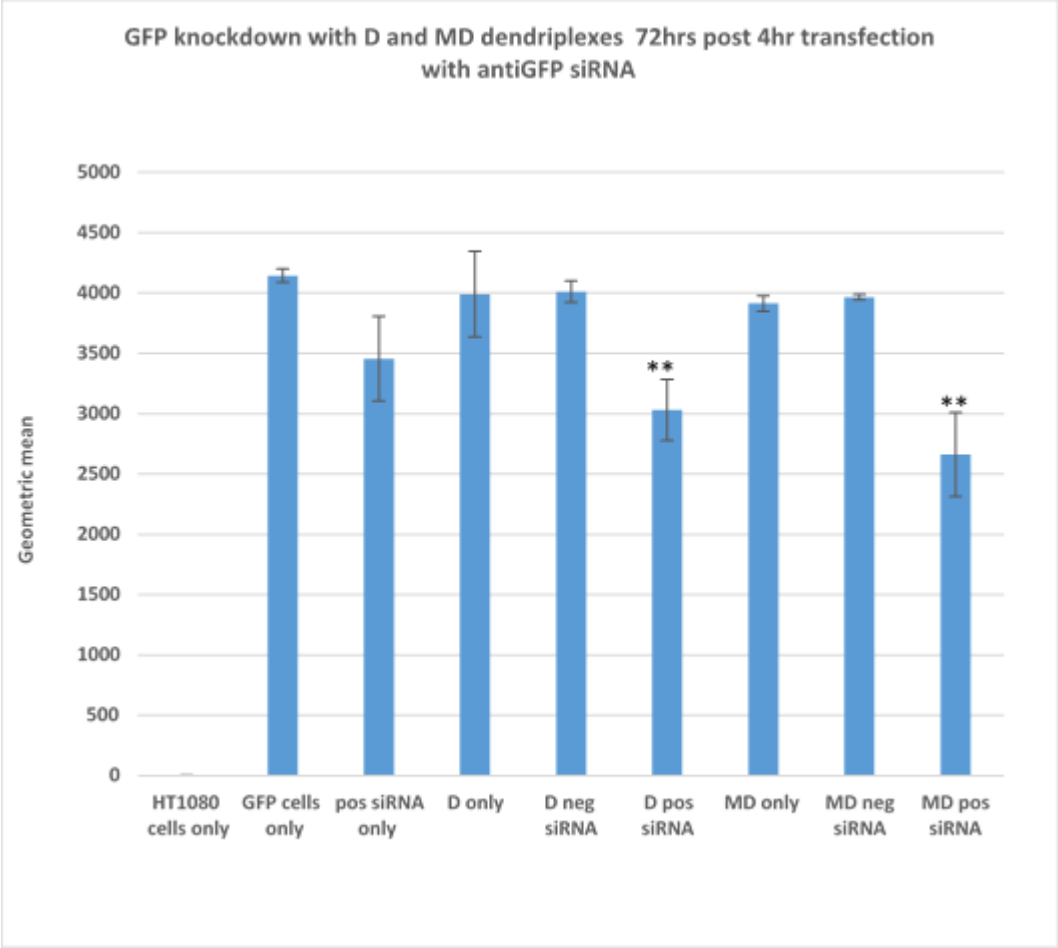

Appendix 3: The transfection efficiency and efficacy of D and MD nanocomplexes at N/P of 8:1, 72hrs post transfection. *HT1080-GFP cells were transfected with D and MD dendriplexes made with 200ng siGFP siNegative (neg siRNA groups) for 4hrs. 72hrs post transfection flow cytometry was used to measure the GFP geometric mean. Non-GFP cells, GFP cells only and siGFP only treated cells were included as negative controls. Data is a representation of an experiment with 3 technical repeats. ** p<0.005 vs respective D/MD negative siRNA controls.*

Appendix 4

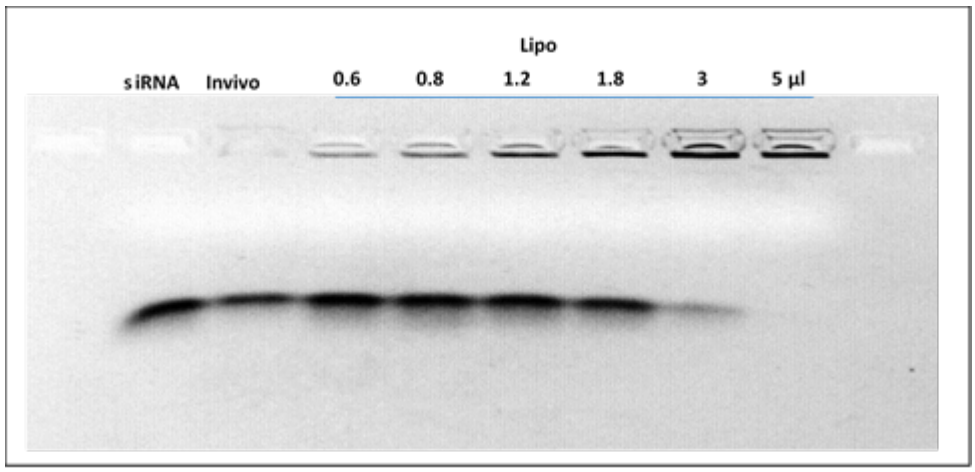

Appendix 4: The binding abilities of Lipofectamine® RNAiMAX at different amounts to siRNA. *A constant amount of 200ng siNegative was used in nanocomplex formation with 0.6-5ul Lipofectamine® RNAiMAX. Free siRNA and Invivofectamine® 3.0 nanocomplexes were included as a controls (complexes made according manufactures guide with no 6X final dilution). Samples were electrophoresed on 2% agarose gel to show siRNA complexation.*

Appendix 5

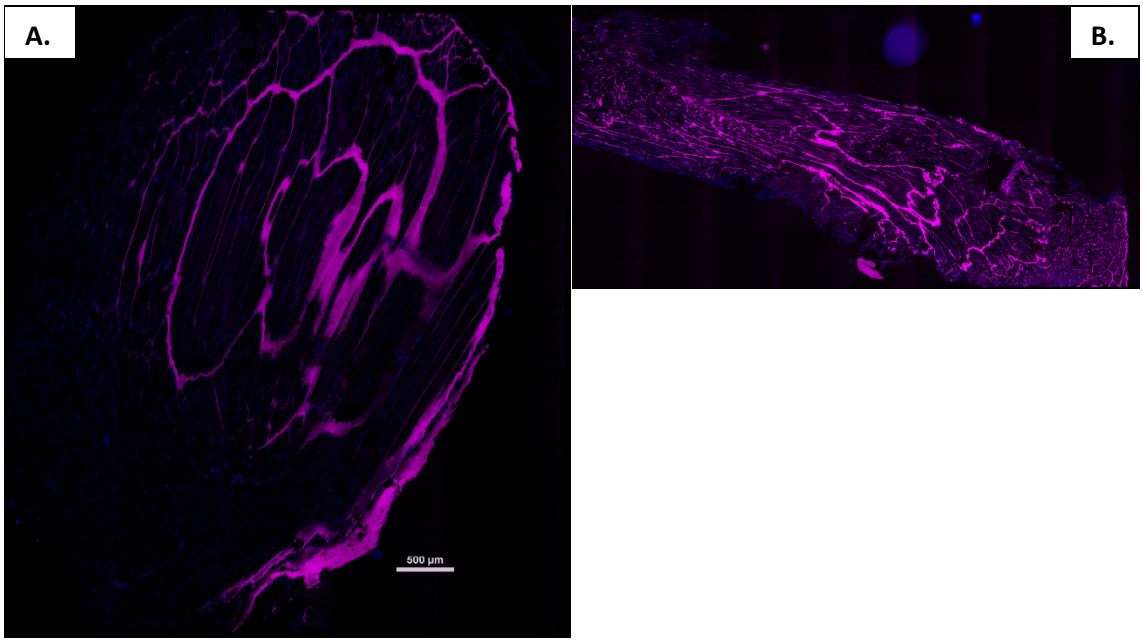

Appendix 5: A representation of optimised injection and distribution of Alexa labelled PEG-VS and fibrin hydrogel in the targeted hind limb tibialis anterior muscle of BALB/c mice. *PEG-VS was labelled with Alexa Fluor® 660 C2-maleimide and Fibrin was labelled with Alexa Fluor™ 647. The micrograph images of the whole TA muscle tissue extracted from BALB/c mice sacrificed 30mins post injecting the muscle with 30µl hydrogel of Alexa (pink) labelled 8-arm 4% PEG-VS (A) hydrogel and fibrin hydrogel (B). The images show successful gel labelling and gel distribution and optimal coverage in the TA muscle. Blue is nuclei DAPI stain of tissue. Scale bar =500µm.*

Appendix 6

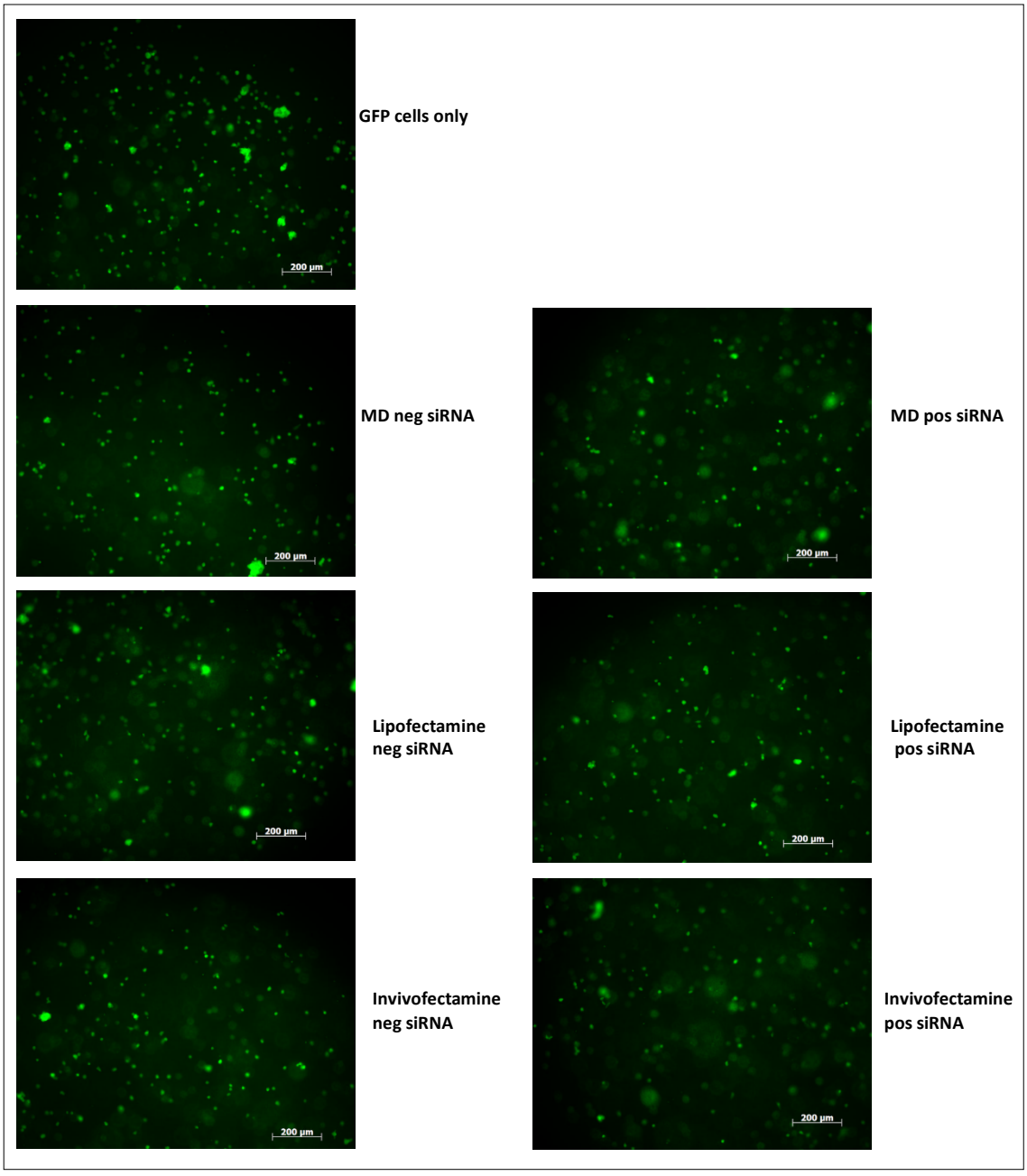

Appendix 6: Fluorescent images of in vitro 3D cell transfection of HT1080-GFP cells at day 0. *Fluorescent images of Day 1 cell seeding set up of the 3D assay. These are maximal projection Z-stack images of cells encapsulated in 5ul 5:1 PEGylated fibrin gel droplet covered with a layer of 50µl 5:1 PEGylated fibrin gel containing: MD/Lipofectamine® RNAiMAX/ Invivofectamine® 3.0 nanocomplexes made with 500ng siDeath (pos siRNA groups) or siDeath-Negative control (neg siRNA groups). Scale bar =200µm.*

Appendix 7

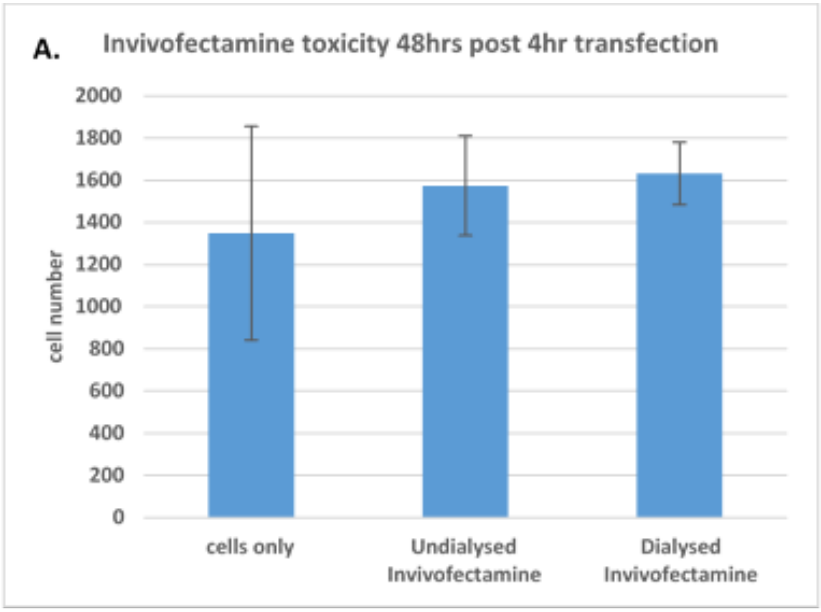

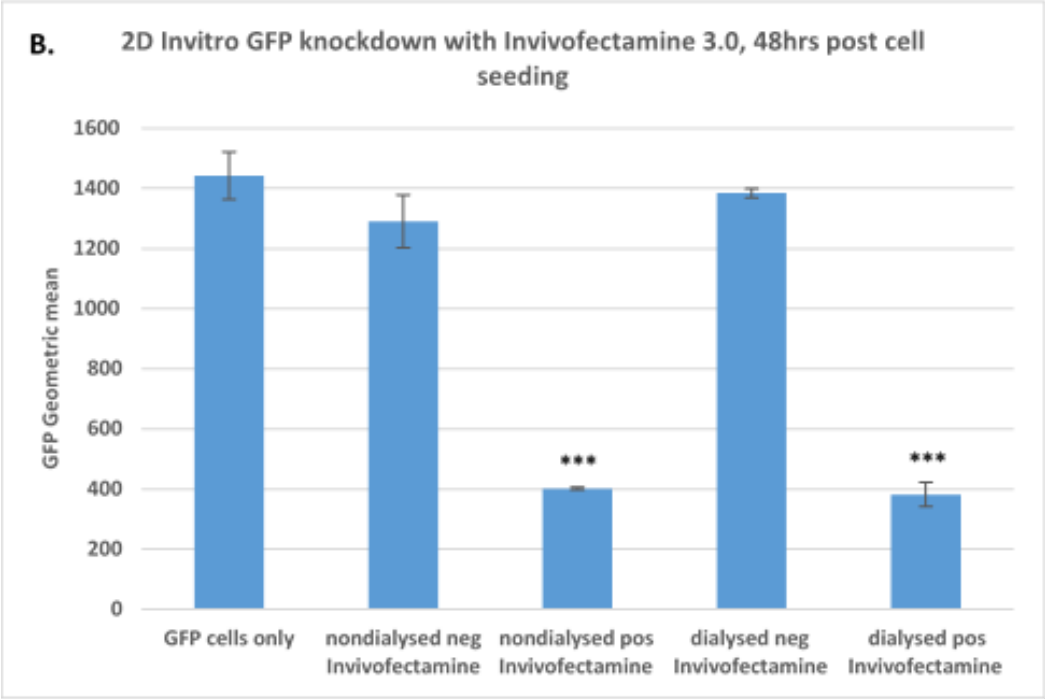

Appendix 7: Cytotoxic effects of Invivofectamine® 3.0 nanocomplexes and the GFP knockdown effects of dialysing and non-dialysed nanocomplexes. *Invivofectamine® 3.0 nanocomplexes made with siMstn-Cy3 (neg Invivofectamine group) or siGFP-Cy3 (pos Invivofectamine group) were dialysed or not in preparation for the in vivo assay. Their cytoxicity (A) and efficacy (B) on HT1080-GFP cells was assessed by CellTiter-Glo® luminescent Cell Viability Assay and flow cytometry respectively. Cells were transfected with nanocomplexes, Invivofectamine® 3.0-siMstn 200ng in (A) or Invivofectamine® 3.0-siMstn/siGFP 500ng in (B) from the dialysed or non-dialysed groups for 4hrs. 48hrs post transfection, cell death and geometric mean was determined. Untreated HT1080-GFP cells (GFP cells only) were used as negative controls in both experiments. siMstn was used as negative control GFP knockdown in (B). *** $p<0.0005$ vs respective nondialysed/dialysed neg Invivofectamine groups.*

Appendix 8

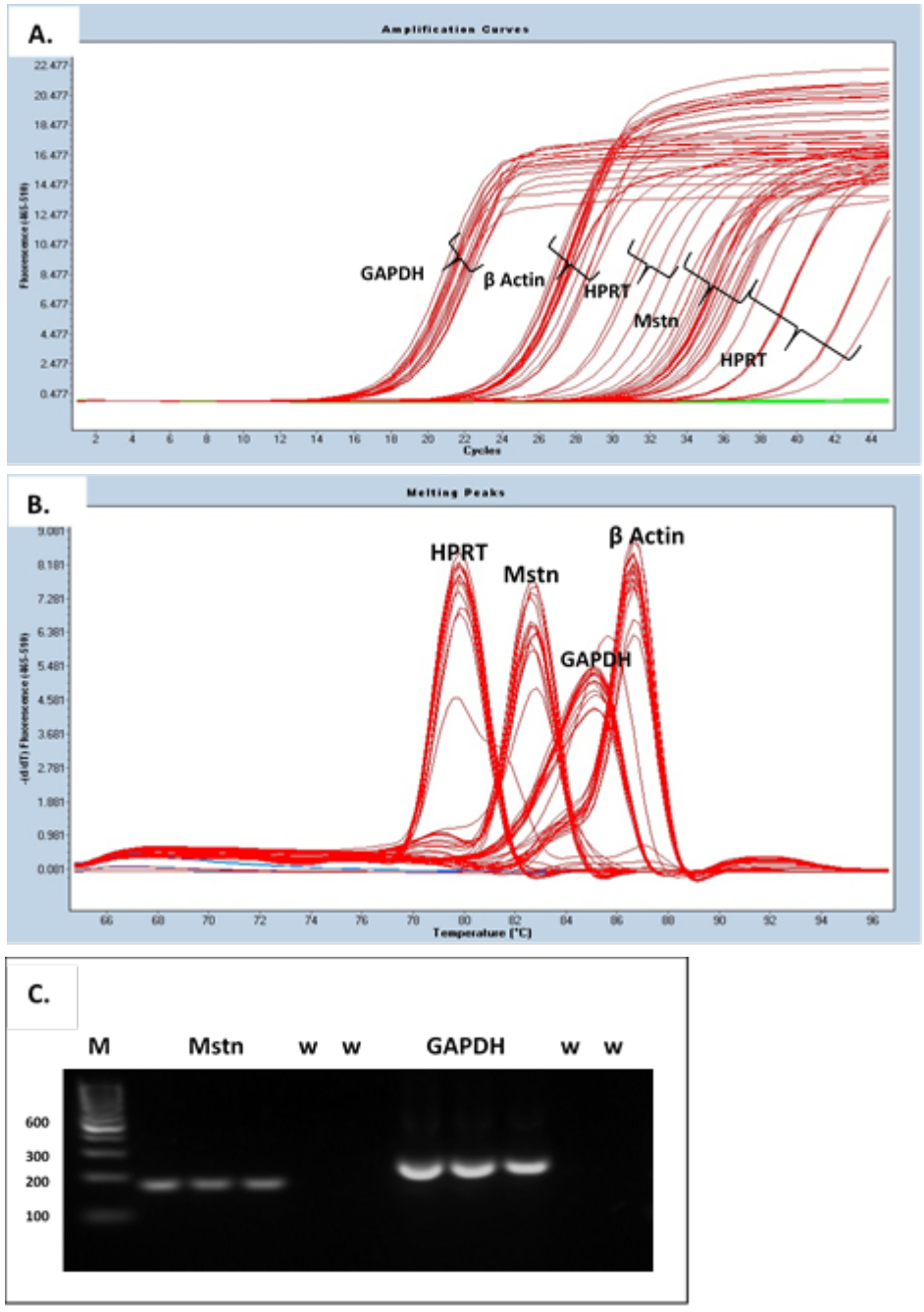

Appendix 8: RT-PCR of housekeeping genes and Mstn primer optimisation. *The amplification (A) and melting (B) curves of HPRT (500nM), GPDH (500nM), β-Actin (500nM) and Mstn (150nM) primers in 16 TA muscle tissue samples extracted from 8 untreated BALB/c GFP transgenic mice. The melting temperatures of GAPDH, β Actin, Mstn and HPRT RT-PCR products. (C) Image shows the RT-PCR single product size from GAPDH (237 bp) and Mstn (167 bp) RT-PCR amplification after 2% agarose gel electrophoresis. M= 100 bp DNA Ladder, W= water control.*

Appendix 9

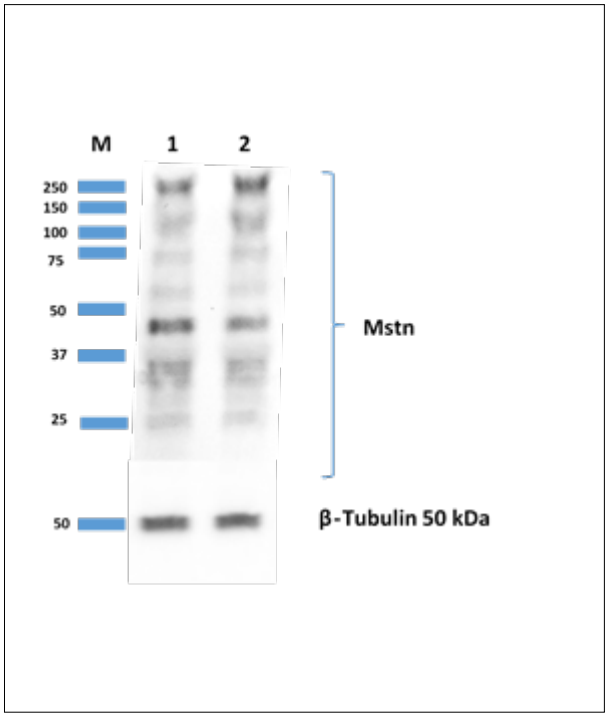

Appendix 9: Myostatin protein expression in tibialis anterior muscle tissue samples of BALB/c GFP transgenic mice. *Mstn expression in the tissue samples from two TA muscle, mice, lane 1 and 2, was analysed by western blot analysis. The image is a representations of 3 immunoblot repeats carried out after Mstn antibody optimisation by dot blot. β-Tubulin was included as loading control. The blot shows multiple unspecific bands and no clear identification of myostatin specific bands, that is: myostatin precursor 50 kDa, myostatin propeptide 39 kDa and myostatin mature inactive N terminal 27 kDa for quantification. Mstn = myostatin, M=molecular weight marker in kDa.*

Appendix 10

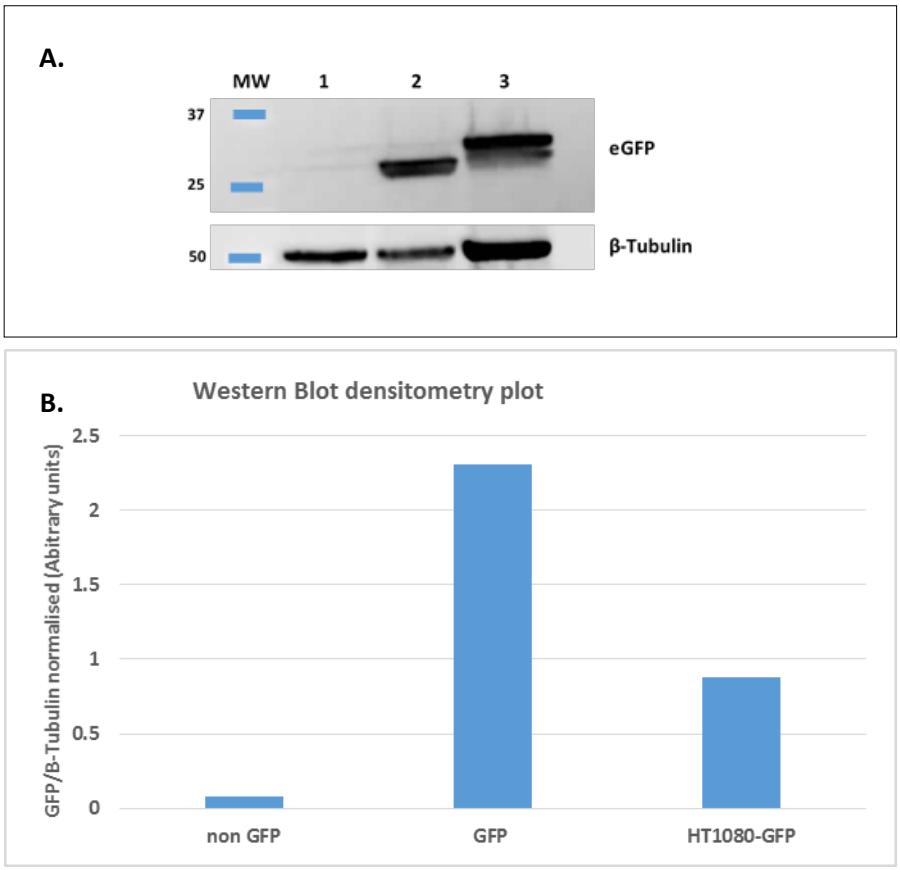

Appendix 10: GFP protein expression from TA muscle tissue of BALB/c GFP transgenic mice. *Total protein was extracted from mouse tissue and 30ug subjected to western blot analysis. Immunoblot image in (A) shows the expression of eGFP protein in the mouse tissue and quantified in (B). Lane 1 is non GFP BALB/c mouse sample negative control, lane 2 is BALB/c GFP mouse TA tissue lysate and lane 3 is HT1080-GFP cell lysate positive control. MW= molecular weight marker in kDa.*

Appendix 11

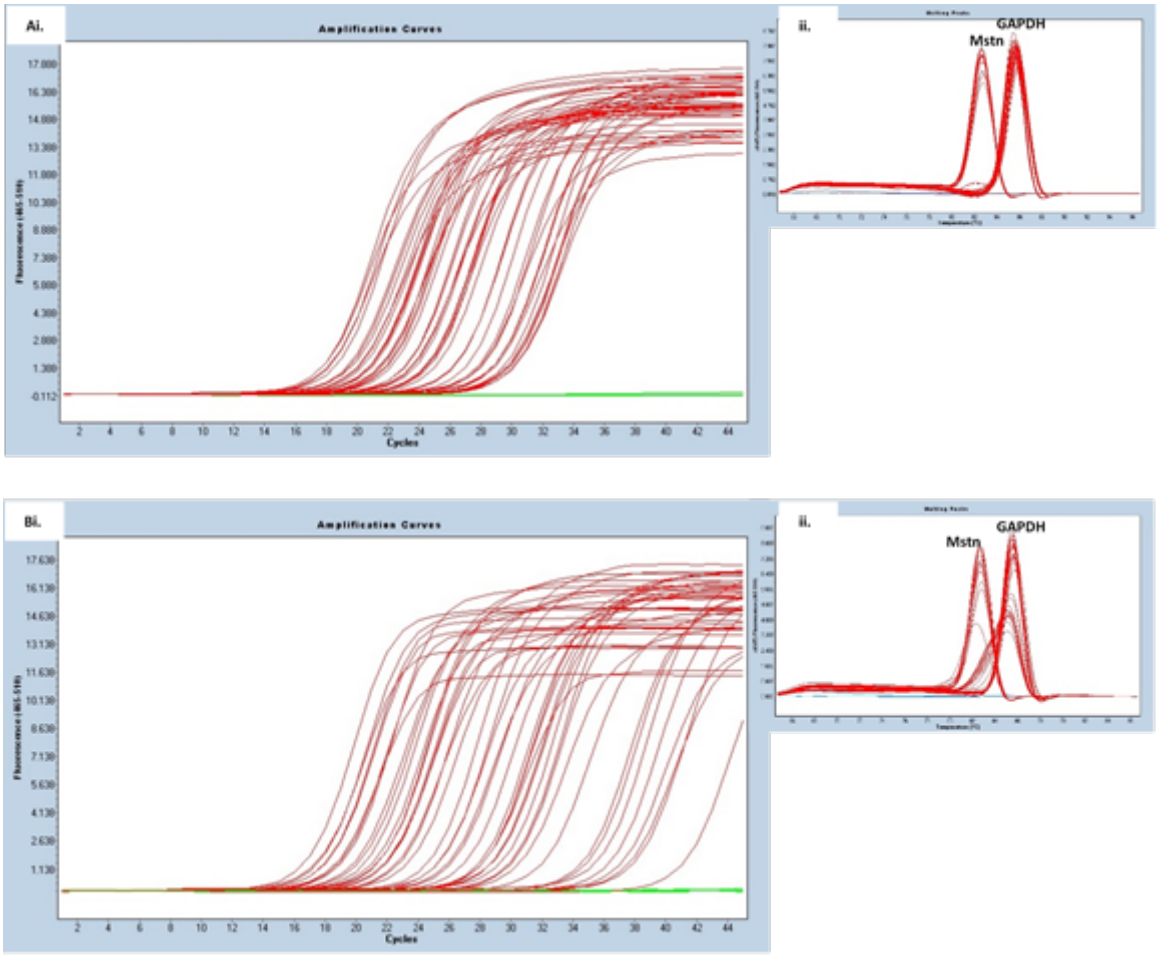

Appendix 11: RT-PCR of Mstn in BALB/c transgenic mice treated with Invivofectamine® 3.0 nanocomplexes with or without 5:1 PEGylated fibrin hydrogel. *7 days post treatment post treatement of mice with Invivofectamine ® 3.0 nanocomplexes made with 5µg siMstn-Cy3 or siGFP-Cy3 with or without. 5:1 PEGylated fibrin hydrogel encapsulation (8 legs per group). Mstn expression was quantified by RT-PCR normalised to GAPDH. (A.i) The amplification and melting curves (A.ii) of Mstn and GPDH from samples treated with Invivofectamine® 3.0-siGFP/siMstn free nanocomplexes. (B.i) The amplification and melting curves (B.ii) of Mstn and GAPDH from samples treated with Invivofectamine® 3.0-siGFP/siMstn encapsulated in 5:1 PEGylated hydrogel.*

Appendix 12

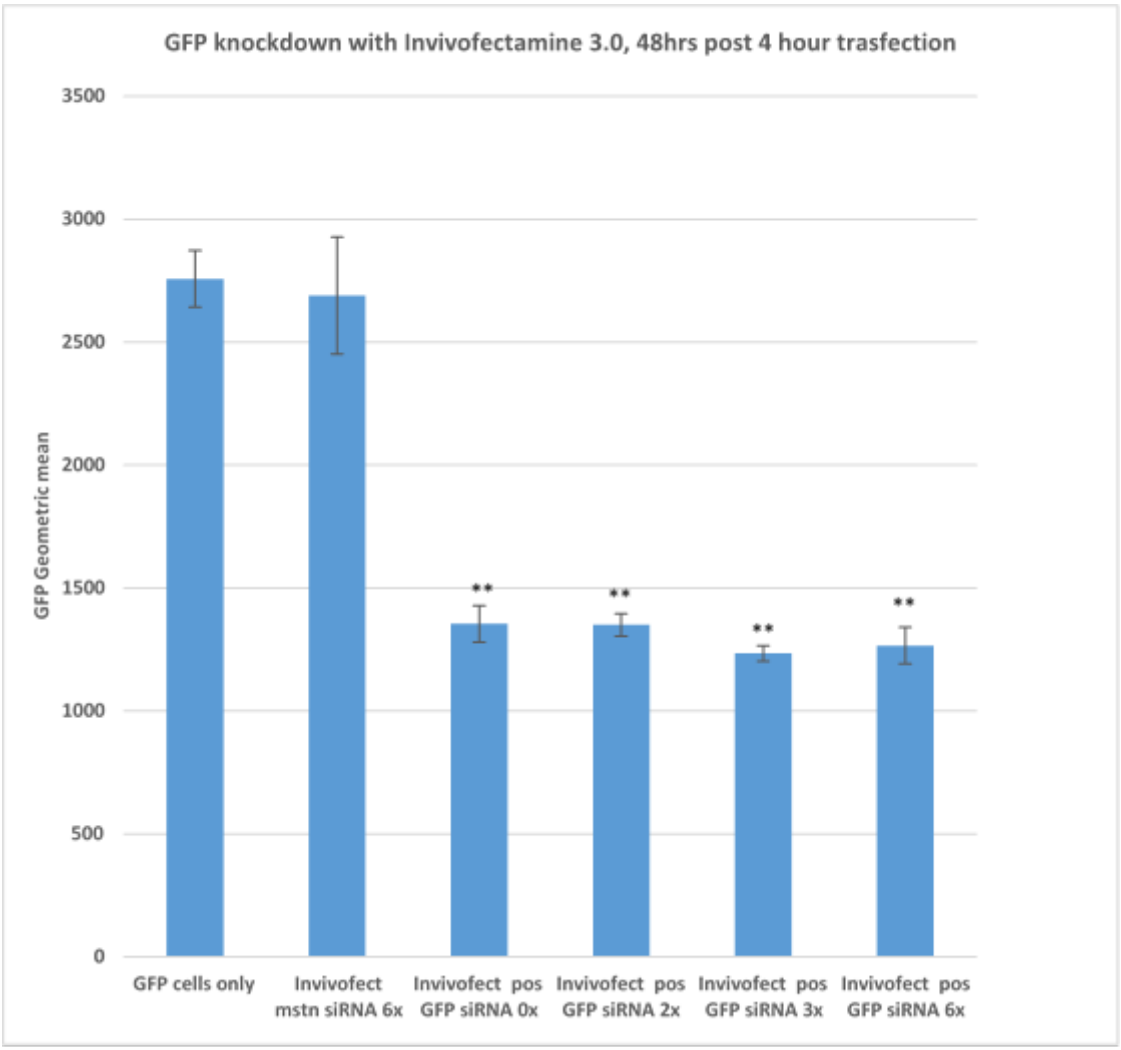

Appendix 12: GFP knockdown in GFP-HT1080 cells with Invivofectamine® 3.0 nanocomplexes in different dilution forms*. HT1080-GFP cells were transfected by Invivofectamine® 3.0 nanocomplexes made with 1000ng siGFP-Cy3 (pos GFP siRNA groups) or siMstn-Cy3 as a control (mstn siRNA group) for 4hrs. The nanocomplexes to use in the transfections were made according to manufacturer's protocol which suggests 6X dilution of the final nanocomplex solution. 3X, 2X and 0X dilution were included ensure efficacy of the nanocomplexes maintained when used in their concentrated form. This would allow smaller volumes with more siRNA to be loaded in the 30µl volume hydrogels without compromising nanocomplex efficacy. Flow cytometry was used to measure the GFP geometric mean.. ** p<0.005 vs Mstn siRNA control group.*

Appendix 13

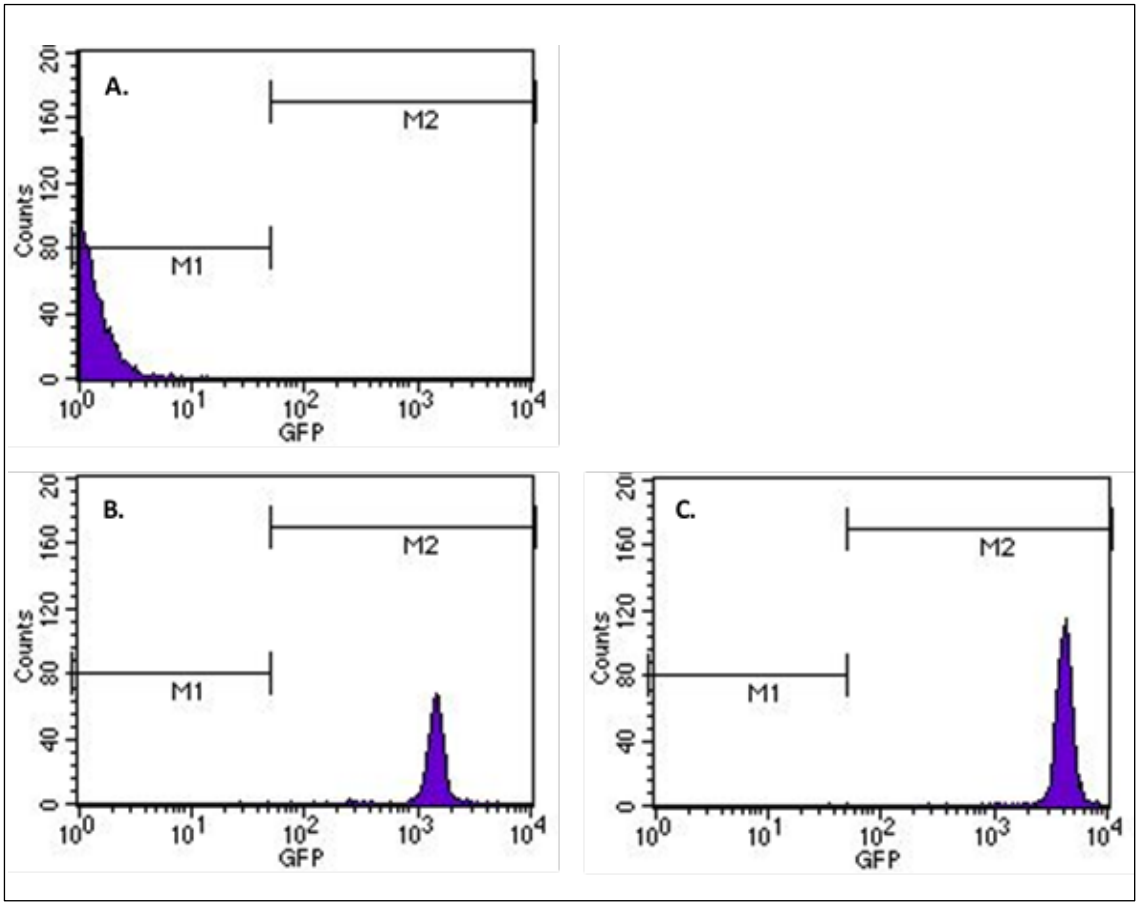

Appendix 13: Geometric means for BALB/c GFP or non-GFP mice to determine genotype*. This was assayed by few cytometry of white cells obtained from mice blood. The GFP deficiency (A), heterozygote (B) homozygote (C) genotype of each mouse was determined by the level GFP fluorescence. M1=GFP geometric mean of non-fluorescent cells, M2=GFP Geometric mean of fluorescent cells.*

Appendix 14

Reagents recipes

1. BHG Buffer pH 7.4

5% glucose
HEPES 20mM
Make up volume with dH_2O to 50ml
pH and sterilise

2. 0.1% DEPC treated water

500µl DEPC
Make up volume to 500ml with dH2O
Leave overnight and pH

3. DTT solution

1.7mg DTT
10ml PBS pH 7.4

4. Alexa dye solution

1mg Alexa Fluor® 660 C2-maleimide
100µl DMSO

5. 10X PBS pH 7.4

8mM $Na_2HPO_4.12H_2O$
1.4mM KH_2PO_4
2.7mM KCl
137mM NaCl
Make up volume to 1L with dH_2O and pH

6. 1X TE buffer pH 8

1M Tris pH 8
0.5M EDTA pH 8
Make up volume to 500ml with dH_2O

7. 10X TBE buffer

890mM Tris Base
890mM Boric acid
20mM EDTA
Make up volume to 500ml with RNase free treated H_2O

8. 1X Iso-osmotic PBS pH 7.4 (iso-PBS)

Solution A: 0.15M $NaH_2PO_4.H_2O$ in 1L dH_2O
Solution B: 0.15M $Na_2HPO_4.12H_2O$ in 1L dH_2O
0.15M NaCl in 500ml dH_2O
Combine 13ml of (A) + 87ml (B) + 100ml 0.15M NaCl
Adjust pH with solution A or B to maintain osmolality

9. Fibrin Gel reagents:

a. HEPES buffered saline 50ml (HBS) pH 7.4 or 7.8
   NaCl 410mg
   HEPES 297.5mg
   Na_2HPO_4 5mg
   pH
   Make up volume to 50ml and filter sterilize

b. HEPES buffered saline with Ca^{2+} 50ml (HBS/Ca^{2+})
   NaCl 410mg
   HEPES 297.5mg
   Na_2HPO_4 5mg
   Add 1ml 2mM $CaCl_2$
   pH to 7.8 and make up volume to 50ml and filter sterilize

c. Fibrinogen stock 40mg/ml
   40mg fibrinogen
   1ml HBS buffer
   Make 100µl aliquots to store at -20^0C

d. Thrombin stock 1000U/5ml
   33.3mg thrombin
   5ml HBS
   Filter sterilize and store 50µl (10U thrombin) aliquots at -20^0C

e. Thrombin working solution (1.4U/ml)
   50µl (10U) thrombin
   7172µl HBS/Ca^{2+}
   Filter sterilize and store 50µl aliquots at -20^0C

10. Western Blotting reagents10X running buffer

10g SDS30g Tris

144g glycine
Make up to 1L with distilled water

a. 10% APS (10ml)
10% (w/v) Ammonium persulfate
10ml distilled water

b. 2X reducing Loading dye pH (6.8) (10ml)
125mM Tris-HCl
4% (m/v) SDS
20% (v/v) glycerol
10% (v/v) 2-mercaptoethanol
Make up the volume to 10ml with distilled water.

c. 10% SDS (100ml)
10% (w/v) SDS
Dissolve in 100ml distilled water

d. 1X Transfer buffer
6.05g Tris
14.4g Glycine
Dissolve in 800ml distilled water
1ml 10% SDS
Add 200ml methanol fresh

e. Ponceau Stain (100ml)
0.1% (w/v) Ponceau S
15% (v/v) Acetic acid
Make up volume to100ml with distilled water

f. TBS Tween pH 7.5 (1L)
20mM Tris
150mM NaCl
0.05% Tween-20
Make up volume to 1L with distilled water

11. Red Blood Cell lysis buffer
8.29g NH_4Cl (0.15M)
1g $KHCO_3$ (10.0mM)
37.2mg Na_2EDTA (0.1mM)
Make up volume to 1L with distilled water
pH. 7.2 - 7.4

12. FACS Buffer
2% fetal culf serum
1mM EDTA
PBS pH 7.4 to 200ml volume

Appendix 15

List of materials

1, 2-dioleoyl-sn-glycero-3-phosphoethanolamine (DOPE), Avanti Polar Lipids (AL, USA).
8-arm 20PEG-VS, Nektar therapeutics, AL.
8-arm 20PEG-AC, Nektar therapeutics, AL.
7.5% SDS-PAGE gel reagents TGX™ FastCast™ Acrylamide Solutions, Bio-Rad (CA, USA).
12% SDS-PAGE gel reagents TGX™ FastCast™ Acrylamide Solutions, Bio-Rad (CA, USA).
100 bp DNA Ladder, ThermoFisher scientific.
Agarose powder, Sigma-Aldrich® (St Louis, MO).
Alexa Fluor® 660 C2-maleimide, Invitrogen Life technologies.
Anti-GFP - ChIP Grade rabbit polyclonal (ab290), Abcam.
anti-Mstn - GDF-8(N-19)-R rabbit polyclonal IgG (SC-688J-R), Santa cruz.
Anti-Rabbit Goat IgG H&L (HRP) (ab97051) antibodies, Abcam.
Anti-β Tubulin antibody (ab6046), Abcam.
CellTiter-Glo® luminescent Cell Viability Assay, Promega (WI, USA).
Cellulose ester dialysis membrane (12-14000 kDa MWCO), Sigma-Aldrich® (St Louis, MO).
Chemiluminescent detection kit WesternBright™ ECL, Advasta (CA, USA).
Chloroform, Sigma-Aldrich® (St Louis, MO)
Dimethyl sulfoxide (DMSO), Sigma-Aldrich® (St Louis, MO).

Dithiothreitol (DTT), Sigma-Aldrich® (St Louis, MO).
Eth D-1 stain for from Live/Dead™ cell viability assay kit from Molecular Probes Inc. (Eugene, OR).
Fetal bovine serum (FBS), Biochrom GmbH (Berlin, Germany).
Fibrinogen from human plasma, Alexa Fluor™ 647 conjugate, ThermoFisher scientific.
Fibrinogen from human serum (T-3879), Sigma-Aldrich® (St Louis, MO).
Forward and reverse GAPDH primers, Qiagen (MD, USA).
Forward and reverse HPRT primers, Qiagen (MD, USA).
Forward and reverse Mstn primers, Qiagen (MD, USA).
Forward and reverse β Actin primers, Qiagen (MD, USA).
G418 neomycin selection antibiotic, Sigma-Aldrich® (St Louis, MO).
GelRed™ Nucleic Acid gel stain (41003), Biotium (CA, USA) respectively.
Heparin sodium salt, Sigma-Aldrich® (St Louis, MO).
HEPES, Sigma-Aldrich® (St Louis, MO)
Hoechst stain, Molecular Probes Inc. (Eugene, OR).
Human fibrosarcoma HT-1080 cell line, The American Type Culture Collection (ATCC).
Hydrochloric acid, Sigma-Aldrich® (St Louis, MO)
Invivofectamine® 3.0 reagents, Life Technologies (CA, USA).
LightCycler® 480 SYBR Green I master mix, Qiagen (MD, USA).
Lipofectamine® RNAiMAX, Life Technologies (CA, USA).
MCDB media, Sigma-Aldrich® (St Louis, MO).
mirVana™ miRNA Isolation Kit and RNAlater® Solution, ThermoFischer Scientific.

MMP1 peptide: GCREGPQGIWGQERCG (1733 Da MW), GenScript (USA Inc, NJ)
N, N-Dimethylformamide, Sigma-Aldrich® (St Louis, MO)
Nitrophenyl Carbonate-Poly (Ethylene-glycol)-Nitrophenyl Carbonate with average MW 2000 (PEG2K-NPC2), Laysan Bio (AL, USA),
Nuclei stains Fluoroshield™ with DAPI, Molecular Probes Inc. (Eugene, OR).
PAMAM Dendrimer, ethylenediamine core, generation 4 [G(4)-D], 10 weight % solution in Methanol, Sigma-Aldrich® (St Louis, MO)
PEG – (Succinimidyl Carboxymethyl Ester)2 MW3500 (PEG-SMC2), JenKem Technology (Beijing, China).
pEGFP-C1 plasmid, Clontech.
Penicillin streptomycin solution (10X), Sigma-Aldrich® (St Louis, MO).
Pierce™ Detergent Compatible Bradford Assay Kit, Sigma-Aldrich® (St Louis, MO).
PolyFect transfection reagent, Qiagen (MD, USA).
Precision Plus Protein™ Dual Colour standard molecular weight marker (161-0374), Bio-Rad (CA, USA).
Protease inhibitor (PI) cocktail, Sigma-Aldrich® (St Louis, MO).
Proteinase K (Sigma Aldrich).
Quant-iT™ RiboGreen™ RNA Reagent, Life Technologies (CA, USA)
RIPA buffer, Sigma-Aldrich® (St Louis, MO).
Roche Transcriptor first strand cDNA synthesis kit, Qiagen (MD, USA).
siDeath - AllStars Hs Cell Death positive control siRNA (1027299), Qiagen (MD, USA).
siDeath-Negative - AllStars Hs Cell Death scramble negative control siRNA, Qiagen (MD, USA).

siFITC - Fluorescein isothiocyanate labelled scramble siNegative, Bioneer Corp (Daedeok District, South Korea).
siGFP - Green fluorescence proteins: GCAUCAAGGUGAACUUCAAdTdT (sense), Bioneer Corp (Daedeok District, South Korea).
siGFP-Cy3 - Cy3 labelled siGFP: GCAUCAAGGUGAACUUCAAdTdT Cy3 (sense), GE Healthcare Dharmacon.
Sigmacote®, Sigma-Aldrich® (St Louis, MO).
siMstn-Cy3 - Cy3 labelled siMstn: AAGAUGACGAUUAUCACGCUA-dTdT-Cy3 (sense), GE Healthcare Dharmacon.
siNegative - Negative scramble control siRNA, Bioneer Corp (Daedeok District, South Korea).
siNegative-Cy3 - AllStars negative Scramble Cy3 labelled siRNA (AF555), Qiagen (MD, USA).
Slide – A - Lyzer®mini dialysis device (10000 MWCO), Sigma-Aldrich® (St Louis, MO).
Thrombin from bovine plasma (T-4648), Sigma-Aldrich® (St Louis, MO).
Triethylamine (TEA), Sigma-Aldrich® (St Louis, MO).
Tris-Borate-EDTA (TBE), Sigma-Aldrich® (St Louis, MO).

7 References

1. Wang, L.L., et al., *Injectable and protease-degradable hydrogel for siRNA sequestration and triggered delivery to the heart.* J Control Release, 2018. **285**: p. 152-161.
2. Xia, Y., J. Tian, and X. Chen, *Effect of surface properties on liposomal siRNA delivery.* Biomaterials, 2016. **79**: p. 56-68.
3. Kim, Y.M., M.R. Park, and S.C. Song, *An injectable cell penetrable nano-polyplex hydrogel for localized siRNA delivery.* Biomaterials, 2013. **34**(18): p. 4493-500.
4. Chakraborty, C., et al., *Therapeutic miRNA and siRNA: Moving from Bench to Clinic as Next Generation Medicine.* Molecular Therapy. Nucleic Acids, 2017. **8**: p. 132-143.
5. Fire, A., et al., *Potent and specific genetic interference by double-stranded RNA in Caenorhabditis elegans.* Nature, 1998. **391**(6669): p. 806-811.
6. Berns, K., et al., *A large-scale RNAi screen in human cells identifies new components of the p53 pathway.* Nature, 2004. **428**(6981): p. 431-7.
7. Elbashir, S.M., et al., *Duplexes of 21-nucleotide RNAs mediate RNA interference in cultured mammalian cells.* Nature, 2001. **411**(6836): p. 494-8.
8. Zheng, L., et al., *An approach to genomewide screens of expressed small interfering RNAs in mammalian cells.* Proceedings of the National Academy of Sciences of the United States of America, 2004. **101**(1): p. 135-40.
9. Bobbin, M.L. and J.J. Rossi, *RNA Interference (RNAi)-Based Therapeutics: Delivering on the Promise?* Annu Rev Pharmacol Toxicol, 2016. **56**: p. 103-22.
10. Moore, C.B., et al., *Short hairpin RNA (shRNA): design, delivery, and assessment of gene knockdown.* Methods Mol Biol, 2010. **629**: p. 141-58.
11. Lee, Y.K., et al., *MicroRNA genes are transcribed by RNA polymerase II.* The EMBO Journal, 2004. **23**(20): p. 4051-4060.
12. Mohan, N., et al., *Combination of LC3 shRNA Plasmid Transfection and Genistein Treatment Inhibited Autophagy and Increased Apoptosis in Malignant Neuroblastoma in Cell Culture and Animal Models.* PLoS ONE, 2013. **8**(10): p. e78958.
13. Silva, J.M., et al., *Second-generation shRNA libraries covering the mouse and human genomes.* Nat Genet, 2005. **37**(11): p. 1281-8.
14. Subramanya, S., et al., *RNA interference-based therapeutics for human immunodeficiency virus HIV-1 treatment: synthetic siRNA or vector-based shRNA?* Expert Opin Biol Ther, 2010. **10**(2): p. 201-13.
15. Nicholson, A.W., *Ribonuclease III mechanisms of double-stranded RNA cleavage.* Wiley Interdiscip Rev RNA, 2014. **5**(1): p. 31-48.
16. Bartel, D.P., *MicroRNAs: genomics, biogenesis, mechanism, and function.* Cell, 2004. **116**(2): p. 281-97.
17. Carthew, R.W. and E.J. Sontheimer, *Origins and Mechanisms of miRNAs and siRNAs.* Cell, 2009. **136**(4): p. 642-55.
18. Treiber, T., N. Treiber, and G. Meister, *Regulation of microRNA biogenesis and function.* Thromb Haemost, 2012. **107**(4): p. 605-10.
19. Valencia-Sanchez, M.A., et al., *Control of translation and mRNA degradation by miRNAs and siRNAs.* Genes Dev, 2006. **20**(5): p. 515-24.
20. He, L. and G.J. Hannon, *MicroRNAs: small RNAs with a big role in gene regulation.* Nat Rev Genet, 2004. **5**(7): p. 522-31.
21. Cooper, T.A., L. Wan, and G. Dreyfuss, *RNA and Disease.* 2009. **136**(4): p. 777-93.
22. El-Brolosy, M.A. and D.Y.R. Stainier, *Genetic compensation: A phenomenon in search of mechanisms.* PLoS Genet, 2017. **13**(7): p. e1006780.

23. Cejka, D., D. Losert, and V. Wacheck, *Short interfering RNA (siRNA): tool or therapeutic?* Clinical science, 2006. **110**(1): p. 47-58.
24. de Fougerolles, A., et al., *Interfering with disease: a progress report on siRNA-based therapeutics.* Nature reviews. Drug discovery, 2007. **6**(6): p. 443-53.
25. Azarmi, S., W.H. Roa, and R. Lobenberg, *Targeted delivery of nanoparticles for the treatment of lung diseases.* Advanced drug delivery reviews, 2008. **60**(8): p. 863-75.
26. Hattori, Y., et al., *In vivo siRNA delivery system for targeting to the liver by poly-l-glutamic acid-coated lipoplex.* Results in pharma sciences, 2014. **4**: p. 1-7.
27. Schiffelers, R.M., et al., *Cancer siRNA therapy by tumor selective delivery with ligand-targeted sterically stabilized nanoparticle.* Nucleic acids research, 2004. **32**(19): p. e149.
28. Omi, K., et al., *siRNA-mediated inhibition of endogenous Huntington disease gene expression induces an aberrant configuration of the ER network in vitro.* Biochemical and biophysical research communications, 2005. **338**(2): p. 1229-35.
29. van Rooij, E., W.S. Marshall, and E.N. Olson, *Toward microRNA-based therapeutics for heart disease: the sense in antisense.* Circulation research, 2008. **103**(9): p. 919-28.
30. Wong, E. and T. Goldberg, *Mipomersen (kynamro): a novel antisense oligonucleotide inhibitor for the management of homozygous familial hypercholesterolemia.* P t, 2014. **39**(2): p. 119-22.
31. Adams, D., et al., *Patisiran, an RNAi Therapeutic, for Hereditary Transthyretin Amyloidosis.* New England Journal of Medicine, 2018. **379**(1): p. 11-21.
32. Jackson, A.L., et al., *Widespread siRNA "off-target" transcript silencing mediated by seed region sequence complementarity.* RNA, 2006. **12**(7): p. 1179-87.
33. Judge, A.D., et al., *Design of noninflammatory synthetic siRNA mediating potent gene silencing in vivo.* Molecular therapy : the journal of the American Society of Gene Therapy, 2006. **13**(3): p. 494-505.
34. Wang, J., et al., *Delivery of siRNA therapeutics: barriers and carriers.* The AAPS journal, 2010. **12**(4): p. 492-503.
35. van de Water, F.M., et al., *Intravenously administered short interfering RNA accumulates in the kidney and selectively suppresses gene function in renal proximal tubules.* Drug metabolism and disposition: the biological fate of chemicals, 2006. **34**(8): p. 1393-7.
36. Grimm, D., et al., *Fatality in mice due to oversaturation of cellular microRNA/short hairpin RNA pathways.* Nature, 2006. **441**(7092): p. 537-41.
37. Aagaard, L. and J.J. Rossi, *RNAi therapeutics: principles, prospects and challenges.* Adv Drug Deliv Rev, 2007. **59**(2-3): p. 75-86.
38. Huang, Y., et al., *Pharmacokinetic Behaviors of Intravenously Administered siRNA in Glandular Tissues.* Theranostics, 2016. **6**(10): p. 1528-1541.
39. Whitehead, K.A., R. Langer, and D.G. Anderson, *Knocking down barriers: advances in siRNA delivery.* Nature reviews. Drug discovery, 2009. **8**(2): p. 129-38.
40. Kim, K.S., G. Khang, and D. Lee, *Application of nanomedicine in cardiovascular diseases and stroke.* Curr Pharm Des, 2011. **17**(18): p. 1825-33.
41. Bobo, D., et al., *Nanoparticle-Based Medicines: A Review of FDA-Approved Materials and Clinical Trials to Date.* Pharm Res, 2016. **33**(10): p. 2373-87.
42. Smith, R.A., et al., *Antisense oligonucleotide therapy for neurodegenerative disease.* The Journal of clinical investigation, 2006. **116**(8): p. 2290-6.
43. Morrissey, D.V., et al., *Potent and persistent in vivo anti-HBV activity of chemically modified siRNAs.* Nat Biotechnol, 2005. **23**(8): p. 1002-7.
44. Arnold, A.S., et al., *Specific β1-adrenergic receptor silencing with small interfering RNA lowers high blood pressure and improves cardiac function in myocardial ischemia.* Journal of Hypertension, 2007. **25**(1): p. 197-205.

45. Soutschek, J., et al., *Therapeutic silencing of an endogenous gene by systemic administration of modified siRNAs.* Nature, 2004. **432**: p. 173.
46. Thomas, M., et al., *Non-viral siRNA delivery to the lung.* Advanced Drug Delivery Reviews, 2007. **59**(2): p. 124-133.
47. Zatsepin, T.S., Y.V. Kotelevtsev, and V. Koteliansky, *Lipid nanoparticles for targeted siRNA delivery - going from bench to bedside.* Int J Nanomedicine, 2016. **11**: p. 3077-86.
48. Crooke, S.T. and R.S. Geary, *Clinical pharmacological properties of mipomersen (Kynamro), a second generation antisense inhibitor of apolipoprotein B.* Br J Clin Pharmacol, 2013. **76**(2): p. 269-76.
49. Shemesh, C.S., et al., *Assessment of the Drug Interaction Potential of Unconjugated and GalNAc(3)-Conjugated 2′ -MOE-ASOs.* Molecular Therapy. Nucleic Acids, 2017. **9**: p. 34-47.
50. Gavrilov, K. and W.M. Saltzman, *Therapeutic siRNA: principles, challenges, and strategies.* Yale J Biol Med, 2012. **85**(2): p. 187-200.
51. Lee, S.J., et al., *Structural modification of siRNA for efficient gene silencing.* Biotechnol Adv, 2013. **31**(5): p. 491-503.
52. Mook, O.R., et al., *Evaluation of locked nucleic acid-modified small interfering RNA in vitro and in vivo.* Mol Cancer Ther, 2007. **6**(3): p. 833-43.
53. Barquinero, J., H. Eixarch, and M. Perez-Melgosa, *Retroviral vectors: new applications for an old tool.* Gene Ther, 2004. **11 Suppl 1**: p. S3-9.
54. Escors, D. and K. Breckpot, *Lentiviral vectors in gene therapy: their current status and future potential.* Arch Immunol Ther Exp (Warsz), 2010. **58**(2): p. 107-19.
55. Couto, L.B. and K.A. High, *Viral vector-mediated RNA interference.* Curr Opin Pharmacol, 2010. **10**(5): p. 534-42.
56. Blaese, R.M., et al., *Treatment of severe combined immunodeficiency disease (SCID) due to adenosine deaminase deficiency with CD34+ selected autologous peripheral blood cells transduced with a human ADA gene. Amendment to clinical research project, Project 90-C-195, January 10, 1992.* Hum Gene Ther, 1993. **4**(4): p. 521-7.
57. Cavazzana-Calvo, M., et al., *Gene therapy of human severe combined immunodeficiency (SCID)-X1 disease.* Science, 2000. **288**(5466): p. 669-72.
58. Levine, F. and T. Friedmann, *Gene therapy techniques.* Curr Opin Biotechnol, 1991. **2**(6): p. 840-4.
59. Mann, R., R.C. Mulligan, and D. Baltimore, *Construction of a retrovirus packaging mutant and its use to produce helper-free defective retrovirus.* Cell, 1983. **33**(1): p. 153-9.
60. Breckpot, K., et al., *Lentivirally transduced dendritic cells as a tool for cancer immunotherapy.* J Gene Med, 2003. **5**(8): p. 654-67.
61. Brown, B.D., et al., *In vivo administration of lentiviral vectors triggers a type I interferon response that restricts hepatocyte gene transfer and promotes vector clearance.* Blood, 2007. **109**(7): p. 2797-805.
62. Aguiar, S., B. van der Gaag, and F.A.B. Cortese, *RNAi mechanisms in Huntington's disease therapy: siRNA versus shRNA.* Translational Neurodegeneration, 2017. **6**(1): p. 30.
63. Lundstrom, K., *Viral Vectors in Gene Therapy.* Diseases, 2018. **6**(2).
64. Check, E., *Gene therapy: shining hopes dented - but not dashed.* Nature, 2002. **420**(6917): p. 735.
65. Check, E., *Regulators split on gene therapy as patient shows signs of cancer.* Nature, 2002. **419**(6907): p. 545-6.
66. Niidome, T. and L. Huang, *Gene therapy progress and prospects: nonviral vectors.* Gene therapy, 2002. **9**(24): p. 1647-52.
67. Raper, S.E., et al., *A pilot study of in vivo liver-directed gene transfer with an adenoviral vector in partial ornithine transcarbamylase deficiency.* Human gene therapy, 2002. **13**(1): p. 163-75.

68. Hacein-Bey-Abina, S., et al., *LMO2-associated clonal T cell proliferation in two patients after gene therapy for SCID-X1.* Science, 2003. **302**(5644): p. 415-9.
69. Bear, A.S., et al., *Replication-competent retroviruses in gene-modified T cells used in clinical trials: is it time to revise the testing requirements?* Mol Ther, 2012. **20**(2): p. 246-9.
70. Milone, M.C. and U. O'Doherty, *Clinical use of lentiviral vectors.* Leukemia, 2018. **32**(7): p. 1529-1541.
71. Nayerossadat, N., T. Maedeh, and P.A. Ali, *Viral and nonviral delivery systems for gene delivery.* Advanced Biomedical Research, 2012. **1**: p. 27.
72. Caster, J.M., et al., *Investigational nanomedicines in 2016: a review of nanotherapeutics currently undergoing clinical trials.* Wiley Interdiscip Rev Nanomed Nanobiotechnol, 2017. **9**(1).
73. Hoshyar, N., et al., *The effect of nanoparticle size on in vivo pharmacokinetics and cellular interaction.* Nanomedicine (Lond), 2016. **11**(6): p. 673-92.
74. McCarthy, J.R., *Nanomedicine and Cardiovascular Disease.* Curr Cardiovasc Imaging Rep, 2010. **3**(1): p. 42-49.
75. Gupta, A.K. and S. Wells, *Surface-modified superparamagnetic nanoparticles for drug delivery: preparation, characterization, and cytotoxicity studies.* IEEE Trans Nanobioscience, 2004. **3**(1): p. 66-73.
76. Senior, J., J.C. Crawley, and G. Gregoriadis, *Tissue distribution of liposomes exhibiting long half-lives in the circulation after intravenous injection.* Biochimica et biophysica acta, 1985. **839**(1): p. 1-8.
77. Stolnik, S., L. Illum, and S.S. Davis, *Long circulating microparticulate drug carriers.* Advanced Drug Delivery Reviews, 1995. **16**(2): p. 195-214.
78. Campbell, F., et al., *Directing Nanoparticle Biodistribution through Evasion and Exploitation of Stab2-Dependent Nanoparticle Uptake.* ACS Nano, 2018. **12**(3): p. 2138-2150.
79. Wilhelm, S., et al., *Analysis of nanoparticle delivery to tumours.* Nature Reviews Materials, 2016. **1**: p. 16014.
80. Zhang, Y.N., et al., *Nanoparticle-liver interactions: Cellular uptake and hepatobiliary elimination.* J Control Release, 2016. **240**: p. 332-348.
81. Choi, H.S., et al., *Renal clearance of quantum dots.* Nat Biotechnol, 2007. **25**(10): p. 1165-70.
82. Fox, M.E., F.C. Szoka, and J.M.J. Fréchet, *Soluble Polymer Carriers for the Treatment of Cancer: The Importance of Molecular Architecture.* Accounts of chemical research, 2009. **42**(8): p. 1141-1151.
83. Frohlich, E., *The role of surface charge in cellular uptake and cytotoxicity of medical nanoparticles.* Int J Nanomedicine, 2012. **7**: p. 5577-91.
84. Jiang, Y., et al., *The Interplay of Size and Surface Functionality on the Cellular Uptake of Sub-10 nm Gold Nanoparticles.* ACS Nano, 2015. **9**(10): p. 9986-93.
85. Harush-Frenkel, O., et al., *Surface charge of nanoparticles determines their endocytic and transcytotic pathway in polarized MDCK cells.* Biomacromolecules, 2008. **9**(2): p. 435-43.
86. Yue, Z.G., et al., *Surface charge affects cellular uptake and intracellular trafficking of chitosan-based nanoparticles.* Biomacromolecules, 2011. **12**(7): p. 2440-6.
87. He, C., et al., *Effects of particle size and surface charge on cellular uptake and biodistribution of polymeric nanoparticles.* Biomaterials, 2010. **31**(13): p. 3657-66.
88. Hirn, S., et al., *Particle size-dependent and surface charge-dependent biodistribution of gold nanoparticles after intravenous administration.* European journal of pharmaceutics and biopharmaceutics : official journal of Arbeitsgemeinschaft fur Pharmazeutische Verfahrenstechnik e.V, 2011. **77**(3): p. 407-416.
89. Liu, X., et al., *Surface and size effects on cell interaction of gold nanoparticles with both phagocytic and nonphagocytic cells.* Langmuir, 2013. **29**(29): p. 9138-48.

90. Khine, Y.Y., et al., *Direct Correlation Between Zeta Potential and Cellular Uptake of Poly(methacrylic acid) Post-Modified with Guanidinium Functionalities.* Macromolecular Chemistry and Physics, 2016. **217**(20): p. 2302-2309.
91. Lorenz, M.R., et al., *Uptake of functionalized, fluorescent-labeled polymeric particles in different cell lines and stem cells.* Biomaterials, 2006. **27**(14): p. 2820-8.
92. Chauhan, A.S., et al., *Unexpected in vivo anti-inflammatory activity observed for simple, surface functionalized poly(amidoamine) dendrimers.* Biomacromolecules, 2009. **10**(5): p. 1195-202.
93. Naha, P.C., et al., *Reactive oxygen species (ROS) induced cytokine production and cytotoxicity of PAMAM dendrimers in J774A.1 cells.* Toxicol Appl Pharmacol, 2010. **246**(1-2): p. 91-9.
94. Schaeublin, N.M., et al., *Surface charge of gold nanoparticles mediates mechanism of toxicity.* Nanoscale, 2011. **3**(2): p. 410-20.
95. Wilczewska, A.Z., et al., *Nanoparticles as drug delivery systems.* Pharmacological reports : PR, 2012. **64**(5): p. 1020-37.
96. Scomparin, A., et al., *Achieving successful delivery of oligonucleotides - From physico-chemical characterization to in vivo evaluation.* Biotechnology advances, 2015.
97. Etheridge, M.L., et al., *The big picture on nanomedicine: the state of investigational and approved nanomedicine products.* Nanomedicine, 2013. **9**(1): p. 1-14.
98. Hassan, S., et al., *Evolution and clinical translation of drug delivery nanomaterials.* Nano Today, 2017. **15**: p. 91-106.
99. Tatiparti, K., et al., *siRNA Delivery Strategies: A Comprehensive Review of Recent Developments.* Nanomaterials (Basel), 2017. **7**(4).
100. Shi, J., et al., *Cancer nanomedicine: progress, challenges and opportunities.* Nat Rev Cancer, 2017. **17**(1): p. 20-37.
101. Yang, Y., et al., *Nanoparticle delivery of pooled siRNA for effective treatment of non-small cell lung cancer.* Mol Pharm, 2012. **9**(8): p. 2280-9.
102. Helmschrodt, C., et al., *Polyethylenimine Nanoparticle-Mediated siRNA Delivery to Reduce alpha-Synuclein Expression in a Model of Parkinson's Disease.* Mol Ther Nucleic Acids, 2017. **9**: p. 57-68.
103. Zhou, J., et al., *Octa-functional PLGA nanoparticles for targeted and efficient siRNA delivery to tumors.* Biomaterials, 2012. **33**(2): p. 583-91.
104. Davis, M.E., et al., *Evidence of RNAi in humans from systemically administered siRNA via targeted nanoparticles.* Nature, 2010. **464**(7291): p. 1067-70.
105. Yang, C., et al., *Chitosan/siRNA nanoparticles targeting cyclooxygenase type 2 attenuate unilateral ureteral obstruction-induced kidney injury in mice.* Theranostics, 2015. **5**(2): p. 110-23.
106. Christie, R.J., et al., *Targeted polymeric micelles for siRNA treatment of experimental cancer by intravenous injection.* ACS Nano, 2012. **6**(6): p. 5174-89.
107. Aldrian, G., et al., *PEGylation rate influences peptide-based nanoparticles mediated siRNA delivery in vitro and in vivo.* J Control Release, 2017. **256**: p. 79-91.
108. Ren, L., et al., *Functionalized graphene oxide for anti-VEGF siRNA delivery: preparation, characterization and evaluation in vitro and in vivo.* RSC Advances, 2017. **7**(33): p. 20553-20566.
109. Lu, W., et al., *Tumor site-specific silencing of NF-kappaB p65 by targeted hollow gold nanosphere-mediated photothermal transfection.* Cancer Res, 2010. **70**(8): p. 3177-88.
110. Mahajan, U.M., et al., *Tumour-specific delivery of siRNA-coupled superparamagnetic iron oxide nanoparticles, targeted against PLK1, stops progression of pancreatic cancer.* Gut, 2016. **65**(11): p. 1838-1849.
111. Paul, A., et al., *Injectable graphene oxide/hydrogel-based angiogenic gene delivery system for vasculogenesis and cardiac repair.* ACS Nano, 2014. **8**(8): p. 8050-62.

112. Kim, M.W., et al., *Cancer-targeted Nucleic Acid Delivery and Quantum Dot Imaging Using EGF Receptor Aptamer-conjugated Lipid Nanoparticles.* Sci Rep, 2017. **7**(1): p. 9474.
113. Bi, Y., et al., *Gene-silencing effects of anti-survivin siRNA delivered by RGDV-functionalized nanodiamond carrier in the breast carcinoma cell line MCF-7.* Int J Nanomedicine, 2016. **11**: p. 5771-5787.
114. Du, J., et al., *Biodegradable nanoparticles of mPEG-PLGA-PLL triblock copolymers as novel non-viral vectors for improving siRNA delivery and gene silencing.* Int J Mol Sci, 2012. **13**(1): p. 516-33.
115. Yang, X.Z., et al., *Systemic delivery of siRNA with cationic lipid assisted PEG-PLA nanoparticles for cancer therapy.* J Control Release, 2011. **156**(2): p. 203-11.
116. Singh, R.P., et al., *Self-Assembled Cationic beta-Cyclodextrin Nanostructures for siRNA Delivery.* Mol Pharm, 2019. **16**(3): p. 1358-1366.
117. Saraogi, G.K., et al., *Gelatin nanocarriers as potential vectors for effective management of tuberculosis.* Int J Pharm, 2010. **385**(1-2): p. 143-9.
118. Mao, H.Q., et al., *Chitosan-DNA nanoparticles as gene carriers: synthesis, characterization and transfection efficiency.* J Control Release, 2001. **70**(3): p. 399-421.
119. Rejinold, N.S., et al., *Biodegradable and thermo-sensitive chitosan-g-poly(N-vinylcaprolactam) nanoparticles as a 5-fluorouracil carrier.* Carbohydrate Polymers, 2011. **83**(2): p. 776-786.
120. Prabhu, R.H., V.B. Patravale, and M.D. Joshi, *Polymeric nanoparticles for targeted treatment in oncology: current insights.* Int J Nanomedicine, 2015. **10**: p. 1001-18.
121. Nikitenko, N.A. and V.S. Prassolov, *Non-Viral Delivery and Therapeutic Application of Small Interfering RNAs.* Acta naturae, 2013. **5**(3): p. 35-53.
122. Panyam, J. and V. Labhasetwar, *Biodegradable nanoparticles for drug and gene delivery to cells and tissue.* Advanced drug delivery reviews, 2003. **55**(3): p. 329-47.
123. Kumari, A., S.K. Yadav, and S.C. Yadav, *Biodegradable polymeric nanoparticles based drug delivery systems.* Colloids Surf B Biointerfaces, 2010. **75**(1): p. 1-18.
124. Bilensoy, E., *Cationic nanoparticles for cancer therapy.* Expert Opinion on Drug Delivery, 2010. **7**(7): p. 795-809.
125. Lin, J. and A. Alexander-Katz, *Cell Membranes Open "Doors" for Cationic Nanoparticles/Biomolecules: Insights into Uptake Kinetics.* ACS Nano, 2013. **7**(12): p. 10799-10808.
126. Boussif, O., et al., *A versatile vector for gene and oligonucleotide transfer into cells in culture and in vivo: polyethylenimine.* Proceedings of the National Academy of Sciences of the United States of America, 1995. **92**(16): p. 7297-301.
127. Nguyen, J. and F.C. Szoka, *Nucleic acid delivery: the missing pieces of the puzzle?* Acc Chem Res, 2012. **45**(7): p. 1153-62.
128. Zhang, X.Q., et al., *Interactions of nanomaterials and biological systems: Implications to personalized nanomedicine.* Adv Drug Deliv Rev, 2012. **64**(13): p. 1363-84.
129. des Rieux, A., et al., *Nanoparticles as potential oral delivery systems of proteins and vaccines: a mechanistic approach.* J Control Release, 2006. **116**(1): p. 1-27.
130. Lunov, O., et al., *Differential uptake of functionalized polystyrene nanoparticles by human macrophages and a monocytic cell line.* ACS nano, 2011. **5**(3): p. 1657-69.
131. Saptarshi, S.R., A. Duschl, and A.L. Lopata, *Interaction of nanoparticles with proteins: relation to bio-reactivity of the nanoparticle.* Journal of nanobiotechnology, 2013. **11**: p. 26.
132. Gibaud, S., et al., *Cells involved in the capture of nanoparticles in hematopoietic organs.* Journal of pharmaceutical sciences, 1996. **85**(9): p. 944-50.
133. Walkey, C.D., et al., *Nanoparticle size and surface chemistry determine serum protein adsorption and macrophage uptake.* Journal of the American Chemical Society, 2012. **134**(4): p. 2139-47.

134. Jain, R.K. and T. Stylianopoulos, *Delivering nanomedicine to solid tumors.* Nature reviews. Clinical oncology, 2010. **7**(11): p. 653-64.
135. Riezman, H., et al., *Molecular mechanisms of endocytosis.* Cell, 1997. **91**(6): p. 731-8.
136. Wattiaux, R., et al., *Endosomes, lysosomes: their implication in gene transfer.* Advanced drug delivery reviews, 2000. **41**(2): p. 201-8.
137. Bazile, D., et al., *Stealth Me.PEG-PLA nanoparticles avoid uptake by the mononuclear phagocytes system.* Journal of pharmaceutical sciences, 1995. **84**(4): p. 493-8.
138. Illum, L. and S.S. Davis, *The organ uptake of intravenously administered colloidal particles can be altered using a non-ionic surfactant (Poloxamer 338).* FEBS letters, 1984. **167**(1): p. 79-82.
139. Norman, M.E., P. Williams, and L. Illum, *Influence of block copolymers on the adsorption of plasma proteins to microspheres.* Biomaterials, 1993. **14**(3): p. 193-202.
140. Biswas, S., et al., *Lipid modified triblock PAMAM-based nanocarriers for siRNA drug co-delivery.* Biomaterials, 2013. **34**(4): p. 1289-301.
141. Fach, M., L. Radi, and P.R. Wich, *Nanoparticle Assembly of Surface-Modified Proteins.* Journal of the American Chemical Society, 2016. **138**(45): p. 14820-14823.
142. Liu, X., et al., *Promoting siRNA delivery via enhanced cellular uptake using an arginine-decorated amphiphilic dendrimer.* Nanoscale, 2015. **7**(9): p. 3867-3875.
143. Peracchia, M.T., et al., *Stealth PEGylated polycyanoacrylate nanoparticles for intravenous administration and splenic targeting.* Journal of controlled release : official journal of the Controlled Release Society, 1999. **60**(1): p. 121-8.
144. Kim, Y., E.J. Park, and D.H. Na, *Recent progress in dendrimer-based nanomedicine development.* Arch Pharm Res, 2018. **41**(6): p. 571-582.
145. Cavallaro, G., et al., *Polymeric nanoparticles for siRNA delivery: Production and applications.* Int J Pharm, 2017. **525**(2): p. 313-333.
146. Bolhassani, A., et al., *Polymeric nanoparticles: potent vectors for vaccine delivery targeting cancer and infectious diseases.* Hum Vaccin Immunother, 2014. **10**(2): p. 321-32.
147. Ragelle, H., G. Vandermeulen, and V. Preat, *Chitosan-based siRNA delivery systems.* J Control Release, 2013. **172**(1): p. 207-218.
148. Zhao, Q.Q., et al., *Gene-carried hepatoma targeting complex induced high gene transfection efficiency with low toxicity and significant antitumor activity.* Int J Nanomedicine, 2012. **7**: p. 3191-202.
149. Lungwitz, U., et al., *Polyethylenimine-based non-viral gene delivery systems.* Eur J Pharm Biopharm, 2005. **60**(2): p. 247-66.
150. Kwok, A. and S.L. Hart, *Comparative structural and functional studies of nanoparticle formulations for DNA and siRNA delivery.* Nanomedicine, 2011. **7**(2): p. 210-9.
151. Patnaik, S. and K.C. Gupta, *Novel polyethylenimine-derived nanoparticles for in vivo gene delivery.* Expert Opin Drug Deliv, 2013. **10**(2): p. 215-28.
152. Rhim, A.D., et al., *Stromal elements act to restrain, rather than support, pancreatic ductal adenocarcinoma.* Cancer Cell, 2014. **25**(6): p. 735-47.
153. Rouanet, M., et al., *Gene Therapy for Pancreatic Cancer: Specificity, Issues and Hopes.* Int J Mol Sci, 2017. **18**(6).
154. Gonzalez, H., S.J. Hwang, and M.E. Davis, *New class of polymers for the delivery of macromolecular therapeutics.* Bioconjug Chem, 1999. **10**(6): p. 1068-74.
155. Heidel, J.D., et al., *Potent siRNA inhibitors of ribonucleotide reductase subunit RRM2 reduce cell proliferation in vitro and in vivo.* Clin Cancer Res, 2007. **13**(7): p. 2207-15.
156. Heidel, J.D., et al., *Administration in non-human primates of escalating intravenous doses of targeted nanoparticles containing ribonucleotide reductase subunit M2 siRNA.* Proc Natl Acad Sci U S A, 2007. **104**(14): p. 5715-21.

157. Davis, M.E., *The first targeted delivery of siRNA in humans via a self-assembling, cyclodextrin polymer-based nanoparticle: from concept to clinic.* Mol Pharm, 2009. **6**(3): p. 659-68.
158. Wu, J., W. Huang, and Z. He, *Dendrimers as carriers for siRNA delivery and gene silencing: a review.* ScientificWorldJournal, 2013. **2013**: p. 630654.
159. Svenson, S. and D.A. Tomalia, *Dendrimers in biomedical applications--reflections on the field.* Adv Drug Deliv Rev, 2005. **57**(15): p. 2106-29.
160. Taratula, O., et al., *Surface-engineered targeted PPI dendrimer for efficient intracellular and intratumoral siRNA delivery.* J Control Release, 2009. **140**(3): p. 284-93.
161. Merkel, O.M., et al., *Molecular modeling and in vivo imaging can identify successful flexible triazine dendrimer-based siRNA delivery systems.* Journal of controlled release : official journal of the Controlled Release Society, 2011. **153**(1): p. 23-33.
162. Weber, N., et al., *Characterization of carbosilane dendrimers as effective carriers of siRNA to HIV-infected lymphocytes.* J Control Release, 2008. **132**(1): p. 55-64.
163. Jiménez, J.L., et al., *Carbosilane dendrimers as carriers of siRNA*. Vol. 22. 2012. 75-82.
164. Fischer, W., et al., *Dendritic polyglycerols with oligoamine shells show low toxicity and high siRNA transfection efficiency in vitro.* Bioconjug Chem, 2010. **21**(10): p. 1744-52.
165. Guerra, J., et al., *Carbon nanohorns functionalized with polyamidoamine dendrimers as efficient biocarrier materials for gene therapy*. Vol. 50. 2012. 2832-2844.
166. Caminade, A.M., R. Laurent, and J.P. Majoral, *Characterization of dendrimers.* Advanced drug delivery reviews, 2005. **57**(15): p. 2130-46.
167. Shah, N., R.J. Steptoe, and H.S. Parekh, *Low-generation asymmetric dendrimers exhibit minimal toxicity and effectively complex DNA.* Journal of peptide science : an official publication of the European Peptide Society, 2011. **17**(6): p. 470-8.
168. Tang, Y., et al., *Efficient in vitro siRNA delivery and intramuscular gene silencing using PEG-modified PAMAM dendrimers.* Molecular pharmaceutics, 2012. **9**(6): p. 1812-21.
169. Jevprasesphant, R., et al., *The influence of surface modification on the cytotoxicity of PAMAM dendrimers.* International journal of pharmaceutics, 2003. **252**(1-2): p. 263-6.
170. Kojima, C., et al., *Influence of dendrimer generation and polyethylene glycol length on the biodistribution of PEGylated dendrimers.* International journal of pharmaceutics, 2010. **383**(1-2): p. 293-6.
171. Liu, C., et al., *Arginine-terminated generation 4 PAMAM dendrimer as an effective nanovector for functional siRNA delivery in vitro and in vivo.* Bioconjugate chemistry, 2014. **25**(3): p. 521-32.
172. Thuy le, T., S. Mallick, and J.S. Choi, *Polyamidoamine (PAMAM) dendrimers modified with short oligopeptides for early endosomal escape and enhanced gene delivery.* International journal of pharmaceutics, 2015. **492**(1-2): p. 233-43.
173. Singh, P., et al., *Folate and folate-PEG-PAMAM dendrimers: synthesis, characterization, and targeted anticancer drug delivery potential in tumor bearing mice.* Bioconjugate chemistry, 2008. **19**(11): p. 2239-52.
174. Biswas, S., et al., *Liposomes loaded with paclitaxel and modified with novel triphenylphosphonium-PEG-PE conjugate possess low toxicity, target mitochondria and demonstrate enhanced antitumor effects in vitro and in vivo.* J Control Release, 2012. **159**(3): p. 393-402.
175. Biswas, S., et al., *Development of the novel PEG-PE-based polymer for the reversible attachment of specific ligands to liposomes: synthesis and in vitro characterization.* Bioconjugate chemistry, 2011. **22**(10): p. 2005-2013.
176. Alshamsan, A., et al., *Formulation and delivery of siRNA by oleic acid and stearic acid modified polyethylenimine.* Mol Pharm, 2009. **6**(1): p. 121-33.

177. Yu, T., et al., *An amphiphilic dendrimer for effective delivery of small interfering RNA and gene silencing in vitro and in vivo.* Angew Chem Int Ed Engl, 2012. **51**(34): p. 8478-84.
178. Liu, J., et al., *Functionalized Dendrimer-Based Delivery of Angiotensin Type 1 Receptor siRNA for Preserving Cardiac Function Following Infarction.* Biomaterials, 2013. **34**(14): p. 3729-3736.
179. Medicine, U.S.N.L.o. *ClinicalTrials.gov*. Available from: https://clinicaltrials.gov/ct2/home.
180. Li, W. and F.C. Szoka, Jr., *Lipid-based nanoparticles for nucleic acid delivery.* Pharm Res, 2007. **24**(3): p. 438-49.
181. Puri, A., et al., *Lipid-based nanoparticles as pharmaceutical drug carriers: from concepts to clinic.* Crit Rev Ther Drug Carrier Syst, 2009. **26**(6): p. 523-80.
182. Torchilin, V.P., *Micellar nanocarriers: pharmaceutical perspectives.* Pharm Res, 2007. **24**(1): p. 1-16.
183. Marquez, A.R., C.O. Madu, and Y. Lu, *An Overview of Various Carriers for siRNA Delivery.* oncomedicine, 2018. **3**: p. 48-58.
184. Husseini, G.A. and W.G. Pitt, *Micelles and nanoparticles for ultrasonic drug and gene delivery.* Adv Drug Deliv Rev, 2008. **60**(10): p. 1137-52.
185. Kim, H.J., et al., *siRNA delivery from triblock copolymer micelles with spatially-ordered compartments of PEG shell, siRNA-loaded intermediate layer, and hydrophobic core.* Biomaterials, 2014. **35**(15): p. 4548-56.
186. Ko, Y.T., et al., *Self-assembling micelle-like nanoparticles based on phospholipid-polyethyleneimine conjugates for systemic gene delivery.* J Control Release, 2009. **133**(2): p. 132-8.
187. Patil, Y.B., et al., *The use of nanoparticle-mediated targeted gene silencing and drug delivery to overcome tumor drug resistance.* Biomaterials, 2010. **31**(2): p. 358-65.
188. Sun, T.M., et al., *Simultaneous delivery of siRNA and paclitaxel via a "two-in-one" micelleplex promotes synergistic tumor suppression.* ACS Nano, 2011. **5**(2): p. 1483-94.
189. Xiong, X.B. and A. Lavasanifar, *Traceable multifunctional micellar nanocarriers for cancer-targeted co-delivery of MDR-1 siRNA and doxorubicin.* ACS Nano, 2011. **5**(6): p. 5202-13.
190. Tseng, Y.C., S. Mozumdar, and L. Huang, *Lipid-based systemic delivery of siRNA.* Advanced drug delivery reviews, 2009. **61**(9): p. 721-31.
191. Xu, Y. and F.C. Szoka, Jr., *Mechanism of DNA release from cationic liposome/DNA complexes used in cell transfection.* Biochemistry, 1996. **35**(18): p. 5616-23.
192. Eloy, J.O., et al., *Liposomes as carriers of hydrophilic small molecule drugs: strategies to enhance encapsulation and delivery.* Colloids Surf B Biointerfaces, 2014. **123**: p. 345-63.
193. Ozpolat, B., A.K. Sood, and G. Lopez-Berestein, *Liposomal siRNA nanocarriers for cancer therapy.* Adv Drug Deliv Rev, 2014. **66**: p. 110-6.
194. Dokka, S., et al., *Oxygen radical-mediated pulmonary toxicity induced by some cationic liposomes.* Pharm Res, 2000. **17**(5): p. 521-5.
195. Lv, H., et al., *Toxicity of cationic lipids and cationic polymers in gene delivery.* J Control Release, 2006. **114**(1): p. 100-9.
196. Zhong, Y.Q., et al., *[Toxicity of cationic liposome Lipofectamine 2000 in human pancreatic cancer Capan-2 cells].* Nan Fang Yi Ke Da Xue Xue Bao, 2008. **28**(11): p. 1981-4.
197. Lechanteur, A., et al., *Cationic Liposomes Carrying siRNA: Impact of Lipid Composition on Physicochemical Properties, Cytotoxicity and Endosomal Escape.* Nanomaterials, 2018. **8**(5): p. 270.
198. Li, J., et al., *Biodegradable calcium phosphate nanoparticle with lipid coating for systemic siRNA delivery.* J Control Release, 2010. **142**(3): p. 416-21.

199. Buyens, K., et al., *Liposome based systems for systemic siRNA delivery: stability in blood sets the requirements for optimal carrier design.* J Control Release, 2012. **158**(3): p. 362-70.
200. Ho, W., X.Q. Zhang, and X. Xu, *Biomaterials in siRNA Delivery: A Comprehensive Review.* Adv Healthc Mater, 2016. **5**(21): p. 2715-2731.
201. Geisbert, T.W., et al., *Postexposure protection of non-human primates against a lethal Ebola virus challenge with RNA interference: a proof-of-concept study.* Lancet, 2010. **375**(9729): p. 1896-905.
202. Li, L., et al., *Tumor vasculature is a key determinant for the efficiency of nanoparticle-mediated siRNA delivery.* Gene therapy, 2012. **19**(7): p. 775-780.
203. Zimmermann, T.S., et al., *RNAi-mediated gene silencing in non-human primates.* Nature, 2006. **441**(7089): p. 111-4.
204. Morrissey, D.V., et al., *Activity of stabilized short interfering RNA in a mouse model of hepatitis B virus replication.* Hepatology, 2005. **41**(6): p. 1349-56.
205. Coelho, T., et al., *Safety and efficacy of RNAi therapy for transthyretin amyloidosis.* N Engl J Med, 2013. **369**(9): p. 819-29.
206. Suhr, O.B., et al., *Efficacy and safety of patisiran for familial amyloidotic polyneuropathy: a phase II multi-dose study.* Orphanet Journal of Rare Diseases, 2015. **10**: p. 109.
207. Akinc, A., et al., *A combinatorial library of lipid-like materials for delivery of RNAi therapeutics.* Nat Biotechnol, 2008. **26**(5): p. 561-9.
208. Frank-Kamenetsky, M., et al., *Therapeutic RNAi targeting PCSK9 acutely lowers plasma cholesterol in rodents and LDL cholesterol in nonhuman primates.* Proc Natl Acad Sci U S A, 2008. **105**(33): p. 11915-20.
209. Fitzgerald, K., et al., *Effect of an RNA interference drug on the synthesis of proprotein convertase subtilisin/kexin type 9 (PCSK9) and the concentration of serum LDL cholesterol in healthy volunteers: a randomised, single-blind, placebo-controlled, phase 1 trial.* Lancet, 2014. **383**(9911): p. 60-68.
210. Hsu, S.H., et al., *Cationic lipid nanoparticles for therapeutic delivery of siRNA and miRNA to murine liver tumor.* Nanomedicine, 2013. **9**(8): p. 1169-80.
211. Jensen, K., J.A. Anderson, and E.J. Glass, *Comparison of small interfering RNA (siRNA) delivery into bovine monocyte-derived macrophages by transfection and electroporation.* Veterinary Immunology and Immunopathology, 2014. **158**(3-4): p. 224-232.
212. Zuris, J.A., et al., *Cationic lipid-mediated delivery of proteins enables efficient protein-based genome editing in vitro and in vivo.* Nat Biotechnol, 2015. **33**(1): p. 73-80.
213. Lesizza, P., et al., *Single-Dose Intracardiac Injection of Pro-Regenerative MicroRNAs Improves Cardiac Function After Myocardial Infarction.* Circ Res, 2017. **120**(8): p. 1298-1304.
214. Eulalio, A., et al., *Functional screening identifies miRNAs inducing cardiac regeneration.* Nature, 2012. **492**(7429): p. 376-81.
215. Eguchi, A., et al., *Liver Bid-suppression for treatment of fibrosis associated with nonalcoholic steatohepatitis.* Journal of hepatology, 2016. **64**(3): p. 699-707.
216. Schlosser, K., et al., *Systemic delivery of MicroRNA mimics with polyethylenimine elevates pulmonary microRNA levels, but lacks pulmonary selectivity.* Pulmonary Circulation, 2018. **8**(1): p. 2045893217750613.
217. Tian, L., et al., *Cannabinoid Receptor 1 Participates in Liver Inflammation by Promoting M1 Macrophage Polarization via RhoA/NF-kappaB p65 and ERK1/2 Pathways, Respectively, in Mouse Liver Fibrogenesis.* Front Immunol, 2017. **8**: p. 1214.
218. Sysol, J.R., et al., *Micro-RNA-1 is decreased by hypoxia and contributes to the development of pulmonary vascular remodeling via regulation of sphingosine kinase 1.* Am J Physiol Lung Cell Mol Physiol, 2018. **314**(3): p. L461-l472.

219. Smith, S., et al., *MicroRNA-302d targets IRF9 to regulate the IFN-induced gene expression in SLE.* J Autoimmun, 2017. **79**: p. 105-111.
220. Sultana, N., et al., *Optimizing Cardiac Delivery of Modified mRNA.* Mol Ther, 2017. **25**(6): p. 1306-1315.
221. Tekedereli, I., et al., *Therapeutic Silencing of Bcl-2 by Systemically Administered siRNA Nanotherapeutics Inhibits Tumor Growth by Autophagy and Apoptosis and Enhances the Efficacy of Chemotherapy in Orthotopic Xenograft Models of ER (-) and ER (+) Breast Cancer.* Mol Ther Nucleic Acids, 2013. **2**: p. e121.
222. Wu, S.Y. and N.A.J. McMillan, *Lipidic Systems for In Vivo siRNA Delivery.* The AAPS Journal, 2009. **11**(4): p. 639-652.
223. Semple, S.C., et al., *Efficient encapsulation of antisense oligonucleotides in lipid vesicles using ionizable aminolipids: formation of novel small multilamellar vesicle structures.* Biochim Biophys Acta, 2001. **1510**(1-2): p. 152-66.
224. Miller, C.R., et al., *Liposome-cell interactions in vitro: effect of liposome surface charge on the binding and endocytosis of conventional and sterically stabilized liposomes.* Biochemistry, 1998. **37**(37): p. 12875-83.
225. Landen, C.N., Jr., et al., *Therapeutic EphA2 gene targeting in vivo using neutral liposomal small interfering RNA delivery.* Cancer Res, 2005. **65**(15): p. 6910-8.
226. Nogueira, E., et al., *Neutral PEGylated liposomal formulation for efficient folate-mediated delivery of MCL1 siRNA to activated macrophages.* Colloids Surf B Biointerfaces, 2017. **155**: p. 459-465.
227. Sakurai, H., et al., *Innate immune response induced by gene delivery vectors.* International journal of pharmaceutics, 2008. **354**(1-2): p. 9-15.
228. Szebeni, J., *Complement activation-related pseudoallergy: a new class of drug-induced acute immune toxicity.* Toxicology, 2005. **216**(2-3): p. 106-21.
229. Yu, B., et al., *Lipid nanoparticles for hepatic delivery of small interfering RNA.* Biomaterials, 2012. **33**(25): p. 5924-34.
230. Tao, W., et al., *Noninvasive imaging of lipid nanoparticle-mediated systemic delivery of small-interfering RNA to the liver.* Molecular therapy : the journal of the American Society of Gene Therapy, 2010. **18**(9): p. 1657-66.
231. Liu, L., et al., *Efficient and Tumor Targeted siRNA Delivery by Polyethylenimine-graft-polycaprolactone-block-poly(ethylene glycol)-folate (PEI-PCL-PEG-Fol).* Mol Pharm, 2016. **13**(1): p. 134-43.
232. Burnett, J.C., J.J. Rossi, and K. Tiemann, *Current progress of siRNA/shRNA therapeutics in clinical trials.* Biotechnology journal, 2011. **6**(9): p. 1130-46.
233. Monaghan, M. and A. Pandit, *RNA interference therapy via functionalized scaffolds.* Advanced drug delivery reviews, 2011. **63**(4-5): p. 197-208.
234. Li, Y., J. Rodrigues, and H. Tomas, *Injectable and biodegradable hydrogels: gelation, biodegradation and biomedical applications.* Chem Soc Rev, 2012. **41**(6): p. 2193-221.
235. Wang, L.L. and J.A. Burdick, *Engineered Hydrogels for Local and Sustained Delivery of RNA-Interference Therapies.* Adv Healthc Mater, 2017. **6**(1).
236. Takahashi, Y., et al., *Quantitative and temporal analysis of gene silencing in tumor cells induced by small interfering RNA or short hairpin RNA expressed from plasmid vectors.* Journal of pharmaceutical sciences, 2009. **98**(1): p. 74-80.
237. O'Brien, F.J., *Biomaterials & scaffolds for tissue engineering.* Materials Today, 2011. **14**(3): p. 88-95.
238. Nelson, C.E., et al., *siRNA Delivery from an Injectable Scaffold for Wound Therapy.* Adv Wound Care (New Rochelle), 2013. **2**(3): p. 93-99.
239. Nelson, C.E., et al., *Sustained local delivery of siRNA from an injectable scaffold.* Biomaterials, 2012. **33**(4): p. 1154-61.
240. Mountziaris, P.M., et al., *Intra-articular controlled release of anti-inflammatory siRNA with biodegradable polymer microparticles ameliorates temporomandibular joint inflammation.* Acta Biomater, 2012. **8**(10): p. 3552-60.

241. Pradhan, P., et al., *The effect of combined IL10 siRNA and CpG ODN as pathogen-mimicking microparticles on Th1/Th2 cytokine balance in dendritic cells and protective immunity against B cell lymphoma.* Biomaterials, 2014. **35**(21): p. 5491-504.
242. Cao, H., et al., *RNA interference by nanofiber-based siRNA delivery system.* J Control Release, 2010. **144**(2): p. 203-12.
243. Rujitanaroj, P.O., et al., *Controlling fibrous capsule formation through long-term down-regulation of collagen type I (COL1A1) expression by nanofiber-mediated siRNA gene silencing.* Acta Biomater, 2013. **9**(1): p. 4513-24.
244. Rujitanaroj, P.O., et al., *Nanofiber-mediated controlled release of siRNA complexes for long term gene-silencing applications.* Biomaterials, 2011. **32**(25): p. 5915-23.
245. Pinese, C., et al., *Sustained delivery of siRNA/mesoporous silica nanoparticle complexes from nanofiber scaffolds for long-term gene silencing.* Acta Biomater, 2018. **76**: p. 164-177.
246. Sarett, S.M., C.E. Nelson, and C.L. Duvall, *Technologies for controlled, local delivery of siRNA.* J Control Release, 2015. **218**: p. 94-113.
247. Hasan, A., et al., *Injectable Hydrogels for Cardiac Tissue Repair after Myocardial Infarction.* Adv Sci (Weinh), 2015. **2**(11): p. 1500122.
248. Park, H., et al., *Injectable biodegradable hydrogel composites for rabbit marrow mesenchymal stem cell and growth factor delivery for cartilage tissue engineering.* Biomaterials, 2007. **28**(21): p. 3217-27.
249. Tous, E., et al., *Injectable acellular hydrogels for cardiac repair.* Journal of cardiovascular translational research, 2011. **4**(5): p. 528-42.
250. Saul, J.M. and D.F. Williams, *12 - Hydrogels in Regenerative Medicine*, in *Handbook of Polymer Applications in Medicine and Medical Devices*, K. Modjarrad and S. Ebnesajjad, Editors. 2011, William Andrew Publishing: Oxford. p. 279-302.
251. Bezuidenhout, D., et al., *Covalent incorporation and controlled release of active dexamethasone from injectable polyethylene glycol hydrogels.* Journal of biomedical materials research. Part A, 2013. **101**(5): p. 1311-8.
252. Davies, N., et al., *The dosage dependence of VEGF stimulation on scaffold neovascularisation.* Biomaterials, 2008. **29**(26): p. 3531-8.
253. Davies, N.H., et al., *Sustaining neovascularization of a scaffold through staged release of vascular endothelial growth factor-A and platelet-derived growth factor-BB.* Tissue engineering. Part A, 2012. **18**(1-2): p. 26-34.
254. Drury, J.L. and D.J. Mooney, *Hydrogels for tissue engineering: scaffold design variables and applications.* Biomaterials, 2003. **24**(24): p. 4337-4351.
255. Han, H.D., et al., *Chitosan hydrogel for localized gene silencing.* Cancer Biol Ther, 2011. **11**(9): p. 839-45.
256. Guo, D.D., et al., *Synergistic effects of Akt1 shRNA and paclitaxel-incorporated conjugated linoleic acid-coupled poloxamer thermosensitive hydrogel on breast cancer.* Biomaterials, 2012. **33**(7): p. 2272-81.
257. Ma, H., et al., *PLK1shRNA and doxorubicin co-loaded thermosensitive PLGA-PEG-PLGA hydrogels for osteosarcoma treatment.* Biomaterials, 2014. **35**(30): p. 8723-34.
258. Segovia, N., et al., *Hydrogel doped with nanoparticles for local sustained release of siRNA in breast cancer.* Adv Healthc Mater, 2015. **4**(2): p. 271-80.
259. Conde, J., et al., *Self-assembled RNA-triple-helix hydrogel scaffold for microRNA modulation in the tumour microenvironment.* Nat Mater, 2016. **15**(3): p. 353-63.
260. Browne, S., et al., *Modulation of inflammation and angiogenesis and changes in ECM GAG-activity via dual delivery of nucleic acids.* Biomaterials, 2015. **69**: p. 133-47.
261. Peng, H., et al., *Sustained delivery of siRNA/PEI complex from in situ forming hydrogels potently inhibits the proliferation of gastric cancer.* J Exp Clin Cancer Res, 2016. **35**: p. 57.

262. Kim, Y.M., M.R. Park, and S.C. Song, *Injectable polyplex hydrogel for localized and long-term delivery of siRNA.* ACS Nano, 2012. **6**(7): p. 5757-66.
263. Kim, Y.M. and S.C. Song, *Targetable micelleplex hydrogel for long-term, effective, and systemic siRNA delivery.* Biomaterials, 2014. **35**(27): p. 7970-7.
264. Kim, Y.-M., C.-H. Kim, and S.-C. Song, *Injectable Ternary Nanocomplex Hydrogel for Long-Term Chemical Drug/Gene Dual Delivery.* ACS Macro Letters, 2016. **5**(3): p. 297-300.
265. Laroui, H., et al., *Targeting intestinal inflammation with CD98 siRNA/PEI-loaded nanoparticles.* Molecular therapy : the journal of the American Society of Gene Therapy, 2014. **22**(1): p. 69-80.
266. Cao, C., et al., *Potential application of injectable chitosan hydrogel treated with siRNA in chronic rhinosinusitis therapy.* Mol Med Rep, 2015. **12**(5): p. 6688-94.
267. Kanazawa, T., et al., *Topical Anti-Nuclear Factor-Kappa B Small Interfering RNA with Functional Peptides Containing Sericin-Based Hydrogel for Atopic Dermatitis.* Pharmaceutics, 2015. **7**(3): p. 294-304.
268. Manaka, T., et al., *Local delivery of siRNA using a biodegradable polymer application to enhance BMP-induced bone formation.* Biomaterials, 2011. **32**(36): p. 9642-8.
269. Li, Y., et al., *The promotion of bone regeneration through positive regulation of angiogenic-osteogenic coupling using microRNA-26a.* Biomaterials, 2013. **34**(21): p. 5048-58.
270. Wang, Y., D.W. Malcolm, and D.S.W. Benoit, *Controlled and sustained delivery of siRNA/NPs from hydrogels expedites bone fracture healing.* Biomaterials, 2017. **139**: p. 127-138.
271. Nguyen, M.K., et al., *RNA interfering molecule delivery from in situ forming biodegradable hydrogels for enhancement of bone formation in rat calvarial bone defects.* Acta Biomater, 2018.
272. San Juan, A., et al., *Development of a functionalized polymer for stent coating in the arterial delivery of small interfering RNA.* Biomacromolecules, 2009. **10**(11): p. 3074-80.
273. Wan, W.G., et al., *Enhanced cardioprotective effects mediated by plasmid containing the short-hairpin RNA of angiotensin converting enzyme with a biodegradable hydrogel after myocardial infarction.* J Biomed Mater Res A, 2014. **102**(10): p. 3452-8.
274. Wang, L.L., et al., *Injectable, Guest-Host Assembled Polyethylenimine Hydrogel for siRNA Delivery.* Biomacromolecules, 2017. **18**(1): p. 77-86.
275. Monaghan, M.G., et al., *Exogenous miR-29B Delivery Through a Hyaluronan-Based Injectable System Yields Functional Maintenance of the Infarcted Myocardium.* Tissue Engineering. Part A, 2018. **24**(1-2): p. 57-67.
276. Wang, L.L., et al., *Local and sustained miRNA delivery from an injectable hydrogel promotes cardiomyocyte proliferation and functional regeneration after ischemic injury.* Nature biomedical engineering, 2017. **1**: p. 983-992.
277. Zhu, J., *Bioactive modification of poly(ethylene glycol) hydrogels for tissue engineering.* Biomaterials, 2010. **31**(17): p. 4639-56.
278. Zhu, J.R., *Bioactive modification of poly(ethylene glycol) hydrogels for tissue engineering.* Biomaterials, 2010. **31**(17): p. 4639-4656.
279. Alconcel, S.N.S.B., A.S.; Maynard, H., *FDA-approved poly(ethylene glycol)-protein conjugate drugs*. Vol. 2. 2011. 1442-1448.
280. Swierczewska, M., K.C. Lee, and S. Lee, *What is the future of PEGylated therapies?* Expert Opinion on Emerging Drugs, 2015. **20**(4): p. 531-536.
281. Nguyen, K.T. and J.L. West, *Photopolymerizable hydrogels for tissue engineering applications.* Biomaterials, 2002. **23**(22): p. 4307-4314.
282. Sanborn, T.J., P.B. Messersmith, and A.E. Barron, *In situ crosslinking of a biomimetic peptide-PEG hydrogel via thermally triggered activation of factor XIII.* Biomaterials, 2002. **23**(13): p. 2703-10.

283. Zhang, L., et al., *Biocompatible and pH-sensitive PEG hydrogels with degradable phosphoester and phosphoamide linkers end-capped with amine for controlled drug delivery.* Polymer Chemistry, 2013. **4**(4): p. 1084-1094.
284. Goetsch, K.P., et al., *Regulation of tissue ingrowth into proteolytically degradable hydrogels.* Acta Biomater, 2015. **24**: p. 44-52.
285. Lutolf, M.P., et al., *Synthetic matrix metalloproteinase-sensitive hydrogels for the conduction of tissue regeneration: engineering cell-invasion characteristics.* Proc Natl Acad Sci U S A, 2003. **100**(9): p. 5413-8.
286. Patterson, J. and J.A. Hubbell, *Enhanced proteolytic degradation of molecularly engineered PEG hydrogels in response to MMP-1 and MMP-2.* Biomaterials, 2010. **31**(30): p. 7836-45.
287. Ciuffreda, M.C., et al., *Synthetic extracellular matrix mimic hydrogel improves efficacy of mesenchymal stromal cell therapy for ischemic cardiomyopathy.* Acta Biomater, 2018. **70**: p. 71-83.
288. Janse van Rensburg, A., et al., *Improved vascularization of porous scaffolds through growth factor delivery from heparinized polyethylene glycol hydrogels.* Acta Biomater, 2017. **49**: p. 89-100.
289. Lutolf, M.P. and J.A. Hubbell, *Synthetic biomaterials as instructive extracellular microenvironments for morphogenesis in tissue engineering.* Nat Biotechnol, 2005. **23**(1): p. 47-55.
290. Bracher, M., et al., *Cell specific ingrowth hydrogels.* Biomaterials, 2013. **34**(28): p. 6797-6803.
291. Lin, C.C. and K.S. Anseth, *PEG hydrogels for the controlled release of biomolecules in regenerative medicine.* Pharm Res, 2009. **26**(3): p. 631-43.
292. Lei, Y. and T. Segura, *DNA delivery from matrix metalloproteinase degradable poly(ethylene glycol) hydrogels to mouse cloned mesenchymal stem cells.* Biomaterials, 2009. **30**(2): p. 254-65.
293. Krebs, M.D., O. Jeon, and E. Alsberg, *Localized and sustained delivery of silencing RNA from macroscopic biopolymer hydrogels.* Journal of the American Chemical Society, 2009. **131**(26): p. 9204-6.
294. Liu, M., et al., *Injectable hydrogels for cartilage and bone tissue engineering.* Bone research, 2017. **5**: p. 17014-17014.
295. Howe, A., et al., *Integrin signaling and cell growth control.* Curr Opin Cell Biol, 1998. **10**(2): p. 220-31.
296. Streuli, C., *Extracellular matrix remodelling and cellular differentiation.* Curr Opin Cell Biol, 1999. **11**(5): p. 634-40.
297. Lister, Z., K.J. Rayner, and E.J. Suuronen, *How Biomaterials Can Influence Various Cell Types in the Repair and Regeneration of the Heart after Myocardial Infarction.* Frontiers in Bioengineering and Biotechnology, 2016. **4**: p. 62.
298. Golan, T., et al., *RNAi therapy targeting KRAS in combination with chemotherapy for locally advanced pancreatic cancer patients.* Oncotarget, 2015. **6**(27): p. 24560-70.
299. Talia, G., et al., *A phase I trial of a local delivery of siRNA against k-ras in combination with chemotherapy for locally advanced pancreatic adenocarcinoma.* Journal of Clinical Oncology, 2013. **31**(15_suppl): p. 4037-4037.
300. Zorde Khvalevsky, E., et al., *Mutant KRAS is a druggable target for pancreatic cancer.* Proc Natl Acad Sci U S A, 2013. **110**(51): p. 20723-8.
301. Kawakami, E., et al., *Local Applications of Myostatin-siRNA with Atelocollagen Increase Skeletal Muscle Mass and Recovery of Muscle Function.* PLoS ONE, 2013. **8**(5): p. e64719.
302. Kinouchi, N., et al., *Atelocollagen-mediated local and systemic applications of myostatin-targeting siRNA increase skeletal muscle mass.* Gene Ther, 2008. **15**(15): p. 1126-30.

303. Kobayashi, H., R. Watanabe, and P.L. Choyke, *Improving conventional enhanced permeability and retention (EPR) effects; what is the appropriate target?* Theranostics, 2013. **4**(1): p. 81-9.
304. Mitragotri, S., et al., *Drug Delivery Research for the Future: Expanding the Nano Horizons and Beyond.* J Control Release, 2017. **246**: p. 183-184.
305. Nguyen, M.K., et al., *Sustained localized presentation of RNA interfering molecules from in situ forming hydrogels to guide stem cell osteogenic differentiation.* Biomaterials, 2014. **35**(24): p. 6278-6286.
306. Kim, N., et al., *Combination of small RNAs for skeletal muscle regeneration*. Vol. 30. 2015.
307. Mori, H., et al., *Effectiveness of cationic liposome-mediated local delivery of myostatin-targeting small interfering RNA in vivo.* Dev Growth Differ, 2014. **56**(3): p. 223-32.
308. Mosler, S., et al., *Combinatory effects of siRNA‐induced myostatin inhibition and exercise on skeletal muscle homeostasis and body composition.* Physiological Reports, 2014. **2**(3): p. e00262.
309. Lee, S.-J., *REGULATION OF MUSCLE MASS BY MYOSTATIN.* Annual Review of Cell and Developmental Biology, 2004. **20**(1): p. 61-86.
310. McPherron, A.C., A.M. Lawler, and S.J. Lee, *Regulation of skeletal muscle mass in mice by a new TGF-beta superfamily member.* Nature, 1997. **387**(6628): p. 83-90.
311. McPherron, A.C. and S.J. Lee, *Double muscling in cattle due to mutations in the myostatin gene.* Proc Natl Acad Sci U S A, 1997. **94**(23): p. 12457-61.
312. Magee, T.R., et al., *Myostatin short interfering hairpin RNA gene transfer increases skeletal muscle mass.* J Gene Med, 2006. **8**(9): p. 1171-81.
313. Miyata, T., T. Taira, and Y. Noishiki, *Collagen engineering for biomaterial use.* Clin Mater, 1992. **9**(3-4): p. 139-48.
314. Hu, S., et al., *MicroRNA-210 as a novel therapy for treatment of ischemic heart disease.* Circulation, 2010. **122**(11 Suppl): p. S124-31.
315. Meloni, M., et al., *Local inhibition of microRNA-24 improves reparative angiogenesis and left ventricle remodeling and function in mice with myocardial infarction.* Molecular therapy : the journal of the American Society of Gene Therapy, 2013. **21**(7): p. 1390-402.
316. Kobara, M., et al., *Effects of ACE inhibition on myocardial apoptosis in an ischemia-reperfusion rat heart model.* J Cardiovasc Pharmacol, 2003. **41**(6): p. 880-9.
317. Pfeffer, M.A., *ACE inhibitors in acute myocardial infarction: patient selection and timing.* Circulation, 1998. **97**(22): p. 2192-4.
318. van Rooij, E., et al., *Dysregulation of microRNAs after myocardial infarction reveals a role of miR-29 in cardiac fibrosis.* Proc Natl Acad Sci U S A, 2008. **105**(35): p. 13027-32.
319. Burmeister, D.M., et al., *In Situ Delivery of Fibrin-Based Hydrogels Prevents Contraction and Reduces Inflammation.* Journal of Burn Care & Research, 2018. **39**(1): p. 40-53.
320. Li, Y., et al., *Fibrin Gel as an Injectable Biodegradable Scaffold and Cell Carrier for Tissue Engineering.* The Scientific World Journal, 2015. **2015**: p. 10.
321. Weisel, J.W. and R.I. Litvinov, *Fibrin Formation, Structure and Properties.* Sub-cellular biochemistry, 2017. **82**: p. 405-456.
322. Chung, D.W. and E.W. Davie, *gamma and gamma' chains of human fibrinogen are produced by alternative mRNA processing.* Biochemistry, 1984. **23**(18): p. 4232-6.
323. Weisel, J.W., *The electron microscope band pattern of human fibrin: Various stains, lateral order, and carbohydrate localization.* Journal of Ultrastructure and Molecular Structure Research, 1986. **96**(1): p. 176-188.
324. Crabtree, G.R., *The molecular biology of fibrinogen*, in *The molecular basis of blood diseases, G. Stamatoyannopoulos, et al., Editors. 1987, Saunders W.B*.

325. Undas, A. and R.A. Ariens, *Fibrin clot structure and function: a role in the pathophysiology of arterial and venous thromboembolic diseases.* Arterioscler Thromb Vasc Biol, 2011. **31**(12): p. e88-99.
326. Henschen, A. and J. Mcdonagh, *Fibrinogen, fibrin and factor XIIIElsevier Science; Amsterdam*, in *Blood Coagulation*, R.F.A.H. Zwaal, H.C., Editor. 1986, Elsevier Science: Amsterdam.
327. Brennan, S.O., et al., *Congenital hypodysfibrinogenaemia (Fibrinogen Des Moines) due to a gamma320Asp deletion at the Ca2+ binding site.* Thromb Haemost, 2007. **98**(2): p. 467-9.
328. Dyr, J.E., et al., *Conversion of fibrinogen to fibrin induced by preferential release of fibrinopeptide B.* Biochim Biophys Acta, 1989. **990**(1): p. 18-24.
329. Chernysh, I.N. and J.W. Weisel, *Dynamic imaging of fibrin network formation correlated with other measures of polymerization.* Blood, 2008. **111**(10): p. 4854-61.
330. Longstaff, C. and K. Kolev, *Basic mechanisms and regulation of fibrinolysis.* J Thromb Haemost, 2015. **13 Suppl 1**: p. S98-105.
331. Weisel, J.W. and R.I. Litvinov, *The biochemical and physical process of fibrinolysis and effects of clot structure and stability on the lysis rate.* Cardiovasc Hematol Agents Med Chem, 2008. **6**(3): p. 161-80.
332. Janmey, P.A., J.P. Winer, and J.W. Weisel, *Fibrin gels and their clinical and bioengineering applications.* Journal of The Royal Society Interface, 2009. **6**(30): p. 1-10.
333. Collet, J.P., et al., *Influence of fibrin network conformation and fibrin fiber diameter on fibrinolysis speed: dynamic and structural approaches by confocal microscopy.* Arterioscler Thromb Vasc Biol, 2000. **20**(5): p. 1354-61.
334. Cakmak, O., et al., *Injectable tissue-engineered cartilage using commercially available fibrin glue.* Laryngoscope, 2013. **123**(12): p. 2986-92.
335. Christman, K.L., et al., *Fibrin glue alone and skeletal myoblasts in a fibrin scaffold preserve cardiac function after myocardial infarction.* Tissue Eng, 2004. **10**(3-4): p. 403-9.
336. Christman, K.L., et al., *Injectable fibrin scaffold improves cell transplant survival, reduces infarct expansion, and induces neovasculature formation in ischemic myocardium.* J Am Coll Cardiol, 2004. **44**(3): p. 654-60.
337. Drinnan, C.T., et al., *Multimodal release of transforming growth factor-beta1 and the BB isoform of platelet derived growth factor from PEGylated fibrin gels.* J Control Release, 2010. **147**(2): p. 180-6.
338. Lee, J.C., et al., *Synovium-derived mesenchymal stem cells encapsulated in a novel injectable gel can repair osteochondral defects in a rabbit model.* Tissue Eng Part A, 2012. **18**(19-20): p. 2173-86.
339. Mazlyzam, A.L., et al., *Reconstruction of living bilayer human skin equivalent utilizing human fibrin as a scaffold.* Burns, 2007. **33**(3): p. 355-63.
340. Taylor, S.J., J.W. McDonald, 3rd, and S.E. Sakiyama-Elbert, *Controlled release of neurotrophin-3 from fibrin gels for spinal cord injury.* J Control Release, 2004. **98**(2): p. 281-94.
341. de Boer, M.T., et al., *Role of fibrin sealants in liver surgery.* Dig Surg, 2012. **29**(1): p. 54-61.
342. Jackson, M.R., *Fibrin sealants in surgical practice: An overview.* The American Journal of Surgery, 2001. **182**(2, Supplement 1): p. S1-S7.
343. Ratnalingam, V., et al., *Fibrin adhesive is better than sutures in pterygium surgery.* Cornea, 2010. **29**(5): p. 485-9.
344. Chung, Y.I., et al., *Efficient revascularization by VEGF administration via heparin-functionalized nanoparticle-fibrin complex.* J Control Release, 2010. **143**(3): p. 282-9.

345. Grainger, D.J., et al., *Release and activation of platelet latent TGF-beta in blood clots during dissolution with plasmin.* Nat Med, 1995. **1**(9): p. 932-7.
346. Layman, H., et al., *Enhanced angiogenic efficacy through controlled and sustained delivery of FGF-2 and G-CSF from fibrin hydrogels containing ionic-albumin microspheres.* J Biomater Sci Polym Ed, 2012. **23**(1-4): p. 185-206.
347. Lee, K., E.A. Silva, and D.J. Mooney, *Growth factor delivery-based tissue engineering: general approaches and a review of recent developments.* Journal of the Royal Society Interface, 2011. **8**(55): p. 153-170.
348. Lei, P., R.M. Padmashali, and S.T. Andreadis, *Cell-controlled and spatially arrayed gene delivery from fibrin hydrogels.* Biomaterials, 2009. **30**(22): p. 3790-9.
349. Ryu, J.H., et al., *Implantation of bone marrow mononuclear cells using injectable fibrin matrix enhances neovascularization in infarcted myocardium.* Biomaterials, 2005. **26**(3): p. 319-26.
350. Torio-Padron, N., et al., *Engineering of adipose tissue by injection of human preadipocytes in fibrin.* Aesthetic Plast Surg, 2007. **31**(3): p. 285-93.
351. Zhang, G., et al., *A PEGylated fibrin patch for mesenchymal stem cell delivery.* Tissue Eng, 2006. **12**(1): p. 9-19.
352. Juliar, B.A., et al., *Sprouting angiogenesis induces significant mechanical heterogeneities and ECM stiffening across length scales in fibrin hydrogels.* Biomaterials, 2018. **162**: p. 99-108.
353. Matthias, N., et al., *Volumetric muscle loss injury repair using in situ fibrin gel cast seeded with muscle-derived stem cells (MDSCs).* Stem Cell Res, 2018. **27**: p. 65-73.
354. des Rieux, A., A. Shikanov, and L.D. Shea, *Fibrin hydrogels for non-viral vector delivery in vitro.* J Control Release, 2009. **136**(2): p. 148-54.
355. Saul, J.M., et al., *Delivery of non-viral gene carriers from sphere-templated fibrin scaffolds for sustained transgene expression.* Biomaterials, 2007. **28**(31): p. 4705-16.
356. Kowalczewski, C.J. and J.M. Saul, *Surface-mediated delivery of siRNA from fibrin hydrogels for knockdown of the BMP-2 binding antagonist noggin.* Acta Biomater, 2015. **25**: p. 109-20.
357. Huang, S. and X. Fu, *Naturally derived materials-based cell and drug delivery systems in skin regeneration.* J Control Release, 2010. **142**(2): p. 149-59.
358. Chung, E., et al., *Fibrin-based 3D matrices induce angiogenic behavior of adipose-derived stem cells.* Acta biomaterialia, 2015. **17**: p. 78-88.
359. Ricles, L.M., et al., *Therapeutic assessment of mesenchymal stem cells delivered within a PEGylated fibrin gel following an ischemic injury.* Biomaterials, 2016. **102**: p. 9-19.
360. Hammers, D.W., et al., *Controlled release of IGF-I from a biodegradable matrix improves functional recovery of skeletal muscle from ischemia/reperfusion.* Biotechnology and bioengineering, 2012. **109**(4): p. 1051-1059.
361. Zhang, G., et al., *Enhancing efficacy of stem cell transplantation to the heart with a PEGylated fibrin biomatrix.* Tissue Eng Part A, 2008. **14**(6): p. 1025-36.
362. Chung, E., et al., *Fibrin-based stem cell containing scaffold improves the dynamics of burn wound healing.* Wound Repair Regen, 2016. **24**(5): p. 810-819.
363. Bajaj, A., et al., *Effect of the headgroup variation on the gene transfer properties of cholesterol based cationic lipids possessing ether linkage.* Biochim Biophys Acta, 2008. **1778**(5): p. 1222-36.
364. Bartlett, D.W. and M.E. Davis, *Effect of siRNA nuclease stability on the in vitro and in vivo kinetics of siRNA-mediated gene silencing.* Biotechnol Bioeng, 2007. **97**(4): p. 909-21.
365. Shen, Y., et al., *Efficient protection and transfection of small interfering RNA by cationic shell-crosslinked knedel-like nanoparticles.* Nucleic Acid Ther, 2013. **23**(2): p. 95-108.

366. Jain, R.K., et al., *Oligomerization of green fluorescent protein in the secretory pathway of endocrine cells.* The Biochemical journal, 2001. **360**(Pt 3): p. 645-649.
367. Mann, M. and O.N. Jensen, *Proteomic analysis of post-translational modifications.* Nat Biotechnol, 2003. **21**(3): p. 255-61.
368. Zhang, Y., et al., *DC-Chol/DOPE cationic liposomes: a comparative study of the influence factors on plasmid pDNA and siRNA gene delivery.* Int J Pharm, 2010. **390**(2): p. 198-207.
369. Bulbake, U., et al., *Comparison of Cationic Liposome and PAMAM Dendrimer for Delivery of Anti-Plk1 siRNA in Breast Cancer Treatment.* Pharmaceutical Development and Technology, 2019: p. 1-27.
370. Pandi, P., et al., *Dendrimer as a new potential carrier for topical delivery of siRNA: A comparative study of dendriplex vs. lipoplex for delivery of TNF-alpha siRNA.* Int J Pharm, 2018. **550**(1-2): p. 240-250.
371. Zheng, X., et al., *A novel in vivo siRNA delivery system specifically targeting dendritic cells and silencing CD40 genes for immunomodulation.* Blood, 2009. **113**(12): p. 2646-54.
372. Chernousova, S. and M. Epple, *Live-cell imaging to compare the transfection and gene silencing efficiency of calcium phosphate nanoparticles and a liposomal transfection agent.* Gene Therapy, 2017. **24**: p. 282.
373. Neuhaus, B., et al., *Nanoparticles as transfection agents: a comprehensive study with ten different cell lines.* RSC Advances, 2016. **6**(22): p. 18102-18112.
374. Wang, T., et al., *Systematic Screening of Commonly Used Commercial Transfection Reagents towards Efficient Transfection of Single-Stranded Oligonucleotides.* Molecules, 2018. **23**(10).
375. Fittkau, M.H., et al., *The selective modulation of endothelial cell mobility on RGD peptide containing surfaces by YIGSR peptides.* Biomaterials, 2005. **26**(2): p. 167-74.
376. Dobner, S., et al., *A synthetic non-degradable polyethylene glycol hydrogel retards adverse post-infarct left ventricular remodeling.* Journal of cardiac failure, 2009. **15**(7): p. 629-36.
377. Kadner, K., et al., *The beneficial effects of deferred delivery on the efficiency of hydrogel therapy post myocardial infarction.* Biomaterials, 2012. **33**(7): p. 2060-6.
378. Johnson, N.R., et al., *Coacervate Delivery of Growth Factors Combined with a Degradable Hydrogel Preserves Heart Function after Myocardial Infarction.* ACS Biomaterials Science & Engineering, 2015. **1**(9): p. 753-759.
379. Chatani, S., D.P. Nair, and C.N. Bowman, *Relative reactivity and selectivity of vinyl sulfones and acrylates towards the thiol–Michael addition reaction and polymerization.* Polymer Chemistry, 2013. **4**(4): p. 1048-1055.
380. Liu, H., S.F. Collins, and L.J. Suggs, *Three-dimensional culture for expansion and differentiation of mouse embryonic stem cells.* Biomaterials, 2006. **27**(36): p. 6004-6014.
381. Rytlewski, J.A., et al., *Mechanisms of tubulogenesis and endothelial phenotype expression by MSCs.* Microvasc Res, 2015. **99**: p. 26-35.
382. Bezuidenhout, D., N. Davies, and P. Zilla, *Effect of well defined dodecahedral porosity on inflammation and angiogenesis.* Asaio j, 2002. **48**(5): p. 465-71.
383. Konings, J., et al., *Factor XIIa regulates the structure of the fibrin clot independently of thrombin generation through direct interaction with fibrin.* Blood, 2011. **118**(14): p. 3942-51.
384. Galler, K.M., et al., *Bioengineering of dental stem cells in a PEGylated fibrin gel.* Regen Med, 2011. **6**(2): p. 191-200.
385. Geuss, L.R., et al., *Maintenance of HL-1 cardiomyocyte functional activity in PEGylated fibrin gels.* Biotechnol Bioeng, 2015. **112**(7): p. 1446-56.
386. Seetharaman, S., et al., *A PEGylated fibrin-based wound dressing with antimicrobial and angiogenic activity.* Acta Biomater, 2011. **7**(7): p. 2787-96.

387. Shpichka, A., et al., *Transparent PEG-Fibrin Gel as a Flexible Tool for Cell Encapsulation*. Vol. 10. 2018. 64.
388. Chan, C., et al., *Optimizing Cationic and Neutral Lipids for Efficient Gene Delivery at High Serum Content.* The journal of gene medicine, 2014. **16**(0): p. 84-96.
389. Zhao, W., S. Zhuang, and X.R. Qi, *Comparative study of the in vitro and in vivo characteristics of cationic and neutral liposomes.* Int J Nanomedicine, 2011. **6**: p. 3087-98.
390. Zylberberg, C., et al., *Engineering liposomal nanoparticles for targeted gene therapy.* Gene Ther, 2017. **24**(8): p. 441-452.
391. Nguyen, M.K., et al., *Photocrosslinkable, biodegradable hydrogels with controlled cell adhesivity for prolonged siRNA delivery to hMSCs to enhance their osteogenic differentiation.* Journal of materials chemistry. B, Materials for biology and medicine, 2017. **5**(3): p. 485-495.
392. Chen, M., et al., *Chitosan/siRNA nanoparticles encapsulated in PLGA nanofibers for siRNA delivery.* ACS nano, 2012. **6**(6): p. 4835-44.
393. Singh, A., S. Suri, and K. Roy, *In-situ crosslinking hydrogels for combinatorial delivery of chemokines and siRNA-DNA carrying microparticles to dendritic cells.* Biomaterials, 2009. **30**(28): p. 5187-200.
394. Wieland, J.A., T.L. Houchin-Ray, and L.D. Shea, *Non-viral vector delivery from PEG-hyaluronic acid hydrogels.* Journal of controlled release : official journal of the Controlled Release Society, 2007. **120**(3): p. 233-41.
395. Schwabe, K., et al., *Sustained delivery of siRNA poly- and lipopolyplexes from porous macromer-crosslinked gelatin gels.* International Journal of Pharmaceutics, 2017. **526**(1): p. 178-187.
396. Dean, D.A., *Nonviral gene transfer to skeletal, smooth, and cardiac muscle in living animals.* Am J Physiol Cell Physiol, 2005. **289**(2): p. C233-45.
397. Lu, Q.L., G. Bou-Gharios, and T.A. Partridge, *Non-viral gene delivery in skeletal muscle: a protein factory.* Gene Ther, 2003. **10**(2): p. 131-42.
398. Mir, L.M., et al., *High-efficiency gene transfer into skeletal muscle mediated by electric pulses.* Proc Natl Acad Sci U S A, 1999. **96**(8): p. 4262-7.
399. Ahlen, G., et al., *A targeted controlled force injection of genetic material in vivo.* Mol Ther Methods Clin Dev, 2016. **5**: p. 16016.
400. Aihara, H. and J. Miyazaki, *Gene transfer into muscle by electroporation in vivo.* Nat Biotechnol, 1998. **16**(9): p. 867-70.
401. Broderick, K.E. and L.M. Humeau, *Enhanced Delivery of DNA or RNA Vaccines by Electroporation.* Methods Mol Biol, 2017. **1499**: p. 193-200.
402. Mathiesen, I., *Electropermeabilization of skeletal muscle enhances gene transfer in vivo.* Gene Ther, 1999. **6**(4): p. 508-14.
403. Kulkarni, S.S., et al., *Suppression of 5'-nucleotidase enzymes promotes AMP-activated protein kinase (AMPK) phosphorylation and metabolism in human and mouse skeletal muscle.* J Biol Chem, 2011. **286**(40): p. 34567-74.
404. Takemasa, T., et al., *Fundamental study of detection of muscle hypertrophy-oriented gene doping by myostatin knock down using RNA interference.* Journal of sports science & medicine, 2012. **11**(2): p. 294-303.
405. Zhu, H., et al., *Skeletal muscle IP3R1 receptors amplify physiological and pathological synaptic calcium signals.* J Neurosci, 2011. **31**(43): p. 15269-83.
406. Kawakami, E., et al., *Atelocollagen-mediated systemic administration of myostatin-targeting siRNA improves muscular atrophy in caveolin-3-deficient mice.* Dev Growth Differ, 2011. **53**(1): p. 48-54.
407. Ruijter, J.M., et al., *Amplification efficiency: linking baseline and bias in the analysis of quantitative PCR data.* Nucleic Acids Res, 2009. **37**(6): p. e45.
408. Soboleski, M.R., J. Oaks, and W.P. Halford, *Green fluorescent protein is a quantitative reporter of gene expression in individual eukaryotic cells.* Faseb j, 2005. **19**(3): p. 440-2.

409. Chalfie, M., et al., *Green fluorescent protein as a marker for gene expression.* Science, 1994. **263**(5148): p. 802-805.
410. Corish, P. and C. Tyler-Smith, *Attenuation of green fluorescent protein half-life in mammalian cells.* Protein Eng, 1999. **12**(12): p. 1035-40.
411. Li, X., et al., *Generation of destabilized green fluorescent protein as a transcription reporter.* J Biol Chem, 1998. **273**(52): p. 34970-5.
412. Afonin, K.A., et al., *Activation of different split functionalities upon re-association of RNA-DNA hybrids.* Nature nanotechnology, 2013. **8**(4): p. 296-304.
413. Benfer, M. and T. Kissel, *Cellular uptake mechanism and knockdown activity of siRNA-loaded biodegradable DEAPA-PVA-g-PLGA nanoparticles.* Eur J Pharm Biopharm, 2012. **80**(2): p. 247-56.
414. Feldmann, D.P., et al., *In vitro and in vivo delivery of siRNA via VIPER polymer system to lung cells.* J Control Release, 2018. **276**: p. 50-58.
415. Khan, I., et al., *Controlled in-cell activation of RNA therapeutics using bond-cleaving bio-orthogonal chemistry.* Chem Sci, 2017. **8**(8): p. 5705-5712.
416. Kim, S., et al., *Highly efficient gene silencing and bioimaging based on fluorescent carbon dots in vitro and in vivo.* Nano Research, 2017. **10**(2): p. 503-519.
417. Shrivats, A.R., et al., *In Vivo GFP Knockdown by Cationic Nanogel-siRNA Polyplexes.* Bioengineering, 2015. **2**(3): p. 160-175.
418. Tiscornia, G., et al., *A general method for gene knockdown in mice by using lentiviral vectors expressing small interfering RNA.* Proc Natl Acad Sci U S A, 2003. **100**(4): p. 1844-8.
419. Shim, M.S., S. Chang, and Y.K. Kwon, *Stimuli-responsive siRNA carriers for efficient gene silencing in tumors via systemic delivery.* Biomaterials Science, 2014. **2**(1): p. 35-40.
420. Howard, K.A., et al., *RNA interference in vitro and in vivo using a novel chitosan/siRNA nanoparticle system.* Mol Ther, 2006. **14**(4): p. 476-84.
421. Golzio, M., et al., *Inhibition of gene expression in mice muscle by in vivo electrically mediated siRNA delivery.* Gene Therapy, 2005. **12**(3): p. 246-251.
422. Medarova, Z., et al., *In vivo imaging of siRNA delivery and silencing in tumors.* Nat Med, 2007. **13**(3): p. 372-7.
423. Walker, R.G., et al., *Biochemistry and Biology of GDF11 and Myostatin: Similarities, Differences, and Questions for Future Investigation.* Circ Res, 2016. **118**(7): p. 1125-41; discussion 1142.
424. Welle, S., et al., *Relation between extent of myostatin depletion and muscle growth in mature mice.* Am J Physiol Endocrinol Metab, 2009. **297**(4): p. E935-40.
425. Khan, T., et al., *Silencing Myostatin Using Cholesterol-conjugated siRNAs Induces Muscle Growth.* Molecular therapy. Nucleic acids, 2016. **5**(8): p. e342-e342.
426. Torchilin, V.P., et al., *p-Nitrophenylcarbonyl-PEG-PE-liposomes: fast and simple attachment of specific ligands, including monoclonal antibodies, to distal ends of PEG chains via p-nitrophenylcarbonyl groups.* Biochim Biophys Acta, 2001. **1511**(2): p. 397-411.